ABSTRACT

BARRY, JEREMY ALAN. Matrix-Assisted Laser Desorption Electrospray Ionization: Fundamental Principles and Applications Toward Direct Analysis and Molecular Imaging. (Under the direction of Dr. David Charles Muddiman).

The past decade has shown numerous advancements in the field of Ambient Mass Spectrometry. Every year there have been new iterations of existing ionization sources as well as the continued development of new methods of producing ions under atmospheric pressure conditions. Among these ambient ionization techniques is a source that was developed in the Muddiman lab in 2005 that combines features and attributes of the two most commonly used ionization methods for biological analysis. By fusing electrospray ionization with matrix-assisted laser desorption ionization, the matrix assisted laser desorption electrospray ionization (MALDESI) technique demonstrates the advantages to hybrid ionization methods.

Along with advancements in instrumentation, including ionization methods as well as developments in mass analyzer technology, there have also been new ways to apply these scientific innovations to answer complex biological problems. The ability to obtain spatial information of unlabeled analyte with the specificity of mass spectrometric detection in the growing field of mass spectrometry imaging has had a significant impact on a number of research areas including drug development, biomarker discovery, and clinical diagnostics.

This work describes the path along the development of a novel ionization source from inception to its continued advancement and application to real world

problems. The initial goals involved optimizing the technology to determine the limits of what the source is capable of. Along the way MALDESI was improved to allow for the ability to perform mass spectrometry imaging. With this new enhancement, MALDESI has been utilized to determine the distribution of dosed drugs within tissue sections. This spatial information can provide insight into the pharmacokinetic and pharmacodynamic properties of the drug.

In addition to its application in mass spectrometry imaging, the MALDESI source also displays potential as a direct analysis technique. The ambient nature of MALDESI makes it well suited for fast analyses with minimal sample preparation. One such application of these capabilities of MALDESI is shown in the direct analysis of dyed fabric and fibers. This experiment can be performed in seconds and provide valuable information about the identity of the dye as well the fabric polymer type.

Undoubtedly, the MALDESI technology will continue to improve and advance along with other developments in mass spectrometry. New methods of analysis and applications are bound to be developed providing avenues for MALDESI to discover other practical uses.

© Copyright 2014 by Jeremy Alan Barry

All Rights Reserved

Matrix-Assisted Laser Desorption Electrospray Ionization: Fundamental Principles and Applications Towards Molecular Imaging

by
Jeremy Alan Barry

A dissertation submitted to the Graduate Faculty of
North Carolina State University
in partial fulfillment of the
requirements for the Degree of
Doctor of Philosophy

Chemistry

Raleigh, North Carolina

2014

APPROVED BY:

_____	_____
David C. Muddiman Professor, Chemistry Committee Chair	Edmond F. Bowden Professor, Chemistry
_____	_____
Gufeng Wang Professor, Chemistry	H. Troy Ghashghaei Professor, Molecular Biomedical Sciences

DEDICATION

I would like to dedicate this dissertation to my family most importantly my parents John and Joanne. My parents have supported me in every endeavor and I am forever grateful for everything they have done for me. Also, my older brothers Justin and Josh who have been the perfect role models in my life and will always be my best friends. In addition, I could not have persisted so long in graduate school if it weren't for my long-time girlfriend (now fiancée) Amber Lauber. She has stuck with me through good times as well as bad and didn't hassled me too much about waiting so long for a ring…I am thankful and extremely fortunate to have such loving support from all of you and I will be forever indebted for your kindness.

BIOGRAPHY

Jeremy Alan Barry was born in Westfield, Massachusetts on June 20, 1986 to his parents John and Joanne Barry and is the youngest of three brothers. Jeremy attended Westfield High School and graduated in 2004. After high school he chose to attend the University of New Haven in West Haven, Connecticut. Here he earned two Bachelor of Science degrees in the fields of Chemistry and Forensic Science. He then moved to North Carolina and started his graduate career in 2008 at the University of North Carolina at Greensboro where he obtained his Master of Science degree in Analytical Chemistry under the direction of Dr. Brent Dawson. After defending his master's thesis, Jeremy began his Ph.D. career in Raleigh, North Carolina at North Carolina State University in 2010 under the direction of Dr. David Muddiman.

ACKNOWLEDGMENTS

I would like to firstly acknowledge my family and fiancée to whom this thesis is dedicated. Again, without your loving support I would not have made it this far.

My passion for the sciences and chemistry likely started early on in my life but one point that sticks out in my mind was in a high school chemistry course with Mr. Jon Tyler. It may sound corny but his classes made chemistry fun and are what inspired me to further my education in chemistry.

While the chemistry department at the University of New Haven was small, this seemed to make the learning experience more personal. I am grateful for the faculty at UNH for challenging me and guiding me in the right direction.

The chemistry and biochemistry department at the University of North Carolina at Greensboro was another group of passionate professors that truly cared about their students. It was here that I learned firsthand that you never really know something until you have to teach it. The opportunity to teach the general chemistry labs was extremely helpful in furthering my knowledge in chemistry. I will always be grateful for the support system that I developed with the fellow TA's and later long-time friends at UNCG and in the Greensboro area. It was a chapter in my life that I will always cherish.

UNCG was my first real experience with research. I can't express my gratitude towards Dr. Brent Dawson for his patience and his guidance that drove me to become a better researcher.

When I first met with Dr. David Muddiman, I could tell that he was the advisor that I wanted to work with. His research program is the reason that I continued on to NCSU for a doctoral degree. By providing the funding and the general direction of the project, he allowed me to grow as an independent researcher and develop critical thinking skills. I don't want to give the wrong impression; he was always there for advice and guidance when I needed it. His method of mentoring really helped me to establish a useful skill set that will be invaluable for my future and I will be forever grateful for this experience. In addition to Dave's mentorship, the Muddiman alumni and group members have tremendously supportive over the past several years and I can't thank them enough.

TABLE OF CONTENTS

LIST OF TABLES

LIST OF FIGURES

LIST OF PUBLICATIONS

1. Jeremy A. Barry; Guillaume Robichaud; David C. Muddiman. In *Encyclopedia of Analytical Chemistry*; John Wiley & Sons, Ltd, **2014** (Submitted 2/21/2014).

2. Kristin H. Cochran; Jeremy A. Barry; David C. Muddiman; David Hinks. Analysis of Trace Fibers by IR-MALDESI coupled with High Resolution MS. *Anal. Chem.* **2014** (In Preparation).

3. Jeremy A. Barry; Guillaume Robichaud; Corbin Thompson; Craig Sykes; Angela Kashuba; David C. Muddiman. Mapping HIV drugs in tissue using several acquisition modes by IR-MALDESI MSI coupled to the Q Exactive. *J. Am. Soc. Mass Spectrom.* **2014** (Submitted 1/6/2014).

4. Jeremy A. Barry; M. Reid Groseclose; Guillaume Robichaud; Stephen Castellino; David C. Muddiman. Localization of drugs and metabolites determined by MALDI and IR-MALDESI MSI coupled to FT-ICR MS. *Int J. Mass Spectrom.* **2014** (Submitted 12/31/2013).

5. Guillaume Robichaud; Jeremy A. Barry; David Muddiman. IR-MALDESI Mass Spectrometry Imaging of Biological Tissue Sections using Ice as a Matrix. *J. Am. Soc. Mass Spectrom.* **2014**, *25*(3), 319-328.

6. Jeremy A. Barry; Guillaume Robichaud; David C. Muddiman. Mass Recalibration of FT-ICR Mass Spectrometry Imaging Data Using the Average Frequency Shift of Ambient Ions. *J. Am. Soc. Mass Spectrom.* **2013**, *24*(7), 1137-1145.

7. Guillaume Robichaud; Kenneth P. Garrard; Jeremy A. Barry; David C. Muddiman. MSiReader: An Open-Source Interface to View and Analyze High Resolving Power MS Imaging Files on Matlab Platform. *J. Am. Soc. Mass Spectrom.* **2013**, *24*(5), 718-721.

8. Guillaume Robichaud; Jeremy A. Barry; Kenneth P. Garrard; David C. Muddiman. Infrared Matrix-Assisted Laser Desorption Electrospray Ionization (IR-MALDESI) Imaging Source Coupled to a FT-ICR Mass Spectrometer. *J. Am. Soc. Mass Spectrom.* **2013**, *24*(1), 92-100.

9. Kristin H. Cochran; Jeremy A. Barry; David C. Muddiman; David Hinks. Direct Analysis of Textile Fabrics and Dyes Using Infrared Matrix-Assisted Laser Desorption Electrospray Ionization Mass Spectrometry. *Anal. Chem.* **2012**, *85*(2), 831-836.

10. Jeremy A. Barry; David C. Muddiman. Global optimization of the infrared matrix-assisted laser desorption electrospray ionization (IR MALDESI) source for mass spectrometry using statistical design of experiments. *Rapid Commun. Mass Spectrom.* **2011**, *25*(23), 3527-3536.

LIST OF PRESENTATIONS

1. **Oral** - “Drug and Metabolism Studies Using Infrared Matrix-Assisted Laser Desorption Electrospray Ionization Mass Spectrometry Imaging (IR-MALDESI MSI) Coupled to FT-ICR” Jeremy A. Barry, Guillaume Robichaud, Reid Groseclose, David Wagner, Stephen Castellino, David C. Muddiman. *61st American Society for Mass Spectrometry Conference*. Minneapolis, Minnesota, June 2013.

2. **Oral** - “Direct Analysis of Dyed Textile Fabric and Fibers Using IR-MALDESI” Jeremy A. Barry, Kristin H. Cochran, Guillaume Robichaud, David C. Muddiman. *Art and Cultural Heritage Workshop*, *61st American Society for Mass Spectrometry Conference*. Minneapolis, Minnesota, June 2013.

3. **Oral** - “Ambient Molecular Imaging Using Infrared Matrix-Assisted Laser Desorption Electrospray Ionization (IR-MALDESI) Coupled to an FT-ICR Mass Spectrometer” Jeremy A. Barry, Guillaume Robichaud, David C. Muddiman. *IQ Consortium MS Imaging Discussion Group Meeting*. GlaxoSmithKline, Research Triangle Park, North Carolina, May 2013

4. **Oral** - “Molecular Imaging Using Infrared Matrix-Assisted Laser Desorption Electrospray Ionization (IR-MALDESI) Coupled to an FT-ICR Mass Spectrometer” Jeremy A. Barry, Guillaume Robichaud, David C. Muddiman. *Triangle Area Mass Spectrometry Discussion Group*. Research Triangle Park, North Carolina, March 2013.

5. **Poster** - “Molecular Imaging Under Ambient Conditions with Infrared Matrix-Assisted Laser Desorption Electrospray Ionization (IR-MALDESI) Mass Spectrometry Using Ice as a Matrix” Jeremy A. Barry, Guillaume Robichaud, David C. Muddiman. *9th Annual United States Human Proteome Organization Conference*. Baltimore, Maryland, March 2013.

6. **Oral** - “Use of Statistical Design of Experiments for Optimization of the Matrix Assisted Laser Desorption Electrospray Ionization (MALDESI) Source for Mass Spectrometry” Jeremy A. Barry, Guillaume Robichaud, David C. Muddiman. *63rd Southeastern Regional Meeting of the American Chemical Society*. Richmond, Virginia, October 2011.

7. **Poster** - “Characterization of the UV- and IR-Matrix-Assisted Laser Desorption Ionization (MALDESI) Source with Air Amplifier” Jeremy A. Barry, Guillaume Robichaud, David C. Muddiman. *59th American Society for Mass Spectrometry Conference*. Denver, Colorado June 2011.

8. **Poster** - “Characterization of the Matrix Assisted Laser Desorption Electrospray Ionization (MALDESI) Source for Mass Spectrometry Using UV or IR Wavelengths” Jeremy A. Barry, Guillaume Robichaud, David C. Muddiman. *7th Annual United States Human Proteome Organization Conference*. Raleigh, North Carolina, June 2011.

CHAPTER 1

An Introduction to the Development of Ambient Ionization Platforms for Mass Spectrometry

A portion of the following work was reprinted from a recently submitted manuscript: Barry, J. A.; Robichaud, G.; Muddiman, D. C. In *Encyclopedia of Analytical Chemistry*, Submitted: February 2014.

1.1 Methods of Ionization for Mass Spectrometry

1.1.1 Matrix-Assisted Laser Desorption Ionization

Matrix assisted laser desorption/ionization (MALDI) is a technique which utilizes a laser to facilitate the desorption and ionization of a matrix/analyte mixture. Early research in this area was performed on amino acids and small molecules[1-4] but the application to large biomolecules was quickly realized.[5-7] Like ESI, MALDI is a relatively soft ionization technique that results in the generation of intact molecular ions. These two ionization sources provide complementary information and are the most widely used techniques for biological mass spectrometry.

One of earliest ion sources for mass spectrometry was a surface analysis technique where a sample surface was bombarded with an ion beam to generate secondary ions in a technique known as secondary ion mass spectrometry (SIMS).[8,9] Also, not long after the introduction of the laser, it was used as a point source to generate ions directly from surfaces or thin films for mass analysis through a technique that would be later referred to as laser desorption ionization (LDI).[10-13] These surface analysis techniques were around prior to MALDI, however, they were typically limited to the analysis of small molecules and would frequently produce

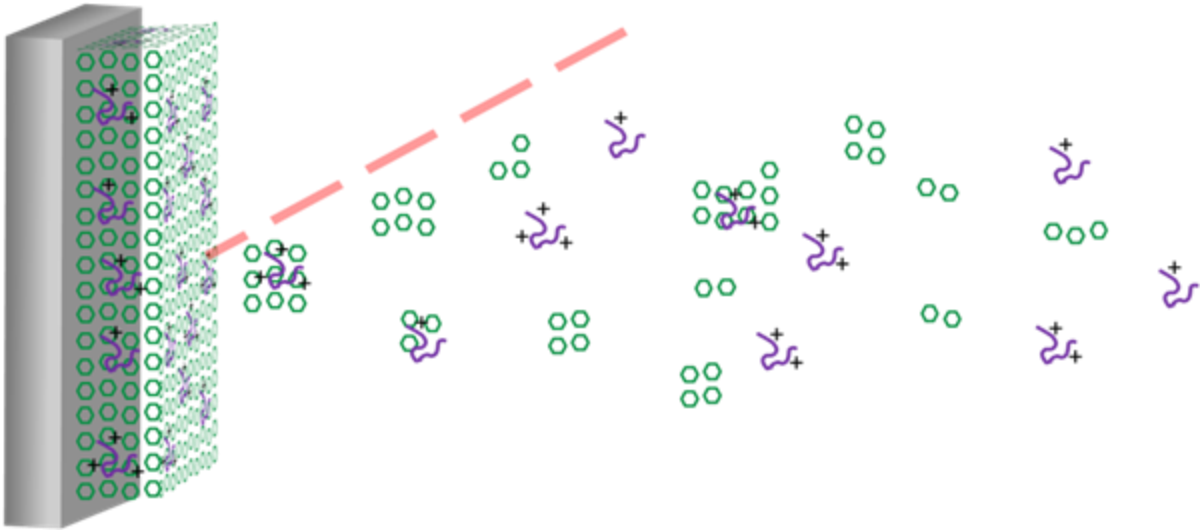

Figure 1.1 Schematic of the MALDI process showing the laser desorption of analyte that is co-crystalized with an organic matrix.

fragments of the molecular ion because of the high energies imparted into the sample. It was observed that mixing the sample with an energy absorbing matrix reduced fragmentation and resulted in an overall enhancement of the mass spectra. These observations are what gave rise to the MALDI technique (**Figure 1.1**).

In a typical MALDI analysis, the analyte is mixed with a large excess of matrix and spotted onto a stainless steel target. Typical qualities of the matrix include the ability to solvate the analyte and to absorb strongly in the wavelength region of the laser emission.[14] This solvation and co-crystallization with an excess of matrix provides isolation of analyte molecules within the matrix lattice to reduce aggregation. Upon irradiation with a short laser pulse, the matrix absorbs a bulk of the energy through electronic excitation. Some of the electronic excitation energy is converted into an expansion of the matrix lattice resulting in sublimation of a layer of

the sample.[15-17] This fast vaporization of the matrix layer also leads to ejection of the imbedded analyte molecules.

While there is still much to learn about the ionization mechanisms involved in MALDI, there are two major theories that have been proposed (**Figure 1.2**). One theory is based on the gas phase protonation of the analyte by photoionized matrix clusters.[18] The photoionization of matrix molecules upon irradiation can produce matrix radical cations which would be highly acidic and likely to donate a proton. This gas phase protonation mechanism is backed by the observation of primarily singly and doubly charged ions. The other theory, referred to as the lucky survivor

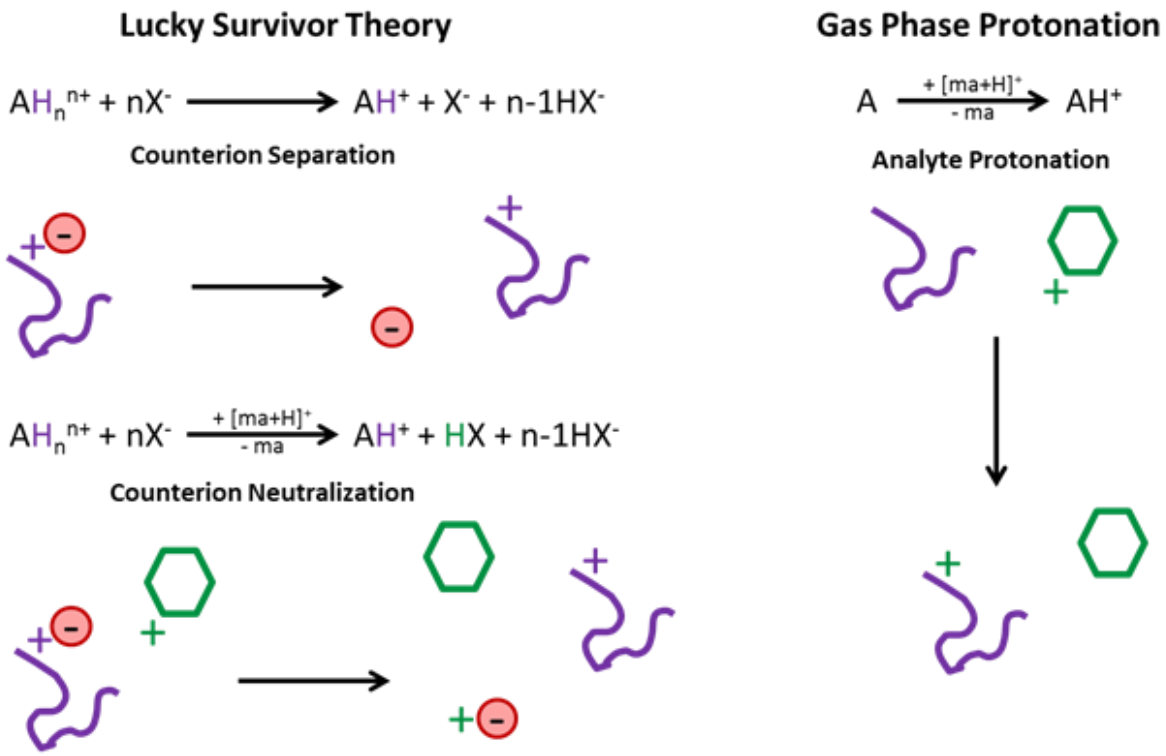

Figure 1.2 The proposed ionization mechanisms in MALDI.

theory, holds that the solution charge states are retained in the condensed phase.[19] Upon drying on the sample plate, the analyte retains the charge state that it had in solution and counterions are present at each charge site to allow for crystallization. After the transition into the gas phase, the analyte ions can be generated through separation of the counterion from the charged analyte or neutralization of the counterion by protonated matrix ions. Here the photoionization of matrix molecules and generation of free electrons and matrix radical cations also plays a significant role. This mechanism does not directly account for the observation of singly and doubly charged species however the authors speculate that the electrons formed from the photoionization of the matrix leads to a rapid re-neutralization of multiply charged ions. They propose that the observed singly and doubly charged ions are the "lucky survivors" of the in plume neutralization. Recent evidence of both protonated and deuterated ions using deuterated matrices provides evidence that both mechanisms may be viable.[20]

MALDI is a robust technique for analyzing biological samples including those with fairly high buffer and salt concentrations.[21] The observation of primarily singly or doubly charged ions makes the analysis of mixtures fairly straightforward. However, this could place a restriction on the observable mass limit depending on the mass analyzer. A major drawback is the poor shot-to-shot reproducibility observed in MALDI which makes quantification difficult.[22] "Sweet spots" are known to form in which there is a large variation in local analyte concentration. This observation is believed to stem from the heterogeneity of the co-crystallization.

Despite there being a large number of options, there is no one matrix choice or sample preparation method which evades the reproducibility issue. Signal suppression from the matrix or analyte is also a common problem in MALDI.[23-25] Another issue that arises in MALDI is the relatively low ion yields. The overall ion to neutral ratio was determined to be around 10^{-4} for a typical MALDI experiment.[26-28]

1.1.2 Electrospray Ionization

Since its inception, electrospray ionization (ESI) has evolved to become one of the most widely utilized ionization techniques for the mass spectrometric analysis of biomacromolecules. In general, the ESI process involves the application of an electric potential to a conductive analyte solution flowing through an emitter to produce a fine mist of charged droplets which eventually generate gas phase ions. The utility of electrospray as a means of producing gas phase macroions was first realized by Malcolm Dole in the late 1960's where he applied electrospray to the analysis of large molecular weight polymers.[29] Inspired in part by the work of Dole, John Fenn demonstrated that ESI could be used as an ion source for mass spectrometry[30,31] to effectively ionize relatively nonvolatile species including high molecular weight polymers,[32] small peptides,[33] and proteins.[34,35] These contributions have revolutionized the field of MS and resulted in the award of a quarter of the Nobel Prize in Chemistry in 2002.[36]

While its application to mass analysis was not realized until the late 1960's, the ideology behind electrospray had been around for some time. The influence of

electric fields on liquid droplets, primarily water, was an area of particular interest to a number of researchers around the turn of the twentieth century. Rayleigh proposed that a charged spherical droplet in an electric field is stable providing that,

$$T > \frac{Q^2}{16\pi a_0^3} \qquad \textbf{(Equation 1.1)}$$

where *T* is the surface tension of the liquid, *Q* is the electric charge, and a_0 is the radius of the drop.[37] However, if the right hand term becomes sufficiently large either by increasing the charge or decreasing the droplet radius, the droplet becomes unstable resulting in liquid being "thrown from the droplet in fine jets." This condition of instability was then later studied by Zeleny for a charged liquid meniscus at the end of a cylindrical tube.[38-40] Zeleny demonstrated that when the conditions of instability are met (by applying an adequately large potential to the solution), the meniscus deforms to a conical shape and a thin jet is pulled from the point where the electric density is the greatest. This jet eventually breaks up into small droplets which then spread into a plume due to mutual electric repulsion. These observations spurred more investigations into the effects of electric fields on liquid droplets,[41-44] the ions produced from electrical discharges at liquid surfaces,[45-47] and the disintegration of charged liquid jets.[48-54] One of the more comprehensive theoretical evaluations of the processes involved in Zeleny's experiments was performed by Taylor where he was able to model the electrohydrodynamics involved with the formation of the cone shape and ejection of droplets.[55] These observations and theories provided the groundwork upon which the electrospray process was

built. Prior to its application to mass spectrometry, electrospray had been utilized in numerous other fields including fuel atomization, electrospinning, and as an efficient means of painting automobiles.[56,57]

A diagram of the ESI process is outlined in **Figure 1.3**. In positive ion mode ESI, a positive electric potential is applied to a conductive analyte solution flowing through a silica capillary. The water is oxidized at the liquid junction where this potential is applied resulting in the generation of excess protons in solution. This excess charge builds up at the capillary emitter causing a deformation of the solution meniscus into a conical shape referred to as the "Taylor Cone".[58] At the apex of this cone a thin jet of the charged solution is emitted from which charged analyte-

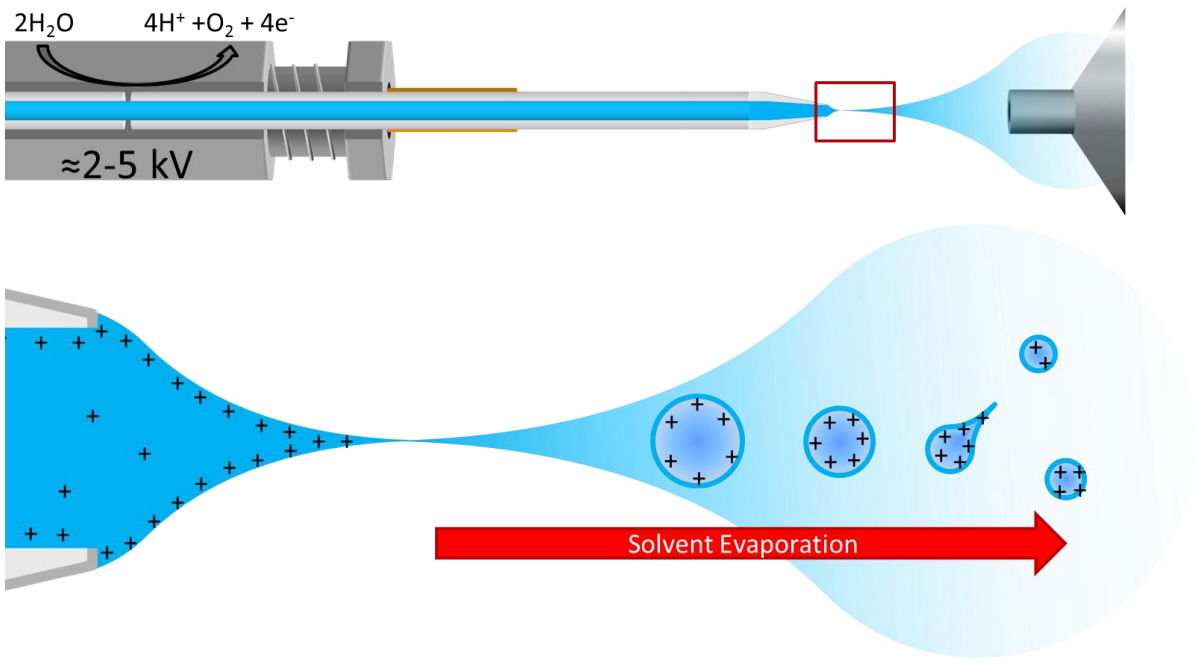

Figure 1.3 Schematic of the electrospray process.

containing solvent droplets are generated. The generation of these charged solvent droplets is the result of axisymmetric and non-axisymmetric disturbances along the jet surface.[54] The size of the droplets that are produced is dependent on a few parameters including the applied potential, the surface tension and conductivity of the solution, the solution flow rate, and the diameter of the emitter tip.[59-61] Conditions typical of contemporary ESI result in droplet sizes on the order of hundreds of nanometers to a micrometer.[62-64] As these solvent droplets are released they spread into a plume due to mutual repulsion. While traveling towards the inlet to the mass spectrometer, the droplets collide with gas molecules from the ambient air and the heat from the resulting friction causes evaporation of the droplet solvent. This solvent evaporation reduces the size of the droplet thereby increasing its overall charge density until it reaches the stability limit, discussed previously, that is referred to as the Rayleigh limit. At this point, where the Coulombic repulsion due to the increased charge density overcomes the surface tension, the droplet will deform and a thin jet will protrude and generate smaller highly charged progeny droplets to reduce stress on the parent droplet.[65-67] It is estimated that roughly 15% of the overall charge from the parent droplet is imparted into these progeny droplets which constitute about 2% of the parent droplet mass.[65,66] The progression of solvent evaporation and droplet fission is repeated until the droplets are small enough to generate gas phase ions.

The production of gas phase ions is proposed to occur by one of two mechanisms known as the charged residue model and the ion evaporation model

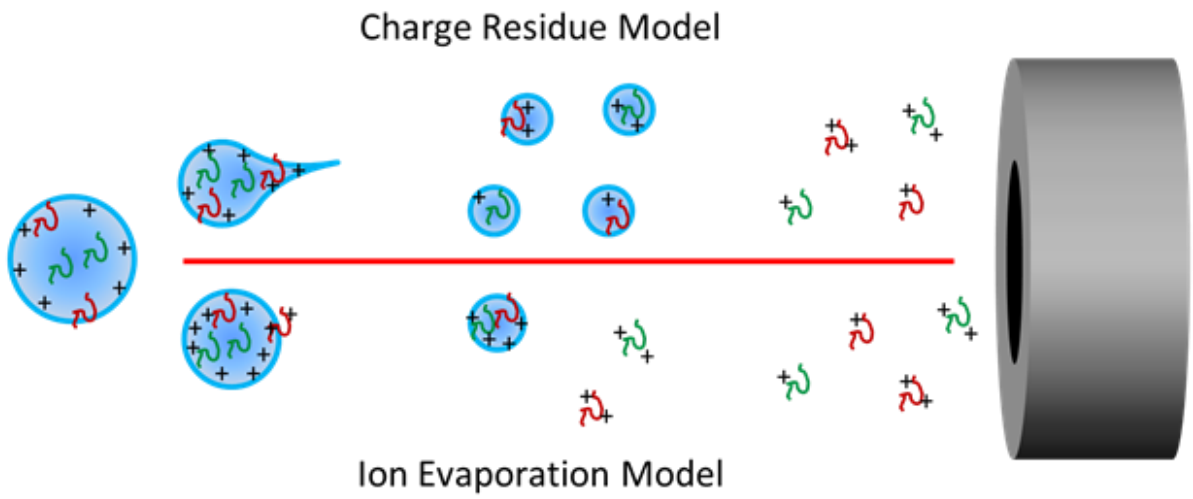

Figure 1.4 Ionization mechanisms in ESI.

(**Figure 1.4**). In both models the droplet evaporation and fission process continues until the diameter is sufficiently small enough to produce ions and it is from this point forward that the two mechanisms differ. Dole proposed that fission continues until the charged droplets reach a point where they are small enough to contain a single analyte molecule.[29,68,69] Upon evaporation of the solvent from that progeny droplet, the confined charge would be imparted onto the analyte and the analyte ion would be transferred into the gas phase. The other more supported mechanism proposed by Iribarne and Thomson is referred to as the ion evaporation model.[70-72] Similar to the charged residue model, droplet evaporation and fission continues until the droplets reach a certain size. However, the authors refer to a situation where these progeny droplets contain multiple elementary charges and analyte species but are still below the Rayleigh instability limit. The local electrostatic field produced by the charges on the surface of these droplets would be capable of ejecting surface active

analytes as gas phase ions and they indeed provide evidence that these conditions are kinetically and thermodynamically favorable for small molecules. While there is still debate over which of these theories is most likely to occur, there has been some acknowledge that large molecules are likely to be ionized by the charged residue model[73] whereas the ion evaporation model is predominant for smaller molecules.[74]

One of the key features of ESI is its ability to produce multiply charged analyte species.[32,34] While this caveat does increase spectral complexity by generating multiple peaks for a single species, it provides a means of detecting large molecules that would be above the upper *m/z* limit of most mass analyzers if they were otherwise singly charged (increasing the charge, z, would decrease the m/z of the ion). This multiple charging effect also makes the molecules more amenable to structural characterization through fragmentation. This is because fragmentation of a singly charged ion would result in a single observable fragment whereas fragmentation of a multiply charged species has the potential to produce multiple observable ions. Another feature that has aided in the popularity of ESI is its compatibility with liquid chromatography techniques.[33] Despite the advantages that were discussed, there are a few drawbacks to this technique. ESI is highly sensitive to the presence of foreign electrolytes, such as inorganic salts that may be present in the matrix of biological samples, which can suppress analyte signal.[75] This ion suppression is also observed in multicomponent samples where species in the same droplet must compete for charge.[76] While the ionization efficiency in ESI is likely to be close to 100%, studies have shown that only about <1% of those ions actually

make it through the interface between the ambient environment where the ions are generated and the vacuum where they are analyzed.[77,78]

1.1.3 Ambient Ionization Sources

By definition, ambient ionization techniques are those which produce ions at atmospheric pressure and temperature. However, this definition has been narrowed to only include ionization techniques that not only meet the atmospheric conditions but also analyze the sample under native conditions. In this case native conditions refer to requiring little to no sample preparation prior to analysis. One of the first ionization sources capable of native sample analysis was desorption electrospray ionization (DESI) which, as the acronym describes, utilizes an electrospray plume to both desorb and analyze analyte directly from a sample.[79] This technique has been cited as the start of an ambient ionization revolution where since the introduction of DESI, more than 30 new ambient ionization sources have been introduced.[80] Most of these ion sources are hybrids of ionization technologies that were already developed, however, this short review will focus on those which involve laser desorption followed by post-ionization by ESI.

Since it is known that laser desorption produces poor ion yields, other methods have been utilized to post-ionize the neutral molecules which are more prevalent in the ablated plume.[81-83] Following the theme of ambient ionization, two methods were introduced which utilized atmospheric pressure laser desorption and post-ionization by ESI: they are referred to as electrospray assisted laser desorption

ionization (ELDI)[84] and matrix assisted laser desorption electrospray ionization (MALDESI).[85]

ELDI involves the non-resonant laser desorption of the sample followed by post-ionization by ESI. A typical ELDI analysis involves spotting the liquid sample onto a stainless steel plate. Once dried the sample plate is placed below the axis made with the electrospray emitter and mass spectrometer inlet. A UV laser is then used to desorb the sample. The particulate matter and neutral analyte molecules that are produced upon desorption partition into the charged electrospray droplets and are ionized via and ESI process. The initial studies with ELDI involved the laser desorption of proteins that include tryptophan residues. While the tryptophan residues could resonantly absorb some of the laser energy, the desorption process is still likely to proceed through a non-resonant thermal process. In fact, the authors have stated that the addition of a matrix to resonantly absorb the laser energy reduces the spectral quality and ion abundance.[86] To date, ELDI has been used to directly detect proteins from biological fluids,[86] lipids from brain tissue, dyes from paintings, active ingredients from drug tablets, [87] and for continuously monitoring ongoing chemical reactions.[88]

The MALDESI process may seem somewhat similar to ELDI in that they both involve laser desorption and electrospray post-ionization, however, MALDESI utilizes an endogenous or exogenous matrix to resonantly absorb the laser energy and facilitate the analyte desorption. A schematic of the MALDESI process is outlined in **Figure 1.5**. Because it is a hybrid of both MALDI and ESI, MALDESI

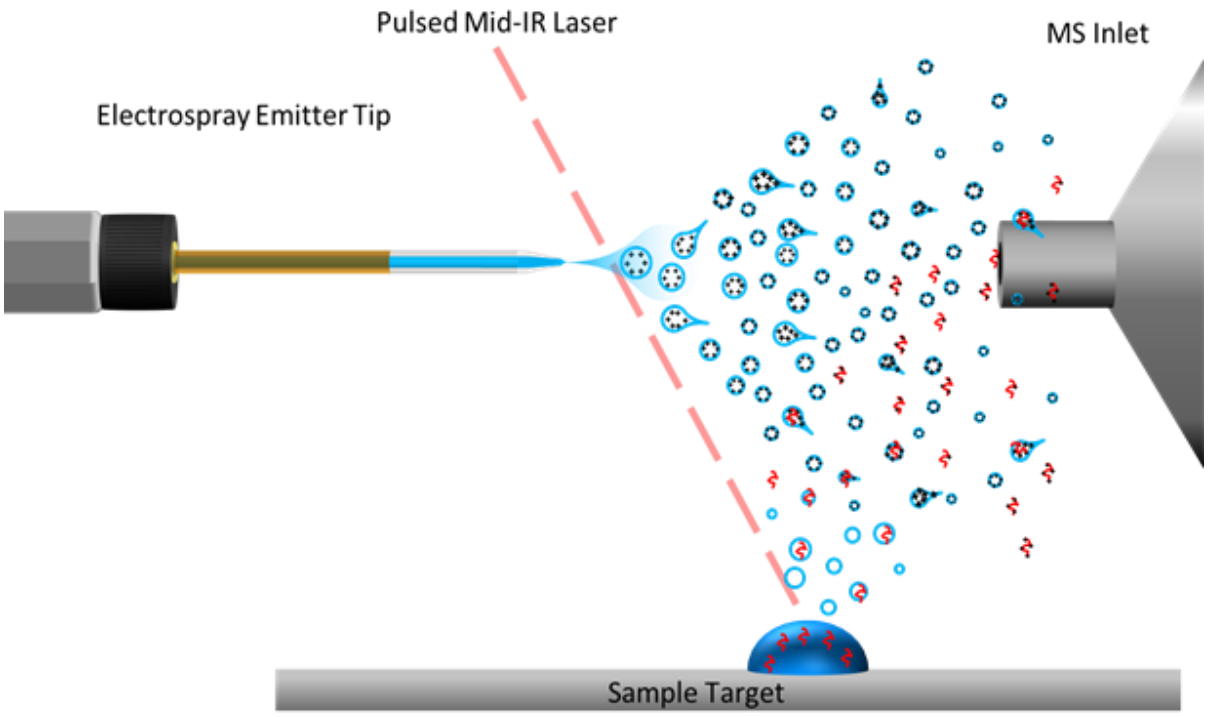

Figure 1.5 Schematic of the IR-MALDESI process.

combines features and benefits of each including analyte multiple charging, soft desorption and ionization, high salt tolerances, and the capability for direct analysis. MALDESI has been demonstrated using UV lasers with emission at 337 and 349 nm in conjunction organic acid matrices, as well as *IR* lasers at the wavelengths of 2.94 and 10.6 μm using glycerol, sinapic acid, or water as a matrix.[85,89-92] In addition to the various laser wavelengths that have been investigated, desorption from both the solid state, in the case of condensed phase organic matrices, and liquid state have also been presented.

Desorption of analyte from condensed phase organic matrices is likely to occur through a mechanism similar to that previously described for MALDI. The

plume expansion, however, could be different because desorption for MALDI takes place under vacuum whereas desorption in MALDESI is as atmospheric pressure. The mechanisms of analyte desorption at atmospheric pressure from liquid matrices, such as water and glycerol, have been described previously and these processes are relevant to MALDESI. IR ablation of water rich material is characterized by a two-step process. Upon irradiation with a laser pulse of a few nanoseconds, the surface layer of water is nearly instantaneously vaporized in a process that is referred to as phase explosion. This initial plume is a mixture of vapor and fine droplets and travels at velocities upwards of 4100 m/s which drives the emission of an equally fast shockwave.[93,94] The recoil stress induced by the expansion of the primary ablation results in a secondary emission of larger droplets that can last up to roughly 1 ms.

After neutral analyte desorption, it has been proposed that the analyte partitions into the charged electrospray droplets. Evidence for this theory can be found in the effects that changes in the electrospray composition have on the observed mass spectra. Loo and coworkers demonstrated that by increasing the organic of the electrospray solvent, the laser desorbed protein conformation can shift from a native folded state to a denatured unfolded state.[95] They also show that adding dithiothreitol, a strong reducing agent, to the electrospray solvent could reduce the disulfide bonds of the oxidized form of insulin. Vertes has shown that adding lithium sulfate to the electrospray solvent for the analysis of lipids allows for structure specific fragmentation of the ester bonds in order to identify the acyl chain

lengths.[96] These observations provide evidence that the desorbed analyte must first partition into the electrospray droplets prior to ionization.

Ionization in MALDESI is believed to take place through an ESI-like mechanism after the desorbed neutral molecules partition into the charged droplets. This hypothesis is based mainly on the observation that MALDESI mass spectra are nearly identical to those observed in ESI. An investigation into the source of analyte ion protonation was carried out by separating the desorption and ionization processes in space and time through a remote sampling device termed the remote analyte sampling, transport, and ionization relay (RASTIR).[97] When using deuterated electrospray solvents with RASTIR, a one Dalton shift was observed in the protonated mass of reserpine which corresponds to the incorporation of a deuteron in place of a proton.[98] This implies that the electrospray is the source of the ionizing proton in MALDESI. Other groups have shown, using an analog of MALDESI known as laser ablation electrospray ionization (LAESI),[99] that the internal energies of MALDESI ions are indistinguishable from ESI generated ions.[100]

1.2 Atmospheric Pressure Mass Spectrometry Imaging

1.2.1 Introduction to Mass Spectrometry Imaging

Mass spectrometry imaging (MSI) involves generating mass spectra from discreet locations in an array pattern over the surface of a sample. By relating the position where each mass spectrum was obtained to the abundance of any ion in those spectra, a heat map can be generated that displays the distribution of that ion

within the sample. Given the high specificity and sensitivity of mass spectrometric detection, this technique demonstrates significant potential for application in a wide number of areas.

The concept of MSI was initially conceived by Castaing and Slodzian in the 1960's with the introduction of Secondary ion mass spectrometry (SIMS).[101] Over the years, however, significant advancements have been made in instrumentation that has allowed for the analysis of molecules up to about 1 kDa with currently unsurpassed spatial resolution.[102-105] Given the softness of matrix-assisted laser desorption ionization (MALDI) towards the analysis of large biomolecules and the capability to generate ions from a position on the sample, MALDI would appear to be a prime candidate for MSI analysis. Indeed, in 1994 Spengler presented on the ability of MALDI to be used for biological ion imaging.[106] Caprioli et al. subsequently published on using MALDI MSI to determine the spatial distribution of peptides and proteins in biological tissue.[107] Since that time, a number of reviews for MSI have been presented covering advancements in methodologies[108-115] and applications in metabolomics,[116,117] proteomics,[116,118-120] lipidomics,[121-124] as well as dosed xenobiotics.[104,125-128] While MALDI is undoubtedly the most used ionization source for MSI, there are a few drawbacks that are associated primarily with the requirement that the sample must be amenable to high vacuum. Sample introduction into high vacuum restricts throughput, sample size and type, as well as negates the analysis of volatile species. The introduction of ionization techniques that operate under atmospheric pressure conditions provided alternative approaches

for MSI that refuted these restrictions.[80,129-132] A few of these sources have been used for MSI which in and of itself is a subject of review.[133]

As mentioned previously, MSI is used to obtain spatial information of multiple ions from the sample surface. The sample is often scanned or rastered in such a way that mass spectra are generated from discreet positions along the sample. The distance between each position where a mass spectra is generated relates to the spatial resolution of the resulting ion image. Different methods have been proposed to define and report spatial resolution in mass spectrometry imaging. The most intuitive and common approach is to define the spatial resolution as the smallest feature that can be resolved on an ion image.[134-136] Others have also defined the spatial resolution as the minimum step size or pixel-to-pixel distance for which an increase in signal abundance from 20% to 80% of the maximum value is measured.[137-139] The later definition is more quantitative and in appearance less subjective. It is also somewhat popular since this calculated value is often smaller than the value determined using the feature based approach, allowing authors to claim a smaller spatial resolution.

Actual spatial resolution in great part defined by the size of the MSI probe (e.g. laser focal diameter, DESI spot size) and the distance between each scan or mass spectra collected (step distance). When imaging in undersampling mode, the step distance is set to be larger than the diameter of the probe size so that there is no overlap. When operating in oversampling mode, the step distance is smaller than the spot size such that sampling areas are overlapping. It has been demonstrated

that the oversampling technique can be used to obtain spatial resolution significantly smaller than the actual probe diameter.[136,139]

Data processing workflow to convert the raw mass spectrometry data collected during an imaging experiment to a 2D heatmap is relatively simple and an example case is presented in **Figure 1.6**. As many authors or research groups will opt to implement their own data processing algorithms, others will use one of the 20 existing software tools for viewing and processing MSI data that are available.

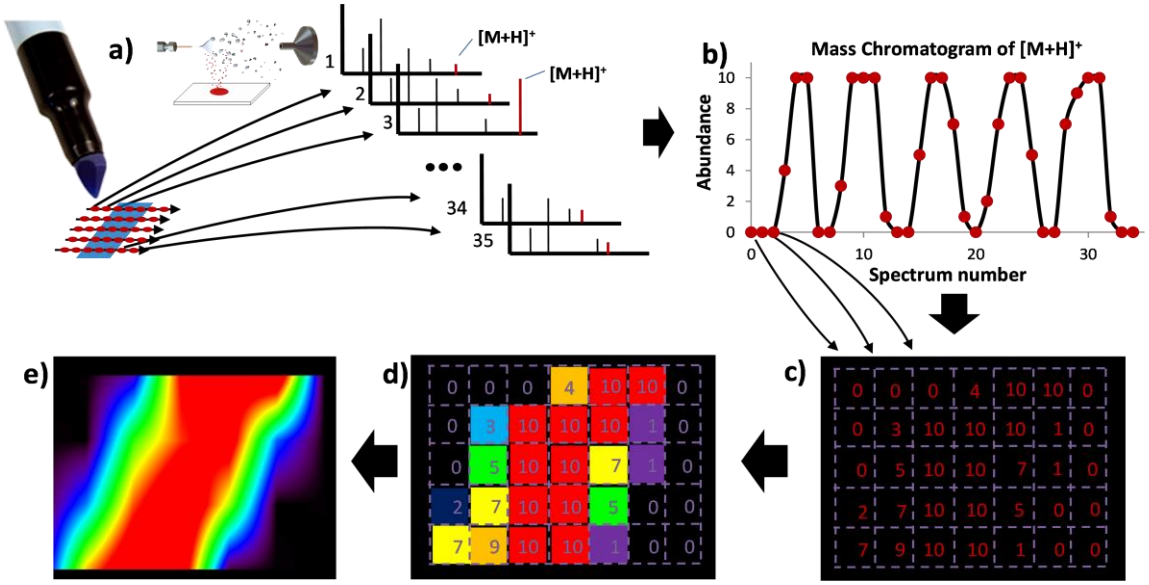

Figure 1.6 Simplified example showing the data processing steps to generate molecular image from mass spectrometry data. **a)** Mass spectra are collected at discrete and monitored spatial locations over the sample surface using a mass spectrometry imaging source. **b)** Typical ion chromatogram of analyte molecule (e.g. dye from felt pen) extracted from the raw data file, before **c)** ion signal abundance of each mass spectra is transposed on 2D data matrix at the spatial location where it was collected. **d)** Signal abundance matrix is then converted to a heat map where intensity values are represented as colors on a heatmap. **e)** Heatmap can be post processed and by adding an optional pixel interpolation steps for smoother contours.

Among those are the MSI software tools that most vendors provide to view the imaging data collected by their instrument. There are also many other MSI software that are platform independent and can process custom MSI data or files from instrument different instrument platforms. This is possible because of the existence of multiple vendor-neutral MS data format such as mzML,[140] mzXML,[141] imZML,[142,143] and the availability of MS data converters to generate those files.[144,145] Many of the vendor neutral MSI software are free and readily available for download[146-149] and some are also open source.[146,148] Most of the imaging software offer basic features such as image colocalization, MS spectra viewing, peak picking, and data extraction from region of interest. More advanced data analysis tools also offer features such as automatic peak detection, normalization, background subtraction, principal component analysis and more.

1.2.2 Atmospheric Pressure Laser Desorption Ionization (AP-LDI) and Atmospheric Pressure Matrix-Assisted Laser Desorption Ionization (AP-MALDI)

1.2.2.1 Introduction to AP-LDI and AP-MALDI

Not long after laser technology was invented, lasers were used for direct desorption and ionization from solid surfaces for mass spectrometry in a technique that later became referred to as laser desorption ionization (LDI).[10] LDI was primarily used in the analysis of small organic compounds.[12,150] Direct coupling of the laser energy to the analyte of interest, however, could produce ions with large internal energies that ultimately result in the observation of fragment ions rather than

molecular ions. The use of a matrix (an endogenous or exogenous component that strongly absorbs in the wavelength region of laser emission) was shown to provide a more efficient desorption and much softer ionization in a technique known as matrix-assisted LDI (MALDI).[4] These improvements in desorption and ionization observed with MALDI provided the opportunity to analyze of large biomolecules by mass spectrometry.[4-6] By allowing for the analysis of proteins, peptides, and other biological molecules, the MALDI technique together with electrospray ionization (ESI)[35] have unequivocally advanced the utility of mass spectrometry.

Since its introduction, MALDI has demonstrated several advantageous features including its ability to produce primarily singly charged ions for simplified spectral interpretation, multiple interrogations from a single position, and minimal sample cleanup due to a high tolerance to salts. In its original arrangement, desorption and ionization in MALDI took place under high vacuum. While this may be beneficial for efficiently collecting/accumulating the generated ions, it does place restrictions on throughput and the type of samples that can be analyzed. These restrictions were lifted when Laiko and Burlingame introduced an atmospheric pressure (AP) MALDI source.[151-153] Aside from being able to handle the sample under atmospheric pressure conditions, AP-MALDI also allowed for even softer ionization due to collisional cooling at AP and greater flexibility by being capable of coupling to any mass spectrometer with an AP interface. This flexibility provides the opportunity to use a single instrument for ESI, atmospheric pressure chemical ionization (APCI), or AP-MALDI through a quick change of the ionization source.

However, a limiting factor that was realized early in the development of AP-MALDI was that the inefficient transfer of ions from AP into the vacuum region for mass analysis (a nuance shared by all AP ionization sources) resulted in reduced sensitivity compared with its vacuum counterpart.

There have been several design iterations of the AP-MALDI source that have aimed at improving the figures of merit of the technique. The initial design used a probe that was held parallel to and within a few mm of the AP interface inlet of the mass spectrometer (**Figure 1.7a**).[153] A flow of nitrogen gas across the sample was used to sweep the ions generated from the laser pulse into the mass spectrometer. In order to improve the efficiency of ion capture by the AP interface, the source was redesigned such that the sample plate was perpendicular to the mass spectrometer inlet as shown in **Figure 1.7b**.[154] With this design, the expansion of the ablation plume occurs in the direction of the mass spectrometer inlet providing improved sampling of the generated ions. Further improvements in ion transmission into the mass spectrometer were realized with the implementation of pulsed dynamic focusing (PDF).[155] In previous designs of AP-MALDI a continuous electric potential was applied to the sample late to provide a static electric field which extracts the laser generated ions towards the AP interface. This, however, can cause ions to be neutralized on the API inlet. With PDF, the potential on the sample plate is lowered to ground as the ions reach the inlet allowing the gas flow from the mass spectrometer to guide the ions into the AP interface. This theory behind the observed enhancement in signal using PDF was later supported by computational

modeling.[156] In addition to the traditional reflection geometry that is commonly used in MALDI, several groups have investigated the use of the transmission geometry arrangement (**Figure 1.7c**).[157,158] However, in order to avoid stifling of the ablated plume, much larger fluences were typically required in order to ablate completely through the sample.

Sample preparation in AP-MALDI is nearly identical to that of vacuum MALDI. All of the matrices and matrix application methods that are commonly used in vacuum MALDI are also applicable to AP-MALDI. In addition, volatile matrices and preparations that were previously impractical because of the requirement of vacuum compatibility became suitable for AP-MALDI. Of primary interest is the use of liquid

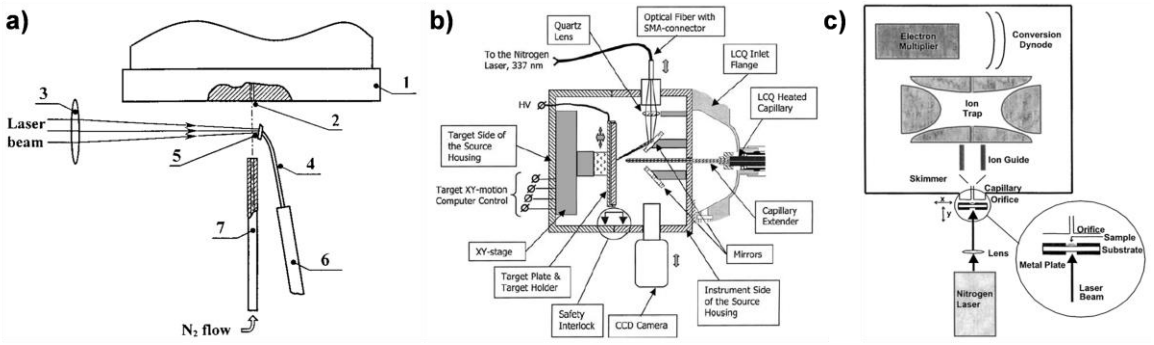

Figure 1.7 The several iterations of the AP-MALDI/AP-LDI source design. **a)** The probe design was the initial proof of concept which led the way to the **b)** more highly engineered source. AP-MALDI can be performed in the reflection geometry where ablation takes place from the top surface of the sample or the **c)** transmission geometry where ablation is initiated from the back of the sample. **a)** Adapted with permission from (V.V. Laiko, M.A. Baldwin, A.L. Burlingame, Anal. Chem., 72, 652-657 (2000)). Copyright (2000) American Chemical Society. **b)** Adapted from (V.M. Doroshenko, V.V. Laiko, N.I. Taranenko, V.D. Berkout, H.S. Lee, Int. J. Mass Spectrom., 221, 39-58 (2002)) with permission from Elsevier. **c)** Adapted with permission from (M.C. Galicia, A. Vertes, J.H. Callahan, Anal. Chem., 74, 1891-1895 (2002)). Copyright (2002) American Chemical Society.

matrices which provide significantly better shot to shot reproducibility compared with solid preparations. Direct analysis from aqueous samples became possible using an IR laser that couples to the O-H stretching vibrations of water essentially allowing water to be used as the matrix which nearly eliminates matrix-related background.[159,160] By adding common UV matrices to liquid supports (i.e. water, glycerol), AP UV-MALDI with liquid matrices is also possible.[161] While the use of ice as a matrix for laser desorption had been demonstrated previously,[162-170] Von Seggern et al. extented its utility as a matrix for AP IR-MALDI by using a Peltier cooled stage to freeze aqueous samples prior to analysis.[171] An AP-MALDI technique using colloidal graphite as the matrix also produced spectra with no matrix-related background interference.[172]

Aside from the observation of labile ions and non-covalent interactions in AP-MALDI,[152,173-178] several studies have been conducted to demonstrate the effective "softness" of ionization. One of the most common methods to elucidate this attribute is through the determination of the ion internal energy using benzylpyridinium ions.[179] With this approach it was determined that because of collisional cooling at AP, fragmentation associated with ion extraction is not observed with AP-MALDI and it was noted signal stability was significantly more reproducible in AP-MALDI compared to vacuum MALDI. A separate study compared the internal energy of peptide ions from ESI with those from AP-MALDI.[180] It was determined that the internal energy of ions produced by AP-MALDI increased with an increasing difference between the gas-phase basicities of the matrix and analyte. Due to a

fundamental flaw in the experimental design in reference [180], Remes and Glish re-examined this comparison and found that the fragmentation onset voltage for peptides ions produced by nanoflow ESI and AP-MALDI were nearly identical.[181]

The observation of primarily singly charged ions in MALDI is oftentimes seen as an advantage because it significantly reduces the complexity of mass spectra from complex mixtures. While this is true, the generation of singly charged ions also presents a limitation given that the upper *m/z* limit of most mass spectrometers is around 2000-4000 *m/z*. This would place ions larger than 2-4 kDa outside the observable mass range which is why most MALDI sources are coupled to time of flight (TOF) mass spectrometers. The ability then to produce multiply charged ions would significantly extend the observable mass range. The generation of ions with high charge states is a trait that is typically reserved for ESI, however there has been some investigation into the ability to generate multiply charged ions by AP-MALDI. König et al. presented AP IR-MALDI of myoglobin from an acidified aqueous droplet (mixed with glycerol) that produced charge states up to 13+.[182] The authors commented that the mechanism of ion generation is likely a cross between ESI and MALDI because a voltage was applied to the sample plate which could likely results in the desorption of charged droplets. Similar observations from other groups support these findings.[91,183-185] Trimpin et al. has shown that multiply charged proteins can be generated by AP-MALDI from crystalline samples by using a field free approach and increasing the temperature of the AP interface inlet.[158] The potential applied to the target was shown to greatly influence the charge state

as when no potential was applied multiply charged ions were observed but when the target potential was present, primarily singly charged ions were observed.[186] While these observations are exciting, the mechanisms underlying the production of multiply charged ions from solid matrix preparations in AP-MALDI have yet to be determined.

A majority of this section has been dedicated to AP-MALDI techniques primarily because AP-LDI techniques are much less frequently observed in the literature. Most of the instrumental improvements that have been realized for AP-MALDI would also be transferable to AP-LDI as the primary distinction between the two is the lack of an energy absorbing matrix in the latter. Despite this, there have been a few instances using AP-LDI to analyze carbonaceous material.[187,188] AP laser desorption and ionization from porous silicon (AP-DIOS) was introduced by Laiko et al. in 2002 and uses a commercial AP-MALDI source with a DIOS plate.[189] It is difficult to classify this technique as either AP-MALDI or AP-LDI since the energy of the laser is absorbed by the substrate and is transferred to the sample to facilitate desorption and ionization. One of the benefits of this method is the absence of matrix interferences that are typically observed in MALDI techniques, however, the technique appears to be useful only for compounds with high proton affinity.[190]

1.2.2.2 Application of AP-LDI and AP-MALDI to MSI

AP-MALDI and AP-LDI have been utilized on several occasions for MSI. The benefits of these techniques over their vacuum counterparts are mainly attributed to

the general advantages common to all AP ionization sources. The common MALDI MSI approach requires that the sample be transferred to the vacuum which can inhibit the analysis of volatile compounds as well as restrict the practical sample size.

One of the first examples of AP-MALDI MSI was presented by Li et al.[139] In this work an IR laser was used to map the abundance of substance p from a mock sample. Using oversampling, the lateral resolution was estimated to be 40 μm by using an electron microscopy calibration grid as a mask over a homogeneous surface of the dye toluidine blue. Using the endogenous water from fruit samples as the laser energy absorbing matrix, the authors used AP IR-MALDI to directly profile several fruits and presented imaging of the skin of a strawberry. To avoid oversampling in this imaging experiment it was required that a lateral resolution of 200 μm be used. Crude ion images of sucrose, fructose, and citric acid were correlated with the skin tissue where signal was absent around the seeds. This analysis serves as proof of principle for AP IR-MALDI MSI as well as the use of endogenous water as a matrix for MSI. A similar setup was later used by the same group to image a white lily flower petal (200 μm lateral resolution) where ion maps of several metabolites were suggested to correlate with the petal's vasculature.[191] The letters 'IR' drawn on a mock target with a pencil were also imaged (125 μm lateral resolution) using this technique and ion maps relating to a sodiated disaccharide correlated with the lettering.[192]

Transmission geometry AP-MALDI has been used to image coronal sections of mouse brain in negative ion mode.[193] While the spot size of the laser was determined to be 20 μm from the ablation craters and the line spacing was reported as 100 μm, the distance between adjacent pixels was not mentioned. Several ions, that were suggested to be lipids, showed spatial distributions that correlated well with the large features of the brain tissue. A similar source coupled to an Thermo Orbitrap Exactive was used to image (30 μm lateral resolution) brain and kidney tissue sections from a rat that had been dosed with hydroxychloroquine.[194] Several lipid ions were shown to be localized in the white matter or gray matter of the brain. Analysis of a delipidated brain section resulted in the observation of a tissue-related multiply charged ion correlating to a 6+ charge state of a 4961 Da small protein (**Figure 1.8**). The imaging of the kidney tissue produced ion maps of the dosed drug as well as two of its metabolites.

Sroyraya et al. used an AP MALDI source to image the eyestalk of the blue swimming crab and several lipids were found to be uniquely distributed within the compartments of the tissue that correlated with the hematoxylin and eosin stained tissue.[195] This same source was used to determine the spatial distribution of phospholipids in the retina of salamander.[196]

Over the past several years, Spengler's group has consistently pushed the boundaries of spatial resolution and mass resolution in MSI.[115] The benefits of high resolving power mass spectrometry for MSI analyses are observed in the accurate mass measurements and the ability to distinguish isobaric species. In 2008,

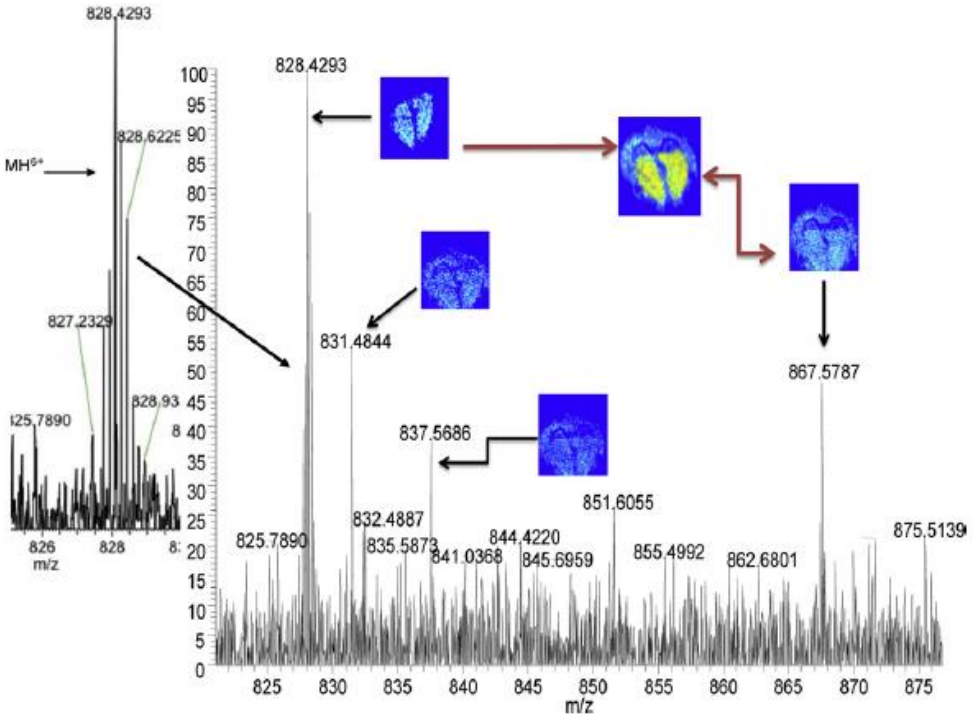

Figure 1.8 Transmission geometry AP-MALDI of rat brain tissue sections showing the distribution of the 6+ charge state of a small protein. Adapted from (A.F. Harron, K. Hoang, C.N. McEwen, Int. J. Mass Spectrom., 352, 65-69 (2013)) with permission from Elsevier.

Koestler et al. reported on a scanning microprobe MALDI source that could be used at AP or intermediate pressure.[197] This source was coupled to an LTQ-FT instrument and synchronization between the pulsing of the laser and ion accumulation provided the ability to obtain a single pulse and a single acquisition per pixel. AP-LDI MSI was performed at 7.5 µm lateral resolution on a marking from a felt tip pen covered by a metallic microgrid. Ions relating to the dye ions from the pen ink corresponded well with the optical image. AP-MALDI MSI was performed using a microgrid to mask a dried droplet preparation of bradykinin and angiotensin

with 8 μm lateral resolution. Ions were analyzed either with the ion trap or the FT-ICR. Both acquisitions resulted in ion images that correlated with the optical image however the FT images were of lower quality due to the higher limit of detection in the FT compared to the ion trap. The same group later published on a detailed characterization of their laser properties and provided implications for high resolution imaging.[198]

Römpp et al. demonstrated AP-MALDI MSI based histology on tissue sections at a spatial resolution of 5 μm.[199] At this spatial resolution, clear distinction of histological features of the tissue can be realized. Ion maps from endogenous species including lipids and neuropeptides produced distributions that were highly correlated with the optical images of the tissue. Römpp et al. has also shown the utility of high spatial resolution imaging in determining the distribution of the anticancer drug imatinib in mouse kidney tissue sections.[200] Preliminary analyses at 35 μm resolution (**Figure 1.9a**) provide the general distribution of the drug in the tissue. Subsequent analyses on targeted areas at higher spatial resolution (5 μm) demonstrate the distribution on a cellular level (**Figure 1.9b**). In addition, this paper also presented an even broader analysis (200 μm lateral resolution) of a portion of a whole body section of a mouse demonstrating the capability to determine drug localization within particular organs.

Keeping with the trend of high resolution AP-MALDI MSI, Guenther et al. published on the imaging of neuropeptides from tissue with a spatial resolution of 5 μm.[201] Distributions of several peptides were demonstrated to be localized in the

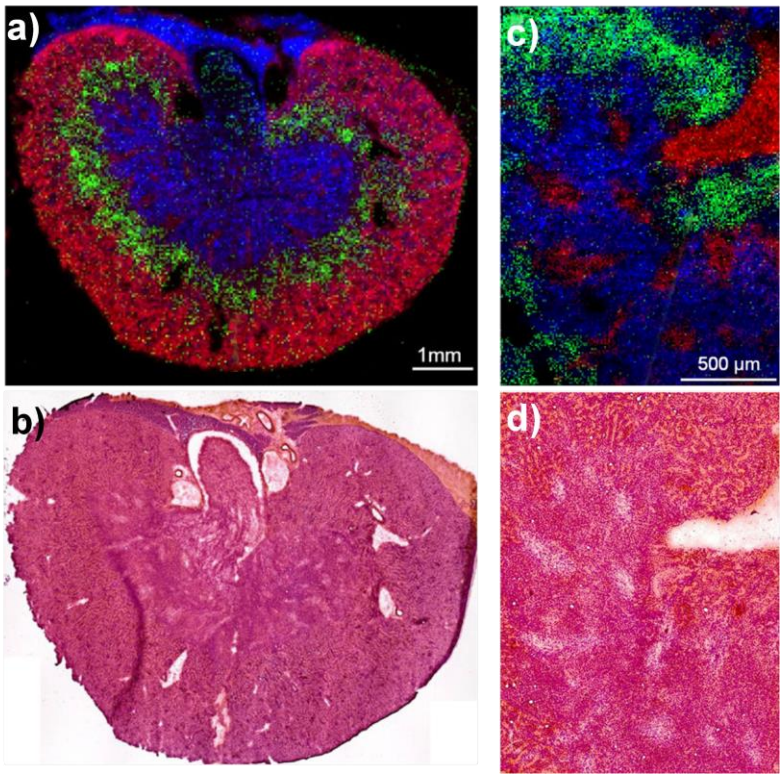

Figure 1.9 a) Overlay of ion maps from AP-MALDI MSI at a spatial resolution of 35 µm: *red,* $[PC(32:0)+K]^+$; g*reen*, imatinib $[M+H]^+$; and *blue* $[PC(34:1)+H]^+$. **b)** Optical image of H&E stained kidney tissue section after MS imaging. **c)** Overlay of ion maps from AP-MALDI MSI at a spatial resolution of 10 µm: *red,* $[heme\ b]^+$; g*reen*, imatinib $[M+H]^+$; and *blue* $[PC(38:5)+K]^+$. **b)** Optical image of H&E stained kidney tissue section after MS imaging. Adapted from (A. Römpp, S. Guenther, Z. Takats, B. Spengler, Anal. Bioanal. Chem., 401, 65-73 (2011)) with kind permission from Springer Science and Business Media.

intermediate or posterior lobe of the pituitary gland. On tissue MS/MS experiments were used to help improve the confidence of peptide identification. In addition, an MS/MS imaging experiment was performed and the colocalization of all of the product ion images with the parent ion image even further validated the identification of that peptide ion.

High resolution imaging of tryptic peptides directly from tissue using AP-MALDI MSI was shown by Schober et al.[202] Mouse brain tissue sections were sprayed with trypsin and incubated to allow for digestion. MSI was then performed at a spatial resolution of 50 µm. Ion maps of several tryptic peptides of myelin basic protein showed spatial distributions that highly correlated with the histological features of a myelin stained mouse brain (**Figure 1.10a**). Schober et al. has also performed single cell AP-MALDI MSI on HeLa cells at 7 µm resolution (**Figure 1.10b**).[203] It was also demonstrated that both high mass resolving power and imaging resolution were required to fully resolve the single cells.

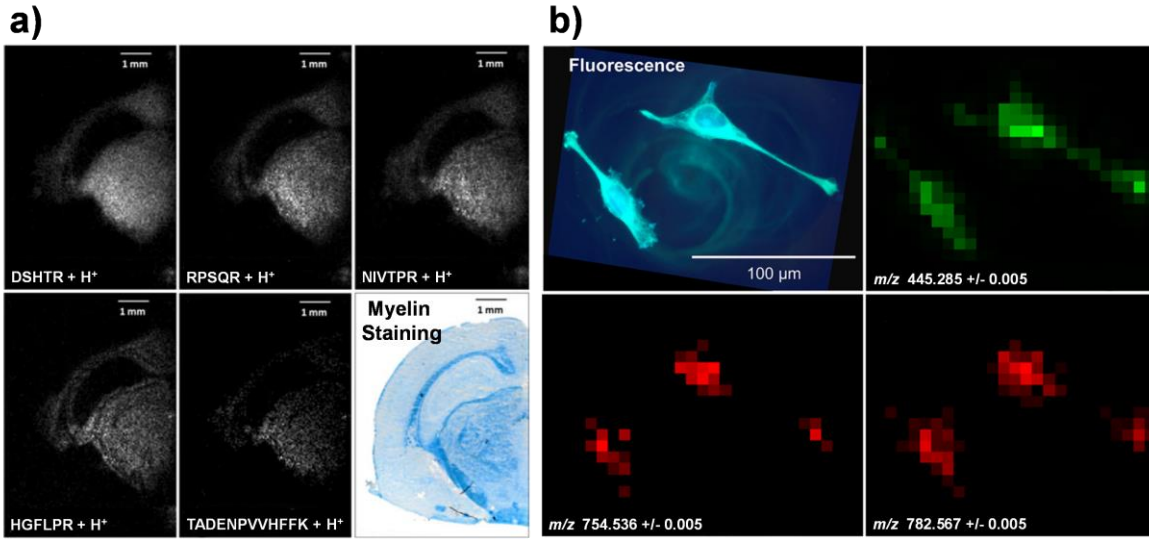

Figure 1.10 **a)** Ion maps of several tryptic peptides of myelin basic protein observed from brain tissue including a myelin stained brain section. Adapted with permission from (Y. Schober, S. Guenther, B. Spengler, A. Römpp, Rapid Commun. Mass Spectrom., 26, 1141-1146 (2012)). Copyright © (2012) JohnWiley & Sons, Ltd. **b)** AP-MALDI MSI of single cells. Adapted with permission from (Y. Schober, S. Guenther, B. Spengler, A. Römpp, Anal. Chem., 84, 6293-6297 (2012)). Copyright (2012) American Chemical Society.

Most recently, Römpp et al. reported on an AP IR-MALDI technique that utilized ice as the matrix.[204] A liquid cooled Peltier stage was used to freeze the tissue and the cold temperature was maintained throughout the imaging experiment. Imaging at spatial resolutions as low as 25 μm was able to produce ion maps from phospholipids that corresponded to features in the brain tissue. The primary benefit of this technique is the use of water as a matrix which removes the reliance on the matrix application step as well as eliminates matrix-related background signal.

There have been only several publications in the literature that utilize AP-LDI for MSI. Once such application has already been discussed, where Koestler et al. used AP-LDI of a marking from a felt tip pen to demonstrate the imaging capabilities of their source design.[197] Bradshaw et al. combined AP-LDI with atomic force microscopy (AFM) to obtain chemical and topographical images of a mock sample.[205] Using oversampling, a spatial resolution of roughly 2 μm was demonstrated for the MSI technique which was suggested to be limited by the detection limit of the mass spectrometer rather than the physical limit. The resulting ion image was found to correlate well with the topographical image (**Figure 1.11**).

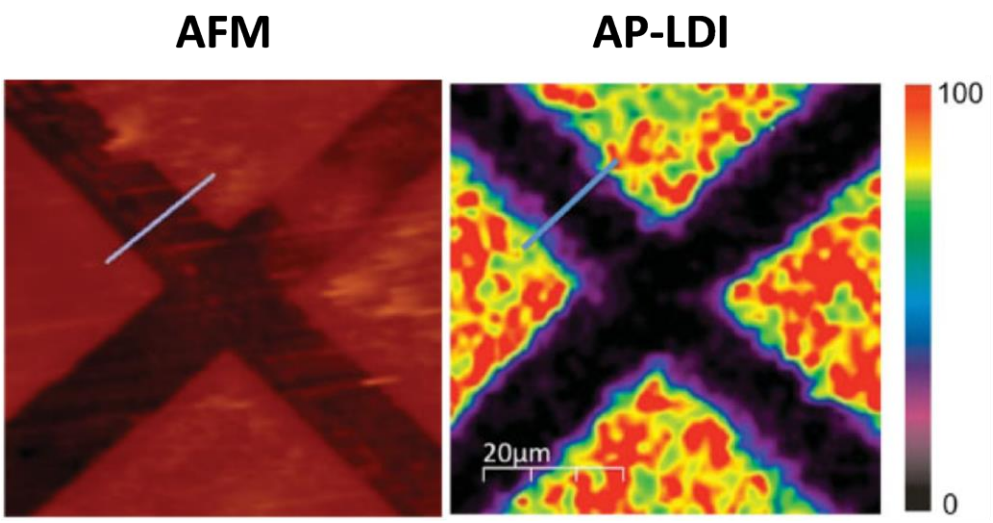

Figure 1.11 Comparison of atomic force microscopy topography image with the ion image from AP-LDI of ablation marks in a rhodamine 6G coating. Adapted with permission from (J.A. Bradshaw, O.S. Ovchinnikova, K.A. Meyer, D.E. Goeringer, Rapid Commun. Mass Spectrom., 23, 3781-3786 (2009)). Copyright © (2009) JohnWiley & Sons, Ltd.

The AP-MALDI source used by Sroyraya et al. was used for AP-LDI imaging of sections of ginger rhizome in both positive and negative ion modes.[206] Features from the tissue were found to align with ion images from both polarities. AP-LDI MSI capabilities have also been demonstrated by Coello et al. using a femtosecond laser to image onion epidermal cells with a spatial resolution of 10 µm.[207] Several plant metabolites were observed and glucose was noted to have a spatial distribution that agreed well with the optical image.

1.2.3 Desorption Electrospray Ionization (DESI)

1.2.3.1 Introduction to DESI

DESI was first introduced by Takats et al.[208] To date, DESI is by far the most studied and most mature technique among all the atmospheric ionization sources. In a typical DESI setup (see **Figure 1.12**), charged droplets are generated using a pneumatically assisted electrospray emitter aimed directly at the surface to be analyzed. Upon interacting with charged droplets and/or gas phase ions hitting the surface with high kinetic energy, secondary charged analyte ions are generated and captured by the inlet of the mass spectrometer instrument. Few ion formation mechanisms have been proposed for DESI, and depend on the source parameters and the analyte.[209,210] The main ion formation pathway has been described as the *droplet pick-up* mechanism where stream of electrospray droplets initially wet and dissolve analyte molecule at the surface. Later collisions of charged primary

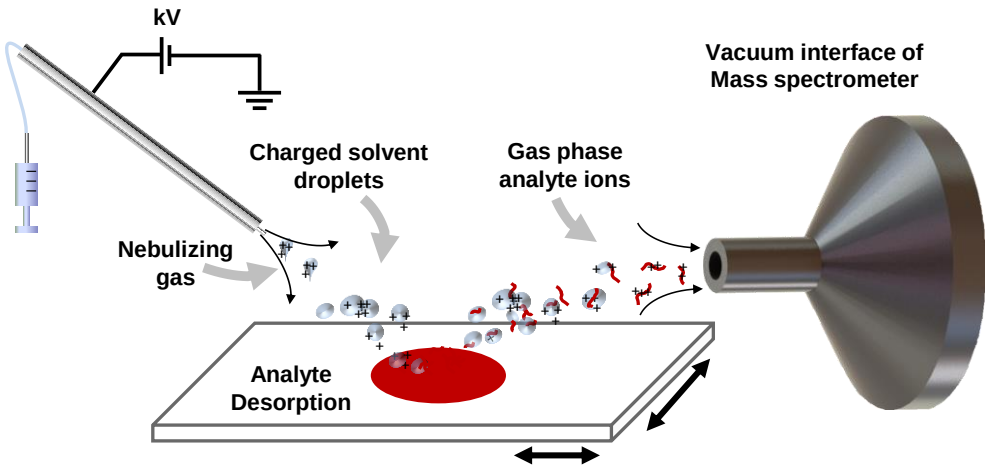

Figure 1.12 DESI experimental setup.

droplets create a splashing effect during which secondary charged droplets containing analyte molecules are ejected. Those charged secondary droplets then undergo an ESI-like desorption/ionization processes, leading to the formation of gas phase analyte ions that are eventually captured by the mass spectrometer inlet tube. This mechanism explains the similarity between the DESI and ESI spectra for some analyte such analyte as peptides or proteins.[210]

The second ion formation mechanism that has been proposed is known as *chemical sputtering*,[211] where desolvated gas phase ions from the primary electrospray plume collide with the surface, ionizing analyte molecules through proton, electron or ion transfer. Charged analyte ions with enough momentum will eventually be ejected from the surface, and captured by the mass spectrometer inlet. Finally the third proposed ionization mechanism involves charge transfer or ion-neutral reactions occurring in the gas phase between desorbed analyte neutrals and gas phase ions generated by ESI. It is more likely that all previously described ionization mechanisms occur simultaneously in DESI, but that some are more predominant depending of the analyte and source parameters. By carefully adjusting the DESI parameters, one can therefore favor the ionization of a specific group of analyte.[129]

Since droplet pickup of analyte molecules followed by ESI-like desorption/ionization of secondary droplets is recognized as the main mechanism leading to the formation of DESI ions, significant effort has been done to better understand the fundamentals of this mechanism. A Phase Doppler Particle Analysis

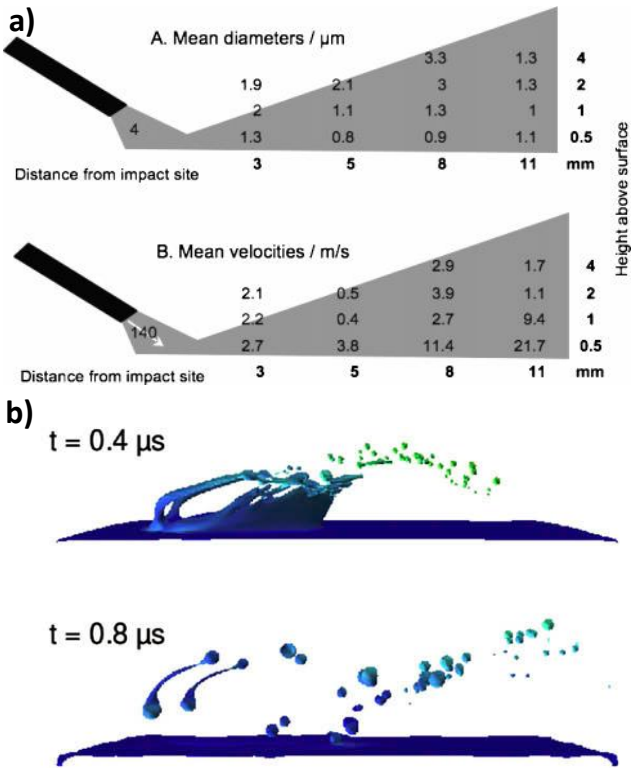

Figure 1.13 **a)** Mean diameters and velocities of DESI droplets measured by Phase Doppler Anemometry and **b)** fluid dynamics simulations of splash for 120 m/s droplet (3.7 µm diameter) impacting wet surface. **a)** Adapted with permission from (A. Venter, P.E. Sojka, R.G. Cooks, Anal. Chem., 78, 8549-8555 (2006)). Copyright (2006) American Chemical Society. **b)** Adapted from (A.B. Costa, R. Graham Cooks, Simulated splashes: Elucidating the mechanism of desorption electrospray ionization mass spectrometry, Chem. Phys. Lett., 464, 1-8 (2008)) with permission from Elsevier.

(PDPA) system was used to investigate the effect of several DESI parameters on the size and velocity of the primary droplets emitted from the ESI emitter and the secondary droplets leaving the surface.[212] Under typical optimal DESI conditions for the analysis of biomolecules, ESI droplets were found to impinge the surface at an average velocity of 120 m/s and have average diameters of 2-4 µm. The kinetic energy resulting from the impact of those droplet with the surface was found to be

relatively low (0.6 meV/droplet), in accordance with the observation that DESI is a soft desorption/ionization technique. Size and velocity of secondary droplets found during those PDPA experiments were also evaluated and later used to build and validate a 2D[213] and later a 3D[214] computational fluid dynamics simulation of the splashing (the effect those results can be seen in **Figure 1.13**). It was then successfully demonstrated using this model that hydrodynamic force/momentum transfer of the primary droplets on a wetted surface was sufficient to create the secondary droplets that are observed experimentally.

Moreover, by comparing the survival yield of thermometer ions, it was also shown that internal energy distribution of ions produced by ESI and DESI was nearly identical,[215] supporting the hypothesis that charged analyte from secondary droplet are formed via similar processes.

Even if DESI is in appearance a relatively simple ionization technique, the list of source parameters that can potentially affect the sensitivity of the source is quite long. The effect of ESI flow, voltage and mass spectrometer inlet capillary temperature on signal intensity has been widely discussed,[216,217] as well as optimization of solvent[218] and geometry.[210,216,219-222]

Adding even more complexity, an optimized combination of parameters that is found to be optimal for one group of analyte might differ for another group[210] as shown in **Figure 1.14**. Because of this strong dependence of signal intensity on source parameters, most commercially available DESI sources are designed so that those parameters can be easily tuned (e.g. adjustable positioners).

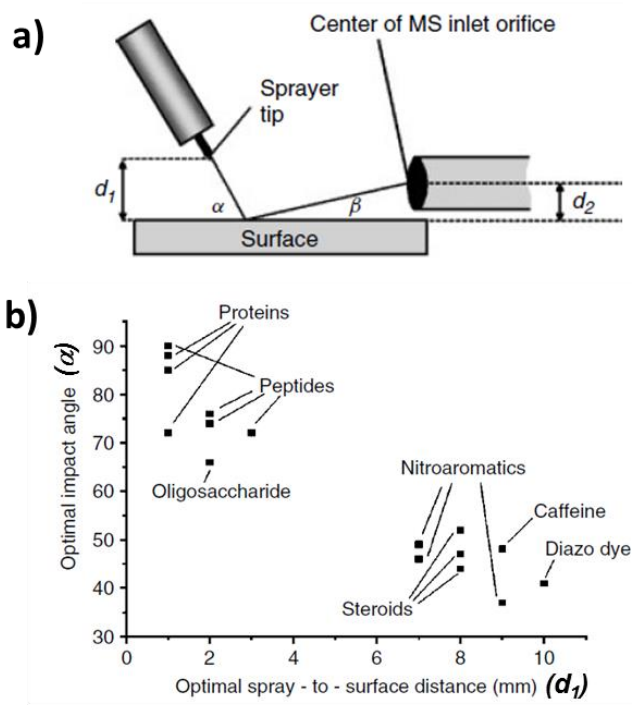

Figure 1.14 **a)** Common DESI parameters and **b)** Optimized impact angle and spray-to-surface distance for several compounds. Adapted with permission from (Z. Takats, J.M. Wiseman, R.G. Cooks, J. Mass Spectrom., 40, 1261-1275 (2005)). Copyright © (2005) JohnWiley & Sons, Ltd.

Some also proposed a geometry independent DESI configuration where both the ESI emitter and the MS inlet are placed normal to the surface and enclosed in a pressure tight enclosure.[223] Mass spectra similar to conventional DESI were reported using this technique, with the added advantage of preventing toxic compounds from being released in the ambient while interrogating the sample. Transmission mode DESI (TM-DESI)[224,225] was also proposed as another simplified, geometry independent DESI configuration, where electrospray is placed directly in front of the MS inlet and transmitting through a mesh on which the analyte is deposited.

The sensitivity of DESI was also investigated and fluorescence spectroscopy used to quantify the amount of analyte consumed during a DESI experiment. It was found that only low attomole amount of rhodamine 6G was necessary to generate a mass spectrum.[226]

Chemical reagents can also be added to the DESI solvent to allow certain reactions with analyte molecules at the surface or in the droplet during the ESI-like desorption process. This technique, called reactive DESI, has been used to improve sensitivity for the detection of cis-Diol,[227] chemical warfare,[228] explosives[209,229] and cholesterol.[230] Reactive DESI was also used to promote the formation of specific non-covalent complexes in counterfeit malarial drugs and improve detection efficiency.[231] 7M ammonium acetate has also been used as ESI solvent additive to reduce the formation of salt adducts and improve sensitivity of DESI under specific conditions.[232]

DESI can be connected to any mass spectrometer instrument with an atmospheric pressure interface. In DESI, ions are generated continuously, compared to pulse laser method that emit packets of ions following each ablation event only such as the laser based desorption techniques. Continuous ion sources are in general easier to integrate with existing mass spectrometers, especially instruments with ion injection that are discrete in time such as LTQ and FT technology based instruments.

1.2.3.2 Application of DESI to MSI

Spatially resolved DESI was demonstrated in the very first DESI article when probe was scanned over the stem section of a poison hemlock plant and abundance of coniceine ion vs distance was reported.[208] The first accounts of using DESI to spatially resolve analyte on a surface was later achieved by coupling thin layer chromatography (TLC) separation with DESI. Dye mixtures separated by TLC were then spatially resolved in 1D by scanning the DESI spot directly on a TLC plate.[233] Application of DESI for 1D profiling of biological tissue was also reported shortly after where changes in sphingomyelin distribution between cancerous and non-cancerous tissue could be detected[234] as shown in **Figure 1.15**.

Computer controlled systems were eventually implemented so that the DESI probe can be used to perform the very first 2D imaging experiments, first using compound mixture eluted on TLC plates,[235] then on biological tissues where several lipids could be identified from coronal brain sections.[236]

Optimization of DESI source parameters was also addressed during these early imaging experiments and it was observed that signal intensity is not the only figure of merit to take into account when optimizing source parameters for DESI imaging. Indeed, scan rate will, in addition to all previously mentioned parameters, not only affect sensitivity but also the spot-to-spot repeatability, the DESI spot size, and the width of each scan line.[237] Those figures of merit are extremely important as they eventually determine the quality and spatial resolution that can be achieved in a mass spectrometry imaging experiment. As it is the case with most of the MS

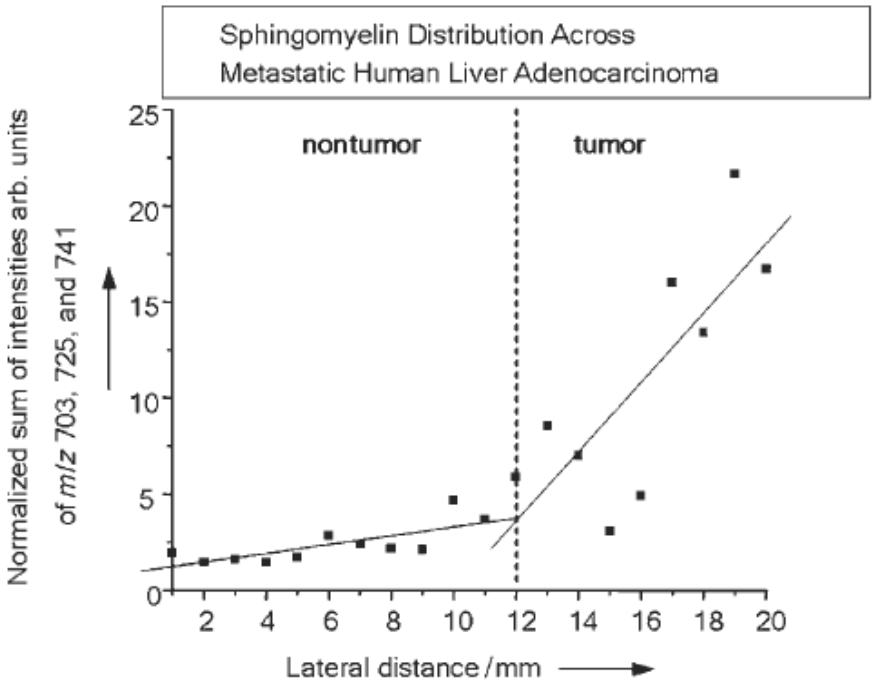

Figure 1.15 Direct tissue profiling of human liver adenocarcinoma using DESI in the positive-ion mode. Ion-intensity distribution of the sum of the m/z values 703, 725, and 741 which correspond to the protonated, sodium, and potassium forms of sphingomyelin (16:0). Adapted with permission from (L.S. Eberlin, D.R. Ifa, C. Wu, R.G. Cooks, Angew. Chem. Int. Ed., 49, 873-876 (2010)). Copyright © (2010) JohnWiley & Sons, Ltd.

imaging techniques, spatial resolution can be improved by reducing the spot size or the line width but it is often at the cost of a reduction in signal intensity. First imaging experiments were achieved with a spatial resolution of 150 μm on glass,[238] 200-250 μm on paper,[239] and about and about 400-500 μm on hydrophobic TLC plates[235] or biological tissue.[239] In all of those experiments, spatial resolution is defined as the smallest feature that can be resolved in the molecular image.

By carefully optimizing DESI source parameters and using a closed loop control system to maintain the distance between the DESI probe tip and the surface,[219] Kertesz and coworkers were able to achieve spatial resolution in the 40-50 μm range on TLC plates.[240,241] Improving spatial resolution on biological tissue was found to be more challenging due the fact that the DESI probe tended to damage the tissue surface. Indeed, under certain conditions, solubilization of extracellular matrix by the action of conventional DESI solvent weakens the tissue structure and makes it more susceptible to be damaged by the high velocity droplets impinging the surface. To minimize the tissue damage during DESI MS interrogation, *morphologically friendly* solvents were proposed, that allow the DESI extraction of analyte molecules of interest while preserving the integrity of the tissue. Rather than using the typical aqueous solutions of MeOH, EtOH or ACN, solvents that are N,N-dimethylformamide (DMF) based were proposed.[242] Using a DMF/EtOH (1:2) morphologically friendly solvent solution, a spatial resolution in the order of 35 μm was demonstrated.[243] Techniques to perform DESI imaging experiments in positive- and negative- ion mode on same tissue were also explored.[244]

1.2.3.2.1 DESI Imaging of Biological Tissue

Soon after reporting the first 1D profiling and spatially resolved DESI analysis of tissue,[234] Wiseman et al. achieved the first DESI (2D) imaging experiment of biological tissues, where distributions of several lipids were determined on the

coronal tissue section of a rat brain in negative ion mode with a spatial resolution of less than 500 μm.[236]

Because of the high ionization efficiency of certain lipid classes, many DESI MS imaging experiments are specifically targeted at lipid distribution in biological tissue.[245] Early DESI experiments effectively took advantage of this efficient lipid detection and successfully used DESI imaging to detect lipids in dog bladder tissue,[246] human blood vessels,[247] and lens.[248]

It was also demonstrated that changes in lipid intensity can be used to successfully differentiate injured spinal cord from healthy controls. During those same experiments, reactive DESI was also used to improve the detection of malondialdehyde by adding dinitrophenylhydrazine to the ESI solvent, also enabling the differentiation of injured specimen from healthy ones.[249]

Thorough investigation of the effect of handling and storage conditions of tissue sections prior to performing DESI imaging revealed that elapsed time between animal sacrifice and flash freezing had little effect on lipid distribution and overall signal intensity. The same conclusion was drawn regarding the tissue thickness and the storage time at -80°C. It was actually found that lipid profiles and intensity would only be impacted significantly if tissue was subjected to extreme and abnormal treatments such as long exposure to 50°C temperature or multiple freeze/thaw cycles.[250]

A 3D model of the mouse brain was also constructed using lipid distributions detected by DESI MS imaging on 36 coronal sections. Correlation could be made

between the distribution of some lipid molecules and the substructure of the brain as shown in **Figure 1.16a**.[251]

DESI imaging has also been coupled to 2D high performance TLC (HPTLC) to characterize complex mixture of lipids eluted directly from rat brain tissue[252] or from lipid extracts.[253] Separating in space the lipid mixture on the HPTLC plate (based on lipid classes) can be used to reduce the ion suppression and improve the detection of less abundant lipids. Reactive DESI was also used and betaine aldehyde added to the electrospray solvent during experiments performed on

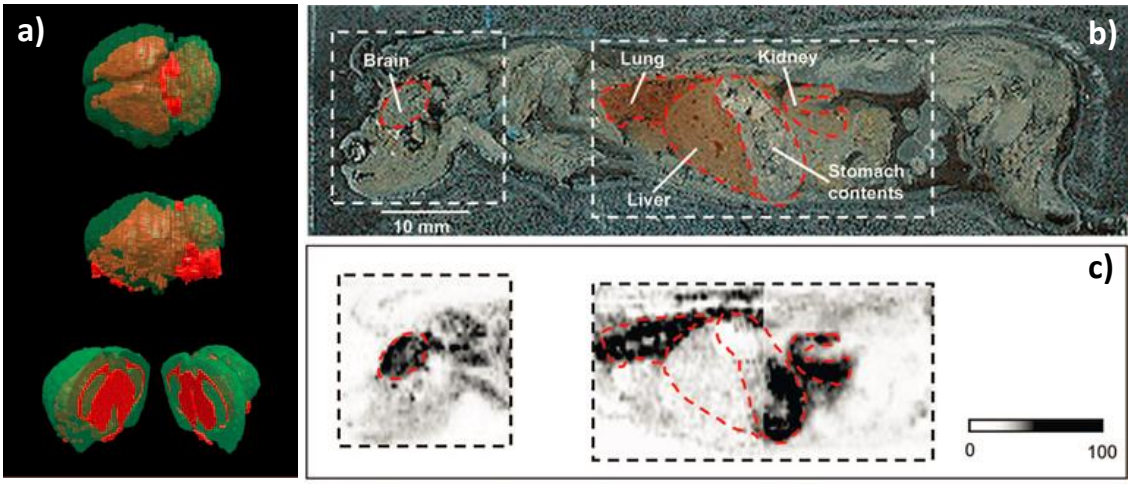

Figure 1.16 a) 3D visualization of DESI MS imaging. The transparent overlaid distribution of lipids outline substructure of mouse brain. Adapted with permission from (L.S. Eberlin, D.R. Ifa, C. Wu, R.G. Cooks, Angew. Chem. Int. Ed., 49, 873-876 (2010)). Copyright © (2010) JohnWiley & Sons, Ltd. **b)** Optical image of a 40 μm thick sagittal section of WB tissue wised with propanonol (7.5 mg/kg). **c)** Distribution of propanonol measured by DESI MS/MS (SRM: m/z 260→116) showing drug distribution in different organs. Adapted with permission from (V. Kertesz, G.J. Van Berkel, M. Vavrek, K.A. Koeplinger, B.B. Schneider, T.R. Covey, Anal. Chem., 80, 5168-5177 (2008)). Copyright (2008) American Chemical Society.

porcine brain extracts to derivatize cholesterol in compounds that can be detected more easily by DESI on the HPTLC plate surface after separation.[253]

In recent experiments, imaging DESI was used to characterize lipid distributions in mouse and bovine embryo/oocyte.[254,255] Lipid profiling using DESI MS has also been use to as a diagnostic method in human cancer research and applied to prostate tissue,[256] kidney,[257] bladder,[258] and brain.[259-261] DESI MS imaging was also used on tumor tissues obtained from surgeries (5 patients). Using a support vector machine (SVM) classification model, diagnostics regarding tumor type (meningioma and glioma), subtype, grade, and cell concentration could be established and correlated with histopathology analysis.[262] These promising results open the door to the development of devices using ambient mass spectrometry to perform real time diagnostic during surgery.

More complete data analysis framework combining mass spectrometry imaging data and co-registered histology images have also been proposed to detect region-specific lipid signature of cancerous cellular regions in tissue. Such workflow has been successfully applied to colorectal cancer tissues using DESI MS imaging data.[263]

In addition to being used for lipid detection, DESI imaging has also been used for the detection of drugs and smaller metabolites. The first account of using DESI-MS imaging for the detection of drugs and metabolites was reported my Wiseman et al, where imaging of tissue harvested from a rat dosed with 50 mg/kg of the antipsychotic drug clozapine was performed.[264] Clozapine was successfully

detected in several organs and good correlation of concentration between LCMS/MS data and DESI MS imaging data was demonstrated. The presence of the N-desmethyl metabolite was also detected in the lung tissue during these experiments. Quantitation of clozapine in rat brain was recently revisited using internal standard spotted atop of tissue to generate calibration curves, enabling quantitative measurement of the amount of drug detected (q-DESI). Concentration results found were cross-validated using LC MS/MS and quantification by [^{14}C]clozapine by extraction scintillation counting.[265]

Drug detection on whole-body (WB) thin tissue sections was also demonstrated in mice that were intravenously dosed with propranolol as shown in **Figure 1.16b-c**. Drug abundance detected by DESI MS/MS imaging and whole-body autoradiography (WBA) were found to corroborate each other.[266] WB DESI MS imaging experiments were also performed on neonate mice drugged with clozapine and three other proprietary drug compounds.[267] Other WB imaging experiments were performed on drug dosed adult rat using an Air Flow-Assisted (AFA)-DESI.[268]

1.2.3.2.2 DESI Imaging for Forensic Applications

The potential of using DESI MS technique for forensic analysis application has been recognized as early as the very first DESI publication.[208] DESI MS has effectively been applied since then to several areas of forensic science such as the detection or identification of explosive, chemical warfare agents, gunshot residue,

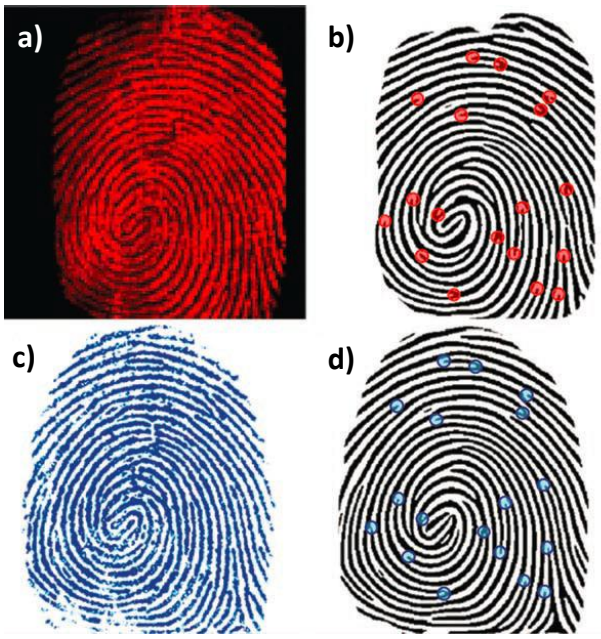

Figure 1.17 a) DESI image of fingerprint on glass showing distribution of cocaine ion with a spatial resolution of 150 μm. **b)** Image processed by fingerprint recognition software showing minutiae that were automatically detected. **c)** Scan image of ink fingerprint blotted on paper. **d)** Processed image showing the same minutiae detected using the DESI imaging data. Adapted from (D.R. Ifa, N.E. Manicke, A.L. Dill, R.G. Cooks, Science, 321, 805-805 (2008)) with permission from AAAS.

and illicit drugs. Forensic application of DESI MS was actually the sole topic of a recent review article.[269] So far, the DESI MS technique has been used mainly as a direct sample analysis tool and very few accounts of DESI MS imaging for forensic application have been reported.

DESI MS imaging was first reported for forensic dye analysis and exposing forged documents.[270] Imaging of fingerprints of cocaine residue on glass was also achieved with a spatial resolution of 150 μm, giving additional orthogonal information that can be used to identify a suspect.[238] The quality of those fingerprint ion images

was sufficient to be used as input for a fingerprint recognition software and minutiae that were automatically identified were similar to those detected using ink fingerprints blotted on paper (see **Figure 1.17**). It was shown that DESI MS imaging could be performed on fingerprints using polymers or additive molecules found in lubricated condoms and eventually be used to provide circumstantial evidence linking a suspect to a crime scene.[271] DESI MS imaging technique has also been used for the detection of counterfeit malarial drug tablets.[272]

1.2.3.2.3 DESI of Plants and Other Natural Products

Mass spectrometry imaging of plants alone has been the topic of several reviews.[273,274] The first account of using DESI MS for the imaging of biological molecules on the surface of natural products was reported by Lane et al.[275,276] They then used DESI imaging to show that bromophycolides, an antifungal chemical, was distributed heterogeneously on the surface of tropical seaweed (*C. serratus*) and found it to be more abundant on distinct, light colored, damaged area the surface as shown in **Figure 1.18a-b**. Additional experiments on seaweed species have also been performed to confirm the presence of neurymenolide-A by DESI MS imaging, an antibacterial metabolite known to cause chemical erosion to coral reefs.[277]

Direct DESI imaging of plants, leaves and flowers can be challenging due to the absorbance of the sample surface or the difficulty to penetrate the plant cuticle which can eventually lead to low and/or unstable DESI signal. Two research groups independently proposed imprinting the sample on a microporous PTFE

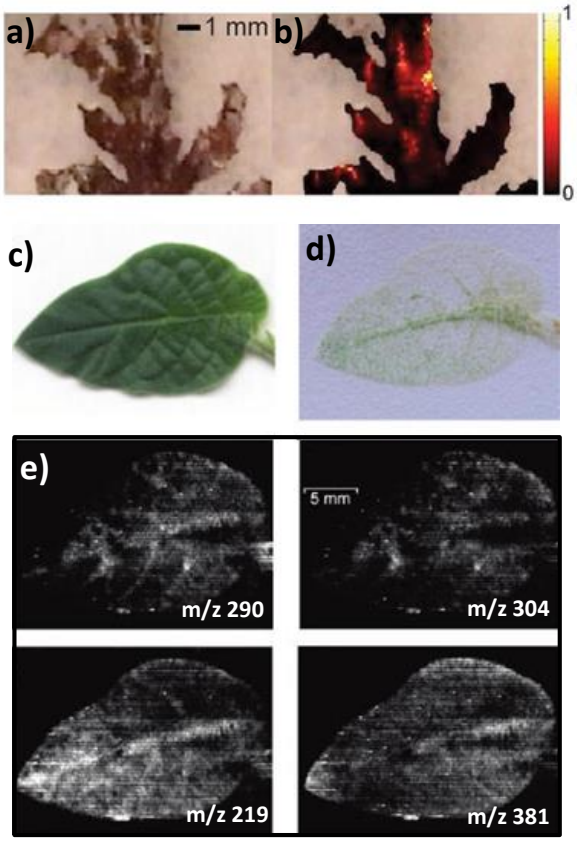

Figure 1.18 **a)** Optical image of the surface of a tropical seaweed plant (*C. serratus)* showing blanched regions and **b)** direct DESI MS image of antifungal bromophycolide A/B ions colocalized with those light colored patches. Adapted from (A.L. Lane, L. Nyadong, A.S. Galhena, T.L. Shearer, E.P. Stout, R.M. Parry, M. Kwasnik, M.D. Wang, M.E. Hay, F.M. Fernandez, Proc. Natl. Acad. Sci. U.S.A., 106, 7314-7319 (2009)) with permission from Proceedings of the National Academy of Sciences USA. Optical images of a **c)** *Datura stramonium* leaf and **d)** its imprint on a Teflon plate. **e)** Indirect DESI MS imaging of imprint showing the distribution of different analyte molecules. Adapted with permission from (J. Thunig, S.H. Hansen, C. Janfelt, Anal. Chem., 83, 3256-3259 (2011)). Copyright (2011) American Chemical Society.

surface,[278,279] a substrate known to be more suitable for DESI analysis.[280] The effect of using the imprint method ranged from significant improvement in signal intensity and stability to literally enabling DESI imaging for cases where no significant signal

could be obtained using standard DESI extraction (e.g. *Datura stramonium*) as shown in **Figure 1.18c-e**.[278] PTFE imprinting techniques were also used to improve detection and DESI MS imaging of non-fluorescent chlorophyll catabolites, a product of the chlorophyll degradation process in plant leaves.[279] Further characterization of the imprint method on porous PTFE was performed on barley leaves, where hydroxynitrile glucosides, a compound located in the leaf epidermis could be imaged using the imprint method on intact leaves as well as using the direct DESI MS method on stripped off epidermis in the first account of direct DESI imaging on plant tissues.[281] DESI MS imaging of plant imprints performed on substrates other than PTFE, such as paper or TLC plates, was also demonstrated.[282-284]

In recent work by Li et al., the metabolite distribution and enzymatic activities on wounded plants was investigated using indirect DESI MS.[285] Also, the direct method for DESI MS imaging of plant leaves was revisited, using a tertiary spray solution of chloroform to remove the cuticular wax layer. This allowed the molecular imaging of metabolites phloroglicinol to be performed directly from the glands of *Hypericum perforatum,* without using the imprint technique.[286] Prebiotic reactions have also been investigated on mineral surfaces.[287]

1.2.4 Resonant (MALDESI) and Off-resonance (ELDI) Laser Desorption with Electrospray Ionization

1.2.4.1 Introduction to ELDI and MALDESI

The interaction of a plume of neutral molecules[98,288-295] or neutral droplets[296-300] with the charged solvent droplets of an electrospray plume to induce ionization has been an area of investigation for some time. However, the union of a neutral plume produced by laser desorption with electrospray ionization presents inherent benefits including the ability to generate ions from a specific spatial location which is a prerequisite for mass spectrometry imaging. There have been several similar techniques described in the literature that combine atmospheric pressure laser desorption with electrospray post-ionization.[84,85,90,99,301-303] These ionization sources can be further classified into two main categories: (1) off-resonance techniques where the laser energy is primarily absorbed by the analyte leading to sample vaporization[84,301,303] and (2) resonant techniques where the laser energy is resonantly absorbed by a matrix leading to the ejection of a large volume of material. This classification is similar in theory to the distinction between laser desorption ionization (LDI) and matrix-assisted laser desorption ionization (MALDI). **Figure 1.19** provides a general schematic of both resonant and non-resonant laser desorption with electrospray post-ionization.

The working principle of laser desorption with electrospray post-ionization was first demonstrated with the off-resonance technique electrospray-assisted laser desorption ionization (ELDI) which was introduced in 2005 by Shiea et al.[84] This

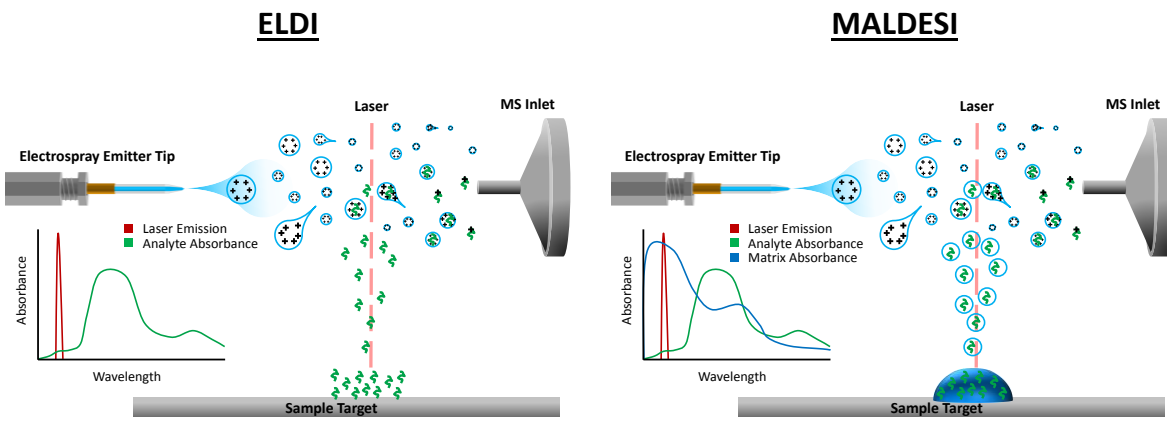

Figure 1.19 Non-resonant (ELDI) and resonant (MALDESI) desorption with electrospray post-ionization.

work used an ultraviolet laser (337 nm) to desorb dried droplets of bovine cytochrome c which were post-ionized by electrospray ionization resulting in the observation of multiply charged ions. The authors also investigated the use of a common MALDI matrix (α-CHCA) and concluded that the matrix was not necessary. ELDI has since found utility in direct analysis[84,86,87,304-306] as well as MSI.[307]

Around the same time, Muddiman et al. introduced matrix-assisted laser desorption electrospray ionization (MALDESI) in 2006.[85] They found that a laser energy absorbing matrix was required in order to observe appreciable signal. This improvement in signal when using a matrix was also noted by others.[88,95,308-311] MALDESI represents the first example in the resonant category whereby a laser is used to resonantly excite an exogenous (or endogenous) matrix to facilitate sample desorption followed by post-ionization by electrospray. This initial MALDESI work used a UV laser to excite an organic acid matrix to desorb peptide and protein

samples. They observed charge state distributions for the proteins that were identical to those obtained by ESI which corroborated the proposed electrospray post-ionization mechanism. A majority of the MALDESI publications have focused on making fundamental measurements to thoroughly characterize the source[85,89,91,98,184,312-314] as well as demonstrating applications in direct analysis[92,315,316] and MSI.[317-321]

Several new acronyms have been introduced in the literature that use different wavelength lasers but employ the same fundamental principles that were established with ELDI and MALDESI. However, both the ELDI and MALDESI techniques are independent of the laser wavelength as a prefix can be added denoting the wavelength region of the laser being used (e.g. IR-, UV-) which is similar to what is commonly done for LDI and MALDI. In the case of MALDESI, an appropriate matrix would be chosen to strongly absorb in the wavelength region of laser emission.

Aside from ELDI, the other off-resonance techniques that have been published include laser electrospray mass spectrometry (LEMS)[301] and laser desorption spray post-ionization (LDSPI).[303] LEMS uses a femtosecond near IR wavelength laser pulse (800 nm) to non-resonantly desorb the sample. Because this technique uses a femtosecond laser, rapid vaporization is achieved without appreciably heating the sample. LEMS has been used for direct analysis of neat samples,[301,322-325] profiling complex samples,[323,326-331] and MSI.[326] LDSPI was

introduced in 2010 and uses an IR laser (1064 nm) for desorption. LDSPI has been used to analyze neat samples as well as sample fingerprinting.[303,332,333]

Those acronyms that fall under MALDESI in the resonant category include laser ablation electrospray ionization (LAESI),[99] laser-assisted desorption electrospray ionization (LADESI),[90] laser ablation mass spectrometry (LAMS).[302] All three of these ionization sources are IR analogs of MALDESI and can be encompassed under the acronym IR-MALDESI. IR-LADESI has since been enveloped by the IR-MALDESI acronym[313] and the LAMS publication investigated analyte surface activity in the sample droplet.[302] To date, LAESI has been used for direct analysis of neat samples,[99,100] complex sample profiling,[96,334-342] as well as MSI[192,343-347] which will be discussed in greater detail later.

1.2.4.2 Application of ELDI to MSI

The benefits of imaging under atmospheric pressure conditions were discussed previously; however there are some additional advantages to using electrospray post-ionization. Firstly, electrospray post-ionization has been suggested to result in improved ion yields when compared with AP-MALDI.[192] Also, the ability to generate multiply charged ions with ELDI and MALDESI makes these techniques more amenable to top-down proteomic analysis and could alleviate the discrimination against larger molecules (>3000 *m/*z) that is observed with AP-MALDI techniques.[139]

There have only been a few examples of MSI using off-resonance laser desorption with electrospray post-ionization (ELDI) presented in the literature. Judge et al. demonstrated the imaging capabilities of ELDI using a non-resonant femtosecond laser for rastering over a dried droplet of oxycodone on a metal slide.[326] The resulting parent ion image for oxycodone showed increased intensity along the outer edge of the dried droplet which is consistent with the contact line deposits of an evaporated droplet. Huang et al. used UV-ELDI to image the surface of slices tissue from two types of fungus (*Ganoderma lucidum* and *Antrodia camphorata*).[307] Because ELDI is an atmospheric pressure ionization source, it was not required that thin cryo-sections (20 μm) be obtained. Therefore, relatively thick sections of fungus tissue (1-5 mm) were able to be imaged. For the *G. lucidum* slice, there were ions that showed increased intensity on the fungus skin compared to the interior of the section. MALDI MS was also performed on an extract of the *G. lucidum* slice and the resulting spectra were similar to what was observed in the ELDI profiling experiment. Several ions in the *A. camphorate* slice were proposed to be volatile analyte ions that were readily ionized when the tissue was placed under the electrospray without requiring laser desorption. However due to the lack of spatial control over desorption and ionization for these volatile ions, the resulting ion maps were of lower quality. A majority of the tissue related ions were tentatively identified as triterpenoids that had been previously recognized as the active components in the fungus tissues. On tissue MS/MS experiments were performed

using ELDI, however, they were unable to make confident identifications of the interrogated ions due to isomeric overlap.

1.2.4.3 Application of MALDESI to MSI

Molecular imaging with resonant laser desorption and electrospray post-ionization (MALDESI) is more prevalent in the literature compared to its off-resonance counterpart. This is likely due to the more efficient desorption of material that can be accomplished when directly coupling the laser energy to a matrix that is mixed with or present in the sample. The term “matrix” is oftentimes misconstrued to be strictly an organic acid when really any molecule that is present in large excess and strongly absorbs in the wavelength region of laser emission can be considered a matrix.[14]

While various laser wavelengths have been investigated for direct analysis applications of MALDESI, imaging applications almost exclusively utilize a mid-IR laser (2.94 μm). By coupling to the O-H vibrational modes, mid-IR laser emission can be strongly absorbed by endogenous or exogenous water which essentially allows water to be used as a matrix. There are inherent benefits that are realized when using water as a matrix such as its naturally occurring in most biological samples and, perhaps most importantly, water does not result in strong matrix interference and background signals that are common to most MALDI matrices.

The first example of using an IR-MALDESI source to obtain spatial information on mock targets was presented by Vertes.[192] A pattern of red and blue

markers was applied to a peace lily leaf which was subsequently imaged by LAESI. Ion maps for the permanent cations of *m/z* 443 (Rhodamine 6G from the red ink) and 478 (Basic Blue 7 from the blue ink) were shown to correlate with the pattern that was drawn on the leaf. Nemes and et al. then used LAESI to map metabolites and secondary metabolites in the leaf of a Zebra plant (*Aphelandra squarrosa*).[343] They were able to identify metabolites that correlated with the green and yellow variegation of the leaf as presented in **Figure 1.20a**. The ion map that is shown is for methoxykaempferol glucuronide (*m/z* 493). Imaging was performed at a spatial resolution of 400 μm which is limited primarily by the spot size of the ablated area which is around 350 μm. The capability to perform depth profiling was also demonstrated. It was estimated that roughly 50 μm of material was removed per pulse and unique mass spectra could be obtained from the various layers of the leaf that were sampled.

After demonstrating that LAESI could be used for depth profiling, Nemes et al. combined lateral imaging with depth profiling resulting in the first report on ambient 3-D mass spectrometry imaging.[344] Preliminary data was presented using a mock sample with marker patterns on the top and bottom of the leaf to show the ability to profile tissue in three dimensions. A Zebra plant leaf was then used for 3-D imaging with a lateral resolution of 500 μm and depth resolution of roughly 30 μm as shown in **Figure 1.20b**. The endogenous metabolite kaempferol (*m/z* 287) was shown to localize specifically in the yellow variegation of the leaf (yellow to red color scale in **Figure 1.20b**). In addition, chlorophyll *a* (*m/z* 893) was found to be most abundant

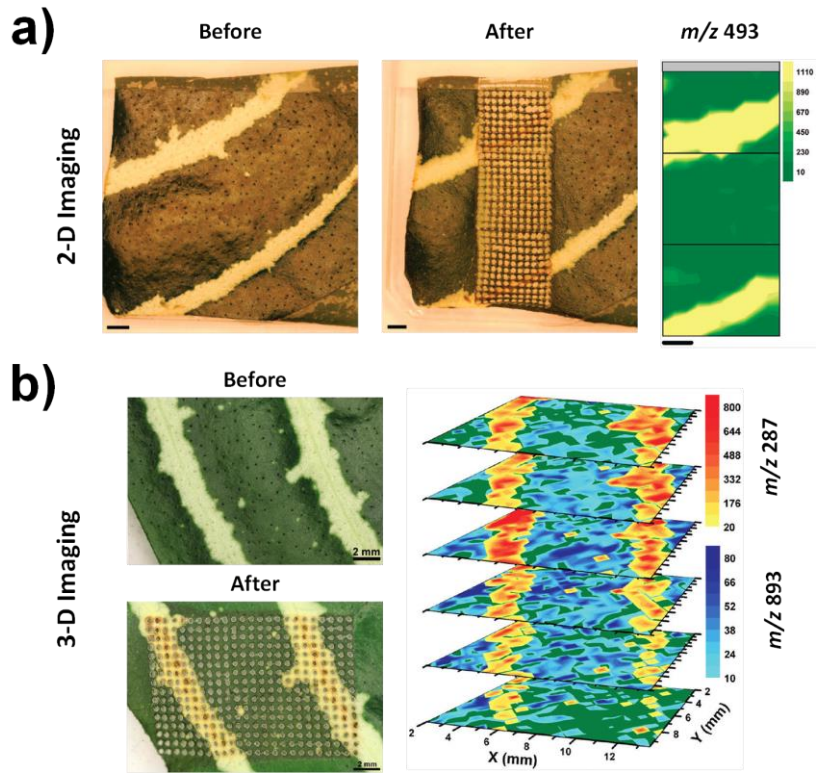

Figure 1.20 **a)** 2-D and **b)** 3-D LAESI MSI of Zebra plant leaf. **a)** Adapted with permission from (P. Nemes, A.A. Barton, Y. Li, A. Vertes, Anal. Chem., 80, 4575-4582 (2008)). Copyright (2008) American Chemical Society. **b)** Adapted with permission from (P. Nemes, A.A. Barton, A. Vertes, Anal. Chem., 81, 6668-6675 (2009)). Copyright (2009) American Chemical Society.

towards the center of the leaf (mesophyll) which is consistent with the location of the chloroplasts. The large variability that is observed from pixel to pixel is likely due to the lack of synchronization between the pulsing of the laser and the collection of mass spectra.

Vaikkinen et al. introduced a new variant of IR-MALDESI that uses heated nitrogen gas to assist with electrospray droplet desolvation in what they refer to as heat-assisted laser ablation electrospray ionization (HA-LAESI).[346] HA-LAESI is

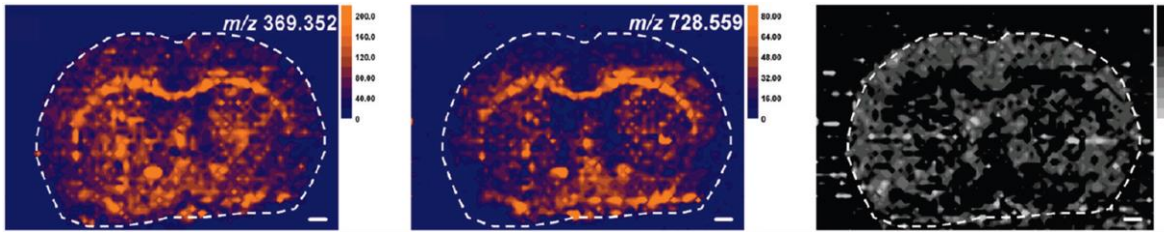

Figure 1.21 LAESI imaging of rat brain tissue sections. Adapted with permission from (P. Nemes, A.S. Woods, A. Vertes, Anal. Chem., 82, 982-988 (2010)). Copyright (2010) American Chemical Society.

similar to the previous LAESI set up, however, the electrospray emitter is off axis from the MS inlet and a heated nebulizer chip is used to introduce a jet of heated nitrogen. This set up was used for imaging of a pansy petal at a spatial resolution of 400 μm and provided comparable results to a LAESI image of a similar petal.

The first application of LAESI imaging to mammalian tissue was presented by Nemes and et al., who imaged coronal sections of rat brain.[345] To prevent the tissue from drying out during imaging, a thermoelectric cooling stage was used to keep the tissue frozen and a nitrogen-purged container was used to prevent ambient water from condensing on the tissue surface. A majority of the ions that were observed related to either lipids or small metabolites as identified through accurate mass measurement and MS/MS. Pearson correlation plots were used to indicate colocalization of observed peaks. The ion maps for cholesterol [M+H-H_2O] and the plasmalogens PC(O-33:3) and/or PE(O-36:3) are shown in **Figure 1.21** along with the corresponding Pearson colocalization map. Despite primarily observing small molecules, the colocalization of heme with a multiply charged ion, tentatively identified as the α-chain of hemoglobin, supported the observation of the protein

subunit. These images were obtained at a spatial resolution of 200 μm which is still relatively large compared with other imaging modalities.

Robichaud et al. presented on a highly engineered IR-MALDESI imaging source coupled to a high resolving power hybrid ion trap – FT-ICR instrument (Thermo LTQ-FT).[317] Because of the long acquisition times associated with FT-ICR MS, synchronization between the pulsing of the laser and the accumulation of ions was required in order to obtain reproducibility from pulse to pulse. Communication between the three major components of the source (IR-laser, stage controller, and mass spectrometer) was achieved in order to ensure that each pixel related to a single acquisition mass spectrum. They showed that despite the spot size being around 250 μm on laser burn paper, the diameter of ablated tissue was closer to 150 μm. Using an undersampling technique, they imaged a section of mouse lung and heart at a spatial resolution of 200 μm. Several lipid ions were presented that related specifically to the heart, lung, or the fatty tissue between them. Over 175 unique peaks were found to correspond to the tissue and of these; a majority of which were proposed to be lipids based off of their correlation with lipid mass excess. Using an electron microscopy grid as a mask over a section of mouse brain tissue, they demonstrated that a spatial resolution of 45 μm was possible using oversampling methods.

Barry et al. presented some IR-MALDESI imaging data of mouse brain tissue as part of a FT-ICR recalibration procedure.[318] Though not the main focus of the article, unique spatial distributions were shown for ions of the same nominal mass

a)

Parameter	Optimized settings for Tissue imaging	Optimized settings for Liquid MALDESI	Optimized settings proposed by others
Spot-Inlet Dist.	3 mm	8 mm	11 mm
ESI tip Diameter	30	30	100
Solvent Comp.	50/50 H_2O/MeOH	50/50 H_2O/ACN	50/50 H_2O/MeOH
Sample Height	5 mm	5 mm	15 mm
Solvent Flow	3 μL/min	0.5 μL/min	0.3 μL/min
ESI-Spot Dist.	1 mm	1 mm	3 mm

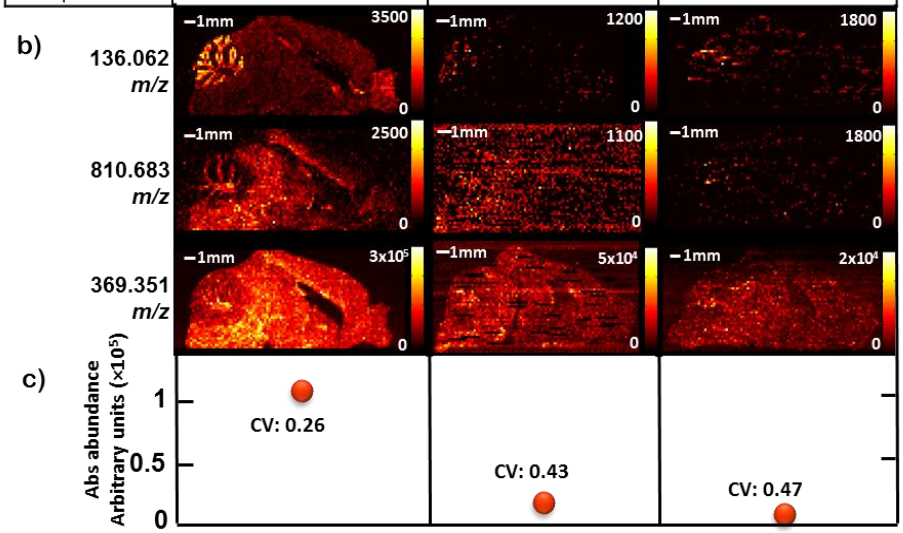

Figure 1.22 Comparison of IR-MALDESI imaging using optimized parameters with those used previously. Adapted from (G. Robichaud, J.A. Barry, D.C. Muddiman, J. Am. Soc. Mass Spectrom., 25, 319-328 (2014)) with kind permission from Springer Science and Business Media.

that were within 50 ppm of each other. This further demonstrated the utility of using high resolving power mass spectrometers for MSI when prior separations are not feasible.

Robichaud et al. reported on the optimization of the geometrical parameters of the IR-MALDESI imaging source using statistically designed experiments (**Figure 1.22**).[319] While previous studies optimized the source geometry for direct analysis of liquid solutions,[314] this work called attention to the fact that the ablated plume

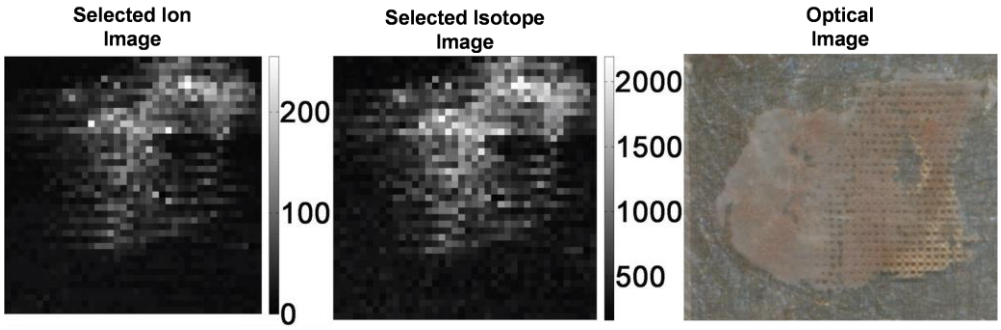

Figure 1.23 Top-down LAESI imaging of hemoglobin alpha directly from lung tissue showing the selected ion image, a sum of all of the isotopes for hemoglobin alpha (selected isotope image) as well as the optical image of the tissue after analysis. Adapted with permission from (A. Kiss, D.F. Smith, B.R. Reschke, M.J. Powel, R.M.A. Heeren, Proteomics, DOI 10.1002/pmic.201300306 (2014)). Copyright © (2014) JohnWiley & Sons, Ltd.

dynamics from a droplet are quite different from the dynamics from a tissue. Shadowgraphic techniques were used in conjunction with the collection of MS signal to correlate the observed plume with the MS signal from that particular ablation event. In this way they were able to demonstrate the utility of ice as a laser energy absorbing matrix for IR-MALDESI. In addition, they investigated the relationship between spatial resolution and sensitivity while taking into account the number of pulses per pixel for conditions with and without ice as a matrix. Nearly an order of magnitude improvement in signal abundance was achieved imaging with the optimized parameters. With this improvement in signal also came an improvement in signal reproducibility from pixel to pixel.

Recent work from Kiss et al. used a modified version of the commercial LAESI source coupled to a hybrid ion trap – FT-ICR instrument for tissue imaging (**Figure 1.23**).[347] This is an exciting development since it described the first top-

down imaging of proteins directly from tissue sections using a LAESI source. Hemoglobin alpha was identified as one of the three proteins detected in the imaging experiment and it was proposed that the other two were also likely to be abundant blood-related proteins because of their correlation with the blood on the tissue. Tandem MS imaging was also presented for hemoglobin. While this is intriguing in concept, there didn't seem to be much correlation between the optical image and the resulting ion images of the fragments.

Barry et al. presented a comparison of IR-MALDESI and UV-MALDI for molecular imaging of the drug lapatinib and its metabolites directly from the liver tissue of a dosed animal.[320] By analyzing serial sections of the same tissue by both methods, they demonstrate that these techniques provide very similar information (**Figure 1.24**). One evident consequence of the UV-MALDI imaging experiment is the importance the matrix application step which must be of high quality to avoid introducing artificial variation in the analyte signal. The influence of the electrospray solvent composition was also investigated by replacing the direct infusion line of the IR-MALDESI source, which usually supplies an isocratic flow of one solvent composition, with a solvent gradient from LC pumps. By tracking the abundance of several molecular classes during the gradient, the ideal solvent composition was chosen to optimize the signal relating to the parent drug and its metabolites.

Most recently, Barry et al. have reported on the coupling of the IR-MALDESI imaging source with the hybrid quadrupole orbitrap (Q Exactive).[321] The Q Exactive offers improvements in acquisition speed that make high resolving power MSI more

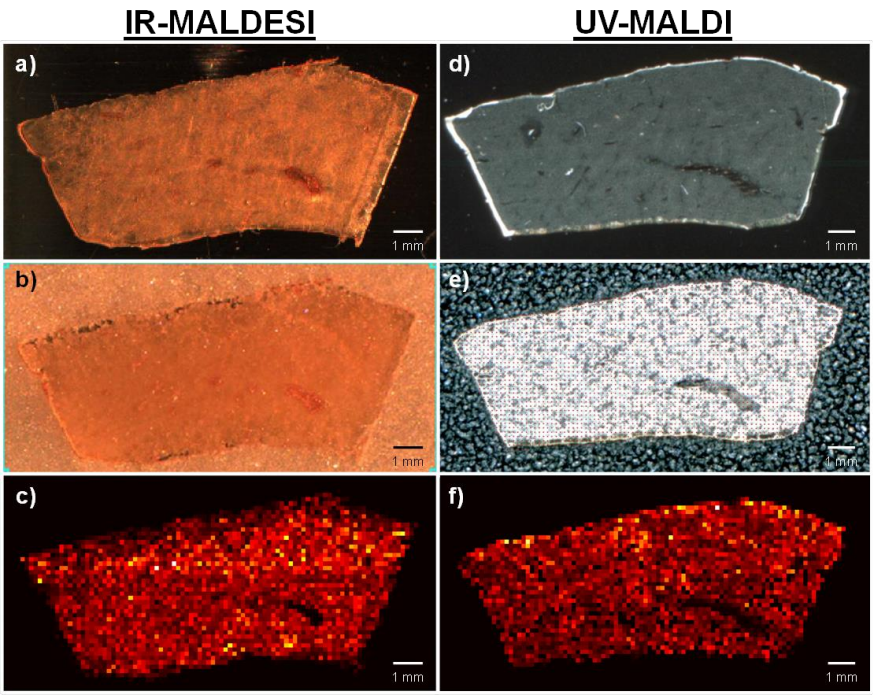

Figure 1.24 Comparison of IR-MALDESI with UV-MALDI for the imaging of drug and metabolites in liver tissue. **a)** Optical image of liver tissue section prior to IR-MALDESI matrix application. **b)** Optical image of liver tissue section after application of the ice matrix for IR-MALDESI. **c)** Ion map of lapatinib from the IR-MALDESI MSI analysis showing homogenous distribution in the liver tissue. **d)** Optical image of liver tissue section prior to UV-MALDI matrix application. **e)** Optical image of liver tissue section after application of matrix (DHB) for UV-MALDI. **f)** Ion map of lapatinib from UV-MALDI MSI analysis showing homogenous distribution in the liver tissue.

practical. IR-MALDESI was used to image tissue that had been incubated with either a high concentration or low concentration of three antiretroviral drugs. The relative intensities of each of the drugs between the high and low concentration tissues were consistent with the exact quantities of each drug as determined by an LC-MS/MS multiple reaction monitoring (MRM) assay that was performed on adjacent tissue sections. This provides the first evidence that IR-MALDESI imaging

data correlates well with a validated MRM assay and displays the potential of using this technology for quantitative imaging. In addition, an IR-MALDESI MRM MSI experiment was performed whereby at each pixel, the *m/z* of raltegravir was isolated and fragmented. Ion images for each of the selected transitions were shown to have excellent correlation with the distribution of the parent ion (**Figure 1.25**). The relative abundances of each of the transitions from the IR-MALDESI MSI experiment were nearly indistinguishable from those obtained from direct infusion ESI which has implications about the similarity of the internal energy of desorption and ionization from both techniques.

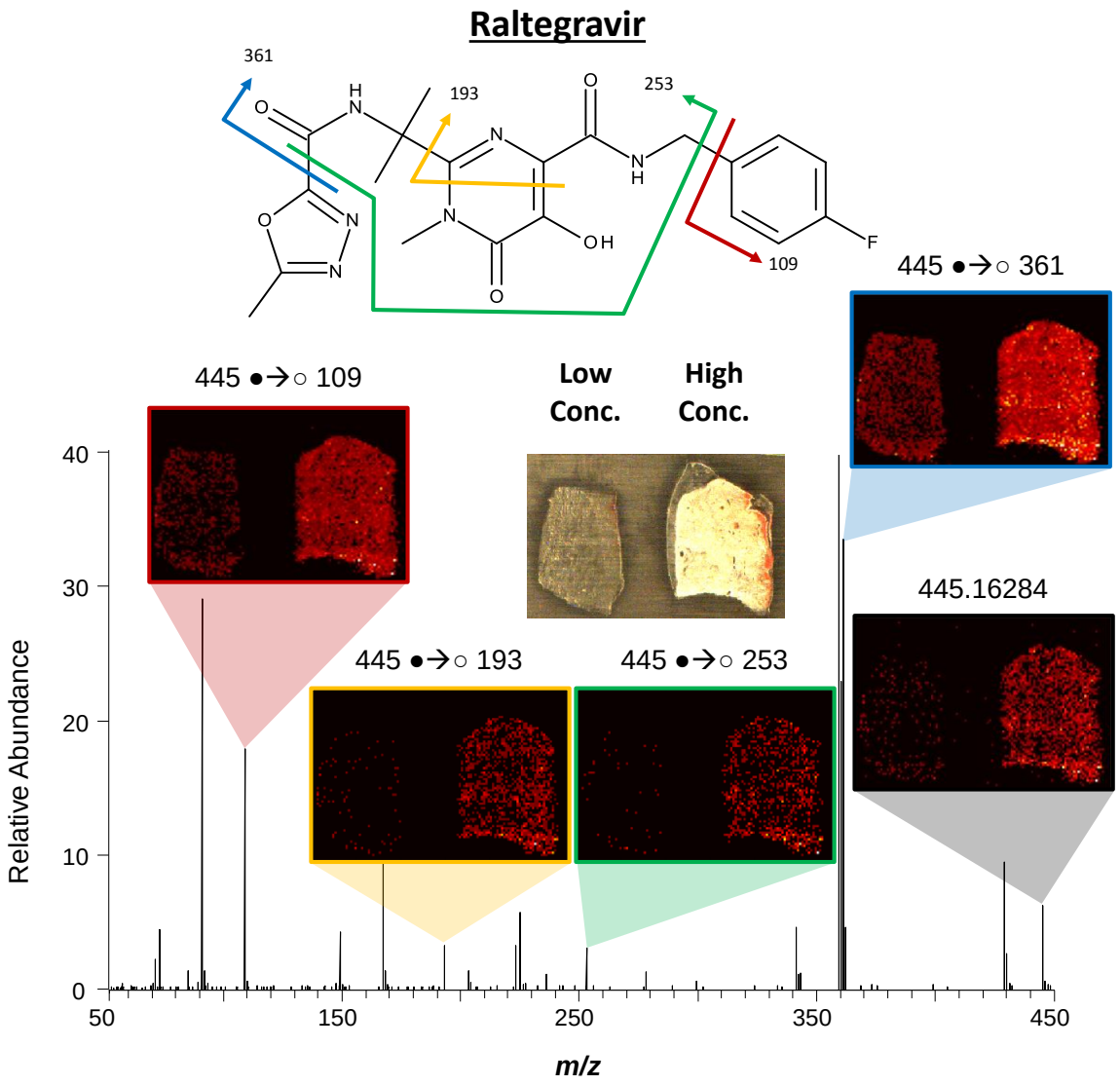

Figure 1.25 IR-MALDESI MRM MSI of raltegravir in tissue sections incubated with a high and low concentration of the drug. Ion maps of selected transitions correlate with the parent ion distribution demonstrating improved selectivity with MRM imaging.

1.2.5 Other Atmospheric Pressure Ionization Techniques for MSI

1.2.5.1 Laser Ablation Flowing Atmospheric Pressure Afterglow (LA-FAPA)

One of the characteristics of most plasma-based sources limiting their use as direct desorption/ionization probes for mass spectrometry imaging is the actual diameter of the plasma plume which is generally in the millimeter range, leading to poor spatial resolution. Shelley et al.[348] were the first to circumvent this limitation by using a 266 nm UV-laser to ablate material from the sample surface and post-ionizing the molecules using a plasma-based modified Flowing Atmospheric-Pressure Afterglow (FAPA) source previously developed.[349] Ablation of the sample was performed in an ablation cell and molecules were carried in a stream of N_2 to be mixed with the afterglow region of the FAPA source, positioned few millimeters in

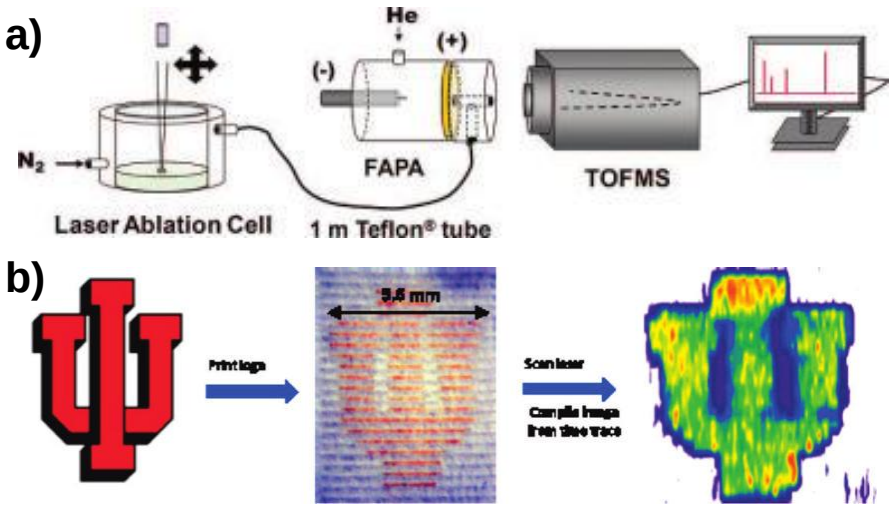

Figure 1.26 a) Schematic of the LA-FAPA imaging source and **b)** LA-FAPA MS imaging of caffeine-dosed ink printed on paper. Adapted with permission from (J.T. Shelley, S.J. Ray, G.M. Hieftje, Anal. Chem., 80, 8308-8313 (2008)). Copyright (2008) American Chemical Society.

front of the mass spectrometer inlet (see **Figure 1.26**).

LA-FAPA MS Imaging of lidocaine spotted biological tissues as well as caffeine dosed celery veins was successfully achieved as proof of concept experiments. A spatial resolution of 20 μm was achieved using this technique, limited mainly by laser spot size. Since LA-FAPA ionization still occurs through relatively high energy chemical ionization processes, this imaging technique is limited to lower mass range (<1 kDa).

1.2.5.2 Infrared Laser Ablation Metastable Induced Chemical Ionization (IR-LAMCI)

In IR-LAMICI, an infrared laser is used to ablate material from sample surface. In the proof of concept experiment reported by Murray,[350] a wavelength of 2.94 μm was used to match the O–H symmetric and asymmetric stretching bands of the naturally occurring water present in the sample. The ablated material, consisting of (mainly) neutral molecules, then reacts with a metastable reactive plume to produce protonated/deprotonated ions by gas-phase chemical ionization. Geometry used in IR-LAMICI, is somewhat similar to the hybrid laser ablation/ESI ionization except that the ESI emitter is replaced by a DART[351]-type gaseous plume of metastable helium or nitrogen molecules formed upstream by electrical discharge and transported via a glass capillary. The plasma-based imaging technique was successfully applied to the detection of acetaminophen monomer and dimer ion on

the surface of the tablets as well as the analysis of counterfeit antimalarial drug tablets.

1.2.5.3 Laser Ablation Atmospheric Pressure Chemical Ionization (LA-APCI)

The idea of post-ionizing laser ablated neutrals using reagent ions produced by corona discharges has been proposed over a decade ago by Coon et al.[352] However, application of LA-APCI to MS imaging is somewhat recent. Indeed, Herdering et al. proposed a MS imaging setup similar to LA-FAPA (**Figure 1.26a**) where a Q-switched Nd:YAG UV laser (λ = 213 nm) is used to desorb material in an ablation cell and resulting aerosol molecules are transported to an ionization source located in front of the mass spectrometer using nitrogen gas flow. In LA-APCI, rather than using a FAPA source, the sample is post-ionized using a commercial APCI source modified to accept analyte in the form of ablated aerosol[353] as opposed to a liquid sample.

Proof of concept imaging experiments were performed on TLC plates where caffeine, acetaminophen, and dissolved Thomapyrin tablets had been separated.[353] All three analytes were detected using the LA-APCI MSI setup interfaced with an orbitrap instrument (Exactive Classic HCD orbitrap mass spectrometer, ThermoFisher Scientific, Bremen, Germany). Imaging results were validated with optical fluorescence images. Additional experiments were performed on untreated Thomapyrin tablets where both caffeine and acetaminophen were resolved with a spatial resolution of 100 μm.

A different LA-APCI MS imaging system was also simultaneously developed and proposed by Lorenz et al.[134] The system adapted a commercial Laser Microdissection system (LMD7000, Leica Microsystems, Wetzel, Germany) so that it can be used for multimodal imaging, i.e. collecting simultaneously fluorescence, bright field and MS imaging data from the same tissue sample. Combining a commercial microscope and laser ablation to perform AP-LDI MS imaging had been explored before.[206] In this case, the integrated UV laser of the LMD system is used to ablate sample tissue material in transmission mode. The ablated material is then

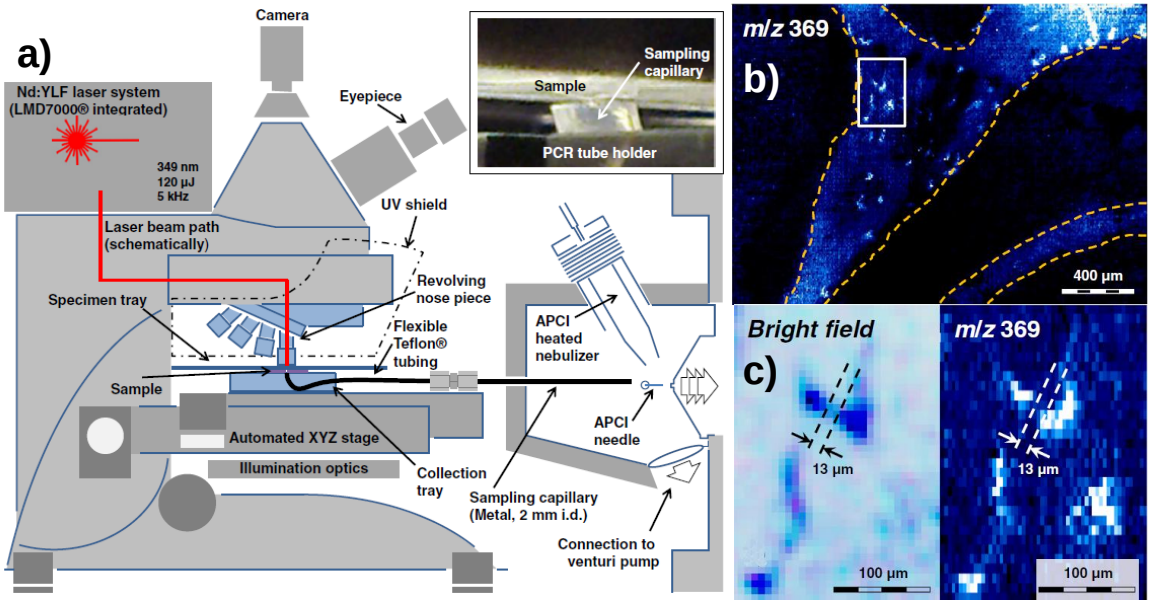

Figure 1.27 **a)** Experimental setup for LA-APCI MS using a LMD microscope. **b)** Different regions of a mouse brain are outlined by the relative abundance of cholesterol $(M+H-H_2O)^+$ and **c)** features as small as 13 µm can be resolved by both bright field microscopy and LA-APCI MS imaging. Adapted with permission from (M. Lorenz, O.S. Ovchinnikova, V. Kertesz, G.J. Van Berkel, Rapid Commun. Mass Spectrom., 27, 1429-1436 (2013)). Copyright © (2013) JohnWiley & Sons, Ltd.

transported via a Teflon tube to a Venturi pumped Ion Max source (ThermoFisher Scientific, Bremen, Germany) equipped with an (unmodified) APCI probe. Sampling tube was positioned inside the source so that neutral molecules are ejected just below the APCI probe. Laser, stage control and triggering of the mass spectrometer were achieved using a software interface developed in-house. The multi-modal system was used to spatially resolve features on mouse brain tissue as small as 13 μm using both bright field microscopy and LA-APCI MS imaging as shown in **Figure 1.27**.

1.2.5.4 Low Temperature Plasma Probe (LTP)

The concept of using the plasma plume created by gas flowing through dielectric barrier discharges as a ionization method (DBDI) was first proposed by Na et Al.[354] In the proposed setup, an electrode plate was placed under a glass slide serving the dual purpose of acting as a dielectric barrier and sample holder while a gas would flow through a hollow stainless steel electrode pointed at the sample. Upon applying an AC excitation, a low temperature plasma plume was formed and could be used to desorb/ionize material from a surface at ambient pressure. Harper et al. later improved the design and proposed a probe with an annular configuration where all DBD components are contained in the probe: the Low Temperature Plasma (LTP) probe.[355] The probe consists of a glass capillary serving as a dielectric barrier through which is inserted an electrode while a conductive film surrounding the capillary serves as the counter electrode. By controlling gas flow

and excitation voltage, a low-temperature plasma plume consisting of high-energy electron and metastable molecules is created and aimed directly at the sample surface for desorption/ionization of analyte. The obvious advantage of the annular LTP probe design is that the interrogated surface does not have to be part of the electrical circuit, making the LTP probe more versatile and even portable.

First application of MS imaging using a LTP probe was presented by Liu et al.[356] where a miniaturized probe was used to successfully identify genuine and counterfeit seals on Chinese calligraphy based on ink content. They were also able to demonstrate a spatial resolution of 250 μm using a LTP probe tip of 150 μm.

1.2.5.5 Desorption Atmospheric Pressure Photoionization (DAPPI)

Atmospheric pressure photoionization (APPI) was developed early on as an ionization source for LC MS systems or direct injection of samples in solution.[357] In APPI, solvent/analyte solution is sprayed and vaporized using a heated nebulizer where nebulizing gas is mixed with an optional dopant. The mixture of gas phase molecules is then exposed to a light source that emits photons at a set energy and ionization occurs through photoionization pathways. DAPPI, first proposed by Haapala et al. ,[358] extended the application of the APPI source to the direct analysis of surface ions. Rather than nebulizing the analyte in solution, the proposed source used a microfluidic device to aim a vaporized heated jet of dopant solvent at the interrogated surface on which is also aimed a discharge lamp emitting photons at a set energy. It was then proposed that surface molecules are thermally desorbed

and ionized by APPI-like gas phase photoionization processes. Ions formed are then captured by the atmospheric pressure sampling inlet of the mass spectrometer, placed few millimeters from the sample spot.

Several ionization pathways have been proposed for DAPPI, depending among others on the ionization energy (IE), proton affinities (PA), and electron affinities (EA) of both the dopant solvent used and the analyte molecules. Indeed ionization pathways leading to the formation of $M^{+\bullet}$, $[M+H]^+$, $M^{-\bullet}$, $[M-H]^-$, $[M-H+O]^-$, $[M-2H+2O]^-$ have been demonstrated depending on the aforementioned factors and polarity.[359] Generally less soft than ESI, DAPPI has demonstrated to be very useful for the ionization of nonpolar analytes. Correlation between the heat conductivity of the sample plate material and the performance of DAPPI source has also been demonstrated where polymers such as PMMA and PTFE lead to higher analyte signal intensity and lower background than surface with higher conductivity such as aluminum. I was also demonstrated that DAPPI technique can be used for the fast screening and detection of illicit drugs confiscated from the streets[360].

First use of DAPPI for mass spectrometry imaging was performed by Pól et al.,[361] where a custom source was adapted so that imaging can be performed alternatively in DESI or DAPPI modes. The integrated imaging source was coupled with a commercial high resolving power FT-ICR instrument. When in DAPPI mode, using a setup similar to Haapala et al. ,[358] the spatial resolution was limited to 1 mm, due to the size of the desorption area created by the heated nebulized gas-dopant jet. Imaging of a dried *Salvia* leaf was perform where several peaks presumed to be

aromatic compounds, esters, and high terpenoids were found in the *m/z* 300-600 range. Imaging of a brain tissue section was also performed where mainly cholesterol $[M-H_2O+H]^+$ could be found when using acetone as a dopant solvent.

1.2.5.6 Probe Electrospray Ionization (PESI)

In proof of concept experiments of probe electrospray ionization (PESI),[362] a sharp metallic needle probe was used to collect sample by dipping its tip in aqueous solution containing analyte of interest in a setup as shown in **Figure 1.28a**. After making contact with the sample, a voltage potential is applied between the solution coated probe and the mass spectrometer inlet positioned few millimeters away. The solution coating the probe tip is then electrosprayed in a pulse-like event due to the low amount of solution and captured by the mass spectrometer. Supporting the hypothesis that PESI ionization pathways are similar to those of conventional ESI, multiply charged ions were detected from melittin, bovine insulin, cytochrome c and polyethylene glycol in aqueous solution. Signal intensity could also be significantly increased by adding acid or ammonium acetate to the solution, which increases the amount of free charges available to take part in the ESI desorption/ionization processes. Additional experiments on biological samples were also performed[363,364] and the fundamentals of the PESI source were investigated using shadowgraphy photography techniques and by assessing the effects of probe shape, viscosity, sampled volume and ESI voltage/current on signal.[365] The PESI source was later adapted to MS imaging of biological tissue sections. A heated capillary sprayer,

aiming at the probe tip was added to the setup. The aqueous or solvent/H_2O solution plume serves the dual purpose of re-wetting the probe tip to enhance signal and also cleaning the needle, minimizing carry-over from pixel to pixel. A PESI MS

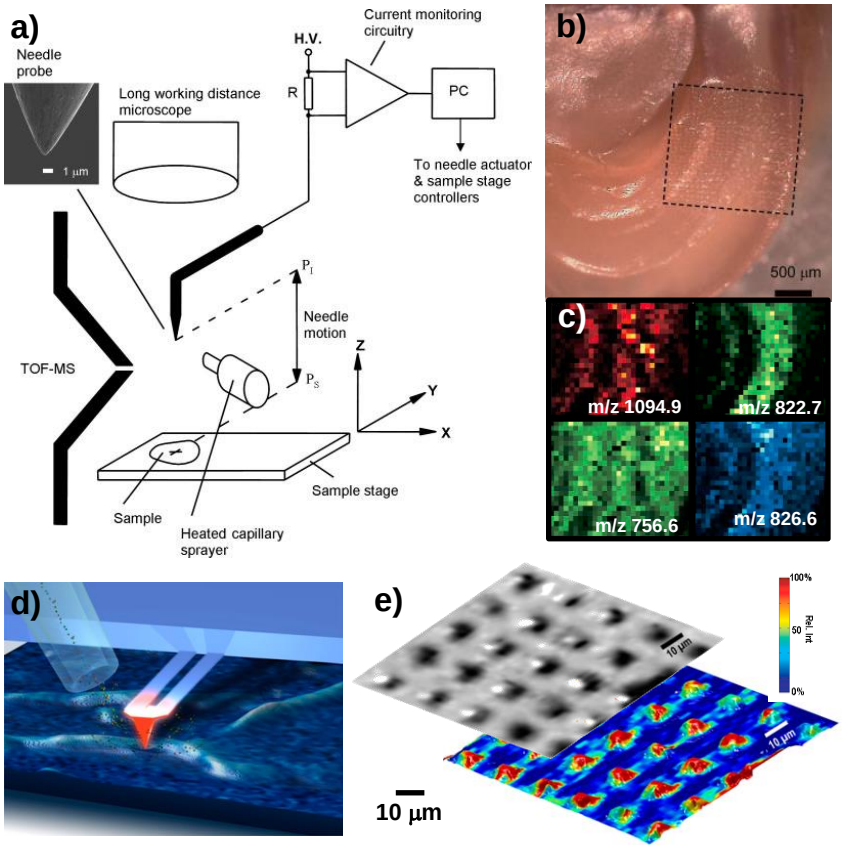

Figure 1.28 **a)** PESI MS imaging experimental setup. **b)** Optical image of mouse brain ROI analyzed by PESI MS imaging and **c)** ion map of different lipids (pixel size is 60 μm). Adapted with permission from (L.C. Chen, K. Yoshimura, Z. Yu, R. Iwata, H. Ito, H. Suzuki, K. Mori, O. Ariyada, S. Takeda, T. Kubota, J. Mass Spectrom., 44, 1469-1477 (2009)). Copyright © (2009) JohnWiley & Sons, Ltd. **d)** Illustration of ion being desorbed in an AFM proximal probe TD/SI MS setup. **e)** Optical image of yellow ink stamped on photo paper (top) and overlay of AFM topography image and TD/SI MS signal intensity of ion of pigment yellow 74 (bottom). Adapted with permission from (O.S. Ovchinnikova, K. Kjoller, G.B. Hurst, D.A. Pelletier, G.J. Van Berkel, Anal. Chem., 86, 1083-1090 (2013)). Copyright (2013) American Chemical Society.

imaging system was implemented where sample stage motion, probe z-axis actuation, ESI voltage application and MS signal acquisition were synchronized using a custom made control system. Imaging of mouse brain was achieved with a spatial resolution of 60 μm, mainly limited by the size of the sampling needle used for those imaging experiments. Detection and mapping of several peaks of phosphatidylcholines (PC) and galactosylceramides (GALCER) was achieved (**Figure 1.28b-c**).[366]

1.2.5.7 Thermal Desorption / Secondary Ionization (TD/SI)

In proximal probe Thermal Desorption/Secondary Ionization Mass Spectrometry (TD/SI MS), a heated probe is positioned near or in contact with the interrogated surface (liquid or solid). The thermally desorbed or vaporized neutral molecules are then transported to a secondary ionization source such as ESI or APCI. The post ionized molecules are captured by the mass spectrometer inlet and analyzed. A typical setup for TD/SI MS is shown in **Figure 1.28d**. This atmospheric ionization technique was first introduced by Ovchinnikova et al.[367] as a method to couple Thin Layer Chromatography (TLC) separation and mass spectrometry. For those early proof-of-concept experiments, the wand of a soldering iron was used as the heated probe and scanned across TLC separated compounds (e.g. pharmaceuticals, dyestuffs, explosives, herbicides). Effects of parameters such as probe diameter, probe temperature, scan speed, and sample-probe distance on the

signal abundance and the spatial resolution were then investigated. Spatial resolution on the order of the probe size radius (mm scale) was then achieved.

The same research group later modified their TD/SI MS source so that it could be used to perform mass spectrometry imaging[368] on sample surfaces. Effects of several source parameters such as scan speed and probe distance were systematically investigated to better understand the fundamentals and to improve the source performance. The abundance of a specific molecule from patterns printed in yellow ink on paper was used as figure of merit for those experiments. It was found that intensity could be significantly improved by reducing the probe-to-surface distance at the cost of increasing the signal variation or relative standard deviation (RSD). Just like with previous settings, the best spatial resolution that could be achieved with this improved source was on the same order as the diameter of the probe size. Indeed, a spatial resolution of *circa* 45 μm was achieved using a probe tip diameter of 50 μm. One of the conclusions from those preliminary imaging experiments is that to further improve image quality and spatial resolution, a smaller heater probe and a means to maintain optimal probe-to-surface distance would be necessary. The same group therefore proposed using a 30 nm diameter heated atomic force microscopy (AFM) probe tip and modified the AFM control system to co-register topographical information and molecular imaging data.[369] For those initial experiments, a thin film of caffeine was deposited on a glass slide. With a probe temperature and a sampling dwell time of 30 s, it was estimated that 2 fg or 10 amol of caffeine was thermally desorbed at each spot, leaving a crater of 250 nm in

diameter and 100 nm deep. Desorbed material was then captured and transported through a long mass spectrometer inlet using the first stage vacuum from the mass spectrometer instrument. The inlet tube was modified so that ions generated by ESI and thermal desorption are mixed in a Y connector in front of the instrument. A 9 x 2 grid was rastered and enough analyte was sampled at each spot to monitor the *m/z* 195→138 transition of the caffeine molecule by ms/ms. More recently, combined AFM topography measurement and mass spectrometry imaging data where ionization of thermally desorbed molecules was achieved by atmospheric pressure chemical ionization (APCI) rather than ESI.[370] Co-registered topographic and MS data were successfully collected on ink patterns (see **Figure 1.28d-e**) and living bacteria colonies on agar gel, where features in the 5-10 μm range were resolved with 2.5 μm × 2 μm MSI pixels.

1.2.5.8 Easy Ambient Sonic Spray Ionization (EASI)

EASI was first introduced to the community under the name Desorption Sonic Spray Ionization (DeSSI),[371] as a (high) voltage-free [*sic*] ambient mass spectrometry ionization method. In a later publication the same research group renamed the source EASI.[372] EASI is fundamentally equivalent to DESI without the use of an ESI voltage. As in DESI, a polar aqueous/solvent solution is aimed at the sample surface using a nebulizer capillary (supersonic pneumatic spray). Typically, a higher solvent flow (3-20 μL/min) is used compared to what is typically used in DESI MS (1-2 μL/min). Just as in DESI, charged droplets collide with the sample

surface, extracting analyte molecules. Through gentle solvent evaporation, a fraction of those molecules will end up as gas phase ions and be captured by the mass spectrometer inlet. Early comparison between DESI and EASI/DeSSI suggested that the ratio of analyte ions/solvent cluster ions was greater in the case of EASI. One of the advantage of proposing a DESI-like ionization method using no voltage is the capability of extending the interrogation technique to applications where using an ESI voltage is not suitable such as *in vivo*/*in situ* analysis of biological tissues during surgical procedures.

EASI imaging was later proposed and the performance of the ionization technique was compared to DESI imaging.[373] In an effort to perform a fair, direct comparison between the two techniques, and account for any biological variation a dual-mode imaging source (DDI) was implemented, allowing for alternation between DESI and EASI from line to line when imaging a tissue sample. It was found that EASI technique is in general less sensitive than DESI.

1.2.5.9 Liquid Microjunction Surface Sampling Probe (LMJ-SSP)

In Liquid Microjunction Surface Sampling Probe (LMJ-SSP), a system of open ended coaxial tubing is positioned few micrometers from the sample surface, wherein solvent solution is delivered toward the sample surface through the outside tubing. A liquid microjunction is formed at the surface where analyte molecules are extracted in the solvent, which is drawn back in through the inner tube and analyzed by ESI MS. While the extraction solvent is actively delivered using a syringe pump,

the driving force pulling the fluid back through the inner tube is provided by the electrostatic pulling force and nebulizing gas at the ESI emitter (see **Figure 1.29**). The setup, as previously described, was proposed by Wachs et al.[374] as a mean to create a liquid junction between devices but Berkel et al. were the first to use a LMJ-SSP source to continuously scan and collect sample over a solid surface.[375] This source was then used to scan over the surface of a thin layer chromatography (TLC) plate on which a 3-dye mixture had been separated and demonstration was made that the three dyes could be spatially resolved in both positive and negative ion mode LMJ-SSP MS. The same group later proposed an improved automated LMJ-

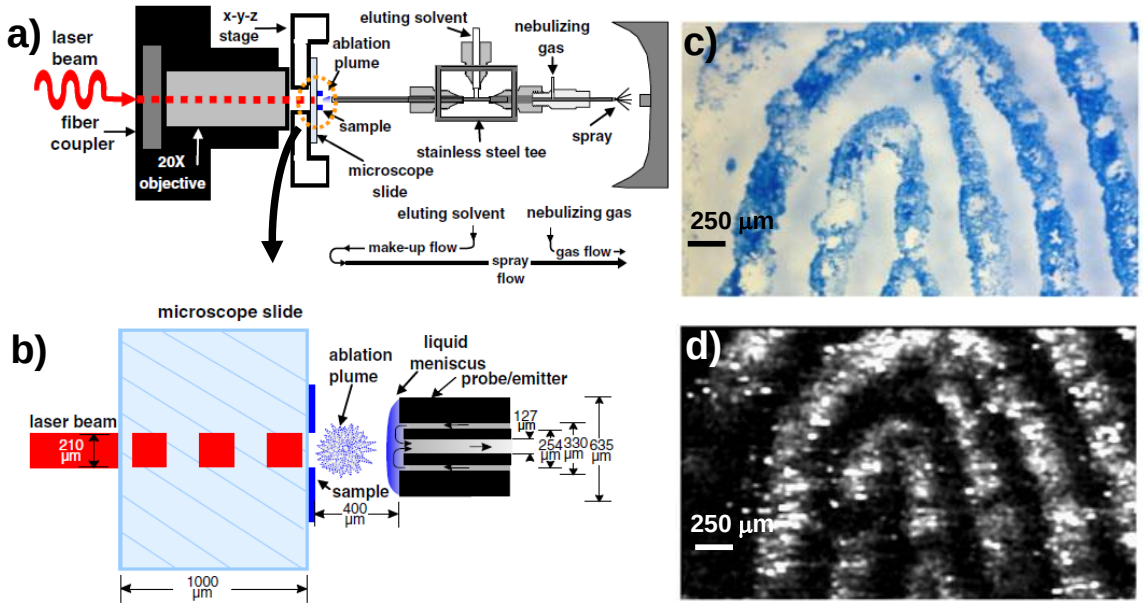

Figure 1.29 **a)** Overview of experimental setup for non-contact transmission geometry laser ablation imaging using LMJ-SSP MS probe and **b)** close-up of desorption at sample surface. **c)** blue ink fingerprint (basic blue 7) and ion image of dye molecule. Adapted with permission from (O.S. Ovchinnikova, V. Kertesz, G.J. Van Berkel, Rapid Commun. Mass Spectrom., 25, 3735-3740 (2011)). Copyright © (2011) JohnWiley & Sons, Ltd.

SSP MS source where x-y position of the probe as well as the tip-probe distance could be precisely controlled and monitored using through a user interface,[376] enabling the use of the source for the first 2D LMJ-SSP MS imaging experiments on elution patterns of analyte on TLC plates and stamped lettering on paper. This same source could also be used to perform direct analysis of surface spotted analyte such as proteins in micro-wells on ceramic or glass plates.[377] LMJ-SSP MS imaging of reserpine spotted on a tissue section was later achieved[378] as well as drug detection in different organs in a sagittal whole-body tissue section from a dosed mouse. Once again, strong dependence of LMJ-SSP MS performance on surface texture and hydrophobicity was confirmed, making tissue imaging quite challenging due to the inherent heterogeneity of those properties in tissue. Indeed, stability of the liquid junction and its diameter (defining the spatial resolution in an imaging experiment) strongly depend on the probe-surface distance, the solvent flow rate, and hydrophobicity of the surface. To enable the LMJ-SSP MS analysis of wettable or absorbent surfaces, typically incompatible with this sampling technique, it was demonstrated that a simple hydrophobic surface treatment could be used.[379] Indeed, by applying a commercially available silicone aerosol it was demonstrated that the LMJ-SSP MS analysis could now be performed on surface like high-performance thin layer chromatography (HPTLC) plates, Kimwipes®, and even dried blood spot paper. Fundamentals of sample extraction at the probe-surface liquid junction were also investigated using visualization tools and computational fluid dynamics (CFD). Capillary diameters, inner capillary position, probe-surface

distance were among the parameters investigated. Both visual observation and CFD analysis confirmed that, by retracting the inner capillary without changing the flow, it was possible to maintain a layer of solvent (plug) at the surface of the sample. It was shown that this plug could be used to manipulate and mix multiple analytes at the sample surface.[380]

Spatial resolution in LMJ-SSP MS is defined mainly by the outside diameter of the probe,[378] scanning speed and wettability of the surface, limiting the best achievable resolution to the millimeter range (diameter of the liquid microjunction). To circumvent this limitation, rather than creating a liquid microjunction with the sample surface, it was proposed to let the probe hover in close proximity of the sample surface and use a laser pulse to ablate material toward the probe in transmission geometry,[381] as shown in **Figure 1.29**. LMJ-SSP MS imaging of a freehand drawing and fingerprints in blue ink (basic blue 7) was performed and spatial resolution of 100 μm was achieved. To improve sample transfer efficiency between the surface and the probe, the same group later proposed to coat the sample surface with thin insoluble film and ablate the material directly in the liquid microjunction.[382] By doing so, a signal improvement of 1 order of magnitude was obtained over the noncontact transmission geometry and spatial resolution of ~50 μm was demonstrated.

In more recent experiments, the LMJ-SSP source was successfully coupled to a HPLC system, such that extracted analyte can undergo chemical separation prior to be analyzed by ESI MS.[383] Propaganol and some of its associated

metabolites were successfully extracted from drug-dosed liver tissue samples, separated by HPLC and detected by ESI MS. Successful experiments were also performed on a dried sheep blood spot, where α and β hemoglobin chains were identified using the same technique.

1.2.5.10 Liquid Extraction Surface Analysis (LESA)

Liquid Extraction Surface Analysis (LESA) was first reported as a variation of LMJ-SSP[384] where, instead of establishing a continuous liquid microjunction with the sample surface using a capillary system, a robotic arm is used to deposit few microliters of extraction solvent on the sample surface using a conductive pipette tip. After a set time, during which sample molecules are extracted at the liquid junction, the fluid is drawn back in the pipette tip and the robotic arm inserts the pipette tip in an ESI chip positioned in front of the mass spectrometer inlet. The solution containing analyte molecules is then electrosprayed in the nano-flow regime and captured by the MS instrument for analysis. A new pipette and chip nozzle is used for each sampling cycle to avoid carry-over and sample contamination. The first demonstration of LESA was performed using commercially available equipment and quantitative analysis of spotted drug samples on MALDI plates and in dried blood spot was achieved. Detection of sulforaphane and propranolol drug was also achieved in mice whole-body thin tissue sections. Similar LESA MS setup, combined with MALDI MSI was also used to investigate the depth of percutaneous absorption of glucocorticoid receptors in porcine ear sections and good correlation

was found between compound penetration in porcine detected and skin blanching degree observed on human skin.[385]

Later, Eikel et al. [386] used a (software) modified TriVersa NanoMate robot (Advion Inc., Ithaca, NY, USA) to profile terfenadine drug and its metabolite fexofenadine in different organs from a whole-body thin mouse tissue section and results were found to corroborate with similar studies performed by others using MALDI MSI and radiolabeled drugs. Imaging capabilities of LESA MS were also demonstrated through this work by profiling terfenadine and fexofenadine in mouse brain with a spatial resolution of 1 mm (limited by the liquid junction area). LESA MS was also used as a complementary technique to quantitative whole-body autoradiography (QWBA) ,[387] to detect pesticides directly from food surfaces,[388] perform clinical analysis of hemoglobin protein from dry blood samples,[389] and to detect additive and degradation products in polymer paint coating.[390] Side by side comparison of LESA with MALDI MSI[391] was performed and it was shown that both techniques could be used to successfully detect the presence of drugs in dosed tissue samples. More information about the spatial distribution of drug can be obtained with MALDI MSI because of the significantly better spatial resolution (10-50 μm vs 1 mm) but, because of its ease of use and ambient nature, LESA remains a valuable tool for applications requiring low spatial resolution or as a screening tool used to confirm the presence of the analyte in a sample (prior to performing a more time consuming analysis such as MALDI MSI). LESA MS was also performed alongside with DESI MSI for the analysis of tryptic digested peptides from protein

mixture on a biomaterial surface.[392] Both techniques have successfully been used to identify endogenous protein species, although LESA MS was shown to be more sensitive than DESI MS. This confirmed once again that LESA can serve as a valuable tool for screening and for rapid detection of analyte. Finally, another automated liquid microjunction probe system was also coupled to an HPLC-ESI MS system and used for the improved detection of drugs in whole-body tissue section.[393]

1.2.5.11 Nanospray Desorption Ionization (nano-DESI)

Nanospray desorption electrospray ionization (Nano-DESI) shares many attributes with the Liquid Microjunction Surface Sampling Probe (LMJ-SSP) method. In nano-DESI,[394] an extraction solvent is actively supplied through an open ended capillary (primary capillary), placed just above the surface of interest as shown in **Figure 1.30a**. Just as in LMJ-SSP, molecules are extracted in the droplet at the liquid-surface interface and analyte rich solution is aspired through a nanospray capillary and electrosprayed in the nano flow regime. ESI potential is typically applied at the primary capillary and extraction solvent flow is adjusted to match the self-aspiring nano-ESI flow so that the size of the liquid bridge remains constant. Nano-DESI has been successfully applied for the direct analysis of, among others, dried samples of drugs, dye, proteins,[394] organic aerosol,[395-397] crude petroleum,[398] and lipids.[399]

One advantage of separating in space the primary and the self-aspiring ESI capillary over the coaxial configuration used in LMJ-SSP is that the size of the liquid junction can be significantly reduced. By carefully controlling the distance between the nano-DESI probe and the sample surface, it was demonstrated that the contact width at the liquid junction could be as small as 8 μm, making it possible to perform

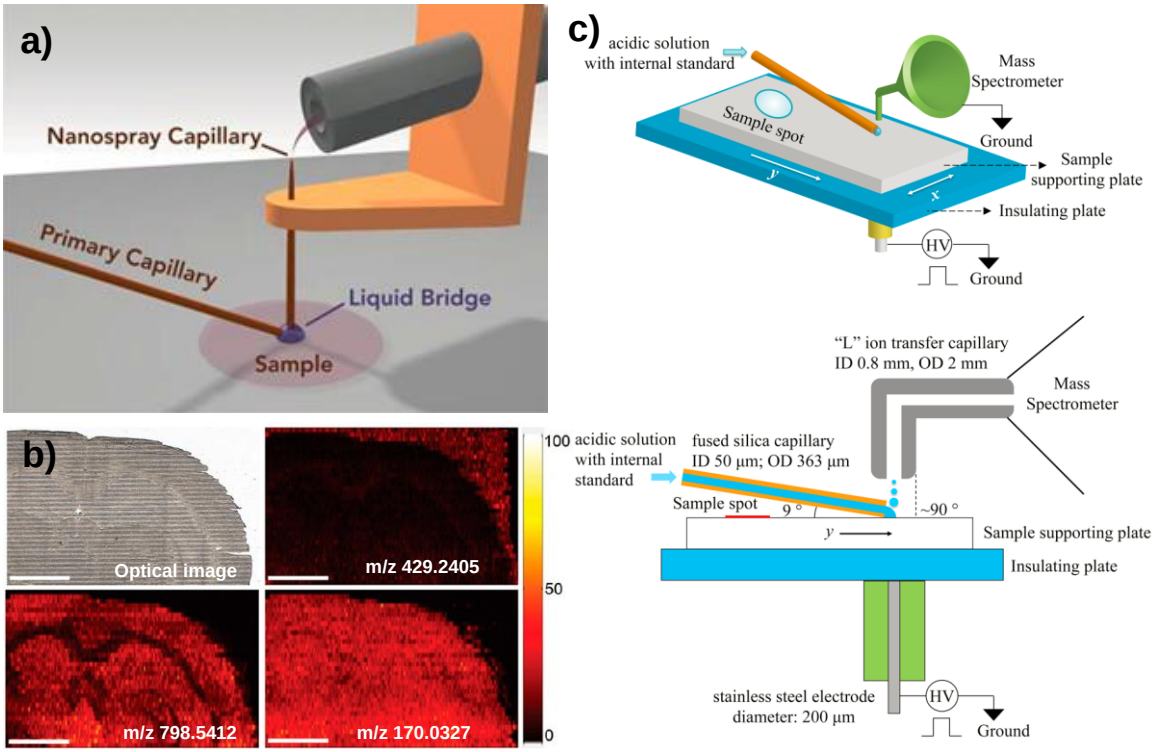

Figure 1.30 **a)** Illustration of nano-DESI setup. Adapted from (P.J. Roach, J. Laskin, A. Laskin, Analyst, 135, 2233-2236 (2010)) with permission of The Royal Society of Chemistry. **b)** An example of nano-DESI imaging data collected on coronal rat brain tissue section. Adapted with permission from (I. Lanekoff, B.S. Heath, A. Liyu, M. Thomas, J.P. Carson, J. Laskin, Anal. Chem., 84, 8351-8356 (2012)). Copyright (2012) American Chemical Society. **c)** ESTASI imaging setup. Adapted with permission from (L. Qiao, E. Tobolkina, A. Lesch, A. Bondarenko, X. Zhong, B. Liu, H.M. Pick, H. Vogel, H.H. Girault, Anal. Chem., (2014)). Copyright (2014) American Chemical Society.

MSI with a high spatial resolution of 12 μm.[400] Nano-DESI MSI was successfully performed on rat brain sections where several lipids were identified on tissue with no sample pre-treatment, corroborating results previously reported in MALDI, DESI or IR-MALDESI (LAESI) experiments. An improved automated nano-DESI imaging platform using computer vision to maintain a constant probe-sample distance was also proposed to control the signal stability and spatial resolution.[401] Nano-DESI images of a coronal section of rat brain tissue collected with that system are presented in **Figure 1.30b**. Among other applications, nano-DESI was used to determine the spatial distribution of drugs and metabolites in nicotine dosed mice brains, while adding an isotopically labeled standard to the nano-DESI solvent to reduce the ion suppression effect on the analyte signal.[402]

1.2.5.12 Electrostatic Spray Ionization (ESTASI)

Electrostatic-Spray Ionization Mass Spectrometry (ESTASI) is a relatively recent ionization technique, where a switched controlled high voltage RC circuit is used to generate alternating pulsed spray of cations and anions from a sample placed on an insulator plate or emitter of different geometries. An electronic circuit and control system used for the ESTASI MS setup has been described in great detail by Qiao et al.[403,404] Direct analysis by ESTASI MS has been coupled to gel electrophoresis for peptide/protein detection.[403] The technique was also used for fingerprinting characterization of perfume fragrance from paper surface.[405] ESTASI MS imaging was recently reported[406] where a wetting capillary was used to deposit

an acidic extraction solvent/internal standard mixture directly on the sample surface (**Figure 1.30c**). Imaging of spotted protein and peptide solutions, inkjet-printed dye as well as melanoma cells on Petri dish was reported. The spatial resolution, which strongly depends on the dimensions of the wetting capillary, was measured at 110 μm.

1.2.5.13 Desorption Atmospheric Pressure Chemical Ionization (DAPCI)

Desorption Atmospheric Pressure Chemical Ionization (DAPCI) was first introduced to help elucidate the ionization mechanisms leading to the formation of gas phase ions using the DESI technique.[407] The ESI capillary was then replaced by a tapered conductor so that, instead of emitting solvent droplets through electrospray mechanisms, gas phase ions were generated by corona discharge ionization in the reagent rich nebulizing gas. Ionization of analyte molecules then occurs by electron or proton transfer chemical ionization in the gas phase. DAPCI was found to be a suitable DESI alternative for the analysis of less polar compounds.[408] It was also shown that DAPCI could be performed without the use of any nebulizing gas while still obtaining great sensitivity, making it convenient for the analysis of volatile powder or for other applications where use of a nebulizing gas is detrimental or prohibited.[409] So far, DAPCI MS has been reported for the direct analysis of several biological and pharmaceutical compounds.[410-413] It was recently demonstrated that DAPCI MS imaging can be used for the forensic examination of handwritten or stamped inks.[414] It was shown that this non-destructive technique

can be used to study the aging of hand writing and has potential use as tool for differentiating documents that have been altered. It was also shown that the ink compound distribution in the lettering, which depends on pen pressure and speed, could be used to discriminate forged signature from the original. DAPCI MS was performed with an estimated spatial resolution of 140 μm.

1.3 Synopsis of Completed Research

The ability to ionize molecules under atmospheric pressure conditions for subsequent mass analysis has significant impact on applications including direct analysis and molecular imaging. Because of this, over the last decade there have been significant developments in ambient mass spectrometry with a large number of novel ionization methods being introduced in the literature every year. One such method, developed in the research laboratory of Dr. David C. Muddiman, combines features and attributes of the two most widely used ionization sources in biological mass spectrometry into a single source, MALDESI. **Chapter 2** describes the incorporation of an infrared laser into the MALDESI source to allow for the use of water as the energy absorbing matrix. Along the development of a novel ionization source there are a number of geometrical parameters which can greatly influence the observed signal and a majority of these parameters, including voltages and distances, can influence each other as well. In order to systematically explore this vast experimental space a Design of Experiments (DOE) was used. Upon optimization of these parameters, an improvement of over four orders of magnitude

was realized in the lowest detectable signal of cytochrome c desorbed from an aqueous solution.

After optimizing the source parameters and developing an ionization source that was capable of performing mass spectrometry imaging, the IR-MALDESI source was used to assess the distribution of lapatinib in the liver tissue of a dosed animal. **Chapter 3** describes this process in detail and, in addition, presents a comparison with UV-MALDI imaging data (the most commonly used ionization source for mass spectrometry imaging) from a serial section. It was determined that both techniques provide similar results, however, IR-MALDESI has the added benefits of an atmospheric pressure ionization source including minimal sample handling.

One of the issues with coupling the IR-MALDESI source to a mass spectrometer (LTQ-FT) that was never intended for use with a pulsed ionization source is a reduced applicability of some of the instrument's features. The LTQ-FT utilizes automatic gain control (AGC) to maintain a consistent number of ions in the ICR cell in order to allow for external mass calibration providing part per million mass accuracy. This AGC feature works well for continuous ionization sources that provide a constant flux of ions but it fails to work when ions are generated in discreet packets as is the case with the pulsed nature of the IR-MALDESI source. Because of this, the AGC feature must be turned off which results in fluctuations in mass accuracy that correlate with the total ion abundance. **Chapter 4** describes a recalibration procedure that accounts for these systematic fluctuations in mass accuracy. This recalibration routine allows for mass measurement accuracies of

within 1 part per million over the course of an imaging experiment which is well within the specifications for the mass spectrometer operating under normal conditions.

Along with developments in ionization sources, the past decade has provided a significant number of improvements in mass spectrometry instrumentation. The orbital trapping technology provides quality mass information that is analogous to what can be obtained from an FT-ICR instrument but in a fraction of the time and often times with improved sensitivity. **Chapter 5** summarizes the coupling of the IR-MALDSI source with one such orbital trapping instrument, the Q Exactive. To demonstrate the utility of this combination, serial sections of tissues that had been incubated in a high or low concentration of three antiretroviral drugs were analyzed by IR-MALDESI MSI or by a validated LC-MS/MS MRM assay. Using isotope dilution techniques, the MRM assay was used to quantify the exact amount of each drug from each tissue section. The relative abundances of the low to high concentration tissues for each drug as determined by IR-MALDESI MSI was found to correlate well with the exact quantities determined by the MRM assay. This correlation has implications into the potential to obtained quantitative information directly from the IR-MALDESI MSI experiment.

In addition to applications in mass spectrometry imaging, the IR-MALDESI source also displays significant potential towards direct analysis. **Chapter 6** describes one such application for the direct analysis of dyed fabrics. Traditional approaches to characterizing trace fiber evidence utilize qualitative measures of the

properties of the dye and fiber. However, these methods will not provide an accurate determination of the actual dye that is present in the fiber which can be an important distinguishing factor. The IR-MALDESI method was thus used to ablate a small portion of the fabric allowing for determination of the dye as well as the fiber polymer in some cases.

1.4 References

(1) Davis, D. V.; Cooks, R. G.; Meyer, B. N.; McLaughlin, J. L. Identification of naturally occurring quaternary compounds by combined laser desorption and tandem mass spectrometry. *Anal. Chem.* **1983**, *55*(8), 1302-1305.

(2) Wright, L. G.; Cooks, R. G.; Wood, K. V. Matrix enhanced laser desorption in mass spectrometry and tandem mass spectrometry. *Biol. Mass Spectrom.* **1985**, *12*(4), 159-162.

(3) Karas, M.; Bachmann, D.; Hillenkamp, F. Influence of the wavelength in high-irradiance ultraviolet laser desorption mass spectrometry of organic molecules. *Anal. Chem.* **1985**, *57*(14), 2935-2939.

(4) Karas, M.; Bachmann, D.; Bahr, U.; Hillenkamp, F. Matrix-assisted ultraviolet laser desorption of non-volatile compounds. *Int. J. Mass Spectrom. Ion Processes* **1987**, *78*(0), 53-68.

(5) Karas, M.; Hillenkamp, F. Laser desorption ionization of proteins with molecular masses exceeding 10,000 daltons. *Anal. Chem.* **1988**, *60*(20), 2299-2301.

(6) Tanaka, K.; Waki, H.; Ido, Y.; Akita, S.; Yoshida, Y.; Yoshida, T.; Matsuo, T. Protein and polymer analyses up to m/z 100 000 by laser ionization time-of-flight mass spectrometry. *Rapid Commun. Mass Spectrom.* **1988**, *2*(8), 151-153.

(7) Karas, M.; Bahr, U.; Hillenkamp, F. UV laser matrix desorption/ionization mass spectrometry of proteins in the 100 000 dalton range. *Int. J. Mass Spectrom. Ion Processes* **1989**, *92*(0), 231-242.

(8) Thomson, J. J. LXXXIII. Rays of positive electricity. *Philosophical Magazine Series 6* **1910**, *20*(118), 752-767.

(9) Herzog, R. F. K.; Viehböck, F. P. Ion Source for Mass Spectrography. *PhRv* **1949**, *76*(6), 855-856.

(10) Honig, R. E.; Woolston, J. R. Laser-Induced Emission of Electrons, Ions, and Neutral Atoms from Solid Surfaces. *Appl. Phys. Lett.* **1963**, *2*(7), 138-139.

(11) Fenner, N. C.; Daly, N. R. Laser Used for Mass Analysis. *Rev. Sci. Instrum.* **1966**, *37*(8), 1068-1070.

(12) Vastola, F. J.; Mumma, R. O.; Pirone, A. J. Analysis of organic salts by laser ionization. *Org. Mass Spectrom.* **1970**, *3*(1), 101-104.

(13) Posthumus, M. A.; Kistemaker, P. G.; Meuzelaar, H. L. C.; Ten Noever de Brauw, M. C. Laser desorption-mass spectrometry of polar nonvolatile bio-organic molecules. *Anal. Chem.* **1978**, *50*(7), 985-991.

(14) Levis, R. J. Laser Desorption and Ejection of Biomolecules From the Condensed Phase into the Gas Phase. *Annu. Rev. Phys. Chem.* **1994**, *45*(1), 483-518.

(15) Vertes, A.; Levine, R. D. Sublimation versus fragmentation in matrix-assisted laser desorption. *Chem. Phys. Lett.* **1990**, *171*(4), 284-290.

(16) Vertes, A.; Gijbels, R.; Levine, R. D. Homogeneous bottleneck model of matrix-assisted ultraviolet laser desorption of large molecules. *Rapid Commun. Mass Spectrom.* **1990**, *4*(6), 228-233.

(17) Johnson, R. E. Models for matrix-assisted desorption by a laser-pulse. *Int. J. Mass Spectrom. Ion Processes* **1994**, *139*(0), 25-38.

(18) Ehring, H.; Karas, M.; Hillenkamp, F. Role of photoionization and photochemistry in ionization processes of organic molecules and relevance for matrix-assisted laser desorption Ionization mass spectrometry. *Org. Mass Spectrom.* **1992**, *27*(4), 472-480.

(19) Karas, M.; Glückmann, M.; Schäfer, J. Ionization in matrix-assisted laser desorption/ionization: singly charged molecular ions are the lucky survivors. *J. Mass Spectrom.* **2000**, *35*(1), 1-12.

(20) Jaskolla, T.; Karas, M. Compelling Evidence for Lucky Survivor and Gas Phase Protonation: The Unified MALDI Analyte Protonation Mechanism. *J. Am. Soc. Mass Spectrom.* **2011**, *22*(6), 976-988.

(21) Beavis, R. C.; Chait, B. T. High-accuracy molecular mass determination of proteins using matrix-assisted laser desorption mass spectrometry. *Anal. Chem.* **1990**, *62*(17), 1836-1840.

(22) Szájli, E.; Fehér, T.; Medzihradszky, K. F. Investigating the Quantitative Nature of MALDI-TOF MS. *Mol. Cell. Proteomics* **2008**, *7*(12), 2410-2418.

(23) Knochenmuss, R.; Dubois, F.; Dale, M. J.; Zenobi, R. The Matrix Suppression Effect and Ionization Mechanisms in Matrix-assisted Laser

Desorption/Ionization. *Rapid Commun. Mass Spectrom.* **1996**, *10*(8), 871-877.

(24) Knochenmuss, R.; Karbach, V.; Wiesli, U.; Breuker, K.; Zenobi, R. The matrix suppression effect in matrix-assisted laser desorption/ionization: application to negative ions and further characteristics. *Rapid Commun. Mass Spectrom.* **1998**, *12*(9), 529-534.

(25) Lou, X.; van Dongen, J. L. J.; Vekemans, J. A. J. M.; Meijer, E. W. Matrix suppression and analyte suppression effects of quaternary ammonium salts in matrix-assisted laser desorption/ionization time-of-flight mass spectrometry: an investigation of suppression mechanism. *Rapid Commun. Mass Spectrom.* **2009**, *23*(19), 3077-3082.

(26) Mowry, C. D.; Johnston, M. V. Internal Energy of Neutral Molecules Ejected by Matrix-Assisted Laser Desorption. *The Journal of Physical Chemistry* **1994**, *98*(7), 1904-1909.

(27) Puretzky, A. A.; Geohegan, D. B. Gas-phase diagnostics and LIF-imaging of 3-hydroxypicolinic acid maldi-matrix plumes. *Chem. Phys. Lett.* **1998**, *286*(5–6), 425-432.

(28) Zenobi, R.; Knochenmuss, R. Ion formation in MALDI mass spectrometry. *Mass Spectrom. Rev.* **1998**, *17*(5), 337-366.

(29) Dole, M.; Mack, L. L.; Hines, R. L. Molecular Beams of Macroions. *J. Chem. Phys.* **1968**, *49*(5), 2240-&.

(30) Yamashita, M.; Fenn, J. B. Electrospray ion source. Another variation on the free-jet theme. *The Journal of Physical Chemistry* **1984**, *88*(20), 4451-4459.

(31) Yamashita, M.; Fenn, J. B. Negative ion production with the electrospray ion source. *The Journal of Physical Chemistry* **1984**, *88*(20), 4671-4675.

(32) Wong, S. F.; Meng, C. K.; Fenn, J. B. Multiple charging in electrospray ionization of poly(ethylene glycols). *The Journal of Physical Chemistry* **1988**, *92*(2), 546-550.

(33) Whitehouse, C. M.; Dreyer, R. N.; Yamashita, M.; Fenn, J. B. Electrospray interface for liquid chromatographs and mass spectrometers. *Anal. Chem.* **1985**, *57*(3), 675-679.

(34) Meng, C. K.; Mann, M.; Fenn, J. B. Of protons or proteins. *Zeitschrift für Physik D Atoms, Molecules and Clusters* **1988**, *10*(2), 361-368.

(35) Fenn, J. B.; Mann, M.; Meng, C. K.; Wong, S. F.; Whitehouse, C. M. Electrospray Ionization for Mass Spectrometry of Large Biomolecules. *Sci* **1989**, *246*(4926), 64-71.

(36) http://www.nobelprize.org/nobel_prizes/chemistry/laureates/2002/

(37) Rayleigh, L. XXVI. On the electrical capacity of approximate spheres and cylinders. *Philosophical Magazine Series 6* **1916**, *31*(183), 177-186.

(38) Zeleny, J. The Electrical Discharge from Liquid Points, and a Hydrostatic Method of Measuring the Electric Intensity at Their Surfaces. *PhRv* **1914**, *3*(2), 69-91.

(39) Zeleny, J. On the conditions of instability of electrified drops, with applications to the electric discharge from liquid points. *Proceedings of the Cambridge Philosophical Society* **1915**, *18*71–83.

(40) Zeleny, J. Instability of Electrified Liquid Surfaces. *PhRv* **1917**, *10*(1), 1-6.

(41) Wilson, C. T. R.; Taylor, G. I. The bursting of soap-bubbles in a uniform electric field. *MPCPS* **1925**, *22*(05), 728-730.

(42) Nolan, J. J. The Breaking of Water Drops by Electric Fields. *Proceedings of the Royal Irish Academy, Section A: Mathematical and Physical Sciences* **1926**, *38*28-39.

(43) Macky, W. A. Some Investigations on the Deformation and Breaking of Water Drops in Strong Electric Fields. *Proceedings of the Royal Society of London. Series A* **1931**, *133*(822), 565-587.

(44) Brazier-Smith, P. R. The stability of a water drop oscillating with finite amplitude in an electric field. *J. Fluid Mech.* **1971**, *50*(03), 417-430.

(45) Nolan, J. J. The Nature of the Ions Produced by the Spraying of Water. *Proceedings of the Royal Society of London. Series A* **1918**, *94*(658), 112-136.

(46) Nolan, J. J. Ions Produced by Discharges at Liquid Surfaces. *Proceedings of the Royal Irish Academy, Section A: Mathematical and Physical Sciences* **1929**, *39*21.

(47) Nolan, J. J.; Nevin, T. E. The Effect of Water Vapour on Diffusion Coefficients and Mobilities of Ions in Air. *Proceedings of the Royal Society of London. Series A* **1930**, *127*(804), 155-174.

(48) Vonnegut, B.; Neubauer, R. L. Production of monodisperse liquid particles by electrical atomization. *J. Colloid Sci.* **1952**, *7*(6), 616-622.

(49) Drozin, V. G. The electrical dispersion of liquids as aerosols. *J. Colloid Sci.* **1955**, *10*(2), 158-164.

(50) Magarvey, R. H.; Outhouse, L. E. Note on the break-up of a charged liquid jet. *J. Fluid Mech.* **1962**, *13*(01), 151-157.

(51) Schneider, J. M.; Lindblad, N. R.; C. D. Hendricks, J.; Crowley, J. M. Stability of an Electrified Liquid Jet. *J. Appl. Phys.* **1967**, *38*(6), 2599-2605.

(52) Huebner, A. L. Disintegration of charged liquid jets. *J. Fluid Mech.* **1969**, *38*(04), 679-688.

(53) Huebner, A. L. Disintegration of Charged Liquid Jets: Results with Isopropyl Alcohol. *Sci* **1970**, *168*(3927), 118-119.

(54) Huebner, A. L.; Chu, H. N. Instability and breakup of charged liquid jets. *J. Fluid Mech.* **1971**, *49*(02), 361-372.

(55) Taylor, G. Disintegration of Water Drops in an Electric Field. *Proceedings of the Royal Society of London. Series A, Mathematical and Physical Sciences* **1964**, *280*(1382), 383-397.

(56) Tilney, R. Electrostatic coating processes. *BJAP* **1953**, *4*(S2), S51.

(57) Hines, R. L. Electrostatic Atomization and Spray Painting. *J. Appl. Phys.* **1966**, *37*(7), 2730-2736.

(58) Taylor, G. I.; McEwan, A. D. The stability of a horizontal fluid interface in a vertical electric field. *J. Fluid Mech.* **1965**, *22*(01), 1-15.

(59) Joffre, G. H.; Cloupeau, M. Characteristic forms of electrified menisci emitting charges. *J. Electrostatics* **1986**, *18*(2), 147-161.

(60) Cloupeau, M.; Prunet-Foch, B. Electrostatic spraying of liquids in cone-jet mode. *J. Electrostatics* **1989**, *22*(2), 135-159.

(61) Gañán-Calvo, A. M.; Dávila, J.; Barrero, A. Current and droplet size in the electrospraying of liquids. Scaling laws. *J. Aerosol Sci.* **1997**, *28*(2), 249-275.

(62) Meesters, G. M. H.; Vercoulen, P. H. W.; Marijnissen, J. C. M.; Scarlett, B. Generation of micron-sized droplets from the Taylor cone. *J. Aerosol Sci.* **1992**, *23*(1), 37-49.

(63) Wilm, M. S.; Mann, M. Electrospray and Taylor-Cone theory, Dole's beam of macromolecules at last? *Int. J. Mass Spectrom. Ion Processes* **1994**, *136*(2–3), 167-180.

(64) Wilm, M.; Mann, M. Analytical Properties of the Nanoelectrospray Ion Source. *Anal. Chem.* **1996**, *68*(1), 1-8.

(65) Doyle, A.; Moffett, D. R.; Vonnegut, B. Behavior of evaporating electrically charged droplets. *J. Colloid Sci.* **1964**, *19*(2), 136-143.

(66) Gomez, A.; Tang, K. Charge and fission of droplets in electrostatic sprays. *Phys. Fluids* **1994**, *6*(1), 404-414.

(67) Duft, D.; Achtzehn, T.; Muller, R.; Huber, B. A.; Leisner, T. Coulomb fission: Rayleigh jets from levitated microdroplets. *Nature* **2003**, *421*(6919), 128-128.

(68) Dole, M.; Hines, R. L.; Mack, L. L.; Mobley, R. C.; Ferguson, L. D.; Alice, M. B. Gas Phase Macroions. *Macromolecules* **1968**, *1*(1), 96-97.

(69) Röllgen, F., W.; Bramer-Weger, E.; Bütfering, L. FIELD ION EMISSION FROM LIQUID SOLUTIONS : ION EVAPORATION AGAINST ELECTROHYDRODYNAMIC DISINTEGRATION. *J. Phys. Colloques* **1987**, *48*(C6), C6-253-C6-256.

(70) Iribarne, J. V.; Thomson, B. A. On the evaporation of small ions from charged droplets. *J. Chem. Phys.* **1976**, *64*(6), 2287-2294.

(71) Thomson, B. A.; Iribarne, J. V. Field induced ion evaporation from liquid surfaces at atmospheric pressure. *J. Chem. Phys.* **1979**, *71*(11), 4451-4463.

(72) Iribarne, J. V.; Dziedzic, P. J.; Thomson, B. A. Atmospheric pressure ion evaporation-mass spectrometry. *Int. J. Mass Spectrom. Ion Phys.* **1983**, *50*(3), 331-347.

(73) Fernandez de la Mora, J. Electrospray ionization of large multiply charged species proceeds via Dole's charged residue mechanism. *Anal. Chim. Acta* **2000**, *406*(1), 93-104.

(74) Kebarle, P.; Peschke, M. On the mechanisms by which the charged droplets produced by electrospray lead to gas phase ions. *Anal. Chim. Acta* **2000**, *406*(1), 11-35.

(75) Ikonomou, M. G.; Blades, A. T.; Kebarle, P. Investigations of the electrospray interface for liquid chromatography/mass spectrometry. *Anal. Chem.* **1990**, *62*(9), 957-967.

(76) Sterner, J. L.; Johnston, M. V.; Nicol, G. R.; Ridge, D. P. Signal suppression in electrospray ionization Fourier transform mass spectrometry of multi-component samples. *J. Mass Spectrom.* **2000**, *35*(3), 385-391.

(77) Smith, R. D.; Loo, J. A.; Edmonds, C. G.; Barinaga, C. J.; Udseth, H. R. New developments in biochemical mass spectrometry: electrospray ionization. *Anal. Chem.* **1990**, *62*(9), 882-899.

(78) Page, J.; Kelly, R.; Tang, K.; Smith, R. Ionization and transmission efficiency in an electrospray ionization—mass spectrometry interface. *J. Am. Soc. Mass Spectrom.* **2007**, *18*(9), 1582-1590.

(79) Takáts, Z.; Wiseman, J. M.; Gologan, B.; Cooks, R. G. Mass Spectrometry Sampling Under Ambient Conditions with Desorption Electrospray Ionization. *Sci* **2004**, *306*(5695), 471-473.

(80) Weston, D. J. Ambient ionization mass spectrometry: current understanding of mechanistic theory; analytical performance and application areas. *Analyst* **2010**, *135*(4), 661-668.

(81) Cotter, R. J. Laser desorption chemical ionization mass spectrometry. *Anal. Chem.* **1980**, *52*(11), 1767-1770.

(82) Boesl, U.; Grotemeyer, J.; Walter, K.; Schlag, E. W. A High-Resolution Time-of-Flight Mass Spectrometer With Laser Desorption and a Laser Ionization Source. *Instrum. Sci. Technol.* **1987**, *16*(1), 151-171.

(83) Coon, J. J.; McHale, K. J.; Harrison, W. W. Atmospheric pressure laser desorption/chemical ionization mass spectrometry: a new ionization method based on existing themes. *Rapid Commun. Mass Spectrom.* **2002**, *16*(7), 681-685.

(84) Shiea, J.; Huang, M.-Z.; Hsu, H.-J.; Lee, C.-Y.; Yuan, C.-H.; Beech, I.; Sunner, J. Electrospray-assisted laser desorption/ionization mass spectrometry for direct ambient analysis of solids. *Rapid Commun. Mass Spectrom.* **2005**, *19*(24), 3701-3704.

(85) Sampson, J.; Hawkridge, A.; Muddiman, D. Generation and detection of multiply-charged peptides and proteins by matrix-assisted laser desorption electrospray ionization (MALDESI) fourier transform ion cyclotron resonance mass spectrometry. *J. Am. Soc. Mass Spectrom.* **2006**, *17*(12), 1712-1716.

(86) Huang, M.-Z.; Hsu, H.-J.; Lee, J.-Y.; Jeng, J.; Shiea, J. Direct Protein Detection from Biological Media through Electrospray-Assisted Laser Desorption Ionization/Mass Spectrometry. *J. Proteome Res.* **2006**, *5*(5), 1107-1116.

(87) Huang, M.-Z.; Hsu, H.-J.; Wu, C.-I.; Lin, S.-Y.; Ma, Y.-L.; Cheng, T.-L.; Shiea, J. Characterization of the chemical components on the surface of different solids with electrospray-assisted laser desorption ionization mass spectrometry. *Rapid Commun. Mass Spectrom.* **2007**, *21*(11), 1767-1775.

(88) Cheng, C.-Y.; Yuan, C.-H.; Cheng, S.-C.; Huang, M.-Z.; Chang, H.-C.; Cheng, T.-L.; Yeh, C.-S.; Shiea, J. Electrospray-Assisted Laser Desorption/Ionization Mass Spectrometry for Continuously Monitoring the States of Ongoing Chemical Reactions in Organic or Aqueous Solution under Ambient Conditions. *Anal. Chem.* **2008**, *80*(20), 7699-7705.

(89) Sampson, J.; Hawkridge, A.; Muddiman, D. Construction of a versatile high precision ambient ionization source for direct analysis and imaging. *J. Am. Soc. Mass Spectrom.* **2008**, *19*(10), 1527-1534.

(90) Rezenom, Y. H.; Dong, J.; Murray, K. K. Infrared laser-assisted desorption electrospray ionization mass spectrometry. *Analyst* **2008**, *133*(2), 226-232.

(91) Sampson, J. S.; Muddiman, D. C. Atmospheric pressure infrared (10.6 μm) laser desorption electrospray ionization (IR-LDESI) coupled to a LTQ Fourier transform ion cyclotron resonance mass spectrometer. *Rapid Commun. Mass Spectrom.* **2009**, *23*(13), 1989-1992.

(92) Sampson, J. S.; Murray, K. K.; Muddiman, D. C. Intact and Top-Down Characterization of Biomolecules and Direct Analysis Using Infrared Matrix-Assisted Laser Desorption Electrospray Ionization Coupled to FT-ICR Mass Spectrometry. *J. Am. Soc. Mass Spectrom.* **2009**, *20*(4), 667-673.

(93) Apitz, I.; Vogel, A., Jacques, S. L.; Duncan, D. D.; Kirkpatrick, S. J.; Kriete, A., Eds.; SPIE: San Jose, CA, USA, 2003, pp 48-59.

(94) Vogel, A.; Venugopalan, V. Kinetics of phase transitions in pulsed IR laser ablation of biological tissues. **2003**66-74.

(95) Peng, I. X.; Ogorzalek Loo, R. R.; Shiea, J.; Loo, J. A. Reactive-Electrospray-Assisted Laser Desorption/Ionization for Characterization of Peptides and Proteins. *Anal. Chem.* **2008**, *80*(18), 6995-7003.

(96) Shrestha, B.; Nemes, P.; Nazarian, J.; Hathout, Y.; Hoffman, E. P.; Vertes, A. Direct analysis of lipids and small metabolites in mouse brain tissue by AP IR-MALDI and reactive LAESI mass spectrometry. *Analyst* **2010**, *135*(4), 751-758.

(97) Dixon, R. B.; Sampson, J. S.; Hawkridge, A. M.; Muddiman, D. C. Ambient Aerodynamic Ionization Source for Remote Analyte Sampling and Mass Spectrometric Analysis. *Anal. Chem.* **2008**, *80*(13), 5266-5271.

(98) Dixon, R. B.; Muddiman, D. C. Study of the ionization mechanism in hybrid laser based desorption techniques. *Analyst* **2010**, *135*(5), 880-882.

(99) Nemes, P.; Vertes, A. Laser Ablation Electrospray Ionization for Atmospheric Pressure, in Vivo, and Imaging Mass Spectrometry. *Anal. Chem.* **2007**, *79*(21), 8098-8106.

(100) Nemes, P.; Huang, H.; Vertes, A. Internal energy deposition and ion fragmentation in atmospheric-pressure mid-infrared laser ablation electrospray ionization. *Phys. Chem. Chem. Phys.* **2012**, *14*(7), 2501-2507.

(101) Castaing, R.; Slodzian, G. Microanalysis by secondary ionic emission. *J. Microscopie* **1962**, *1*395-410.

(102) Pacholski, M. L.; Winograd, N. Imaging with Mass Spectrometry. *Chem. Rev.* **1999**, *99*(10), 2977-3006.

(103) Brunelle, A.; Laprevote, O. Recent Advances in Biological Tissue Imaging with Time-of-Flight Secondary Ion Mass Spectrometry: Polyatomic Ion Sources, Sample Preparation, and Applications. *Curr. Pharm. Des.* **2007**, *13*(32), 3335-3343.

(104) Rubakhin, S. S.; Jurchen, J. C.; Monroe, E. B.; Sweedler, J. V. Imaging mass spectrometry: fundamentals and applications to drug discovery. *Drug Discovery Today* **2005**, *10*(12), 823-837.

(105) Solon, E.; Schweitzer, A.; Stoeckli, M.; Prideaux, B. Autoradiography, MALDI-MS, and SIMS-MS Imaging in Pharmaceutical Discovery and Development. *The AAPS Journal* **2010**, *12*(1), 11-26.

(106) Spengler, B.; Hubert, M.; Kaufman, R. In *Proceedings of the 42nd Annual Conference on Mass Spectrometry and Allied Topics*: Chicago, Illinois, 1994, p 1041.

(107) Caprioli, R. M.; Farmer, T. B.; Gile, J. Molecular Imaging of Biological Samples: Localization of Peptides and Proteins Using MALDI-TOF MS. *Anal. Chem.* **1997**, *69*(23), 4751-4760.

(108) Chaurand, P.; Schwartz, S. A.; Reyzer, M. L.; Caprioli, R. M. Imaging Mass Spectrometry: Principles and Potentials. *Toxicol. Pathol.* **2005**, *33*(1), 92-101.

(109) McDonnell, L. A.; Heeren, R. M. A. Imaging mass spectrometry. *Mass Spectrom. Rev.* **2007**, *26*(4), 606-643.

(110) Heeren, R. M. A.; Smith, D. F.; Stauber, J.; Kükrer-Kaletas, B.; MacAleese, L. Imaging Mass Spectrometry: Hype or Hope? *J. Am. Soc. Mass Spectrom.* **2009**, *20*(6), 1006-1014.

(111) Balluff, B.; Schöne, C.; Höfler, H.; Walch, A. MALDI imaging mass spectrometry for direct tissue analysis: technological advancements and recent applications. *Histochem. Cell Biol.* **2011**, *136*(3), 227-244.

(112) Goodwin, R. J. A. Sample preparation for mass spectrometry imaging: Small mistakes can lead to big consequences. *J. Proteomics* **2012**, *75*(16), 4893-4911.

(113) Chaurand, P. Imaging mass spectrometry of thin tissue sections: A decade of collective efforts. *J. Proteomics* **2012**, *75*(16), 4883-4892.

(114) Jungmann, J. H.; Heeren, R. M. A. Emerging technologies in mass spectrometry imaging. *J. Proteomics* **2012**, *75*(16), 5077-5092.

(115) Römpp, A.; Spengler, B. Mass spectrometry imaging with high resolution in mass and space. *Histochem. Cell Biol.* **2013**, *139*(6), 759-783.

(116) Reyzer, M. L.; Caprioli, R. M. MALDI-MS-based imaging of small molecules and proteins in tissues. *Curr. Opin. Chem. Biol.* **2007**, *11*(1), 29-35.

(117) Svatoš, A. Mass spectrometric imaging of small molecules. *Trends Biotechnol.* **2010**, *28*(8), 425-434.

(118) Burnum, K. E.; Frappier, S. L.; Caprioli, R. M. Matrix-Assisted Laser Desorption/Ionization Imaging Mass Spectrometry for the Investigation of Proteins and Peptides. *Annu. Rev. Anal. Chem.* **2008**, *1*(1), 689-705.

(119) Goodwin, R. J. A.; Pennington, S. R.; Pitt, A. R. Protein and peptides in pictures: Imaging with MALDI mass spectrometry. *Proteomics* **2008**, *8*(18), 3785-3800.

(120) Cillero-Pastor, B.; Heeren, R. M. A. Matrix-Assisted Laser Desorption Ionization Mass Spectrometry Imaging for Peptide and Protein Analyses: A Critical Review of On-Tissue Digestion. *J. Proteome Res.* **2014**, *13*(2), 325-335.

(121) Fernández, J.; Ochoa, B.; Fresnedo, O.; Giralt, M.; Rodríguez-Puertas, R. Matrix-assisted laser desorption ionization imaging mass spectrometry in lipidomics. *Anal. Bioanal. Chem.* **2011**, *401*(1), 29-51.

(122) Murphy, R. C.; Merrill Jr, A. H. Lipidomics and Imaging Mass Spectrometry. *Biochimica et Biophysica Acta (BBA) - Molecular and Cell Biology of Lipids* **2011**, *1811*(11), 635-636.

(123) Goto-Inoue, N.; Hayasaka, T.; Zaima, N.; Setou, M. Imaging mass spectrometry for lipidomics. *Biochimica et Biophysica Acta - Molecular and Cell Biology of Lipids* **2011**, *1811*(11), 961-969.

(124) Touboul, D.; Brunelle, A.; Laprévote, O. Mass spectrometry imaging: Towards a lipid microscope? *Biochimie* **2011**, *93*(1), 113-119.

(125) Rudin, M.; Weissleder, R. Molecular imaging in drug discovery and development. *Nat Rev Drug Discov* **2003**, *2*(2), 123-131.

(126) Rudin, M.; Rausch, M.; Stoeckli, M. Molecular Imaging in Drug Discovery and Development: Potential and Limitations of Nonnuclear Methods. *Mol. Imag. Biol.* **2005**, *7*(1), 5-13.

(127) Castellino, S.; Groseclose, M. R.; Wagner, D. MALDI imaging mass spectrometry: bridging biology and chemistry in drug development. *Bioanalysis* **2011**, *3*(21), 2427-2441.

(128) Greer, T.; Sturm, R.; Li, L. Mass spectrometry imaging for drugs and metabolites. *J. Proteomics* **2011**, *74*(12), 2617-2631.

(129) Cooks, R. G.; Ouyang, Z.; Takats, Z.; Wiseman, J. M. Ambient Mass Spectrometry. *Sci* **2006**, *311*(5767), 1566-1570.

(130) Van Berkel, G. J.; Pasilis, S. P.; Ovchinnikova, O. Established and emerging atmospheric pressure surface sampling/ionization techniques for mass spectrometry. *J. Mass Spectrom.* **2008**, *43*(9), 1161-1180.

(131) Chen, H.; Gamez, G.; Zenobi, R. What can we learn from ambient ionization techniques? *J. Am. Soc. Mass Spectrom.* **2009**, *20*(11), 1947-1963.

(132) Covey, T. R.; Thomson, B. A.; Schneider, B. B. Atmospheric pressure ion sources. *Mass Spectrom. Rev.* **2009**, *28*(6), 870-897.

(133) Wu, C.; Dill, A. L.; Eberlin, L. S.; Cooks, R. G.; Ifa, D. R. Mass spectrometry imaging under ambient conditions. *Mass Spectrom. Rev.* **2013**, *32*(3), 218-243.

(134) Lorenz, M.; Ovchinnikova, O. S.; Kertesz, V.; Van Berkel, G. J. Laser microdissection and atmospheric pressure chemical ionization mass spectrometry coupled for multimodal imaging. *Rapid Commun. Mass Spectrom.* **2013**, *27*(13), 1429-1436.

(135) Campbell, D. I.; Ferreira, C. R.; Eberlin, L. S.; Cooks, R. G. Improved spatial resolution in the imaging of biological tissue using desorption electrospray ionization. *Anal. Bioanal. Chem.* **2012**, *404*(2), 389-98.

(136) Jurchen, J. C.; Rubakhin, S. S.; Sweedler, J. V. MALDI-MS imaging of features smaller than the size of the laser beam. *J. Am. Soc. Mass Spectrom.* **2005**, *16*(10), 1654-1659.

(137) Colliver, T. L.; Brummel, C. L.; Pacholski, M. L.; Swanek, F. D.; Ewing, A. G.; Winograd, N. Atomic and molecular imaging at the single-cell level with TOF-SIMS. *Anal Chem* **1997**, *69*(13), 2225-31.

(138) Luxembourg, S. L.; Mize, T. H.; McDonnell, L. A.; Heeren, R. M. High-spatial resolution mass spectrometric imaging of peptide and protein distributions on a surface. *Anal. Chem.* **2004**, *76*(18), 5339-44.

(139) Li, Y.; Shrestha, B.; Vertes, A. Atmospheric Pressure Molecular Imaging by Infrared MALDI Mass Spectrometry. *Anal. Chem.* **2007**, *79*(2), 523-532.

(140) Martens, L.; Chambers, M.; Sturm, M.; Kessner, D.; Levander, F.; Shofstahl, J.; Tang, W. H.; Rompp, A.; Neumann, S.; Pizarro, A. D.; Montecchi-Palazzi, L.; Tasman, N.; Coleman, M.; Reisinger, F.; Souda, P.; Hermjakob, H.; Binz, P. A.; Deutsch, E. W. mzML--a community standard for mass spectrometry data. *Mol. Cell. Proteomics* **2011**, *10*(1), R110 000133.

(141) Pedrioli, P. G.; Eng, J. K.; Hubley, R.; Vogelzang, M.; Deutsch, E. W.; Raught, B.; Pratt, B.; Nilsson, E.; Angeletti, R. H.; Apweiler, R.; Cheung, K.; Costello, C. E.; Hermjakob, H.; Huang, S.; Julian, R. K.; Kapp, E.; McComb, M. E.; Oliver, S. G.; Omenn, G.; Paton, N. W.; Simpson, R.; Smith, R.; Taylor, C. F.; Zhu, W.; Aebersold, R. A common open representation of mass spectrometry data and its application to proteomics research. *Nat. Biotechnol.* **2004**, *22*(11), 1459-66.

(142) Schramm, T.; Hester, A.; Klinkert, I.; Both, J. P.; Heeren, R. M.; Brunelle, A.; Laprevote, O.; Desbenoit, N.; Robbe, M. F.; Stoeckli, M.; Spengler, B.; Rompp, A. imzML - A common data format for the flexible exchange and processing of mass spectrometry imaging data. *J. Proteomics* **2012**, *75*(16), 5106-10.

(143) Römpp, A. S., T.; Hester, A.; Klinkert, I.; Heeren, R.; Stöckli, M.; et al. *Data Mining in Proteomics*; Humana Press: New York, 2010.

(144) Race, A. M.; Styles, I. B.; Bunch, J. Inclusive sharing of mass spectrometry imaging data requires a converter for all. *J Proteomics* **2012**, *75*(16), 5111-2.

(145) Kessner, D.; Chambers, M.; Burke, R.; Agus, D.; Mallick, P. ProteoWizard: open source software for rapid proteomics tools development. *Bioinformatics* **2008**, *24*(21), 2534-6.

(146) Robichaud, G.; Garrard, K.; Barry, J.; Muddiman, D. MSiReader: An Open-Source Interface to View and Analyze High Resolving Power MS Imaging Files on Matlab Platform. *J. Am. Soc. Mass Spectrom.* **2013**, *24*(5), 718-721.

(147) Stoeckli, M.; Staab, D.; Staufenbiel, M.; Wiederhold, K. H.; Signor, L. Molecular imaging of amyloid beta peptides in mouse brain sections using mass spectrometry. *Anal. Biochem.* **2002**, *311*(1), 33-39.

(148) Parry, R. M.; Galhena, A. S.; Gamage, C. M.; Bennett, R. V.; Wang, M. D.; Fernández, F. M. OmniSpect: An Open MATLAB-Based Tool for Visualization and Analysis of Matrix-Assisted Laser Desorption/Ionization and Desorption Electrospray Ionization Mass Spectrometry Images. *J. Am. Soc. Mass Spectrom.* **2013**1-4.

(149) http://www.amolf.nl/download/datacubeexplorer/

(150) Hillenkamp, F.; Unsold, E.; Kaufmann, R.; Nitsche, R. Laser Microprobe Mass Analysis of Organic Materials. *Nature* **1975**, *256*(5513), 119-120.

(151) Laiko, V. V.; Burlingame, A. L. Atmospheric pressure matrix assisted laser desorption. 5965884, **1999**.

(152) Wolfender, J.-L.; Chu, F.; Ball, H.; Wolfender, F.; Fainzilber, M.; Baldwin, M. A.; Burlingame, A. L. Identification of tyrosine sulfation in Conus pennaceus conotoxins α-PnIA and α-PnIB: further investigation of labile sulfo- and phosphopeptides by electrospray, matrix-assisted laser desorption/ionization (MALDI) and atmospheric pressure MALDI mass spectrometry. *J. Mass Spectrom.* **1999**, *34*(4), 447-454.

(153) Laiko, V. V.; Baldwin, M. A.; Burlingame, A. L. Atmospheric Pressure Matrix-Assisted Laser Desorption/Ionization Mass Spectrometry. *Anal. Chem.* **2000**, *72*(4), 652-657.

(154) Doroshenko, V. M.; Laiko, V. V.; Taranenko, N. I.; Berkout, V. D.; Lee, H. S. Recent developments in atmospheric pressure MALDI mass spectrometry. *Int. J. Mass Spectrom.* **2002**, *221*(1), 39-58.

(155) Tan, P. V.; Laiko, V. V.; Doroshenko, V. M. Atmospheric Pressure MALDI with Pulsed Dynamic Focusing for High-Efficiency Transmission of Ions into a Mass Spectrometer. *Anal. Chem.* **2004**, *76*(9), 2462-2469.

(156) Berkout, V. D.; Kryuchkov, S. I.; Doroshenko, V. M. Modeling of ion processes in atmospheric pressure matrix-assisted laser desorption/ionisation. *Rapid Commun. Mass Spectrom.* **2007**, *21*(13), 2046-2050.

(157) Galicia, M. C.; Vertes, A.; Callahan, J. H. Atmospheric Pressure Matrix-Assisted Laser Desorption/Ionization in Transmission Geometry. *Anal. Chem.* **2002**, *74*(8), 1891-1895.

(158) Trimpin, S.; Herath, T. N.; Inutan, E. D.; Cernat, S. A.; Miller, J. B.; Mackie, K.; Walker, J. M. Field-free transmission geometry atmospheric pressure matrix-assisted laser desorption/ionization for rapid analysis of unadulterated tissue samples. *Rapid Commun. Mass Spectrom.* **2009**, *23*(18), 3023-3027.

(159) Laiko, V.; Taranenko, N.; Berkout, V.; Yakshin, M.; Prasad, C.; Lee, H.; Doroshenko, V. Desorption/ionization of biomolecules from aqueous solutions at atmospheric pressure using an infrared laser at 3 μm. *J. Am. Soc. Mass Spectrom.* **2002**, *13*(4), 354-361.

(160) Von Seggern, C. E.; Moyer, S. C.; Cotter, R. J. Liquid Infrared Atmospheric Pressure Matrix-Assisted Laser Desorption/Ionization Ion Trap Mass Spectrometry of Sialylated Carbohydrates. *Anal. Chem.* **2003**, *75*(13), 3212-3218.

(161) Turney, K.; Harrison, W. W. Liquid supports for ultraviolet atmospheric pressure matrix-assisted laser desorption/ionization. *Rapid Commun. Mass Spectrom.* **2004**, *18*(6), 629-635.

(162) Nelson, R.; Rainbow, M.; Lohr, D.; Williams, P. Volatilization of high molecular weight DNA by pulsed laser ablation of frozen aqueous solutions. *Sci* **1989**, *246*(4937), 1585-1587.

(163) Becker, C. H.; Jusinski, L. E.; Moro, L. Infrared laser-induced desorption of neutral organic compounds from frozen aqueous solution followed by single-photon ionization. *Int. J. Mass Spectrom. Ion Processes* **1990**, *95*(3), R1-R4.

(164) Williams, P. Time of flight mass spectrometry of DNA laser-ablated from frozen aqueous solutions: applications to the Human Genome Project. *International Journal of Mass Spectrometry and Ion Processes* **1994**, *131*335-344.

(165) Berkenkamp, S.; Karas, M.; Hillenkamp, F. Ice as a matrix for IR-matrix-assisted laser desorption/ionization: mass spectra from a protein single crystal. *Proc. Natl. Acad. Sci. U. S. A.* **1996**, *93*(14), 7003-7.

(166) Hunter, J. M.; Lin, H.; Becker, C. H. Cryogenic Frozen Solution Matrixes for Analysis of DNA by Time-of-Flight Mass Spectrometry. *Anal. Chem.* **1997**, *69*(17), 3608-3612.

(167) Kraft, P.; Alimpiev, S.; Dratz, E.; Sunner, J. Infrared, surface-assisted laser desorption ionization mass spectrometry on frozen aqueous solutions of proteins and peptides using suspensions of organic solids. *J. Am. Soc. Mass Spectrom.* **1998**, *9*(9), 912-924.

(168) Sheffer, J. D.; Murray, K. K. Infrared matrix-assisted laser desorption/ionization using a frozen alcohol matrix. *J. Mass Spectrom.* **2000**, *35*(1), 95-97.

(169) Naito, Y.; Miyabayashi, K.; Tsujimoto, K. Development of cryostage for matrix-assisted laser desorption/ionization Fourier transform ion cyclotron resonance mass spectrometry. *Int. J. Mass Spectrom.* **2002**, *221*(2), 83-92.

(170) Berry, J. I.; Sun, S.; Dou, Y.; Wucher, A.; Winograd, N. Laser Desorption and Imaging of Proteins from Ice via UV Femtosecond Laser Pulses. *Anal. Chem.* **2003**, *75*(19), 5146-5151.

(171) Von Seggern, C. E.; Gardner, B. D.; Cotter, R. J. Infrared Atmospheric Pressure MALDI Ion Trap Mass Spectrometry of Frozen Samples Using a Peltier-Cooled Sample Stage. *Anal. Chem.* **2004**, *76*(19), 5887-5893.

(172) Perdian, D. C.; Schieffer, G. M.; Houk, R. S. Atmospheric pressure laser desorption/ionization of plant metabolites and plant tissue using colloidal graphite. *Rapid Commun. Mass Spectrom.* **2010**, *24*(4), 397-402.

(173) Keough, T.; Lacey, M. P.; Strife, R. J. Atmospheric pressure matrix-assisted laser desorption/ionization ion trap mass spectrometry of sulfonic acid derivatized tryptic peptides. *Rapid Commun. Mass Spectrom.* **2001**, *15*(23), 2227-2239.

(174) Moyer, S. C.; Cotter, R. J.; Woods, A. S. Fragmentation of phosphopeptides by atmospheric pressure MALDI and ESI/ion trap mass spectrometry. *J. Am. Soc. Mass Spectrom.* **2002**, *13*(3), 274-283.

(175) Moyer, S. C.; VonSeggern, C. E.; Cotter, R. J. Fragmentation of cationized phosphotyrosine containing peptides by atmospheric pressure MALDI/Ion trap mass spectrometry. *J. Am. Soc. Mass Spectrom.* **2003**, *14*(6), 581-592.

(176) Von Seggern, C. E.; Zarek, P. E.; Cotter, R. J. Fragmentation of Sialylated Carbohydrates Using Infrared Atmospheric Pressure MALDI Ion Trap Mass Spectrometry from Cation-Doped Liquid Matrixes. *Anal. Chem.* **2003**, *75*(23), 6523-6530.

(177) Von Seggern, C. E.; Cotter, R. J. Fragmentation studies of noncovalent sugar–sugar complexes by infrared atmospheric pressure MALDI. *J. Am. Soc. Mass Spectrom.* **2003**, *14*(10), 1158-1165.

(178) Von Seggern, C. E.; Cotter, R. J. Study of peptide–sugar non-covalent complexes by infrared atmospheric pressure matrix-assisted laser desorption/ionization. *J. Mass Spectrom.* **2004**, *39*(7), 736-742.

(179) Gabelica, V.; Schulz, E.; Karas, M. Internal energy build-up in matrix-assisted laser desorption/ionization. *J. Mass Spectrom.* **2004**, *39*(6), 579-593.

(180) Konn, D. O.; Murrell, J.; Despeyroux, D.; Gaskell, S. J. Comparison of the Effects of Ionization Mechanism, Analyte Concentration, and Ion “Cool-Times” on the Internal Energies of Peptide Ions Produced by Electrospray and Atmospheric Pressure Matrix-Assisted Laser Desorption Ionization. *J. Am. Soc. Mass Spectrom.* **2005**, *16*(5), 743-751.

(181) Remes, P. M.; Glish, G. L. On The Time Scale of Internal Energy Relaxation of AP-MALDI and nano-ESI Ions in a Quadrupole Ion Trap. *J. Am. Soc. Mass Spectrom.* **2009**, *20*(10), 1801-1812.

(182) König, S.; Kollas, O.; Dreisewerd, K. Generation of Highly Charged Peptide and Protein Ions by Atmospheric Pressure Matrix-Assisted Infrared Laser Desorption/Ionization Ion Trap Mass Spectrometry. *Anal. Chem.* **2007**, *79*(14), 5484-5488.

(183) Jorabchi, K.; Westphall, M. S.; Smith, L. M. Charge Assisted Laser Desorption/Ionization Mass Spectrometry of Droplets. *J. Am. Soc. Mass Spectrom.* **2008**, *19*(6), 833-840.

(184) Sampson, J. S.; Hawkridge, A. M.; Muddiman, D. C. Development and Characterization of an Ionization Technique for Analysis of Biological Macromolecules: Liquid Matrix-Assisted Laser Desorption Electrospray Ionization. *Anal. Chem.* **2008**, *80*(17), 6773-6778.

(185) Ren, X.; Liu, J.; Zhang, C.; Luo, H. Direct analysis of samples under ambient condition by high-voltage-assisted laser desorption ionization mass spectrometry in both positive and negative ion mode. *Rapid Commun. Mass Spectrom.* **2013**, *27*(5), 613-620.

(186) Trimpin, S.; Inutan, E. D.; Herath, T. N.; McEwen, C. N. Matrix-Assisted Laser Desorption/Ionization Mass Spectrometry Method for Selectively Producing

Either Singly or Multiply Charged Molecular Ions. *Anal. Chem.* **2009**, *82*(1), 11-15.

(187) Michela, A.; Barbara, A.; Antonio, T.; Anna, C. Identification of large polycyclic aromatic hydrocarbons in carbon particulates formed in a fuel-rich premixed ethylene flame. *Carbon* **2008**, *46*(15), 2059-2066.

(188) Apicella, B.; Alfè, M.; Amoresano, A.; Galano, E.; Ciajolo, A. Advantages and limitations of laser desorption/ionization mass spectrometric techniques in the chemical characterization of complex carbonaceous materials. *Int. J. Mass Spectrom.* **2010**, *295*(1–2), 98-102.

(189) Laiko, V. V.; Taranenko, N. I.; Berkout, V. D.; Musselman, B. D.; Doroshenko, V. M. Atmospheric pressure laser desorption/ionization on porous silicon. *Rapid Commun. Mass Spectrom.* **2002**, *16*(18), 1737-1742.

(190) Huikko, K.; Östman, P.; Sauber, C.; Mandel, F.; Grigoras, K.; Franssila, S.; Kotiaho, T.; Kostiainen, R. Feasibility of atmospheric pressure desorption/ionization on silicon mass spectrometry in analysis of drugs. *Rapid Commun. Mass Spectrom.* **2003**, *17*(12), 1339-1343.

(191) Li, Y.; Shrestha, B.; Vertes, A. Atmospheric Pressure Infrared MALDI Imaging Mass Spectrometry for Plant Metabolomics. *Anal. Chem.* **2008**, *80*(2), 407-420.

(192) Vertes, A.; Nemes, P.; Shrestha, B.; Barton, A.; Chen, Z.; Li, Y. Molecular imaging by Mid-IR laser ablation mass spectrometry. *Appl. Phys. A: Mater. Sci. Process.* **2008**, *93*(4), 885-891.

(193) Richards, A. L.; Lietz, C. B.; Wager-Miller, J. B.; Mackie, K.; Trimpin, S. Imaging mass spectrometry in transmission geometry. *Rapid Commun. Mass Spectrom.* **2011**, *25*(6), 815-820.

(194) Harron, A. F.; Hoang, K.; McEwen, C. N. High mass resolution tissue imaging at atmospheric pressure using laserspray ionization mass spectrometry. *Int. J. Mass Spectrom.* **2013**, *352*(0), 65-69.

(195) Sroyraya, M.; Goto-Inoue, N.; Zaima, N.; Hayasaka, T.; Chansela, P.; Tanasawet, S.; Shrivas, K.; Sobhon, P.; Setou, M. Visualization of biomolecules in the eyestalk of the blue swimming crab, Portunus pelagicus, by imaging mass spectrometry using the atmospheric-pressure mass microscope. *Surf. Interface Anal.* **2010**, *42*(10-11), 1589-1592.

(196) Roy, M. C.; Nakanishi, H.; Takahashi, K.; Nakanishi, S.; Kajihara, S.; Hayasaka, T.; Setou, M.; Ogawa, K.; Taguchi, R.; Naito, T. Salamander retina phospholipids and their localization by MALDI imaging mass spectrometry at cellular size resolution. *J. Lipid Res.* **2011**, *52*(3), 463-470.

(197) Koestler, M.; Kirsch, D.; Hester, A.; Leisner, A.; Guenther, S.; Spengler, B. A high-resolution scanning microprobe matrix-assisted laser desorption/ionization ion source for imaging analysis on an ion trap/Fourier transform ion cyclotron resonance mass spectrometer. *Rapid Commun. Mass Spectrom.* **2008**, *22*(20), 3275-3285.

(198) Guenther, S.; Koestler, M.; Schulz, O.; Spengler, B. Laser spot size and laser power dependence of ion formation in high resolution MALDI imaging. *Int. J. Mass Spectrom.* **2010**, *294*(1), 7-15.

(199) Römpp, A.; Guenther, S.; Schober, Y.; Schulz, O.; Takats, Z.; Kummer, W.; Spengler, B. Histology by Mass Spectrometry: Label-Free Tissue Characterization Obtained from High-Accuracy Bioanalytical Imaging. *Angew. Chem. Int. Ed.* **2010**, *49*(22), 3834-3838.

(200) Römpp, A.; Guenther, S.; Takats, Z.; Spengler, B. Mass spectrometry imaging with high resolution in mass and space (HR^2 MSI) for reliable investigation of drug compound distributions on the cellular level. *Anal. Bioanal. Chem.* **2011**, *401*(1), 65-73.

(201) Guenther, S.; Römpp, A.; Kummer, W.; Spengler, B. AP-MALDI imaging of neuropeptides in mouse pituitary gland with 50µm spatial resolution and high mass accuracy. *Int. J. Mass Spectrom.* **2011**, *305*(2–3), 228-237.

(202) Schober, Y.; Guenther, S.; Spengler, B.; Römpp, A. High-resolution matrix-assisted laser desorption/ionization imaging of tryptic peptides from tissue. *Rapid Commun. Mass Spectrom.* **2012**, *26*(9), 1141-1146.

(203) Schober, Y.; Guenther, S.; Spengler, B.; Römpp, A. Single Cell Matrix-Assisted Laser Desorption/Ionization Mass Spectrometry Imaging. *Anal. Chem.* **2012**, *84*(15), 6293-6297.

(204) Römpp, A.; Schäfer, K.; Guenther, S.; Wang, Z.; Köstler, M.; Leisner, A.; Paschke, C.; Schramm, T.; Spengler, B. High-resolution atmospheric pressure infrared laser desorption/ionization mass spectrometry imaging of biological tissue. *Anal. Bioanal. Chem.* **2013**, *405*(22), 6959-6968.

(205) Bradshaw, J. A.; Ovchinnikova, O. S.; Meyer, K. A.; Goeringer, D. E. Combined chemical and topographic imaging at atmospheric pressure via microprobe laser desorption/ionization mass spectrometry–atomic force microscopy. *Rapid Commun. Mass Spectrom.* **2009**, *23*(23), 3781-3786.

(206) Harada, T.; Yuba-Kubo, A.; Sugiura, Y.; Zaima, N.; Hayasaka, T.; Goto-Inoue, N.; Wakui, M.; Suematsu, M.; Takeshita, K.; Ogawa, K.; Yoshida, Y.; Setou, M. Visualization of Volatile Substances in Different Organelles with an Atmospheric-Pressure Mass Microscope. *Anal. Chem.* **2009**, *81*(21), 9153-9157.

(207) Coello, Y.; Jones, A. D.; Gunaratne, T. C.; Dantus, M. Atmospheric Pressure Femtosecond Laser Imaging Mass Spectrometry. *Anal. Chem.* **2010**, *82*(7), 2753-2758.

(208) Takats, Z.; Wiseman, J. M.; Gologan, B.; Cooks, R. G. Mass spectrometry sampling under ambient conditions with desorption electrospray ionization. *Sci* **2004**, *306*(5695), 471-3.

(209) Cotte-Rodríguez, I.; Takáts, Z.; Talaty, N.; Chen, H.; Cooks, R. G. Desorption electrospray ionization of explosives on surfaces: Sensitivity and selectivity enhancement by reactive desorption electrospray ionization. *Anal. Chem.* **2005**, *77*(21), 6755-6764.

(210) Takats, Z.; Wiseman, J. M.; Cooks, R. G. Ambient mass spectrometry using desorption electrospray ionization (DESI): instrumentation, mechanisms and applications in forensics, chemistry, and biology. *J. Mass Spectrom.* **2005**, *40*(10), 1261-1275.

(211) Vincenti, M.; Cooks, R. Desorption due to charge exchange in low-energy collisions of organofluorine ions at solid surfaces. *Org. Mass Spectrom.* **1988**, *23*(5), 317-326.

(212) Venter, A.; Sojka, P. E.; Cooks, R. G. Droplet dynamics and ionization mechanisms in desorption electrospray ionization mass spectrometry. *Anal. Chem.* **2006**, *78*(24), 8549-8555.

(213) Costa, A. B.; Cooks, R. G. Simulation of atmospheric transport and droplet–thin film collisions in desorption electrospray ionization. *Chem. Commun.* **2007**(38), 3915-3917.

(214) Costa, A. B.; Graham Cooks, R. Simulated splashes: Elucidating the mechanism of desorption electrospray ionization mass spectrometry. *Chem. Phys. Lett.* **2008**, *464*(1), 1-8.

(215) Nefliu, M.; Smith, J. N.; Venter, A.; Cooks, R. G. Internal energy distributions in desorption electrospray ionization (DESI). *J. Am. Soc. Mass Spectrom.* **2008**, *19*(3), 420-427.

(216) Talaty, N.; Takáts, Z.; Cooks, R. G. Rapid in situ detection of alkaloids in plant tissue under ambient conditions using desorption electrospray ionization. *Analyst* **2005**, *130*(12), 1624-1633.

(217) Chen, H.; Talaty, N. N.; Takáts, Z.; Cooks, R. G. Desorption Electrospray Ionization Mass Spectrometry for High-Throughput Analysis of Pharmaceutical Samples in the Ambient Environment. *Anal. Chem.* **2005**, *77*(21), 6915-6927.

(218) Badu-Tawiah, A.; Bland, C.; Campbell, D. I.; Cooks, R. G. Non-aqueous spray solvents and solubility effects in desorption electrospray ionization. *J. Am. Soc. Mass Spectrom.* **2010**, *21*(4), 572-579.

(219) Kertesz, V.; Van Berkel, G. J. Scanning and surface alignment considerations in chemical imaging with desorption electrospray mass spectrometry. *Anal. Chem.* **2008**, *80*(4), 1027-1032.

(220) Kertesz, V.; Van Berkel, G. J. Improved desorption electrospray ionization mass spectrometry performance using edge sampling and a rotational sample stage. *Rapid Commun. Mass Spectrom.* **2008**, *22*(23), 3846-3850.

(221) Green, F.; Stokes, P.; Hopley, C.; Seah, M.; Gilmore, I.; O'Connor, G. Developing repeatable measurements for reliable analysis of molecules at surfaces using desorption electrospray ionization. *Anal. Chem.* **2009**, *81*(6), 2286-2293.

(222) Bodzon-Kulakowska, A.; Drabik, A.; Ner, J.; Kotlinska, J. H.; Suder, P. Desorption electrospray ionisation (DESI) for beginners–how to adjust settings for tissue imaging. *Rapid Commun. Mass Spectrom.* **2014**, *28*(1), 1-9.

(223) Venter, A.; Cooks, R. G. Desorption electrospray ionization in a small pressure-tight enclosure. *Anal. Chem.* **2007**, *79*(16), 6398-403.

(224) Chipuk, J. E.; Brodbelt, J. S. Transmission mode desorption electrospray ionization. *J. Am. Soc. Mass Spectrom.* **2008**, *19*(11), 1612-1620.

(225) Chipuk, J. E.; Gelb, M. H.; Brodbelt, J. S. Surface-enhanced transmission mode desorption electrospray ionization: increasing the specificity of ambient ionization mass spectrometric analyses. *Anal. Chem.* **2009**, *82*(1), 16-18.

(226) Bereman, M. S.; Muddiman, D. C. Detection of Attomole Amounts of Analyte by Desorption Electrospray Ionization Mass Spectrometry (DESI-MS) Determined Using Fluorescence Spectroscopy. *J. Am. Soc. Mass Spectrom.* **2007**, *18*(6), 1093-1096.

(227) Chen, H.; Cotte-Rodríguez, I.; Cooks, R. G. cis-Diol functional group recognition by reactive desorption electrospray ionization (DESI). *Chem. Commun.* **2006**(6), 597-599.

(228) Song, Y.; Cooks, R. G. Reactive desorption electrospray ionization for selective detection of the hydrolysis products of phosphonate esters. *J. Mass Spectrom.* **2007**, *42*(8), 1086-1092.

(229) Cotte-Rodríguez, I.; Chen, H.; Cooks, R. G. Rapid trace detection of triacetone triperoxide (TATP) by complexation reactions during desorption electrospray ionization. *Chem. Commun.* **2006**(9), 953-955.

(230) Wu, C.; Ifa, D. R.; Manicke, N. E.; Cooks, R. G. Rapid, Direct Analysis of Cholesterol by Charge Labeling in Reactive Desorption Electrospray Ionization. *Anal. Chem.* **2009**, *81*(18), 7618-7624.

(231) Nyadong, L.; Green, M. D.; De Jesus, V. R.; Newton, P. N.; Fernández, F. M. Reactive desorption electrospray ionization linear ion trap mass spectrometry of latest-generation counterfeit antimalarials via noncovalent complex formation. *Anal. Chem.* **2007**, *79*(5), 2150-2157.

(232) Jackson, A. U.; Talaty, N.; Cooks, R. G.; Van Berkel, G. J. Salt tolerance of desorption electrospray ionization (DESI). *J. Am. Soc. Mass Spectrom.* **2007**, *18*(12), 2218-2225.

(233) Van Berkel, G. J.; Ford, M. J.; Deibel, M. A. Thin-layer chromatography and mass spectrometry coupled using desorption electrospray ionization. *Anal. Chem.* **2005**, *77*(5), 1207-1215.

(234) Wiseman, J. M.; Puolitaival, S. M.; Takats, Z.; Cooks, R. G.; Caprioli, R. M. Mass spectrometric profiling of intact biological tissue by using desorption electrospray ionization. *Angew. Chem.* **2005**, *44*(43), 7094-7.

(235) Van Berkel, G. J.; Kertesz, V. Automated sampling and imaging of analytes separated on thin-layer chromatography plates using desorption electrospray ionization mass spectrometry. *Anal. Chem.* **2006**, *78*(14), 4938-4944.

(236) Wiseman, J. M.; Ifa, D. R.; Song, Q.; Cooks, R. G. Tissue imaging at atmospheric pressure using desorption electrospray ionization (DESI) mass spectrometry. *Angewandte Chemie International Edition* **2006**, *45*(43), 7188-7192.

(237) Pasilis, S. P.; Kertesz, V.; Van Berkel, G. J. Surface scanning analysis of planar arrays of analytes with desorption electrospray ionization-mass spectrometry. *Anal. Chem.* **2007**, *79*(15), 5956-5962.

(238) Ifa, D. R.; Manicke, N. E.; Dill, A. L.; Cooks, R. G. Latent fingerprint chemical imaging by mass spectrometry. *Sci* **2008**, *321*(5890), 805-805.

(239) Ifa, D. R.; Wiseman, J. M.; Song, Q.; Cooks, R. G. Development of capabilities for imaging mass spectrometry under ambient conditions with desorption electrospray ionization (DESI). *Int J Mass Spectrom* **2007**, *259*(1), 8-15.

(240) Kertesz, V.; Van Berkel, G. J. Improved imaging resolution in desorption electrospray ionization mass spectrometry. *Rapid Commun. Mass Spectrom.* **2008**, *22*(17), 2639-2644.

(241) Kertesz, V. K. V.; Van Berkel, G. J.; Pasilis, S. P. In *Poster presented at the 55th ASMS Conference on Mass Spectrometry, Indianapolis, IN*, 2007.

(242) Eberlin, L. S.; Ferreira, C. R.; Dill, A. L.; Ifa, D. R.; Cheng, L.; Cooks, R. G. Nondestructive, histologically compatible tissue imaging by desorption electrospray ionization mass spectrometry. *Chembiochem : a European journal of chemical biology* **2011**, *12*(14), 2129-2132.

(243) Campbell, D. I.; Ferreira, C. R.; Eberlin, L. S.; Cooks, R. G. Improved spatial resolution in the imaging of biological tissue using desorption electrospray ionization. *Anal Bioanal Chem* **2012**, *404*(2), 389-398.

(244) Janfelt, C.; Wellner, N.; Hansen, H. S.; Hansen, S. H. Displaced dual-mode imaging with desorption electrospray ionization for simultaneous mass

spectrometry imaging in both polarities and with several scan modes. *J. Mass Spectrom.* **2013**, *48*(3), 361-366.

(245) Eberlin, L. S.; Ferreira, C. R.; Dill, A. L.; Ifa, D. R.; Cooks, R. G. Desorption electrospray ionization mass spectrometry for lipid characterization and biological tissue imaging. *Biochimica et Biophysica Acta (BBA)-Molecular and Cell Biology of Lipids* **2011**, *1811*(11), 946-960.

(246) Dill, A. L.; Ifa, D. R.; Manicke, N. E.; Costa, A. B.; Ramos-Vara, J. A.; Knapp, D. W.; Cooks, R. G. Lipid profiles of canine invasive transitional cell carcinoma of the urinary bladder and adjacent normal tissue by desorption electrospray ionization imaging mass spectrometry. *Anal. Chem.* **2009**, *81*(21), 8758-8764.

(247) Manicke, N. E.; Nefliu, M.; Wu, C.; Woods, J. W.; Reiser, V.; Hendrickson, R. C.; Cooks, R. G. Imaging of lipids in atheroma by desorption electrospray ionization mass spectrometry. *Anal. Chem.* **2009**, *81*(21), 8702-8707.

(248) Ellis, S. R.; Wu, C.; Deeley, J. M.; Zhu, X.; Truscott, R. J.; Cooks, R. G.; Mitchell, T. W.; Blanksby, S. J. Imaging of human lens lipids by desorption electrospray ionization mass spectrometry. *J. Am. Soc. Mass Spectrom.* **2010**, *21*(12), 2095-2104.

(249) Girod, M.; Shi, Y.; Cheng, J.-X.; Cooks, R. G. Mapping lipid alterations in traumatically injured rat spinal cord by desorption electrospray ionization imaging mass spectrometry. *Anal. Chem.* **2010**, *83*(1), 207-215.

(250) Dill, A.; Eberlin, L.; Costa, A.; Ifa, D.; Cooks, R. G. Data quality in tissue analysis using desorption electrospray ionization. *Anal. Bioanal. Chem.* **2011**, *401*(6), 1949-1961.

(251) Eberlin, L. S.; Ifa, D. R.; Wu, C.; Cooks, R. G. Three-Dimensional Vizualization of Mouse Brain by Lipid Analysis Using Ambient Ionization Mass Spectrometry. *Angew. Chem. Int. Ed.* **2010**, *49*(5), 873-876.

(252) Wiseman, J. M.; Li, J. B. Elution, partial separation, and identification of lipids directly from tissue slices on planar chromatography media by desorption electrospray ionization mass spectrometry. *Anal. Chem.* **2010**, *82*(21), 8866-8874.

(253) Paglia, G.; Ifa, D. R.; Wu, C.; Corso, G.; Cooks, R. G. Desorption electrospray ionization mass spectrometry analysis of lipids after two-dimensional high-

performance thin-layer chromatography partial separation. *Anal. Chem.* **2010**, *82*(5), 1744-1750.

(254) Ferreira, C.; Eberlin, L.; Hallett, J.; Cooks, R. Single oocyte and single embryo lipid analysis by desorption electrospray ionization mass spectrometry. *J. Mass Spectrom.* **2012**, *47*(1), 29-33.

(255) Ferreira, C. R.; Pirro, V.; Eberlin, L. S.; Hallett, J. E.; Cooks, R. G. Developmental phases of individual mouse preimplantation embryos characterized by lipid signatures using desorption electrospray ionization mass spectrometry. *Anal. Bioanal. Chem.* **2012**, *404*(10), 2915-2926.

(256) Eberlin, L. S.; Dill, A. L.; Costa, A. B.; Ifa, D. R.; Cheng, L.; Masterson, T.; Koch, M.; Ratliff, T. L.; Cooks, R. G. Cholesterol sulfate imaging in human prostate cancer tissue by desorption electrospray ionization mass spectrometry. *Anal. Chem.* **2010**, *82*(9), 3430-3434.

(257) Dill, A. L.; Eberlin, L. S.; Zheng, C.; Costa, A. B.; Ifa, D. R.; Cheng, L.; Masterson, T. A.; Koch, M. O.; Vitek, O.; Cooks, R. G. Multivariate statistical differentiation of renal cell carcinomas based on lipidomic analysis by ambient ionization imaging mass spectrometry. *Anal. Bioanal. Chem.* **2010**, *398*(7-8), 2969-2978.

(258) Dill, A. L.; Eberlin, L. S.; Costa, A. B.; Zheng, C.; Ifa, D. R.; Cheng, L.; Masterson, T. A.; Koch, M. O.; Vitek, O.; Cooks, R. G. Multivariate statistical identification of human bladder carcinomas using ambient ionization imaging mass spectrometry. *Chemistry-a European Journal* **2011**, *17*(10), 2897-2902.

(259) Eberlin, L. S.; Dill, A. L.; Golby, A. J.; Ligon, K. L.; Wiseman, J. M.; Cooks, R. G.; Agar, N. Y. Discrimination of human astrocytoma subtypes by lipid analysis using desorption electrospray ionization imaging mass spectrometry. *Angew. Chem. Int. Ed.* **2010**, *122*(34), 6089-6092.

(260) Eberlin, L. S.; Norton, I.; Dill, A. L.; Golby, A. J.; Ligon, K. L.; Santagata, S.; Cooks, R. G.; Agar, N. Y. Classifying human brain tumors by lipid imaging with mass spectrometry. *Cancer Res.* **2012**, *72*(3), 645-654.

(261) Abbassi-Ghadi, N.; Veselkov, K.; Kumar, S.; Huang, J.; Jones, E.; Strittmatter, N.; Kudo, H.; Goldin, R.; Takáts, Z.; Hanna, G. Discrimination of lymph node metastases using desorption electrospray ionisation-mass spectrometry imaging. *Chem. Commun.* **2014**.

(262) Eberlin, L. S.; Norton, I.; Orringer, D.; Dunn, I. F.; Liu, X.; Ide, J. L.; Jarmusch, A. K.; Ligon, K. L.; Jolesz, F. A.; Golby, A. J. Ambient mass spectrometry for the intraoperative molecular diagnosis of human brain tumors. *Proc. Natl. Acad. Sci. U.S.A.* **2013**, *110*(5), 1611-1616.

(263) Veselkov, K. A.; Mirnezami, R.; Strittmatter, N.; Goldin, R. D.; Kinross, J.; Speller, A. V.; Abramov, T.; Jones, E. A.; Darzi, A.; Holmes, E. Chemo-informatic strategy for imaging mass spectrometry-based hyperspectral profiling of lipid signatures in colorectal cancer. *Proc. Natl. Acad. Sci. U.S.A.* **2014**201310524.

(264) Wiseman, J. M.; Ifa, D. R.; Zhu, Y. X.; Kissinger, C. B.; Manicke, N. E.; Kissinger, P. T.; Cooks, R. G. Desorption electrospray ionization mass spectrometry: Imaging drugs and metabolites in tissues. *Proc. Natl. Acad. Sci. U. S. A.* **2008**, *105*(47), 18120-18125.

(265) Vismeh, R.; Waldon, D. J.; Teffera, Y.; Zhao, Z. Localization and quantification of drugs in animal tissues by use of desorption electrospray ionization mass spectrometry imaging. *Anal Chem* **2012**, *84*(12), 5439-5445.

(266) Kertesz, V.; Van Berkel, G. J.; Vavrek, M.; Koeplinger, K. A.; Schneider, B. B.; Covey, T. R. Comparison of Drug Distribution Images from Whole-Body Thin Tissue Sections Obtained Using Desorption Electrospray Ionization Tandem Mass Spectrometry and Autoradiography. *Anal. Chem.* **2008**, *80*(13), 5168-5177.

(267) Liu, J.; Gingras, J.; Ganley, K. P.; Vismeh, R.; Teffera, Y.; Zhao, Z. Whole-body tissue distribution study of drugs in neonate mice using desorption electrospray ionization mass spectrometry imaging. *Rapid Commun. Mass Spectrom.* **2014**, *28*(2), 185-190.

(268) Luo, Z.; He, J.; Chen, Y.; He, J.; Gong, T.; Tang, F.; Wang, X.; Zhang, R.; Huang, L.; Zhang, L. Air Flow-Assisted Ionization Imaging Mass Spectrometry Method for Easy Whole-Body Molecular Imaging under Ambient Conditions. *Anal. Chem.* **2013**, *85*(5), 2977-2982.

(269) Morelato, M.; Beavis, A.; Kirkbride, P.; Roux, C. Forensic applications of desorption electrospray ionisation mass spectrometry (DESI-MS). *Forensic Sci. Int.* **2013**, *226*(1), 10-21.

(270) Ifa, D.; Gumaelius, L.; Eberlin, L.; Manicke, N.; Cooks, R. Forensic analysis of inks by imaging desorption electrospray ionization (DESI) mass spectrometry. *Analyst* **2007**, *132*(5), 461-467.

(271) Mirabelli, M. F.; Chramow, A.; Cabral, E. C.; Ifa, D. R. Analysis of sexual assault evidence by desorption electrospray ionization mass spectrometry. *J. Mass Spectrom.* **2013**, *48*(7), 774-778.

(272) Nyadong, L.; Harris, G. A.; Balayssac, S. p.; Galhena, A. S.; Malet-Martino, M.; Martino, R.; Parry, R. M.; Wang, M. D.; Fernández, F. M.; Gilard, V. r. Combining two-dimensional diffusion-ordered nuclear magnetic resonance spectroscopy, imaging desorption electrospray ionization mass spectrometry, and direct analysis in real-time mass spectrometry for the integral investigation of counterfeit pharmaceuticals. *Anal. Chem.* **2009**, *81*(12), 4803-4812.

(273) Bjarnholt, N.; Li, B.; D'Alvise, J.; Janfelt, C. Mass spectrometry imaging of plant metabolites–principles and possibilities. *Nat. Prod. Rep.* **2014**.

(274) Horn, P. J.; Chapman, K. D. Lipidomics in situ: Insights into plant lipid metabolism from high resolution spatial maps of metabolites. *Prog. Lipid Res.* **2014**, *54*32-52.

(275) Lane, A. L.; Nyadong, L.; Galhena, A. S.; Shearer, T. L.; Stout, E. P.; Parry, R. M.; Kwasnik, M.; Wang, M. D.; Hay, M. E.; Fernandez, F. M. Desorption electrospray ionization mass spectrometry reveals surface-mediated antifungal chemical defense of a tropical seaweed. *Proc. Natl. Acad. Sci. U.S.A.* **2009**, *106*(18), 7314-7319.

(276) Esquenazi, E.; Dorrestein, P. C.; Gerwick, W. H. Probing marine natural product defenses with DESI-imaging mass spectrometry. *Proc. Natl. Acad. Sci. U.S.A.* **2009**, *106*(18), 7269-7270.

(277) Andras, T.; Alexander, T.; Gahlena, A.; Parry, R. M.; Fernandez, F.; Kubanek, J.; Wang, M.; Hay, M. Seaweed Allelopathy Against Coral: Surface Distribution of a Seaweed Secondary Metabolite by Imaging Mass Spectrometry. *J. Chem. Ecol.* **2012**, *38*(10), 1203-1214.

(278) Thunig, J.; Hansen, S. H.; Janfelt, C. Analysis of secondary plant metabolites by indirect desorption electrospray ionization imaging mass spectrometry. *Anal. Chem.* **2011**, *83*(9), 3256-9.

(279) Müller, T.; Oradu, S.; Ifa, D. R.; Cooks, R. G.; Kräutler, B. Direct plant tissue analysis and imprint imaging by desorption electrospray ionization mass spectrometry. *Anal. Chem.* **2011**, *83*(14), 5754-5761.

(280) Ifa, D. R.; Manicke, N. E.; Rusine, A. L.; Cooks, R. G. Quantitative analysis of small molecules by desorption electrospray ionization mass spectrometry from polytetrafluoroethylene surfaces. *Rapid Commun. Mass Spectrom.* **2008**, *22*(4), 503-510.

(281) Li, B.; Bjarnholt, N.; Hansen, S. H.; Janfelt, C. Characterization of barley leaf tissue using direct and indirect desorption electrospray ionization imaging mass spectrometry. *J. Mass Spectrom.* **2011**, *46*(12), 1241-1246.

(282) Cabral, E.; Mirabelli, M.; Perez, C.; Ifa, D. Blotting Assisted by Heating and Solvent Extraction for DESI-MS Imaging. *J. Am. Soc. Mass Spectrom.* **2013**, *24*(6), 956-965.

(283) Ifa, D. R.; Srimany, A.; Eberlin, L. S.; Naik, H. R.; Bhat, V.; Cooks, R. G.; Pradeep, T. Tissue imprint imaging by desorption electrospray ionization mass spectrometry. *Analytical Methods* **2011**, *3*(8), 1910-1912.

(284) Hemalatha, R. G.; Pradeep, T. Understanding the Molecular Signatures in Leaves and Flowers by Desorption Electrospray Ionization Mass Spectrometry (DESI MS) Imaging. *J. Agric. Food Chem.* **2013**, *61*(31), 7477-7487.

(285) Li, B.; Knudsen, C.; Hansen, N. K.; Jørgensen, K.; Kannangara, R.; Bak, S.; Takos, A.; Rook, F.; Hansen, S. H.; Møller, B. L.; Janfelt, C.; Bjarnholt, N. Visualizing metabolite distribution and enzymatic conversion in plant tissues by desorption electrospray ionization mass spectrometry imaging. *Plant J.* **2013**, *74*(6), 1059-1071.

(286) Li, B.; Hansen, S. H.; Janfelt, C. Direct imaging of plant metabolites in leaves and petals by desorption electrospray ionization mass spectrometry. *Int. J. Mass Spectrom.* **2013**, *348*(0), 15-22.

(287) Bennett, R. V.; Cleaves, H. J.; Davis, J. M.; Sokolov, D. A.; Orlando, T. M.; Bada, J. L.; Fernández, F. M. Desorption Electrospray Ionization Imaging Mass Spectrometry as a Tool for Investigating Model Prebiotic Reactions on Mineral Surfaces. *Anal. Chem.* **2013**, *85*(3), 1276-1279.

(288) C.M. Whitehouse, F. L., C.K. Meng, J.B. Fenn. In *Proceedings of the 34th ASMS Conference on Mass Spectrometry and Allied Topics*: Cincinnati, Ohio, 1986, p 507.

(289) Chen, Y. H.; Hill, H. H.; Wittmer, D. P. Analytical merit of electrospray ion mobility spectrometry as a chromatographic detector. *J. Microcolumn Sep.* **1994**, *6*(5), 515-524.

(290) Lee, C.-Y.; Shiea, J. Gas Chromatography Connected to Multiple Channel Electrospray Ionization Mass Spectrometry for the Detection of Volatile Organic Compounds. *Anal. Chem.* **1998**, *70*(13), 2757-2761.

(291) Amad, M. a. H.; Cech, N. B.; Jackson, G. S.; Enke, C. G. Importance of gas-phase proton affinities in determining the electrospray ionization response for analytes and solvents. *J. Mass Spectrom.* **2000**, *35*(7), 784-789.

(292) Wu, C.; Siems, W. F.; Hill, H. H. Secondary Electrospray Ionization Ion Mobility Spectrometry/Mass Spectrometry of Illicit Drugs. *Anal. Chem.* **2000**, *72*(2), 396-403.

(293) Hong, C.-M.; Tsai, F.-C.; Shiea, J. A Multiple Channel Electrospray Source Used To Detect Highly Reactive Ketenes from a Flow Pyrolyzer. *Anal. Chem.* **2000**, *72*(6), 1175-1178.

(294) Fernandez de la Mora, J. Ionization of vapor molecules by an electrospray cloud. *Int. J. Mass Spectrom.* **2011**, *300*(2–3), 182-193.

(295) Martinez-Lozano Sinues, P.; Criado, E.; Vidal, G. Mechanistic study on the ionization of trace gases by an electrospray plume. *Int. J. Mass Spectrom.* **2012**, *313*(0), 21-29.

(296) Shiea, J.; Wang, C.-H. Applications of Multiple Channel Electrospray Ionization Sources for Biological Sample Analysis. *J. Mass Spectrom.* **1997**, *32*(2), 247-250.

(297) Lee, C.-C.; Chang, D.-Y.; Jeng, J.; Shiea, J. Generating multiply charged protein ions via two-step electrospray ionization mass spectrometry. *J. Mass Spectrom.* **2002**, *37*(1), 115-117.

(298) Chang, D.-Y.; Lee, C.-C.; Shiea, J. Detecting Large Biomolecules from High-Salt Solutions by Fused-Droplet Electrospray Ionization Mass Spectrometry. *Anal. Chem.* **2002**, *74*(11), 2465-2469.

(299) Chen, H.; Venter, A.; Cooks, R. G. Extractive electrospray ionization for direct analysis of undiluted urine, milk and other complex mixtures without sample preparation. *Chem. Commun.* **2006**(19), 2042-2044.

(300) Law, W. S.; Wang, R.; Hu, B.; Berchtold, C.; Meier, L.; Chen, H.; Zenobi, R. On the Mechanism of Extractive Electrospray Ionization. *Anal. Chem.* **2010**, *82*(11), 4494-4500.

(301) Brady, J. J.; Judge, E. J.; Levis, R. J. Mass spectrometry of intact neutral macromolecules using intense non-resonant femtosecond laser vaporization with electrospray post-ionization. *Rapid Commun. Mass Spectrom.* **2009**, *23*(19), 3151-3157.

(302) Jorabchi, K.; Smith, L. M. Single Droplet Separations and Surface Partition Coefficient Measurements Using Laser Ablation Mass Spectrometry. *Anal. Chem.* **2009**, *81*(23), 9682-9688.

(303) Liu, J.; Qiu, B.; Luo, H. Fingerprinting of yogurt products by laser desorption spray post-ionization mass spectrometry. *Rapid Commun. Mass Spectrom.* **2010**, *24*(9), 1365-1370.

(304) Lin, S.-Y.; Huang, M.-Z.; Chang, H.-C.; Shiea, J. Using Electrospray-Assisted Laser Desorption/Ionization Mass Spectrometry To Characterize Organic Compounds Separated on Thin-Layer Chromatography Plates. *Anal. Chem.* **2007**, *79*(22), 8789-8795.

(305) Cheng, S.-C.; Lin, Y.-S.; Huang, M.-Z.; Shiea, J. Applications of electrospray laser desorption ionization mass spectrometry for document examination. *Rapid Commun. Mass Spectrom.* **2010**, *24*(2), 203-208.

(306) Kao, Y.-Y.; Cheng, C.-N.; Cheng, S.-C.; Ho, H.-O.; Shiea, J. Distinguishing authentic and counterfeit banknotes by surface chemical composition determined using electrospray laser desorption ionization mass spectrometry. *J. Mass Spectrom.* **2013**, *48*(11), 1129-1135.

(307) Huang, M.-Z.; Cheng, S.-C.; Jhang, S.-S.; Chou, C.-C.; Cheng, C.-N.; Shiea, J.; Popov, I. A.; Nikolaev, E. N. Ambient molecular imaging of dry fungus surface by electrospray laser desorption ionization mass spectrometry. *Int. J. Mass Spectrom.* **2012**, *325–327*(0), 172-182.

(308) Peng, I. X.; Shiea, J.; Loo, R. R. O.; Loo, J. A. Electrospray-assisted laser desorption/ionization and tandem mass spectrometry of peptides and proteins. *Rapid Commun. Mass Spectrom.* **2007**, *21*(16), 2541-2546.

(309) Shiea, J.; Yuan, C.-H.; Huang, M.-Z.; Cheng, S.-C.; Ma, Y.-L.; Tseng, W.-L.; Chang, H.-C.; Hung, W.-C. Detection of Native Protein Ions in Aqueous Solution under Ambient Conditions by Electrospray Laser

Desorption/Ionization Mass Spectrometry. *Anal. Chem.* **2008**, *80*(13), 4845-4852.

(310) Huang, M.-Z.; Jhang, S.-S.; Cheng, C.-N.; Cheng, S.-C.; Shiea, J. Effects of matrix, electrospray solution, and laser light on the desorption and ionization mechanisms in electrospray-assisted laser desorption ionization mass spectrometry. *Analyst* **2010**, *135*(4), 759-766.

(311) Peng, I. X.; Ogorzalek Loo, R. R.; Margalith, E.; Little, M. W.; Loo, J. A. Electrospray-assisted laser desorption ionization mass spectrometry (ELDI-MS) with an infrared laser for characterizing peptides and proteins. *Analyst* **2010**, *135*(4), 767-772.

(312) Sampson, J. S.; Hawkridge, A. M.; Muddiman, D. C. Direct characterization of intact polypeptides by matrix-assisted laser desorption electrospray ionization quadrupole Fourier transform ion cyclotron resonance mass spectrometry. *Rapid Commun. Mass Spectrom.* **2007**, *21*(7), 1150-1154.

(313) Huang, F.; Murray, K. K. Continuous flow infrared matrix-assisted laser desorption electrospray ionization mass spectrometry. *Rapid Commun. Mass Spectrom.* **2010**, *24*(19), 2799-2804.

(314) Barry, J. A.; Muddiman, D. C. Global optimization of the infrared matrix-assisted laser desorption electrospray ionization (IR MALDESI) source for mass spectrometry using statistical design of experiments. *Rapid Commun. Mass Spectrom.* **2011**, *25*(23), 3527-3536.

(315) Cochran, K. H.; Barry, J. A.; Muddiman, D. C.; Hinks, D. Direct Analysis of Textile Fabrics and Dyes Using Infrared Matrix-Assisted Laser Desorption Electrospray Ionization Mass Spectrometry. *Anal. Chem.* **2012**, *85*(2), 831-836.

(316) Harris, G. A.; Graf, S.; Knochenmuss, R.; Fernandez, F. M. Coupling laser ablation/desorption electrospray ionization to atmospheric pressure drift tube ion mobility spectrometry for the screening of antimalarial drug quality. *Analyst* **2012**, *137*(13), 3039-3044.

(317) Robichaud, G.; Barry, J. A.; Garrard, K. P.; Muddiman, D. C. Infrared Matrix-Assisted Laser Desorption Electrospray Ionization (IR-MALDESI) Imaging Source Coupled to a FT-ICR Mass Spectrometer. *J. Am. Soc. Mass Spectrom.* **2013**, *24*(1), 92-100.

(318) Barry, J. A.; Robichaud, G.; Muddiman, D. C. Mass Recalibration of FT-ICR Mass Spectrometry Imaging Data Using the Average Frequency Shift of Ambient Ions. *J. Am. Soc. Mass Spectrom.* **2013**, *24*(7), 1137-1145.

(319) Robichaud, G.; Barry, J. A.; Muddiman, D. C. IR-MALDESI Mass Spectrometry Imaging of Biological Tissue Sections using Ice as a Matrix. *J. Am. Soc. Mass Spectrom.* **2014**, *25*(3), 319-328.

(320) Barry, J. A.; Groseclose, M. R.; Robichaud, G.; Castellino, S.; Muddiman, D. C. Assessing drug and metabolite detection in liver tissue by IR-MALDESI mass spectrometry imaging coupled to FT-ICR MS. *Int. J. Mass Spectrom.* **Submitted 12/31/2013**.

(321) Barry, J. A.; Robichaud, G.; Thompson, C.; Sykes, C.; Kashuba, A. D. M.; Muddiman, D. C. Mapping Antiretroviral Drugs in Tissue by IR-MALDESI MSI Coupled to the Q Exactive and Comparison with LC-MS/MS SRM Assay. *J. Am. Soc. Mass Spectrom.* **Submitted 1/6/2014**.

(322) Brady, J. J.; Judge, E. J.; Simon, K.; Levis, R. J., Farkas, D. L.; Nicolau, D. V.; Leif, R. C., Eds.; SPIE: San Francisco, California, USA, 2010, pp 75680R-8.

(323) Brady, J.; Judge, E.; Levis, R. Analysis of Amphiphilic Lipids and Hydrophobic Proteins Using Nonresonant Femtosecond Laser Vaporization with Electrospray Post-Ionization. *J. Am. Soc. Mass Spectrom.* **2011**, *22*(4), 762-772.

(324) Brady, J. J.; Judge, E. J.; Levis, R. J. Nonresonant femtosecond laser vaporization of aqueous protein preserves folded structure. *Proc. Natl. Acad. Sci. U.S.A.* **2011**, *108*(30), 12217-12222.

(325) Perez, J. J.; Flanigan, P. M.; Karki, S.; Levis, R. J. Laser Electrospray Mass Spectrometry Minimizes Ion Suppression Facilitating Quantitative Mass Spectral Response for Multicomponent Mixtures of Proteins. *Anal. Chem.* **2013**, *85*(14), 6667-6673.

(326) Judge, E. J.; Brady, J. J.; Dalton, D.; Levis, R. J. Analysis of Pharmaceutical Compounds from Glass, Fabric, Steel, and Wood Surfaces at Atmospheric Pressure Using Spatially Resolved, Nonresonant Femtosecond Laser Vaporization Electrospray Mass Spectrometry. *Anal. Chem.* **2010**, *82*(8), 3231-3238.

(327) Brady, J. J.; Judge, E. J.; Levis, R. J. Identification of explosives and explosive formulations using laser electrospray mass spectrometry. *Rapid Commun. Mass Spectrom.* **2010**, *24*(11), 1659-1664.

(328) Judge, E. J.; Brady, J. J.; Levis, R. J. Mass Analysis of Biological Macromolecules at Atmospheric Pressure Using Nonresonant Femtosecond Laser Vaporization and Electrospray Ionization. *Anal. Chem.* **2010**, *82*(24), 10203-10207.

(329) Flanigan, P. M.; Brady, J. J.; Judge, E. J.; Levis, R. J. Determination of Inorganic Improvised Explosive Device Signatures Using Laser Electrospray Mass Spectrometry Detection with Offline Classification. *Anal. Chem.* **2011**, *83*(18), 7115-7122.

(330) Judge, E. J.; Brady, J. J.; Barbano, P. E.; Levis, R. J. Nonresonant Femtosecond Laser Vaporization with Electrospray Postionization for ex vivo Plant Tissue Typing Using Compressive Linear Classification. *Anal. Chem.* **2011**, *83*(6), 2145-2151.

(331) Perez, J. J.; Flanigan, P. M.; Brady, J. J.; Levis, R. J. The Classification of Smokeless Gun powders using Laser Electrospray Mass Spectrometry and Offline Multivariate Statistical Analysis. *Anal. Chem.* **2012**, *85*(1), 296-302.

(332) Liu, J.; Zhang, C.; Sun, J.; Luo, H. Unexpected complexation reaction during analysis of proteins using laser desorption spray post-ionization mass spectrometry. *Analyst* **2012**, *137*(8), 1764-1767.

(333) Liu, J.; Zhang, C.; Sun, J.; Ren, X.; Luo, H. Laser desorption dual spray post-ionization mass spectrometry for direct analysis of samples via two informative channels. *J. Mass Spectrom.* **2013**, *48*(2), 250-254.

(334) Shrestha, B.; Vertes, A. In Situ Metabolic Profiling of Single Cells by Laser Ablation Electrospray Ionization Mass Spectrometry. *Anal. Chem.* **2009**, *81*(20), 8265-8271.

(335) Sripadi, P.; Nazarian, J.; Hathout, Y.; Hoffman, E.; Vertes, A. In vitro analysis of metabolites from the untreated tissue of Torpedo californica electric organ by mid-infrared laser ablation electrospray ionization mass spectrometry. *Metabolomics* **2009**, *5*(2), 263-276.

(336) Shrestha, B.; Nemes, P.; Vertes, A. Ablation and analysis of small cell populations and single cells by consecutive laser pulses. *Appl. Phys. A: Mater. Sci. Process.* **2010**, *101*(1), 121-126.

(337) Sripadi, P.; Shrestha, B.; Easley, R. L.; Carpio, L.; Kehn-Hall, K.; Chevalier, S.; Mahieux, R.; Kashanchi, F.; Vertes, A. Direct Detection of Diverse Metabolic Changes in Virally Transformed and Tax-Expressing Cells by Mass Spectrometry. *PLoS One* **2010**, *5*(9), e12590.

(338) Stephens, C. H.; Shrestha, B.; Morris, H. R.; Bier, M. E.; Whitmore, P. M.; Vertes, A. Minimally invasive monitoring of cellulose degradation by desorption electrospray ionization and laser ablation electrospray ionization mass spectrometry. *Analyst* **2010**, *135*(9), 2434-2444.

(339) Parsiegla, G.; Shrestha, B.; Carrière, F.; Vertes, A. Direct Analysis of Phycobilisomal Antenna Proteins and Metabolites in Small Cyanobacterial Populations by Laser Ablation Electrospray Ionization Mass Spectrometry. *Anal. Chem.* **2011**, *84*(1), 34-38.

(340) Shrestha, B.; Patt, J. M.; Vertes, A. In Situ Cell-by-Cell Imaging and Analysis of Small Cell Populations by Mass Spectrometry. *Anal. Chem.* **2011**, *83*(8), 2947-2955.

(341) Shrestha, B.; Sripadi, P.; Walsh, C. M.; Razunguzwa, T. T.; Powell, M. J.; Kehn-Hall, K.; Kashanchi, F.; Vertes, A. Rapid, non-targeted discovery of biochemical transformation and biomarker candidates in oncovirus-infected cell lines using LAESI mass spectrometry. *Chem. Commun.* **2012**, *48*(31), 3700-3702.

(342) Shrestha, B.; Javonillo, R.; Burns, J. R.; Pirger, Z.; Vertes, A. Comparative local analysis of metabolites, lipids and proteins in intact fish tissues by LAESI mass spectrometry. *Analyst* **2013**, *138*(12), 3444-3449.

(343) Nemes, P.; Barton, A. A.; Li, Y.; Vertes, A. Ambient Molecular Imaging and Depth Profiling of Live Tissue by Infrared Laser Ablation Electrospray Ionization Mass Spectrometry. *Anal. Chem.* **2008**, *80*(12), 4575-4582.

(344) Nemes, P.; Barton, A. A.; Vertes, A. Three-Dimensional Imaging of Metabolites in Tissues under Ambient Conditions by Laser Ablation Electrospray Ionization Mass Spectrometry. *Anal. Chem.* **2009**, *81*(16), 6668-6675.

(345) Nemes, P.; Woods, A. S.; Vertes, A. Simultaneous Imaging of Small Metabolites and Lipids in Rat Brain Tissues at Atmospheric Pressure by Laser Ablation Electrospray Ionization Mass Spectrometry. *Anal. Chem.* **2010**, *82*(3), 982-988.

(346) Vaikkinen, A.; Shrestha, B.; Nazarian, J.; Kostiainen, R.; Vertes, A.; Kauppila, T. J. Simultaneous Detection of Nonpolar and Polar Compounds by Heat-Assisted Laser Ablation Electrospray Ionization Mass Spectrometry. *Anal. Chem.* **2012**, *85*(1), 177-184.

(347) Kiss, A.; Smith, D. F.; Reschke, B. R.; Powel, M. J.; Heeren, R. M. A. Top-Down Mass Spectrometry Imaging of Intact Proteins by LAESI FT-ICR MS. *Proteomics* **2013**DOI 10.1002/pmic.201300306.

(348) Shelley, J. T.; Ray, S. J.; Hieftje, G. M. Laser ablation coupled to a flowing atmospheric pressure afterglow for ambient mass spectral imaging. *Anal. Chem.* **2008**, *80*(21), 8308-8313.

(349) Andrade, F. J.; Shelley, J. T.; Wetzel, W. C.; Webb, M. R.; Gamez, G.; Ray, S. J.; Hieftje, G. M. Atmospheric pressure chemical ionization source. 2. Desorption-ionization for the direct analysis of solid compounds. *Anal. Chem.* **2008**, *80*(8), 2654-2663.

(350) Galhena, A. S.; Harris, G. A.; Nyadong, L.; Murray, K. K.; Fernández, F. M. Small molecule ambient mass spectrometry imaging by infrared laser ablation metastable-induced chemical ionization. *Anal. Chem.* **2010**, *82*(6), 2178-2181.

(351) Cody, R. B.; Laramee, J. A.; Durst, H. D. Versatile new ion source for the analysis of materials in open air under ambient conditions. *Anal. Chem.* **2005**, *77*(8), 2297-302.

(352) Coon, J. J.; McHale, K. J.; Harrison, W. Atmospheric pressure laser desorption/chemical ionization mass spectrometry: a new ionization method based on existing themes. *Rapid Commun. Mass Spectrom.* **2002**, *16*(7), 681-685.

(353) Herdering, C.; Reifschneider, O.; Wehe, C. A.; Sperling, M.; Karst, U. Ambient molecular imaging by laser ablation atmospheric pressure chemical ionization mass spectrometry. *Rapid Commun Mass Sp* **2013**, *27*(23), 2595-2600.

(354) Na, N.; Zhang, C.; Zhao, M.; Zhang, S.; Yang, C.; Fang, X.; Zhang, X. Direct detection of explosives on solid surfaces by mass spectrometry with an ambient ion source based on dielectric barrier discharge. *J. Mass Spectrom.* **2007**, *42*(8), 1079-1085.

(355) Harper, J. D.; Charipar, N. A.; Mulligan, C. C.; Zhang, X.; Cooks, R. G.; Ouyang, Z. Low-temperature plasma probe for ambient desorption ionization. *Anal. Chem.* **2008**, *80*(23), 9097-9104.

(356) Liu, Y.; Ma, X.; Lin, Z.; He, M.; Han, G.; Yang, C.; Xing, Z.; Zhang, S.; Zhang, X. Imaging Mass Spectrometry with a Low-Temperature Plasma Probe for the Analysis of Works of Art. *Angew. Chem.* **2010**, *122*(26), 4537-4539.

(357) Robb, D. B.; Covey, T. R.; Bruins, A. P. Atmospheric pressure photoionization: an ionization method for liquid chromatography-mass spectrometry. *Anal. Chem.* **2000**, *72*(15), 3653-3659.

(358) Haapala, M.; Pól, J.; Saarela, V.; Arvola, V.; Kotiaho, T.; Ketola, R. A.; Franssila, S.; Kauppila, T. J.; Kostiainen, R. Desorption atmospheric pressure photoionization. *Anal. Chem.* **2007**, *79*(20), 7867-7872.

(359) Luosujärvi, L.; Arvola, V.; Haapala, M.; Saarela, V.; Franssila, S.; Kotiaho, T.; Kostiainen, R.; Kauppila, T. J. Desorption and ionization mechanisms in desorption atmospheric pressure photoionization. *Anal. Chem.* **2008**, *80*(19), 7460-7466.

(360) Luosujärvi, L.; Laakkonen, U. M.; Kostiainen, R.; Kotiaho, T.; Kauppila, T. J. Analysis of street market confiscated drugs by desorption atmospheric pressure photoionization and desorption electrospray ionization coupled with mass spectrometry. *Rapid Commun. Mass Spectrom.* **2009**, *23*(9), 1401-1404.

(361) Pól, J.; Vidová, V.; Kruppa, G.; Kobliha, V. c.; Novák, P.; Lemr, K.; Kotiaho, T.; Kostiainen, R.; Havlíček, V. r.; Volný, M. Automated ambient desorption−ionization platform for surface imaging integrated with a commercial fourier transform ion cyclotron resonance mass spectrometer. *Anal. Chem.* **2009**, *81*(20), 8479-8487.

(362) Hiraoka, K.; Nishidate, K.; Mori, K.; Asakawa, D.; Suzuki, S. Development of probe electrospray using a solid needle. *Rapid Commun. Mass Spectrom.* **2007**, *21*(18), 3139-3144.

(363) Yoshimura, K.; Chen, L. C.; Asakawa, D.; Hiraoka, K.; Takeda, S. Physical properties of the probe electrospray ionization (PESI) needle applied to the biological samples. *J. Mass Spectrom.* **2009**, *44*(6), 978-985.

(364) Chen, L. C.; Nishidate, K.; Saito, Y.; Mori, K.; Asakawa, D.; Takeda, S.; Kubota, T.; Terada, N.; Hashimoto, Y.; Hori, H. Application of probe

electrospray to direct ambient analysis of biological samples. *Rapid Commun. Mass Spectrom.* **2008**, *22*(15), 2366-2374.

(365) Chen, L. C.; Nishidate, K.; Saito, Y.; Mori, K.; Asakawa, D.; Takeda, S.; Kubota, T.; Hori, H.; Hiraoka, K. Characteristics of probe electrospray generated from a solid needle. *J. Phys. Chem. B* **2008**, *112*(35), 11164-11170.

(366) Chen, L. C.; Yoshimura, K.; Yu, Z.; Iwata, R.; Ito, H.; Suzuki, H.; Mori, K.; Ariyada, O.; Takeda, S.; Kubota, T. Ambient imaging mass spectrometry by electrospray ionization using solid needle as sampling probe. *J. Mass Spectrom.* **2009**, *44*(10), 1469-1477.

(367) Ovchinnikova, O. S.; Van Berkel, G. J. Thin-layer chromatography and mass spectrometry coupled using proximal probe thermal desorption with electrospray or atmospheric pressure chemical ionization. *Rapid Commun. Mass Spectrom.* **2010**, *24*(12), 1721-1729.

(368) Ovchinnikova, O. S.; Kertesz, V.; Van Berkel, G. J. Molecular surface sampling and chemical imaging using proximal probe thermal desorption/secondary ionization mass spectrometry. *Anal. Chem.* **2010**, *83*(2), 598-603.

(369) Ovchinnikova, O. S.; Nikiforov, M. P.; Bradshaw, J. A.; Jesse, S.; Van Berkel, G. J. Combined atomic force microscope-based topographical imaging and nanometer-scale resolved proximal probe thermal desorption/electrospray ionization–mass spectrometry. *ACS Nano* **2011**, *5*(7), 5526-5531.

(370) Ovchinnikova, O. S.; Kjoller, K.; Hurst, G. B.; Pelletier, D. A.; Van Berkel, G. J. Atomic Force Microscope Controlled Topographical Imaging and Proximal Probe Thermal Desorption/Ionization Mass Spectrometry Imaging. *Anal. Chem.* **2014**, *86*(2), 1083-1090.

(371) Haddad, R.; Sparrapan, R.; Eberlin, M. N. Desorption sonic spray ionization for (high) voltage-free ambient mass spectrometry. *Rapid Commun. Mass Spectrom.* **2006**, *20*(19), 2901-2905.

(372) Haddad, R.; Sparrapan, R.; Kotiaho, T.; Eberlin, M. N. Easy ambient sonic-spray ionization-membrane interface mass spectrometry for direct analysis of solution constituents. *Anal. Chem.* **2008**, *80*(3), 898-903.

(373) Janfelt, C.; Nørgaard, A. W. Ambient mass spectrometry imaging: a comparison of desorption ionization by sonic spray and electrospray. *J. Am. Soc. Mass Spectrom.* **2012**, *23*(10), 1670-1678.

(374) Wachs, T.; Henion, J. Electrospray device for coupling microscale separations and other miniaturized devices with electrospray mass spectrometry. *Anal. Chem.* **2001**, *73*(3), 632-638.

(375) Van Berkel, G. J.; Sanchez, A. D.; Quirke, J. M. E. Thin-layer chromatography and electrospray mass spectrometry coupled using a surface sampling probe. *Anal. Chem.* **2002**, *74*(24), 6216-6223.

(376) Kertesz, V.; Ford, M. J.; Van Berkel, G. J. Automation of a surface sampling probe/electrospray mass spectrometry system. *Anal. Chem.* **2005**, *77*(22), 7183-7189.

(377) Van Berkel, G. J.; Ford, M. J.; Doktycz, M. J.; Kennel, S. J. Evaluation of a surface-sampling probe electrospray mass spectrometry system for the analysis of surface-deposited and affinity-captured proteins. *Rapid Commun. Mass Spectrom.* **2006**, *20*(7), 1144-1152.

(378) Van Berkel, G. J.; Kertesz, V.; Koeplinger, K. A.; Vavrek, M.; Kong, A. N. T. Liquid microjunction surface sampling probe electrospray mass spectrometry for detection of drugs and metabolites in thin tissue sections. *J. Mass Spectrom.* **2008**, *43*(4), 500-508.

(379) Walworth, M. J.; Stankovich, J. J.; Van Berkel, G. J.; Schulz, M.; Minarik, S.; Nichols, J.; Reich, E. Hydrophobic treatment enabling analysis of wettable surfaces using a liquid microjunction surface sampling probe/electrospray ionization-mass spectrometry system. *Anal. Chem.* **2010**, *83*(2), 591-597.

(380) ElNaggar, M. S.; Barbier, C.; Van Berkel, G. J. Liquid microjunction surface sampling probe fluid dynamics: Computational and experimental analysis of coaxial intercapillary positioning effects on sample manipulation. *J. Am. Soc. Mass Spectrom.* **2011**, *22*(7), 1157-1166.

(381) Ovchinnikova, O. S.; Kertesz, V.; Van Berkel, G. J. Combining transmission geometry laser ablation and a non-contact continuous flow surface sampling probe/electrospray emitter for mass spectrometry based chemical imaging. *Rapid Commun. Mass Spectrom.* **2011**, *25*(24), 3735-3740.

(382) Ovchinnikova, O. S.; Lorenz, M.; Kertesz, V.; Van Berkel, G. J. Laser Ablation Sampling of Materials Directly into the Formed Liquid Microjunction of a

Continuous Flow Surface Sampling Probe/Electrospray Ionization Emitter for Mass Spectral Analysis and Imaging. *Anal. Chem.* **2013**, *85*(21), 10211-10217.

(383) Van Berkel, G. J.; Kertesz, V. Continuous-flow liquid microjunction surface sampling probe connected on-line with high-performance liquid chromatography/mass spectrometry for spatially resolved analysis of small molecules and proteins. *Rapid Commun. Mass Spectrom.* **2013**, *27*(12), 1329-1334.

(384) Kertesz, V.; Van Berkel, G. J. Fully automated liquid extraction-based surface sampling and ionization using a chip-based robotic nanoelectrospray platform. *J. Mass Spectrom.* **2010**, *45*(3), 252-260.

(385) Marshall, P.; Toteu-Djomte, V.; Bareille, P.; Perry, H.; Brown, G.; Baumert, M.; Biggadike, K. Correlation of Skin Blanching and Percutaneous Absorption for Glucocorticoid Receptor Agonists by Matrix-Assisted Laser Desorption Ionization Mass Spectrometry Imaging and Liquid Extraction Surface Analysis with Nanoelectrospray Ionization Mass Spectrometry. *Anal. Chem.* **2010**, *82*(18), 7787-7794.

(386) Eikel, D.; Vavrek, M.; Smith, S.; Bason, C.; Yeh, S.; Korfmacher, W. A.; Henion, J. D. Liquid extraction surface analysis mass spectrometry (LESA-MS) as a novel profiling tool for drug distribution and metabolism analysis: the terfenadine example. *Rapid Commun. Mass Spectrom.* **2011**, *25*(23), 3587-3596.

(387) Schadt, S.; Kallbach, S.; Almeida, R.; Sandel, J. Investigation of Figopitant and Its Metabolites in Rat Tissue by Combining Whole-Body Autoradiography with Liquid Extraction Surface Analysis Mass Spectrometry. *Drug Metab. Dispos.* **2012**, *40*(3), 419-425.

(388) Eikel, D.; Henion, J. Liquid extraction surface analysis (LESA) of food surfaces employing chip-based nano-electrospray mass spectrometry. *Rapid Commun. Mass Spectrom.* **2011**, *25*(16), 2345-2354.

(389) Edwards, R. L.; Creese, A. J.; Baumert, M.; Griffiths, P.; Bunch, J.; Cooper, H. J. Hemoglobin variant analysis via direct surface sampling of dried blood spots coupled with high-resolution mass spectrometry. *Anal. Chem.* **2011**, *83*(6), 2265-2270.

(390) Paine, M. R.; Barker, P. J.; Maclauglin, S. A.; Mitchell, T. W.; Blanksby, S. J. Direct detection of additives and degradation products from polymers by liquid

extraction surface analysis employing chip-based nanospray mass spectrometry. *Rapid Commun. Mass Spectrom.* **2012**, *26*(4), 412-418.

(391) Blatherwick, E. Q.; Van Berkel, G. J.; Pickup, K.; Johansson, M. K.; Beaudoin, M.-E.; Cole, R. O.; Day, J. M.; Iverson, S.; Wilson, I. D.; Scrivens, J. H. Utility of spatially-resolved atmospheric pressure surface sampling and ionization techniques as alternatives to mass spectrometric imaging (MSI) in drug metabolism. *Xenobiotica* **2011**, *41*(8), 720-734.

(392) Rao, W.; Celiz, A. D.; Scurr, D. J.; Alexander, M. R.; Barrett, D. A. Ambient DESI and LESA-MS Analysis of Proteins Adsorbed to a Biomaterial Surface Using In-Situ Surface Tryptic Digestion. *J. Am. Soc. Mass Spectrom.* **2013**, *24*(12), 1927-1936.

(393) Kertesz, V.; Van Berkel, G. J. Automated liquid microjunction surface sampling-HPLC-MS/MS analysis of drugs and metabolites in whole-body thin tissue sections. *Bioanalysis* **2013**, *5*(7), 819-826.

(394) Roach, P. J.; Laskin, J.; Laskin, A. Nanospray desorption electrospray ionization: an ambient method for liquid-extraction surface sampling in mass spectrometry. *Analyst* **2010**, *135*(9), 2233-2236.

(395) O'Brien, R. E.; Nguyen, T. B.; Laskin, A.; Laskin, J.; Hayes, P. L.; Liu, S.; Jimenez, J. L.; Russell, L. M.; Nizkorodov, S. A.; Goldstein, A. H. Probing molecular associations of field collected and laboratory generated SOA with nano DESI high resolution mass spectrometry. *J. Geophys. Res.-Attmos.* **2013**, *118*(2), 1042-1051.

(396) Roach, P. J.; Laskin, J.; Laskin, A. Molecular Characterization of Organic Aerosols Using Nanospray-Desorption/Electrospray Ionization-Mass Spectrometry†. *Anal. Chem.* **2010**, *82*(19), 7979-7986.

(397) Laskin, J.; Eckert, P. A.; Roach, P. J.; Heath, B. S.; Nizkorodov, S. A.; Laskin, A. Chemical Analysis of Complex Organic Mixtures Using Reactive Nanospray Desorption Electrospray Ionization Mass Spectrometry. *Anal. Chem.* **2012**, *84*(16), 7179-7187.

(398) Eckert, P. A.; Roach, P. J.; Laskin, A.; Laskin, J. Chemical characterization of crude petroleum using nanospray desorption electrospray ionization coupled with high-resolution mass spectrometry. *Anal. Chem.* **2012**, *84*(3), 1517-1525.

(399) Lanekoff, I.; Thomas, M.; Laskin, J. Shotgun Approach for Quantitative Imaging of Phospholipids Using Nanospray Desorption Electrospray Ionization Mass Spectrometry. *Anal. Chem.* **2014**.

(400) Laskin, J.; Heath, B. S.; Roach, P. J.; Cazares, L.; Semmes, O. J. Tissue imaging using nanospray desorption electrospray ionization mass spectrometry. *Anal. Chem.* **2011**, *84*(1), 141-148.

(401) Lanekoff, I.; Heath, B. S.; Liyu, A.; Thomas, M.; Carson, J. P.; Laskin, J. Automated platform for high-resolution tissue imaging using nanospray desorption electrospray ionization mass spectrometry. *Anal. Chem.* **2012**, *84*(19), 8351-8356.

(402) Lanekoff, I.; Thomas, M.; Carson, J. P.; Smith, J. N.; Timchalk, C.; Laskin, J. Imaging Nicotine in Rat Brain Tissue by Use of Nanospray Desorption Electrospray Ionization Mass Spectrometry. *Anal. Chem.* **2013**, *85*(2), 882-889.

(403) Qiao, L.; Tobolkina, E.; Liu, B.; Girault, H. H. Coupling Isoelectric Focusing Gel Electrophoresis to Mass Spectrometry by Electrostatic Spray Ionization. *Anal. Chem.* **2013**, *85*(9), 4745-4752.

(404) Qiao, L.; Sartor, R.; Gasilova, N.; Lu, Y.; Tobolkina, E.; Liu, B.; Girault, H. H. Electrostatic-Spray Ionization Mass Spectrometry. *Anal. Chem.* **2012**, *84*(17), 7422-7430.

(405) Tobolkina, E.; Qiao, L.; Xu, G.; Girault, H. H. Electrostatic-spray ionization mass spectrometry sniffing for perfume fingerprinting. *Rapid Commun. Mass Spectrom.* **2013**, *27*(21), 2310-2316.

(406) Qiao, L.; Tobolkina, E.; Lesch, A.; Bondarenko, A.; Zhong, X.; Liu, B.; Pick, H. M.; Vogel, H.; Girault, H. H. Electrostatic Spray Ionization Mass Spectrometry Imaging. *Anal. Chem.* **2014**, *86*(4), 2033-2041.

(407) Takats, Z.; Cotte-Rodriguez, I.; Talaty, N.; Chen, H.; Cooks, R. G. Direct, trace level detection of explosives on ambient surfaces by desorption electrospray ionization mass spectrometry. *Chem. Commun.* **2005**(15), 1950-1952.

(408) Williams, J. P.; Scrivens, J. H. Rapid accurate mass desorption electrospray ionisation tandem mass spectrometry of pharmaceutical samples. *Rapid Commun. Mass Spectrom.* **2005**, *19*(24), 3643-3650.

(409) Williams, J. P.; Patel, V. J.; Holland, R.; Scrivens, J. H. The use of recently described ionisation techniques for the rapid analysis of some common drugs and samples of biological origin. *Rapid Commun. Mass Spectrom.* **2006**, *20*(9), 1447-1456.

(410) Jia, B.; Ouyang, Y.; Sodhi, R. N.; Hu, B.; Zhang, T.; Li, J.; Chen, H. Differentiation of human kidney stones induced by melamine and uric acid using surface desorption atmospheric pressure chemical ionization mass spectrometry. *J. Mass Spectrom.* **2011**, *46*(3), 313-319.

(411) Huang, D.; Luo, L.; Jiang, C.; Han, J.; Wang, J.; Zhang, T.; Jiang, J.; Zhou, Z.; Chen, H. Sinapine Detection in Radish Taproot Using Surface Desorption Atmospheric Pressure Chemical Ionization Mass Spectrometry. *J. Agric. Food Chem.* **2011**, *59*(6), 2148-2156.

(412) Yang, S.; Ding, J.; Zheng, J.; Hu, B.; Li, J.; Chen, H.; Zhou, Z.; Qiao, X. Detection of melamine in milk products by surface desorption atmospheric pressure chemical ionization mass spectrometry. *Anal. Chem.* **2009**, *81*(7), 2426-2436.

(413) Chen, H.; Zheng, J.; Zhang, X.; Luo, M.; Wang, Z.; Qiao, X. Surface desorption atmospheric pressure chemical ionization mass spectrometry for direct ambient sample analysis without toxic chemical contamination. *J. Mass Spectrom.* **2007**, *42*(8), 1045-1056.

(414) Li, M.; Jia, B.; Ding, L.; Hong, F.; Ouyang, Y.; Chen, R.; Zhou, S.; Chen, H.; Fang, X. Document authentication at molecular levels using desorption atmospheric pressure chemical ionization mass spectrometry imaging. *J. Mass Spectrom.* **2013**, *48*(9), 1042-1049.

CHAPTER 2

Global Optimization of the IR Matrix-Assisted Laser Desorption Electrospray Ionization (IR MALDESI) Source for Mass Spectrometry Using Statistical Design of Experiments

The following work was reprinted with permission from:
Barry, J. A.; Muddiman, D. C. Rapid Commun. Mass Spectrom. 2011, 25(23), 3527-3536.
Copyright © 2011 John Wiley & Sons, Ltd.
The original publication may be accessed directly via the World Wide Web.

2.1 Introduction

With the advent of electrospray ionization (ESI)[1] and matrix-assisted laser desorption ionization (MALDI),[2,3] mass spectrometry (MS) has played an ever increasing role in the analysis of biological systems.[4] These two ionization techniques have emerged as somewhat complementary in biological analysis. ESI generates primarily multiply-charged ions which are more amenable to tandem MS and can increase the mass range of most mass analyzers. This method is also more easily coupled to liquid chromatography. MALDI, on the other hand, is typically limited to singly- or doubly-charged ions which can limit the mass range available to most mass analyzers when sampling large biomolecules. MALDI has a much greater tolerance for high salt samples; however, the vacuum requirement places restrictions on the type of samples that can be analyzed. While both of these techniques provide a wealth of information, they usually require extensive sample preparation in order to make the sample amenable to analysis.

As MS has evolved, the restrictions and limitations of traditional ionization sources such as ESI and MALDI have led to the development of methods for

ambient ionization. These methods are becoming increasingly popular due to their wide applicability to a variety of samples and substrates while requiring little to no sample preparation. The introduction of desorption electrospray ionization (DESI)[5] marked the beginning of the trend towards native sampling in mass spectrometry. The subsequent years led to the release of well over thirty 'novel' ambient ionization sources which have been reviewed extensively.[6-10] A few of these sources have been commercialized and are becoming more universally integrated into industrial and academic laboratories including, but not limited to, DESI, direct analysis in real time (DART),[11] atmospheric pressure solids analysis probe (ASAP),[12] and perhaps most recently laser ablation electrospray ionization (LAESI).[13]

A subdivision of ambient ionization can be dedicated to laser sampling/desorption followed by post-ionization by electrospray. A handful of these ionization sources have been described and include electrospray-assisted laser desorption ionization (ELDI),[14] matrix-assisted laser desorption electrospray ionization (MALDESI),[15] infrared laser assisted desorption electrospray ionization (IR LADESI),[16] laser ablation electrospray ionization (LAESI),[13] laser ablation mass spectrometry (LAMS),[17] and laser electrospray mass spectrometry (LEMS).[18] Most recently a technique was published called laser desorption spray post-ionization (LDSPI)[19] in which the authors state that perhaps all of these techniques could be merged under this one acronym. These methods are relatively similar but some differ by a few of their parameter settings (source geometry, laser wavelength, repetition rate, and pulse width). In MALDESI, it is proposed that the laser (UV or

IR) is used to excite the sample matrix (endogenous or exogenous) thereby facilitating the desorption of the analyte (liquid or solid). The desorbed neutral molecules or particulate matter in the ablated plume are then entrained or are extracted into the electrospray plume which is orthogonal to the ablation plume and on axis with the inlet to the mass spectrometer. Ionization is then presumed to proceed through an ESI-like mechanism where the analyte containing charged droplets undergo multiple events of desorption and fission ultimately resulting in the ionization of the analyte. A major advantage of this technique is that it combines certain benefits of MALDI and ESI. The high spatial resolution, salt tolerance, and extended interrogation capabilities of MALDI along with the multiple charging effects and ambient nature of ESI are also realized in MALDESI.

Post-ionization by ESI provides MALDESI with the ability to include reagents or standards in the electrospray solvent in order to manipulate the analyte or allow for quantitation. This niche of the post-ionization techniques has been used to facilitate protein unfolding, reduce disulfide bonds, super-charge proteins,[20] define neutral capture efficiency,[15,21] determine the source of the charging protons using deuterated solvents,[22] increase lipid dissociation by generating lithiated ions,[23] and as a means of introducing internal calibrants without disrupting the analyte solution.[15,24,25]

Water has a relatively high absorption cross section in the mid-IR due to the asymmetric O-H stretching modes, thus the use of a mid-IR laser allows for endogenous water in the sample to act as a matrix and facilitate analyte

desorption.[26] It has been well studied that IR laser ablation at atmospheric pressure leads to particularly low ionization yields[27] where a larger portion of the ablated plume consists of neutral particles.[28] MALDESI is believed to have higher ionization efficiency than direct laser ionization due to the post-ionization of the more abundant neutral molecules. This hypothesis is supported by the observations of Nemes and coworkers where LAESI was found to produce greater intensity ion signal compared with AP IR-MALDI.[29]

One aspect that is common among all of these ionization sources is the vast experimental space which needs to be explored. There is a multitude of parameters and settings which can have a dramatic impact on the quality and intensity of the signal. Traditionally, the optimization of a multi-parameter system would be performed by what has been called the 'One Factor at a Time' (OFAT) approach by which one factor is varied at a time while the others are held constant in order to achieve the desired response. The OFAT approach makes the assumption that all of the factors are independent from each other which is almost never valid in experimental data.[30] This assumption could then lead to highly confounded and suboptimal results which may result in optimization of signal to a false maximum. The other extreme would be to test all possible combinations of each level for each factor in an approach known as a full factorial design of experiments (DOE). A more feasible approach to this problem would be a fractional factorial DOE in which a large portion of the experimental space is explored but with a significantly smaller number of experiments. Usually this subdivision of DOE arrives at the same

conclusions of a full factorial design but in a fraction of the time and cost. DOE is a statistical tool which can be used to efficiently optimize multiple factors in order to obtain the desired response(s) of a given system while recognizing higher order interactions. In DOE, experiments (different combinations of factor levels) are statistically constructed so the greatest amount of information about the importance of each factor can be extracted from the results of each experiment. It is through this process that DOE can efficiently evaluate a large experimental space. There are many great resources which more thoroughly describe the mathematics behind this principle.[31-33] A tutorial by Riter and coworkers provides a detailed description of DOE and its conceivable role as an important contrivance in mass spectrometry.[34] Our lab has applied DOE to optimization to hydrophobic tagging reactions for glycans,[35] LTQ-Orbitrap instrumental parameters in order to increase proteome coverage,[36] and in the design and development of an Air Amplifier.[37] Other groups have demonstrated this approach's utility in optimizing the operation of ESI and APCI ion sources.[38,39] Statistical experimental design has also been used for optimizing separation conditions in liquid chromatography (LC) and to develop a general LC-MS method.[40] Here, we used fractional factorial DOE in order to efficiently explore and optimize the combination of parameter settings for our IR-MALDESI source for mass spectrometry in order to decrease our detection limits for small to medium sized proteins.

2.2 Experimental

2.2.1 Materials

Bovine cytochrome c, equine cytochrome c, and formic acid were purchased from Sigma Aldrich (St. Louis, MO, USA). HPLC grade acetonitrile and water were purchased from Burdick & Jackson (Muskegon, MI, USA). All materials were used as received without further purification.

2.2.2 Methods

The electrospray solution was prepared by mixing 15:85 acetonitrile and water (v/v) with 0.1 % formic acid. A stock solution of bovine cytochrome c was prepared by dissolving the protein in the electrospray solution to give a 100 nM solution which was used as the electrospray solvent in the DOE and spot down experiments. Solutions of equine cytochrome c were prepared by dissolving the protein in HPLC grade water to give a stock concentration of 100 μM which was serially diluted down to 1 pM for the spot down experiments.

2.2.3 IR-MALDESI Source and LTQ-FTICR Mass Spectrometer

The UV-MALDESI source has been described in detail previously[41] and has been recently modified to accommodate a Mid-IR laser.[42] Briefly, the electrospray solution containing 100 nM bovine cytochrome c was supplied at a flow rate of 400 nL/min - 3 μL/min using a syringe pump (PHD 2000, Harvard Apparatus, Holliston, MA, USA) through a tapered silica emitter tip (75 μm ID, 30 μm tip, New Objective,

Woburn, MA, USA). High voltage, applied to a stainless steel union (MU1XCS6, VICI Valco, Houston, TX, USA) just prior to the emitter tip, was varied between 2.0 and 3.5 kV such that the electrospray was stabilized in cone-jet mode (visual affirmation). This mode of electrospray has been shown to yield higher ionization efficiency.[43,44] The ESI emitter tip was positioned within 5-10 mm of and on axis with the inlet to the mass spectrometer. A 1 µL droplet of 100 µM equine cytochrome c was deposited onto the stainless steel target which was biased (0-1.0 kV) and held 3-20 mm below the electrospray axis. The sample was ablated using an Nd:YAG pumped, wavelength tunable (2.7 - 3.1 µm) optical parametric oscillator (IR Opolette, Opotek, Carlsbad, CA, USA) with a pulse width of 7 ns. The wavelength was tuned to 2.94 µm for all experiments and the repetition rate was varied between 5 and 20 Hz. The laser power was attenuated using an external attenuator to values of 210 µJ/pulse - 1.6 mJ/pulse. The laser beam was directed using two gold coated Pyrex mirrors (Newport Corporation, Irvine, CA, USA) and was focused using a calcium fluoride plano convex lens (Edmund Optics, Barrington, NJ, USA) to a spot size of 200-300 µm in diameter, corresponding to fluence values of 0.5 – 1.5 J/cm^2. The sample droplet was ablated at varying distances from the inlet to the mass spectrometer (1-10 mm). After the interaction of the ablated plume with the ESI plume, the resulting ions were then sampled by an extended inlet capillary, biased at 42 V and heated to 175 °C, for a Thermo LTQ-FT-ICR Ultra mass spectrometer (Thermo Fisher Scientific, San Jose, CA, USA). The tube lens was set to 125 V. The resolving power of the FT-ICR was set to a value of 50,000$_{FWHM}$ at m/z 400 and

a maximum injection time of 500 ms was used which corresponds to ~1 s/scan. The automatic gain control (AGC) limit was reached for every scan implying that the maximum injection time was never reached. These resolving power and ionization time settings reflected a tradeoff between resolution and duty cycle of the instrument. The instrument was mass calibrated just prior to conducting the fractional factorial and full factorial DOEs. Mass spectra were collected in positive-ion mode over 20 scans for a mass range of 500-2000 m/z. Intensity values for both forms of cytochrome c were obtained from single acquisition spectra.

2.2.4 Data Analysis

A seven factor, three level D-optimal screening DOE was designed using JMP 9.0 (SAS Institute, Inc., Cary, NC, USA). The parameters that were studied including their ranges and the motivation for testing them can be found in **Table 2.1.** A pictorial description of the factors is shown in **Figure 2.1**. In a given experiment a solution of bovine cytochrome c is electrosprayed while a 1 µL droplet of equine cytochrome c is desorbed and ionized by IR-MALDESI. The presence of bovine cytochrome c in the electrospray solution provided a measure of electrospray stability throughout the experiments. Bovine and equine cytochrome c share about 97% of their primary sequence. An equimolar mixture of these two species analyzed by ESI shows similar charge states and charge state distributions which are close to a 1:1 ratio (bov:equ).[45] Due to this sequence homology, the ratio of ions produced by IR-MALDESI to those produced by ESI (i.e. equine:bovine) was used as the

Table 2.1 List of the factors and the meaningful ranges over which they were tested. Also noted are some of the motivations for their inclusion in the screening fractional factorial DOE.

Factor	Min.	Mid.	Max	Motivation
Stage Height (mm)	3	11.5	20	Stage height can determine the degree of overlap between the ablated plume and the electrospray plume.
ESI-Inlet Distance (mm)	5	7.5	10	This factor can control the stability of the electrospray as well as the area available for interaction with the ablated plume.
Sample-Inlet Distance (mm)	1	5.5	10	This factor can also affect the degree of overlap between the two plumes as well as the size of the ESI droplets which interact with the ablated plume.
Flow Rate (nL/min.)	400	1700	3000	Flow rate can control the size of the electrospray droplets as well as the efficiency of ionization.
Plate Voltage (V)	0	500	1000	This factor could be used to account for the presence of a grounded stainless steel plate in the electric field created by electrospray.
Laser Fluence (J/cm^2)	0.5	1	1.5	Will probably determine the amount of material which is ablated from the surface as well as the allowable sampling time.
Laser Repetition Rate (Hz)	5	10	20	Repetition rate would affect the number of laser pulses which would be required in order to observe appreciable signal as well as to some degree determining the amount of sample ablated in a given time frame.

experimental response which was set to be maximized in the DOE. Responses for average charge state and ion injection time were included in the design as non-influential responses so that fluctuations in their values could be monitored under the various parameter settings. All single factor, two-factor, and second order interactions were included in the design to be resolved from confounding with each

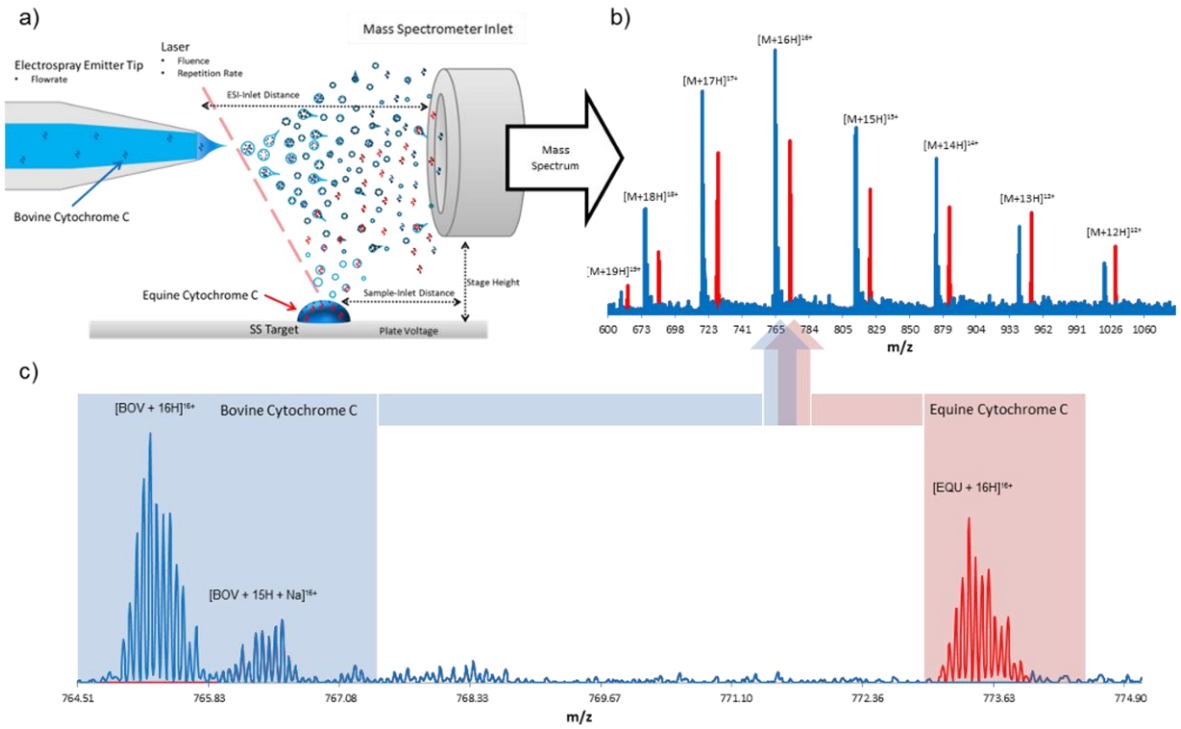

Figure 2.1 **a)** A pictorial description of the experiments which were performed. The inclusion of bovine cytochrome c (BOV) in the electrospray solution during the ionization of equine cytochrome c (EQU) by IR-MALDESI provided a means of tracking electrospray stability and semi-quantitatively determining the ionization efficiency of IR-MALDESI under each set of conditions. **b)** A mass spectrum showing the charge state distributions of both BOV (blue) and EQU (red) captured from a typical experiment. **c)** A zoomed-in portion of the spectrum in showing the isotopic distributions for both analyte and internal standard as well as the observation of salt adduction for the electrosprayed internal standard but not the analyte ionized by IR-MALDESI.

other. Experiments were performed in duplicate and their order was randomized to decrease the influence of experimental and systematic bias respectively. Upon completion of the allotted experiments, signal intensities for the various charge states ($[M+8H]^{8+}$ - $[M+19H]^{19+}$) of both bovine and equine cytochrome c were extracted from a single mass spectrum. Intensities were then normalized for ion

injection time and charge state (due to the increased current induced by higher charge states in ICR). The normalized intensities for each charge state were then summed for both forms of cytochrome c. The ratio of the summed normalized intensities of equine cytochrome c to bovine cytochrome c (EQU:BOV) was then calculated and input into JMP in order to determine the impact of each factor setting. The factors which were deemed to be significant in the screening DOE were then used as the main factors in a full factorial DOE which was designed in JMP.

2.3 Results and Discussion

2.3.1 Screening Design of Experiments

A subgroup of DOE known as fractional factorial DOE allows for systematic examination of multiple factors and interactions simultaneously in order to determine their degree of significance requiring only a small number of experiments. This is in contrast to a full factorial DOE in which the number of experiments required can be represented as L^f, where f is the number of factors (parameters) being studied and L signifies the number of levels (settings) at each factor. For example, a system with 7 factors being tested at 3 levels would require 3^7 or 2,187 experiments in order to test all possible factor combinations. Replicates of these experiments would drive the number of required experiments even higher (duplicate = 4,374 or triplicate = 6,561). This is an astoundingly large number which, due to economic and temporal restraints, is not feasible for most systems. Fractional factorial DOE only requires a fraction of the experiments and will generally still arrive at the same conclusion;

however, there could be some degree of confounding between the main factors and higher order interactions depending on the design resolution. In a typical fractional factorial DOE, two levels are chosen for each factor, a maximum (+) and minimum (-), which reflect that factor's practical range. Here we have also included center points (0) for each factor to account for the possibility that the response may not be linear over the entire range. After incorporating all of this information (factors, levels, responses), the desired resolution of the design is selected. Design resolution represents what degree of aliasing will be allowed. The lowest meaningful resolution is a resolution III design where estimated main effects are confounded with two factor and higher order interactions. In a resolution IV design the main effects may be confounded with three factor or higher interactions but are unconfounded from two factor interactions and two factor interactions may be confounded with other two factor interactions. A resolution V design has main effects and two factor interactions unconfounded from themselves and each other but there may be confounding with three factor or higher order interactions. The highest resolution is a resolution VI design where there is no confounding between main effects, two factor interactions, and three factor interactions but some confounding is possible with higher order interactions. Since our objective was to estimate main effects and two factor interactions, a resolution V design would provide the required information. After selecting the desired resolution the program (JMP) generates a list of experiments to be conducted from which each factor's effect on the system response can be extrapolated. Within the program, the levels

for each factor is assigned as a dimensionless variable with a value of -1 (minimum factor level) to 1 (maximum factor level) with the center point as zero. This approach accounts for differences in the magnitude of the factor range so that it will not influence its significance. The design that was used required 128 total experiments including duplicates and the order of the experiments was randomized.

A screening fractional factorial DOE was used to explore the vast experimental space presented within the many possible parameter settings of the IR-MALDESI source. The seven parameters that were tested are listed in **Table 2.1** including the ranges over which they were studied. The range of values for each parameter was established to reflect the settings that have been used by other labs as well as our own. These seven parameters as well as all two-factor and second order interactions were included in the design. As mentioned previously, two-factor interactions are often ignored in the OFAT approach but can play a significant role in global optimization. A pictorial representation of a typical experiment is depicted in **Figure 2.1**. A 100 nM solution of bovine cytochrome c was electrosprayed through the direct infusion line of the IR-MALDESI source while a 100 μM equine cytochrome c solution (1 μL) was ablated from the sample target then was captured, and ionized in the ESI plume. Both bovine and equine cytochrome c were therefore present in the same mass spectra; one ionized by ESI (BOV) and the other ionized by IR-MALDESI (EQU). This allowed for an estimation of ionization efficiency and provided a means of monitoring the stability of the electrospray under each set of conditions. The ratio (EQU:BOV) accounts for differences in electrospray ionization

efficiency which may arise under the different factor settings and was therefore used as the response metric for the DOE.

The results for the screening DOE are shown in **Figure 2.2**. The half normal probability plot (**Figure 2.2a**) orders the estimated effects of the variables and compares them with a normal quantile distribution. Those variables which diverge

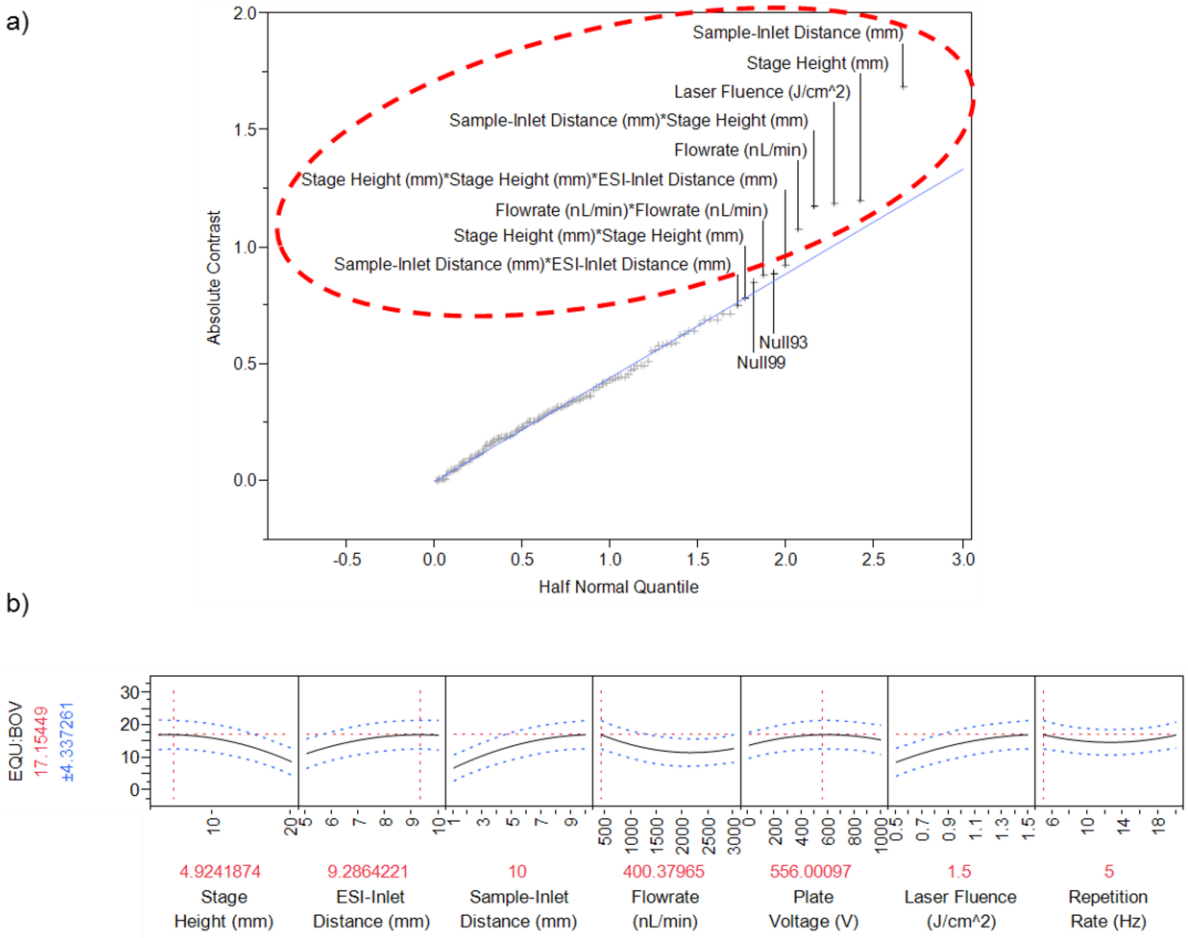

Figure 2.2 Summary of the results of the screening fractional factorial DOE. **a)** A half-normal quantile plot that describes which factors and interactions were found to be significant (hashed red circle). **b)** Prediction profiler which models the system and predicts the optimal combination of settings (shown in red above each factor).

from the normal quantile curve represent those factors (circled in red) which contribute the most to the variance observed in the response. A full list containing all of the main factors and interactions is shown in **Figure 2.3**. The significant variables (highlighted in blue) along with their corresponding contrasts, *t-ratios*, and *p* values can also be found in **Figure 2.3**. A parameter is considered to be significant if its *p* value is smaller than 0.1 (90 % confidence). Those which have *p*-values which are marked with an asterisk define the variance in the data within 95 % confidence (*p*-value smaller than 0.05). The contrasts which are listed give an indication as to which factor setting was preferred as well as the degree to which it influences the response. Those with large, in magnitude, contrast values induced the greatest effect on the EQU:BOV ratio. The sign for contrast (+/-) provides some indication as to whether the maximum (+) or minimum (-) setting provided the best response.

Four of the seven main factors were found to be significant. Among these four were sample to mass spectrometer inlet distance, stage height, flow rate, and laser fluence. The sample to inlet distance defines where the sample is ablated in relation to the mass spectrometer inlet and larger distances were favored. One could reason that this increased distance provides more time and area for the ablated plume to interact with the electrospray plume. Stage height was also found to be statistically significant and has previously been shown to have a rather drastic impact on ion intensity.[29] Nemes and coworkers have shown that signal can be obtained up to 30 mm away from the electrospray axis but the maximum signal

Term	Contrast		t-Ratio	p-Value
Sample-Inlet Distance (mm)	1.68767		3.79	0.0004 *
Laser Fluence (J/cm^2)	1.19075		2.68	0.0098 *
Stage Height (mm)	-1.20027		-2.70	0.0093 *
Flowrate (nL/min)	-1.07838		-2.42	0.0169 *
ESI-Inlet Distance (mm)	0.49661		1.12	0.2616
Repetition Rate (Hz)	0.29798		0.67	0.5049
Plate Voltage (V)	0.25599		0.58	0.5694
Sample-Inlet Distance (mm)*Sample-Inlet Distance (mm)	-0.64106	*	-1.44	0.1489
Sample-Inlet Distance (mm)*Laser Fluence (J/cm^2)	0.69252	*	1.56	0.1211
Laser Fluence (J/cm^2)*Laser Fluence (J/cm^2)	-0.56314	*	-1.27	0.2024
Sample-Inlet Distance (mm)*Stage Height (mm)	-1.17480	*	-2.64	0.0109 *
Laser Fluence (J/cm^2)*Stage Height (mm)	-0.48297	*	-1.09	0.2769
Stage Height (mm)*Stage Height (mm)	-0.78551	*	-1.77	0.0782
Sample-Inlet Distance (mm)*Flowrate (nL/min)	-0.42275	*	-0.95	0.3394
Laser Fluence (J/cm^2)*Flowrate (nL/min)	-0.67266	*	-1.51	0.1318
Stage Height (mm)*Flowrate (nL/min)	0.24844	*	0.56	0.5813
Flowrate (nL/min)*Flowrate (nL/min)	0.88170	*	1.98	0.0473 *
Sample-Inlet Distance (mm)*ESI-Inlet Distance (mm)	0.75075	*	1.69	0.0912
Laser Fluence (J/cm^2)*ESI-Inlet Distance (mm)	0.36265	*	0.82	0.4144
Stage Height (mm)*ESI-Inlet Distance (mm)	-0.43917	*	-0.99	0.3218
Flowrate (nL/min)*ESI-Inlet Distance (mm)	0.22379	*	0.50	0.6181
ESI-Inlet Distance (mm)*ESI-Inlet Distance (mm)	-0.58692	*	-1.32	0.1844
Sample-Inlet Distance (mm)*Repetition Rate (Hz)	0.41379	*	0.93	0.3518
Laser Fluence (J/cm^2)*Repetition Rate (Hz)	-0.42044	*	-0.94	0.3431
Stage Height (mm)*Repetition Rate (Hz)	0.08096	*	0.18	0.8599
Flowrate (nL/min)*Repetition Rate (Hz)	-0.18032	*	-0.41	0.6883
ESI-Inlet Distance (mm)*Repetition Rate (Hz)	-0.16101	*	-0.36	0.7193
Repetition Rate (Hz)*Repetition Rate (Hz)	0.64404	*	1.45	0.1477
Sample-Inlet Distance (mm)*Plate Voltage (V)	0.58005	*	1.30	0.1891
Laser Fluence (J/cm^2)*Plate Voltage (V)	-0.03789	*	-0.09	0.9345
Stage Height (mm)*Plate Voltage (V)	-0.21958	*	-0.49	0.6255
Flowrate (nL/min)*Plate Voltage (V)	0.43088	*	0.97	0.3315
ESI-Inlet Distance (mm)*Plate Voltage (V)	0.39942	*	0.90	0.3671
Repetition Rate (Hz)*Plate Voltage (V)	0.00575	*	0.01	0.9901
Plate Voltage (V)*Plate Voltage (V)	-0.71318	*	-1.60	0.1106
Sample-Inlet Distance (mm)*Sample-Inlet Distance (mm)*Laser Fluence (J/cm^2)	-0.69031	*	-1.55	0.1222
Sample-Inlet Distance (mm)*Laser Fluence (J/cm^2)*Laser Fluence (J/cm^2)	-0.31576	*	-0.71	0.4791
Sample-Inlet Distance (mm)*Sample-Inlet Distance (mm)*Stage Height (mm)	-0.04316	*	-0.10	0.9239
Sample-Inlet Distance (mm)*Laser Fluence (J/cm^2)*Stage Height (mm)	0.25109	*	0.56	0.5775
Laser Fluence (J/cm^2)*Laser Fluence (J/cm^2)*Stage Height (mm)	-0.25832	*	-0.58	0.5657
Sample-Inlet Distance (mm)*Stage Height (mm)*Stage Height (mm)	0.01025	*	0.02	0.9813
Laser Fluence (J/cm^2)*Stage Height (mm)*Stage Height (mm)	-0.47527	*	-1.07	0.2848
Sample-Inlet Distance (mm)*Sample-Inlet Distance (mm)*Flowrate (nL/min)	-0.08206	*	-0.18	0.8582
Sample-Inlet Distance (mm)*Laser Fluence (J/cm^2)*Flowrate (nL/min)	-0.10202	*	-0.23	0.8217
Laser Fluence (J/cm^2)*Laser Fluence (J/cm^2)*Flowrate (nL/min)	0.30530	*	0.69	0.4925
Sample-Inlet Distance (mm)*Stage Height (mm)*Flowrate (nL/min)	0.19631	*	0.44	0.6648
Laser Fluence (J/cm^2)*Stage Height (mm)*Flowrate (nL/min)	0.15611	*	0.35	0.7289
Stage Height (mm)*Stage Height (mm)*Flowrate (nL/min)	0.33861	*	0.76	0.4480
Sample-Inlet Distance (mm)*Flowrate (nL/min)*Flowrate (nL/min)	0.71658	*	1.61	0.1086
Laser Fluence (J/cm^2)*Flowrate (nL/min)*Flowrate (nL/min)	0.35601	*	0.80	0.4231
Stage Height (mm)*Flowrate (nL/min)*Flowrate (nL/min)	-0.27788	*	-0.62	0.5383
Sample-Inlet Distance (mm)*Sample-Inlet Distance (mm)*ESI-Inlet Distance (mm)	0.58584	*	1.32	0.1848
Sample-Inlet Distance (mm)*Laser Fluence (J/cm^2)*ESI-Inlet Distance (mm)	0.34656	*	0.78	0.4360
Laser Fluence (J/cm^2)*Laser Fluence (J/cm^2)*ESI-Inlet Distance (mm)	-0.25447	*	-0.57	0.5724
Sample-Inlet Distance (mm)*Stage Height (mm)*ESI-Inlet Distance (mm)	-0.12598	*	-0.28	0.7790
Laser Fluence (J/cm^2)*Stage Height (mm)*ESI-Inlet Distance (mm)	-0.07945	*	-0.18	0.8629
Stage Height (mm)*Stage Height (mm)*ESI-Inlet Distance (mm)	-0.92503	*	-2.08	0.0382 *
Sample-Inlet Distance (mm)*Flowrate (nL/min)*ESI-Inlet Distance (mm)	-0.59251	*	-1.33	0.1802
Laser Fluence (J/cm^2)*Flowrate (nL/min)*ESI-Inlet Distance (mm)	-0.05417	*	-0.12	0.9045
Stage Height (mm)*Flowrate (nL/min)*ESI-Inlet Distance (mm)	0.69340	*	1.56	0.1204
Flowrate (nL/min)*Flowrate (nL/min)*ESI-Inlet Distance (mm)	0.02454	*	0.06	0.9575
Sample-Inlet Distance (mm)*ESI-Inlet Distance (mm)*ESI-Inlet Distance (mm)	0.51097	*	1.15	0.2495
Laser Fluence (J/cm^2)*ESI-Inlet Distance (mm)*ESI-Inlet Distance (mm)	0.16994	*	0.38	0.7046

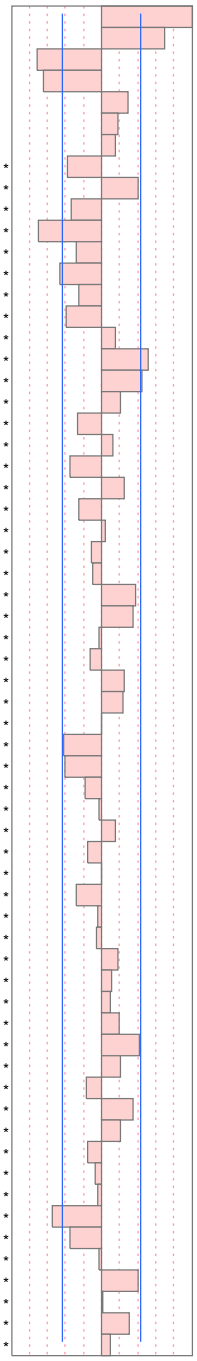

Figure 2.3 Full list of the factors and interactions which were tested providing the contrasts, t-ratios, and p values for each. Those highlighted in blue were found to be significant within 90 % confidence and those with an asterisk on the p value are significant within 95 % confidence.

intensity was observed around 15 mm for bradykinin. They hypothesized that perhaps such a large distance was required due to the large momentum of the ejected particles from the ablated plume. Our results, however, suggest that a shorter stage height led to slightly better ionization efficiency, but this could be attributed to differences in instrumentation. Laser fluence was also concluded to be significant which is not very surprising considering that higher fluences, which were favored, impart more energy into the target and result in the ablation of more material. Plume shielding at higher fluence rates could result in decreased energy deposition in subsequent pulses and would allow explanation for the favoring of short stage heights and the observation that laser repetition rate was found to be insignificant.[46] The final main factor which was found to be significant was the electrospray flow rate. In particular, low flow rates were most influential. Electrospray conducted at low flow rates (nL/min) produces smaller droplets which can lead to more efficient desolvation and ionization in ESI.[47] Small droplets have a larger surface area to volume ratio compared to their larger counterparts which could provide the laser desorbed particles with a greater interaction surface thereby yielding more efficient analyte encapsulation/extraction. A few two factor interactions were found to be vital as well as several second order interactions all of which would have been overlooked if the OFAT approach was conducted. For example, the interactions of sample to inlet distance with both stage height and ESI to inlet distance would have otherwise been ignored. The prediction profiler plot, shown in **Figure 2.2b**, uses standard least squares analysis to model the behavior

of the system based on the results of the measurements which were obtained. Using this model and an iterative approach, the global response can be maximized and the coefficients for each factor that give rise to the maximum response can be obtained. This combination of values, shown in red above each factor, represents the predicted globally optimal settings. It should also be noted that these values are estimates based on a model of the data and therefore may not be accurate out to the number of decimal places shown. A surprising observation is that the lowest repetition rate tested, 5 Hz, was predicted to yield the best response. This prediction could be due to the prolonged observation of signal resulting from fewer laser pulses per scan or the somewhat reduced effects of plume shielding at lower repetition rates. Optimization at 5 Hz also implies that as few as five laser pulses per scan were required to observe appreciable signal. Despite this prediction, it should be mentioned that that laser repetition rate was not considered a significant factor. In fact the estimated response for 5 Hz repetition rate is statistically the same over the entire range tested as shown in **Figure 2.2b** where the maximum response (horizontal dashed red line) is within the 95% confidence interval (blue dashed lines) over the entire range.

2.3.2 Full Factorial Design of Experiments

The variables which were found to be significant from the screening DOE were then analyzed at higher resolution using a full factorial DOE with shorter ranges for each factor. Those factors which were insignificant over the range of

values tested were held constant at the setting which was predicted to yield the optimum response (**Figure 2.2b**). Shorter ranges for the significant variables were established by limiting the range to those values which were within the 95 % confidence interval (where the horizontal red dashed line crosses the blue dashed line in **Figure 2.2b**. These factors including their new ranges are shown in **Table 2.2**. The maximum value for sample to inlet distance was limited to 8 mm to avoid ablating a spot which is behind the optimal ESI emitter distance (9 mm). Plots similar to those shown in **Figure 2.2b** and **Figure 2.3** for the screening DOE were also obtained for the full factorial DOE using the significant variables with the restricted ranges. The factor which was found to be most influential was the sample to inlet distance. The maximum value for this setting was favored which suggests that ablating a spot closer to the ESI emitter generated the greatest ion signal. A large sample distance may provide a greater area for interaction of the two plumes. The position along the electrospray axis where the sample is ablated can also reflect the degree of desolvation which the charged electrospray droplets have undergone.

Table 2.2 List of the factors and the range of settings which were tested at higher resolution in the full factorial DOE.

Factor	Min.	Mid.	Max
Stage Height (mm)	5	10	15
Sample-Inlet Distance (mm)	4	6	8
Flow Rate (nL/min.)	400	1000	1500
Laser Fluence (J/cm^2)	0.8	1.1	1.5

This would, at least partially, control the size of the charged droplets which interact with the ablated neutrals. Laser fluence was found to be important which, again, is not very surprising for the reasons discussed earlier (more ablated material). The prediction profiler was used to model the combination of tested settings which would yield the best response (**Figure 2.4**). The optimal combination is shown in red above each factor. A list of the optimal combination of settings for the all of the parameters that were tested in both DOEs can be found in **Table 2.3**. The lowest flow rate (400 nL/min) was preferred which is likely to be due to higher efficiency of ESI at low flow rates. It would be interesting to see if perhaps even lower flow rates or possibly static nanospray could provide an even better response. Stage height was optimized at 5.5 mm; however, it can be deduced that larger stage heights, at least up to 15 mm, do not produce a significantly different response. This conclusion is supported in **Figure 2.4** where the slope of the modeled line for stage height (black line) is sufficiently close to zero such that the predicted maximum response

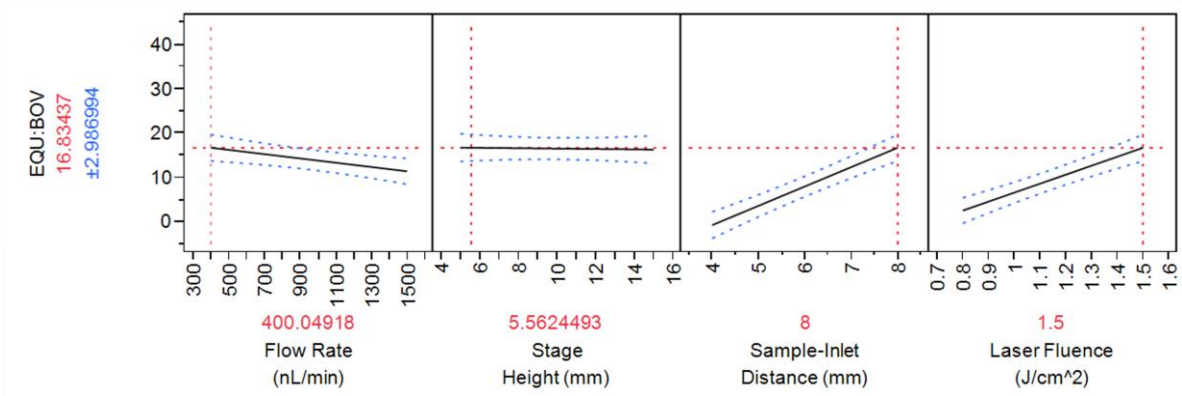

Figure 2.4 Prediction profiler which models the system and predicts the optimal combination of settings (shown in red above each factor).

Table 2.3 The best, worst, and previously used combination of factor settings.

Factor	Best	Previous	Worst
Stage Height (mm)	5.5	5	20
ESI-Inlet Distance (mm)	9	5	10
Sample-Inlet Distance (mm)	8	5	9
Flow Rate (nL/min.)	400	800	1800
Plate Voltage (V)	550	300	0
Laser Fluence (J/cm^2)	1.5	2.2	0.5
Laser Repetition Rate (Hz)	5	10	10

(horizontal dashed red line) falls within 95 % confidence interval (dashed blue lines) over the entire tested range (5 - 15 mm). It is also important to note that the optimal conditions predicted by the model from the screening DOE (**Figure 2.2b**) nearly matches the results which were obtained from the higher resolution full factorial DOE (**Figure 2.4**). This implies that enough information was collected from the screening fractional factorial DOE (128 experiments for 7 factors at 3 levels and performed in duplicate) to accurately predict the overall optimal conditions without strictly requiring the extra experimental results obtained from the higher resolution full factorial DOE (162 experiments for 4 factors at 3 levels and performed in duplicate). We, however, felt it necessary to test the validity of the fractional factorial DOE prediction by conducting the full factorial DOE with the significant variables.

2.3.3 Spot-Down Experiments

In order to quantify the validity of our global optimization, a spot down experiment was performed using the best, worst, and previous parameter settings in

our lab to determine the limit of detection for equine cytochrome c. The chart in **Table 2.3** lists the parameter settings for the best and worst conditions that were investigated as well as our previous settings which were determined using the OFAT approach. As in the DOE experiments, the EQU:BOV ratio was used as the response. Triplicate measurements were obtained for IR-MALDESI of equine cytochrome c at concentrations ranging from 100 µM to 1 pM under each set of conditions. The results shown in **Figure 2.5** demonstrate that the lowest detection

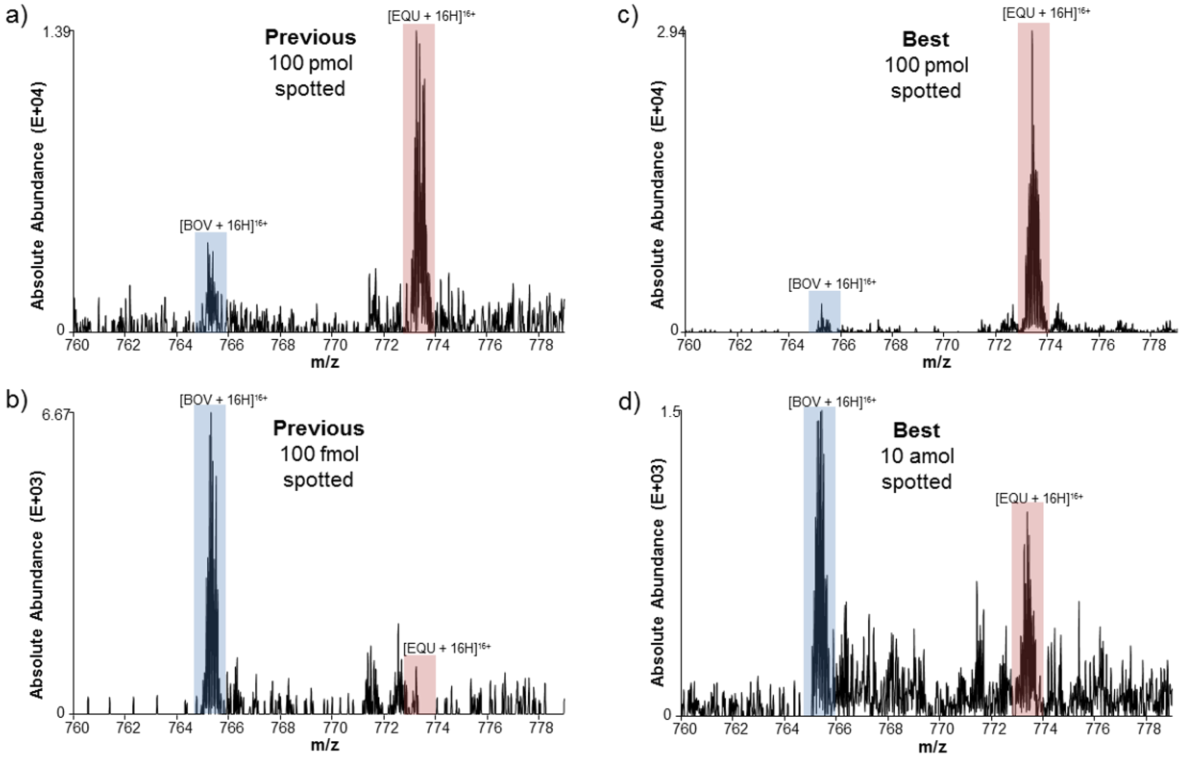

Figure 2.5 Single acquisition mass spectra from the spot down experiment zoomed in on the $[M+16H]^{16+}$ charge states for both equine and bovine cytochrome c. The top spectra (**a, c**) represent the 100 pmol equine cytochrome c spotted on the target and analyzed. The bottom spectra (**b, d**) represent the smallest amount spotted which resulted in detectable signal.

limit (10 amol) was realized using the DOE optimized parameter combination (**Figure 2.5d**) and provided an improvement of at least a four orders of magnitude over our previous settings (100 fmol) (**Figure 2.5b**). Detection limits were calculated by determining the total amount of material spotted for the lowest detected signal. For example, 10pM equine cytochrome c was detected from a 1 µL droplet for the best set of conditions yielding a 10 amol detection limit (1.0E-11 M x 1.0E-6 L = 10.0E-18 mol). These detection limits are conservative estimates since they represent the total amount of material spotted on the surface. The worst parameter combination failed to yield any signal over the range tested. This observation was somewhat surprising given that relatively similar settings, with the exception of laser fluence, were used for LAESI imaging.[48] However, due to inherent differences in the various types of mass spectrometers from one lab to another, it is unlikely that there would be only one set of conditions which works best for all labs. Prior to this work, detection limits for the similarly sized protein ubiquitin (~8.5 kDa) were demonstrated to be around 100 fmol using the IR-ELDI source to ablate the analyte from a water containing droplet.[49] While the differences in detection limits are due mainly to the type of the mass analyzer used, both through this previous work and our current optimization, we are working to get the most out of the front end by driving down the detection limits attainable from the ionization source.

2.4 Conclusions

We have demonstrated the utility of fractional factorial design of experiments as an efficient approach to globally optimizing complex systems which include a wide variety of parameters and settings. Such a vast experimental space would be insufficiently explored using the OFAT approach and would be uneconomically examined by conducting an exhaustive full factorial DOE. The globally optimized combination of parameter settings was validated by comparing it to the worst set of conditions and perhaps more importantly to our previous settings. A limit of detection of 10 attomoles for equine cytochrome c was obtained using our optimized settings. This detection limit corresponds to an improvement of four orders of magnitude over our previous parameter settings[41] which were determined using the OFAT method. The improvement in signal provides evidence of the influences of higher order interactions which are usually not taken into consideration and can have a profound effect on the response of a system. It is possible that these optimal parameter settings may specifically favor ionization of small to medium sized proteins from liquid droplets. However, we have demonstrated that fractional factorial DOE offers a systematic approach to global optimization which can be applied to efficiently and economically enhance conditions for any molecular class or sample state (solid, liquid, tissue) of interest.

2.5 References

(1) Fenn, J. B.; Mann, M.; Meng, C. K.; Wong, S. F.; Whitehouse, C. M. Electrospray Ionization for Mass Spectrometry of Large Biomolecules. *Sci* **1989**, *246*(4926), 64-71.

(2) Tanaka, K.; Waki, H.; Ido, Y.; Akita, S.; Yoshida, Y.; Yoshida, T.; Matsuo, T. Protein and polymer analyses up to m/z 100 000 by laser ionization time-of-flight mass spectrometry. *Rapid Commun. Mass Spectrom.* **1988**, *2*(8), 151-153.

(3) Karas, M.; Hillenkamp, F. Laser desorption ionization of proteins with molecular masses exceeding 10,000 daltons. *Anal. Chem.* **1988**, *60*(20), 2299-2301.

(4) Aebersold, R.; Mann, M. Mass spectrometry-based proteomics. *Nature* **2003**, *422*(6928), 198-207.

(5) Takáts, Z.; Wiseman, J. M.; Gologan, B.; Cooks, R. G. Mass Spectrometry Sampling Under Ambient Conditions with Desorption Electrospray Ionization. *Sci* **2004**, *306*(5695), 471-473.

(6) Cooks, R. G.; Ouyang, Z.; Takats, Z.; Wiseman, J. M. Ambient Mass Spectrometry. *Sci* **2006**, *311*(5767), 1566-1570.

(7) Van Berkel, G. J.; Pasilis, S. P.; Ovchinnikova, O. Established and emerging atmospheric pressure surface sampling/ionization techniques for mass spectrometry. *J. Mass Spectrom.* **2008**, *43*(9), 1161-1180.

(8) Chen, H.; Gamez, G.; Zenobi, R. What can we learn from ambient ionization techniques? *J. Am. Soc. Mass Spectrom.* **2009**, *20*(11), 1947-1963.

(9) Covey, T. R.; Thomson, B. A.; Schneider, B. B. Atmospheric pressure ion sources. *Mass Spectrom. Rev.* **2009**, *28*(6), 870-897.

(10) Weston, D. J. Ambient ionization mass spectrometry: current understanding of mechanistic theory; analytical performance and application areas. *Analyst* **2010**, *135*(4), 661-668.

(11) Cody, R. B.; Laramée, J. A.; Durst, H. D. Versatile New Ion Source for the Analysis of Materials in Open Air under Ambient Conditions. *Anal. Chem.* **2005**, *77*(8), 2297-2302.

(12) McEwen, C. N.; McKay, R. G.; Larsen, B. S. Analysis of Solids, Liquids, and Biological Tissues Using Solids Probe Introduction at Atmospheric Pressure on Commercial LC/MS Instruments. *Anal. Chem.* **2005**, *77*(23), 7826-7831.

(13) Nemes, P.; Vertes, A. Laser Ablation Electrospray Ionization for Atmospheric Pressure, in Vivo, and Imaging Mass Spectrometry. *Anal. Chem.* **2007**, *79*(21), 8098-8106.

(14) Shiea, J.; Huang, M.-Z.; Hsu, H.-J.; Lee, C.-Y.; Yuan, C.-H.; Beech, I.; Sunner, J. Electrospray-assisted laser desorption/ionization mass spectrometry for direct ambient analysis of solids. *Rapid Commun. Mass Spectrom.* **2005**, *19*(24), 3701-3704.

(15) Sampson, J.; Hawkridge, A.; Muddiman, D. Generation and detection of multiply-charged peptides and proteins by matrix-assisted laser desorption electrospray ionization (MALDESI) fourier transform ion cyclotron resonance mass spectrometry. *J. Am. Soc. Mass Spectrom.* **2006**, *17*(12), 1712-1716.

(16) Rezenom, Y. H.; Dong, J.; Murray, K. K. Infrared laser-assisted desorption electrospray ionization mass spectrometry. *Analyst* **2008**, *133*(2), 226-232.

(17) Jorabchi, K.; Smith, L. M. Single Droplet Separations and Surface Partition Coefficient Measurements Using Laser Ablation Mass Spectrometry. *Anal. Chem.* **2009**, *81*(23), 9682-9688.

(18) Brady, J. J.; Judge, E. J.; Levis, R. J. Mass spectrometry of intact neutral macromolecules using intense non-resonant femtosecond laser vaporization with electrospray post-ionization. *Rapid Commun. Mass Spectrom.* **2009**, *23*(19), 3151-3157.

(19) Liu, J.; Qiu, B.; Luo, H. Fingerprinting of yogurt products by laser desorption spray post-ionization mass spectrometry. *Rapid Commun. Mass Spectrom.* **2010**, *24*(9), 1365-1370.

(20) Peng, I. X.; Ogorzalek Loo, R. R.; Shiea, J.; Loo, J. A. Reactive-Electrospray-Assisted Laser Desorption/Ionization for Characterization of Peptides and Proteins. *Anal. Chem.* **2008**, *80*(18), 6995-7003.

(21) Judge, E. J.; Brady, J. J.; Dalton, D.; Levis, R. J. Analysis of Pharmaceutical Compounds from Glass, Fabric, Steel, and Wood Surfaces at Atmospheric Pressure Using Spatially Resolved, Nonresonant Femtosecond Laser Vaporization Electrospray Mass Spectrometry. *Anal. Chem.* **2010**, *82*(8), 3231-3238.

(22) Dixon, R. B.; Muddiman, D. C. Study of the ionization mechanism in hybrid laser based desorption techniques. *Analyst* **2010**, *135*(5), 880-882.

(23) Shrestha, B.; Nemes, P.; Nazarian, J.; Hathout, Y.; Hoffman, E. P.; Vertes, A. Direct analysis of lipids and small metabolites in mouse brain tissue by AP IR-MALDI and reactive LAESI mass spectrometry. *Analyst* **2010**, *135*(4), 751-758.

(24) Sampson, J. S.; Hawkridge, A. M.; Muddiman, D. C. Direct characterization of intact polypeptides by matrix-assisted laser desorption electrospray ionization quadrupole Fourier transform ion cyclotron resonance mass spectrometry. *Rapid Commun. Mass Spectrom.* **2007**, *21*(7), 1150-1154.

(25) Sripadi, P.; Nazarian, J.; Hathout, Y.; Hoffman, E.; Vertes, A. In vitro analysis of metabolites from the untreated tissue of <i>Torpedo californica</i> electric organ by mid-infrared laser ablation electrospray ionization mass spectrometry. *Metabolomics* **2009**, *5*(2), 263-276.

(26) Berkenkamp, S.; Karas, M.; Hillenkamp, F. Ice as a matrix for IR-matrix-assisted laser desorption/ionization: mass spectra from a protein single crystal. *Proc. Natl. Acad. Sci. U. S. A.* **1996**, *93*(14), 7003-7.

(27) Laiko, V.; Taranenko, N.; Berkout, V.; Yakshin, M.; Prasad, C.; Lee, H.; Doroshenko, V. Desorption/ionization of biomolecules from aqueous solutions at atmospheric pressure using an infrared laser at 3 μm. *J. Am. Soc. Mass Spectrom.* **2002**, *13*(4), 354-361.

(28) Jackson, S. N.; Kim, J.-K.; Laboy, J. L.; Murray, K. K. Particle formation by infrared laser ablation of glycerol: implications for ion formation. *Rapid Commun. Mass Spectrom.* **2006**, *20*(8), 1299-1304.

(29) Vertes, A.; Nemes, P.; Shrestha, B.; Barton, A.; Chen, Z.; Li, Y. Molecular imaging by Mid-IR laser ablation mass spectrometry. *Appl. Phys. A: Mater. Sci. Process.* **2008**, *93*(4), 885-891.

(30) Fisher, R. A. *Statistical Methods for Research Workers*; Hafner Publishing Company: New York, New York, 1973.

(31) Tamhane, A. C. *Statistical Analysis of Designed Experiments*, 3rd ed.; John Wiley & Sons: Hoboken, NJ, 2009.

(32) Launsby, R. G. W., D. L. *Straight Talk on Designing Experiments: An Introductory Text for Scientists and Engineers*, 2nd ed.; Launsby Consulting: Colorado, 1995.

(33) http://www.itl.nist.gov/div898/handbook/index.htm.

(34) Riter, L. S.; Vitek, O.; Gooding, K. M.; Hodge, B. D.; Julian, R. K. Statistical design of experiments as a tool in mass spectrometry. *J. Mass Spectrom.* **2005**, *40*(5), 565-579.

(35) Walker, S. H.; Papas, B. N.; Comins, D. L.; Muddiman, D. C. Interplay of Permanent Charge and Hydrophobicity in the Electrospray Ionization of Glycans. *Anal. Chem.* **2010**, *82*(15), 6636-6642.

(36) Andrews, G.; Dean, R.; Hawkridge, A.; Muddiman, D. Improving Proteome Coverage on a LTQ-Orbitrap Using Design of Experiments. *J. Am. Soc. Mass Spectrom.* **2011**, *22*(4), 773-783.

(37) Robichaud, G.; Dixon, R. B.; Potturi, A. S.; Cassidy, D.; Edwards, J. R.; Sohn, A.; Dow, T. A.; Muddiman, D. C. Design, modeling, fabrication, and evaluation of the air amplifier for improved detection of biomolecules by electrospray ionization mass spectrometry. *Int. J. Mass Spectrom.* **2011**, *300*(2–3), 99-107.

(38) Huang, S. K.; Glancy, S. B.; Stansbury, W. F. Optimization of a commercial liquid chromatography/mass spectrometry interface by statistical experimental design. *Rapid Commun. Mass Spectrom.* **1993**, *7*(8), 722-724.

(39) de Sousa, N. D.; Ellett, C. J.; Gilbert, M.; Wright, A. D. Use of Chemometrics To Optimize the Operation of an Ion Source. *Anal. Chem.* **2008**, *80*(3), 873-877.

(40) Seto, C.; Bateman, K. P.; Gunter, B. Development of generic liquid chromatography-mass spectrometry methods using experimental design. *J. Am. Soc. Mass Spectrom.* **2002**, *13*(1), 2-9.

(41) Sampson, J.; Hawkridge, A.; Muddiman, D. Construction of a versatile high precision ambient ionization source for direct analysis and imaging. *J. Am. Soc. Mass Spectrom.* **2008**, *19*(10), 1527-1534.

(42) Sampson, J. S.; Murray, K. K.; Muddiman, D. C. Intact and Top-Down Characterization of Biomolecules and Direct Analysis Using Infrared Matrix-Assisted Laser Desorption Electrospray Ionization Coupled to FT-ICR Mass Spectrometry. *J. Am. Soc. Mass Spectrom.* **2009**, *20*(4), 667-673.

(43) Valaskovic, G.; Murphy, J.; Lee, M. Automated orthogonal control system for electrospray ionization. *J. Am. Soc. Mass Spectrom.* **2004**, *15*(8), 1201-1215.

(44) Nemes, P.; Marginean, I.; Vertes, A. Spraying Mode Effect on Droplet Formation and Ion Chemistry in Electrosprays. *Anal. Chem.* **2007**, *79*(8), 3105-3116.

(45) Gordon, E. F.; Mansoori, B. A.; Carroll, C. F.; Muddiman, D. C. Hydropathic influences on the quantification of equine heart cytochrome c using relative ion abundance measurements by electrospray ionization Fourier transform ion cyclotron resonance mass spectrometry. *J. Mass Spectrom.* **1999**, *34*(10), 1055-1062.

(46) Nahen, K.; Vogel, A. Plume dynamics and shielding by the ablation plume during Er:YAG laser ablation. *J. Biomed. Opt.* **2002**, *7*(2), 165-178.

(47) Valaskovic, G. A.; Kelleher, N. L.; Little, D. P.; Aaserud, D. J.; McLafferty, F. W. Attomole-Sensitivity Electrospray Source for Large-Molecule Mass Spectrometry. *Anal. Chem.* **1995**, *67*(20), 3802-3805.

(48) Nemes, P.; Barton, A. A.; Li, Y.; Vertes, A. Ambient Molecular Imaging and Depth Profiling of Live Tissue by Infrared Laser Ablation Electrospray Ionization Mass Spectrometry. *Anal. Chem.* **2008**, *80*(12), 4575-4582.

(49) Peng, I. X.; Ogorzalek Loo, R. R.; Margalith, E.; Little, M. W.; Loo, J. A. Electrospray-assisted laser desorption ionization mass spectrometry (ELDI-MS) with an infrared laser for characterizing peptides and proteins. *Analyst* **2010**, *135*(4), 767-772.

CHAPTER 3

Assessing Drug and Metabolite Detection in Liver Tissue by IR-MALDESI Mass Spectrometry Imaging Coupled to FT-ICR MS

The following work was reprinted from the recently submitted manuscript: Barry, J. A.; Groseclose, M. R.; Robichaud, G.; Castellino, S.; Muddiman, D. C. *Int. J. Mass Spectrom.* Submitted*:* December 31, 2013.

3.1 Introduction

In drug discovery and development, it is essential to determine and understand the pharmacokinetic (PK) properties of drug candidates including their absorption, distribution, metabolism, and excretion (ADME).[1] Drug efficacy is at least partially dependent on its localization toward its intended target; however, untargeted accumulation of the drug or its metabolites in tissue can result in adverse toxicological effects. While drug levels in plasma do play an important role in pharmacokinetic and pharmacodynamic (PK/PD) studies, it has been suggested that plasma concentrations alone do not accurately reflect the localized drug concentration in tissue.[2]

In 1997 Caprioli et al. demonstrated the molecular imaging of peptides and proteins from biological tissue sections using matrix-assisted laser desorption ionization (MALDI) MSI. There are several key attributes that make MALDI MSI an ideal candidate for the mapping of pharmaceuticals in tissue. MALDI is known to be a highly sensitive technique that is capable of detecting attomole quantities of analyte.[3] Also, detection based on MS allows for multiplexed image acquisition as well as discrimination between parent drug and metabolite distributions. An added

benefit is that MS does not require the use of isotopically labeled standards and therefore distributions studies can be performed as a more cost effective methodology earlier in the drug discovery process to refine the list of potential drug candidates to those that exhibit desirable PK/PD properties. Troendle et al. demonstrated the direct detection of pharmaceuticals from tissue sections by MALDI MS[4] and Caprioli's group presented the first MALDI MSI analysis of dosed drugs in tissue.[5,6] Because whole body autoradiography (WBA) and LC-MS are more commonly used for drug distribution analysis, several groups have validated the observed distributions and relative intensities obtained from MSI by performing autoradiography or LC-MS on serial sections.[6-27]

The multiplexing capabilities of MSI can be realized if a large *m/z* range is acquired from each pixel enabling simultaneous acquisition of spatial information for hundreds of endogenous as well as exogenous molecules (xenobiotics). The additional information obtained from these endogenous molecular distributions could prove to be useful when correlated with drug accumulation.[18,24,28-31] However, because most MALDI MSI analyses are performed with lower resolution mass analyzers, isobaric interferences in the low *m/z* range from endogenous molecules or matrix-related peaks necessitate the use of MS/MS imaging to follow a specific transition which precludes multiplex image acquisition. Several sample preparation methods have been described to circumvent isobaric matrix interferences.[20,32] Despite being less common, the examples of high *spectral* resolution MSI for determining drug distribution in tissue demonstrate the benefits of using FT-ICR or

Orbitrap MS for this type of study.[22,27,29,30,33-38] Most of these groups report on the resolution of several unique species with distinct spatial distributions all resolved at the same nominal mass. This higher resolving power (RP) decreases the risk of an unresolved interfering species, therefore allowing for full mass range MSI to be performed and the benefits of multiplex image acquisition to be realized. In addition to high RP, these instruments also provide high mass measurement accuracy (MMA) which, for small molecules, can provide a unique elemental composition to aid in ion identification.[39]

A majority of the challenges with MALDI MSI are directly related to the matrix application process. This process commonly involves spraying or spotting a saturated solution of organic matrix to extract analyte from within the tissue for co-crystallization with the matrix on the tissue surface.[40] Therefore, variation in extraction efficiency relating either to tissue type or analyte solubility in the matrix solvent can impact the observed relative ion intensities. There is also some debate on the degree of molecular diffusion that can take place during this process. In addition, the homogeneity of matrix application and the size of the resulting matrix crystals directly impact the achievable spatial resolution making sample preparation the most important step in the MALDI MSI process. Because of the large number of variables associated with matrix application (i.e. choice of matrix, choice of matrix solvent composition, application method), there are no standard procedures that work best for all samples. Thus, the decision of which method to use is typically determined empirically for a specific analyte or tissue type. Also, given that the

matrix molecules ionize very well and are present in such large excess, the low mass range is typically dominated by matrix-related peaks making the analysis of small molecules more challenging. Despite these analytical challenges, MALDI has been the most widely implemented method of ionization for imaging of drugs and metabolites in tissues.

Other ionization methods that don't require such extensive sample preparation show a great deal of promise in MSI. Desorption electrospray ionization (DESI) has been used on several occasions for drug distribution studies[13,15,27] and liquid extraction surface analysis (LESA) is capable of providing a quick profiling of drug distribution.[41-45] Another ambient ionization method that has demonstrated potential in MSI is infrared matrix-assisted laser desorption electrospray ionization (IR-MALDESI).[46] MALDESI was the first ambient ionization technique to combine atmospheric pressure matrix-assisted laser desorption with electrospray post-ionization.[47] While first described for UV desorption, the MALDESI process is independent of laser wavelength given that any wavelength laser could be used, provided an appropriate matrix (endogenous or exogenous) is chosen that strongly absorbs the corresponding laser wavelength. The use of an infrared laser is particularly appealing because it allows for the use of ice as the laser energy absorbing matrix which does not produce mass spectral interferences and can be easily applied to the sample if necessary.

Herein we report on the use of both IR-MALDESI and UV-MALDI coupled to FT-ICR for the MSI analysis of lapatinib dosed liver tissue. Both techniques provide

complementary information on the detection of the parent drug and several of its metabolites. An investigation of the role of the electrospray solvent composition on IR-MALDESI signal is also presented.

3.2 Experimental

3.2.1 Materials

Bovine Formic acid was purchased from Sigma Aldrich (St. Louis, MO). HPLC grade acetonitrile, methanol, trifluoroacetic acid, and water were purchased from Burdick & Jackson (Muskegon, MI, USA) or Fisher Scientific (Pittsburgh, PA) and were used as received without further purification. 2,5-dihydroxybenzoic acid, (DHB, purity 98%) was purchased from Sigma Aldrich (St. Louis, MO) and purified by recrystallized prior to use. ITO coated glass microscope slides were purchased from Bruker Daltonics (Billerica, MA). Shandon colorfrost plus positively charged glass microscope slides were purchased from Fisher Scientific (Pittsburgh, PA).

3.2.2 Samples

All studies were conducted in accordance with the GSK Policy on the Care, Welfare and Treatment of Laboratory Animals and were reviewed the Institutional Animal Care and Use Committee either at GSK or by the ethical review process at the institution where the work was performed.

Following repeat oral administration of lapatinib, dog liver tissue was flash frozen in liquid nitrogen at necropsy and stored at -80 °C until sectioning. Frozen

tissues were sectioned at 12 µm for UV-MALDI with serial 50 µm sections collected for IR-MALDESI using a Leica 350S cryostat (Wetzlar, Germany). Sections for IR-MALDESI were thaw mounted onto positively charged glass microscope slides and sections for UV-MALDI were thaw mounted onto ITO coated glass microscope slides.

3.2.3 IR-MALDESI Imaging

For a detailed description of the IR-MALDESI imaging source and source parameters please refer to the following references.[46,48] In short, the sample is placed on the liquid cooled Peltier stage which is cooled to -10 °C while open to the ambient in order to deposit a thin layer of ice over the surface of the tissue section. The energy from a mid IR laser (IR Opolette, Opotek, Carlsbad, CA, USA) pulse is strongly absorbed by the ice matrix to facilitate desorption of the sample. The ablated neutral sample molecules partition into the charged solvent droplets of an electrospray plume generated from an emitter capillary coupled to a syringe pump. Ion production occurs through an ESI-like process and ions are then sampled by the atmospheric pressure interface of the mass spectrometer. The IR-MALDESI source is coupled to a Thermo LTQ-FT Ultra (ThermoFisher Scientific, San Jose, CA, USA). The resolving power of the LTQ-FT was set at 100,000 at *m/z* 400. The automatic gain control (AGC), which controls the number of ions sent to the ICR cell to maintain high MMA with external mass calibration, was turned off for these experiments due to its incompatibility with the pulsed nature of the IR-MALDESI

source. Internal calibration can be performed using the average frequency shift recalibration technique (described in detail elsewhere[49]) to maintain MMA within ± 1 ppm. For these experiments a large *m/z* window (*m/z* 150-1500) was collected in order to obtain spatial information on endogenous species as well as the drug-related peaks. Stage movement, laser ablation, and mass spectrometer acquisition is synchronized as described previously.[46] Three IR pulses are performed at each pixel which ablates all the way through the 50 µm thick tissue section with the ion injection time (length of time that ions are accumulated in the LTQ) set to 200 ms in order to accumulate ions from all three laser pulses (3 pulses at 20 Hz). In this manner, a single acquisition mass spectrum is obtained at each pixel location. Thus, the signal at each pixel in the ion image is representative of an average of ions from the entire voxel of material that is ablated. It should also be noted that liver morphology can vary within these 50 µm thick voxels. A rectangular region of interest (ROI) that defines the boundaries of the MSI experiment was drawn to encompass the entire tissue area The MSI experiments were performed at a spatial resolution of 150 µm.

3.2.4 UV-MALDI Imaging

Immediately following thaw-mounting of the tissue section on the ITO coated glass slide, a matrix solution consisting of DHB (30 mg/mL) in water/methanol/TFA (1:1:.05 v/v/v) was applied using an ImagePrep (Bruker Daltonics, Billerica, MA) automated matrix application device for all UV-MALDI tissue slides. All UV-MALDI

experiments were performed using a Solarix 7T Fourier transform-ion cyclotron resonance mass spectrometer (Bruker Daltonics, Billerica, MA). Data were acquired at a spatial resolution of 150 µm and spectra at each position were generated using 100 laser shots at a frequency of 1 kHz. Dog liver tissue sections consisted of 2962 pixels. Ion images for tissue sections were acquired in 1 hour at a peak resolution of ~125,000 (FWHM, m/z 400).

3.2.5 Data Analysis

The .raw files from the Thermo instrument were converted into mzXML files using the freely available MSConvert tool from Proteowizard [50]. The Bruker files were exported as .ascii files using CompassXport (free data export tool from Bruker). Analysis of both imaging files was performed using the freely available standalone version of the MSiReader software.[51] All images shown have not been normalized or interpolated in order to demonstrate the true quality of the raw data. The observed accurate masses were used to assign the identification of lapatinib and its metabolites. The nomenclature for the observed metabolites is based on a previously published metabolite descriptions of lapatinib.[52] For the pixel by pixel calculation of the percentage of drug-related material (% DRM), the pixel intensities for lapatinib and all of its metabolites were exported from MSiReader by exporting the intensity data for all pixels containing drug related material. These intensity values for all drug-related *m/z*'s were summed on a pixel by pixel basis to obtain a heat map of the total intensity for all DRM. This new heat map was then loaded

back into MSiReader using the load custom data function. By normalizing lapatinib or one of its metabolites with this custom heat map, the percentage of total DRM at each pixel can be determined for each drug component. These heat maps show the distribution of the composition of DRM in each pixel where the intensity scale is % DRM for that particular compound (lapatinib or metabolites). While this is not an exact measure of the % DRM due to potential differences in ionization efficiency, it can provide valuable information about the relative distribution of the parent and its metabolites.

3.2.6 IR-MALDESI Imaging Solvent Composition Analysis

To investigate the effect of the electrospray solvent composition on the observed signal from an IR-MALDESI MSI experiment, the syringe pump was replaced with a HPLC pump (Chorus 220, Leap Technologies, Carrboro, NC). Both methanol and acetonitrile were investigated as the organic solvent. The solvent compositions were as follows; solvent A: 95% water 5% organic (methanol or acetonitrile) 0.2% formic acid and solvent B: 5% water 95% organic (methanol or acetonitrile) 0.2% formic acid. The following solvent gradient was performed during an imaging analysis within the tissue section at a flow rate of 3 µL/min.; 0-5 min 95% A, 5-20 min 95% A to 95% B, 20-25 min 95%B. A rectangular ROI was selected such that every pixel in the imaging experiment was on tissue (Fig. 2a-b). Three separate experiments were performed for each solvent system on serial sections of lapatinib dosed liver tissue. The extracted ion chromatograms for several lipid

species (369.3516, cholesterol, $[M+H-H_2O]^+$; 758.5694, PC(34:2)/PE(37:2), $[M+H]^+$; 786.6007, PC(36:2)/PE(39:2), $[M+H]^+$; 806.5694, PC(38:6)/PE(41:6), $[M+H]^+$; 810.6007, PC(38:4)/PE(41:4), $[M+H]^+$), lapatinib and its metabolites, and several ambient ions (371.1012, pentadimethylcyclocyloxane, $[M+H]^+$; 519.1388, heptadimethylcyclocyloxane, $[M+H]^+$; 536.1654, heptadimethylcyclocyloxane, $[M+NH_4]^+$; 593.1576, octadimethylcyclocyloxane, $[M+H]^+$; 610.1841, octadimethylcyclocyloxane, $[M+NH_4]^+$) were obtained for each experiment using Xcalibur (ThermoFisher Scientific) and exported into Excel. The intensities for each group (lipids, DRM, and ambient ions) were summed for each experiment and the plots in Figure 3.2c) represent a 20 point moving average of all three imaging experiments for both solvent systems.

3.3 Results and Discussion

3.3.1 Preliminary IR-MALDESI Imaging

IR-MALDESI MSI was performed on a 50 µm thick section of dog liver tissue from an animal dosed with the tyrosine kinase inhibitor lapatinib. Because of the increased penetration depth of an IR laser compared to UV, a significantly larger amount of material is ablated with a single IR laser pulse.[53] While drug related signal was observed with 12 µm thick tissue sections, a previous investigation on the effect of tissue thickness on overall IR-MALDESI signal demonstrated that the use of thicker tissue with multiple pulses per pixel provided more consistent results (data not shown). This, however, does come at the cost of loss of spatial resolution in the

z-direction where tissue morphology can vary within the thicker tissue sections. The tissue section was placed on the liquid cooled Peltier stage of the IR-MALDESI source and a thin layer of ice was deposited over the top of the tissue section just prior to analysis. This ice layer has been shown to improve sensitivity and pixel to pixel reproducibility in IR-MALDESI imaging experiments[46,48] as it resonantly absorbs the laser energy and facilitates efficient desorption of the tissue-related material.

The results of the IR-MALDESI MSI experiment are shown in **Figure 3.1a-e**. In addition to detecting lapatinib, IR-MALDESI MSI was capable of determining the spatial distribution for eleven of its metabolites (see supplemental **Figure 3.2** for ion maps of all drug-related material). Optical images of the tissue section before (**Figure 3.1a**) and after the ice matrix deposition (**Figure 3.1b**) demonstrate the uniformity of matrix application. At 150 μm spatial resolution, the distribution of the parent drug as $[M+H]^+$ appears to be homogenously distributed throughout the liver with exception to the area around the blood vessels where little to no lapatinib was detected (**Figure 3.1c**). To highlight the location of these blood vessels, the distribution for heme b as $[M]^+$ is presented in **Figure 3.1d** and an overlay of the lapatinib distribution (blue) with the heme distribution (red) is shown in **Figure 3.1e**. Additionally, there were over 700 peaks relating to endogenous species that were also detected. Based on an accurate mass search of this peak list in the Scripps METLIN database,[54] a majority of these endogenous species were likely to be lipids (primarily phosphocholines). The lower mass limit for the subsequent UV-MALDI

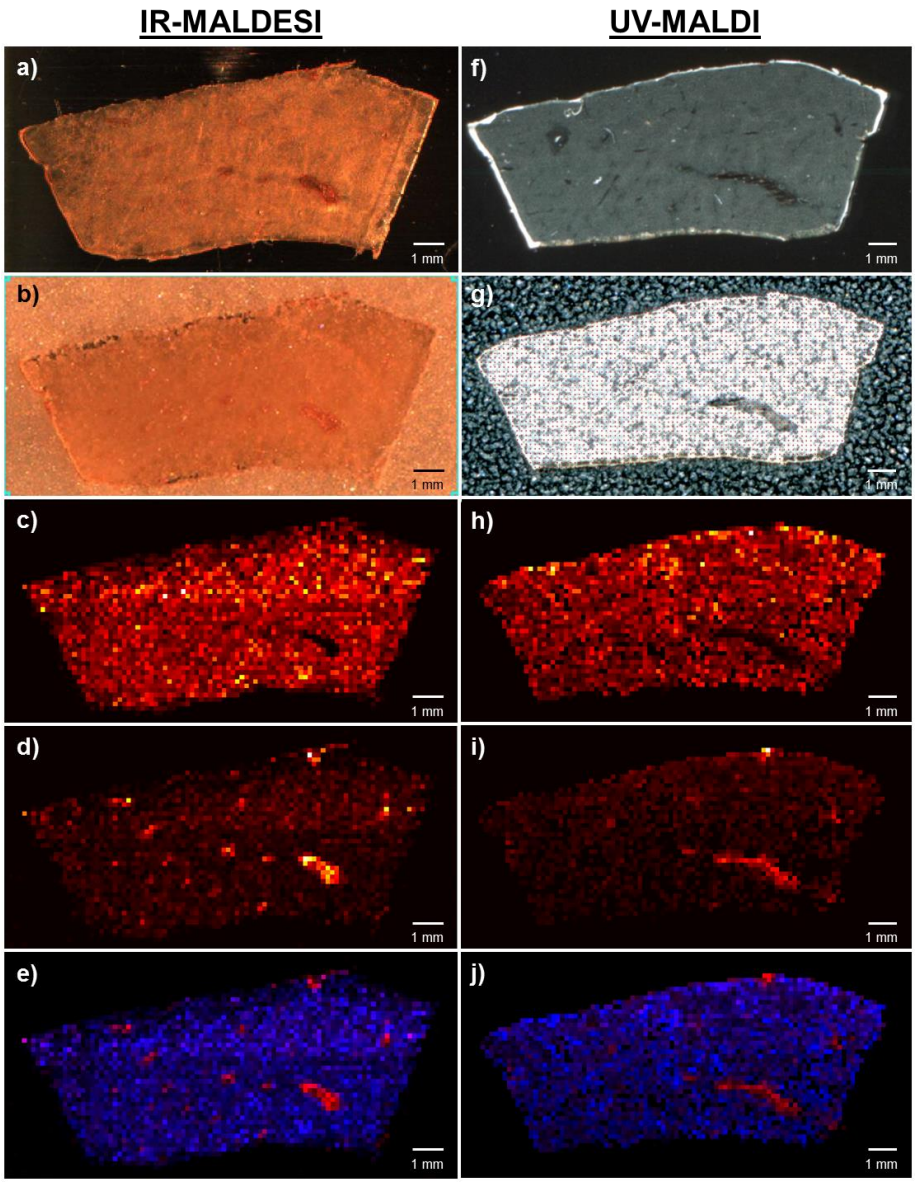

Figure 3.1 IR-MALDESI (**a-e**) and UV-MALDI (**f-j**) MSI of lapatinib dosed liver tissue. **a)** Optical image of liver tissue section analyzed by IR-MALDESI. **b)** Optical image of liver tissue section after deposition of ice matrix. **c)** Ion map of lapatinib $[M+H]^+$. **d)** Ion map of heme b $[M]^+$ showing the distribution of the blood vessels. **e)** Overlay of **c)** and **d)** where blue is the lapatinib and red is the heme b distribution. **f)** Optical image of liver tissue section analyzed by UV-MALDI. **g)** Optical image of liver tissue section after matrix application. **h)** Ion map of lapatinib $[M+H]^+$. **i)** Ion map of SM(34:0) or PE-Cer(37:1) $[M+H]^+$ showing the distribution of the blood vessels. **j)** Overlay of **h)** and **i)** where blue is the lapatinib and red is the blood vessel distribution

analysis was set to *m/z* 340 to avoid low mass interferences from matrix related peaks. Given that the matrix for the IR-MALDESI imaging experiments is ice, there are no low mass matrix interferences allowing for acquisition of a lower mass range (*m/*z 150 for these experiments). Of the endogenous species that were detected, over 40 of them were below the lower mass range for the UV-MALDI acquisition (340 *m/z*). These low m/z peaks include endogenous species such as phenylalanine, spermine, and adenosine just to name a few. The ability to acquire imaging data at such low *m/z* without matrix interference becomes even more significant when investigating the distribution of drugs or endogenous species that fall within this range.

3.3.2 UV-MALDI Imaging

UV-MALDI MSI was performed on a 12 µm thick section of dog liver that was a serial cut to the one analyzed by IR-MALDESI to allow for empirical comparison between the two techniques. The UV-MALDI results are shown in **Figure 3.1f-j**. Images depicting the section before and after the matrix application process are shown in **Figure 3.1f** and **Figure 3.1g** respectively. The spatial resolution of the MALDI experiment was set to 150 µm to match the resolution currently attainable by IR-MALDESI. The conditions used for the matrix application step in MALDI IMS can be adjusted to match the desired spatial resolution. Higher spatial resolution experiments (e.g. 10 µm) require higher quality application (e.g. sublimation) of the matrix to achieve a homogenous coating and avoid introducing artificial variation of

DRM	Formula	Exact Mass $[M+H]^+$	Distribution
Lapatinib	$C_{29}H_{26}ClFN_4O_4S$	581.1420	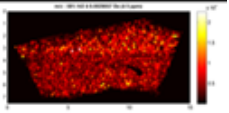
M1	$C_{22}H_{21}ClN_4O_4S$	473.1045	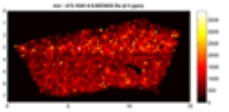
M2	$C_{26}H_{18}ClFN_4O_2$	473.1175	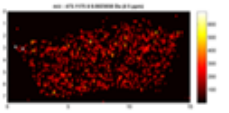
M4	$C_{26}H_{20}ClFN_4O_2$	475.1332	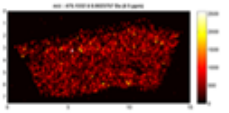
M8	$C_{29}H_{26}ClFN_4O_5S$	597.1369	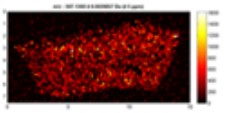
M9/10	$C_{26}H_{18}ClFN_4O_3$	489.1124	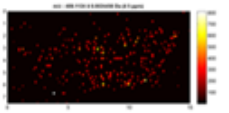
M11	$C_{26}H_{17}ClFN_3O_3$	474.1015	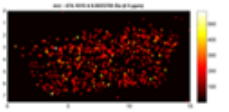
M12	$C_{26}H_{17}ClFN_3O_4$	490.0964	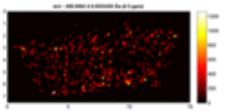
	$C_{26}H_{17}ClFN_3O_2$	458.1066	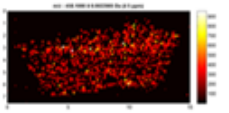
	$C_{26}H_{19}ClFN_3O_2$	460.1223	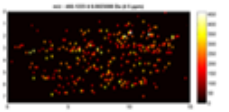
	$C_{22}H_{19}ClN_4O_4S$	471.0888	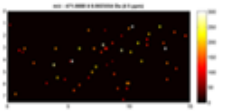
	$C_{27}H_{20}ClFN_4O_3$	503.1281	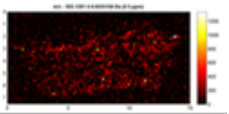

Figure 3.2 Ion maps for all drug related material (lapatinib and metabolites) that were observed from the preliminary IR-MALDESI MSI analysis.

the analyte signal. In these experiments, given the relatively low spatial resolution, the matrix application step was adjusted to enhance for sensitivity by increasing the volume of matrix solution applied during each spray cycle to increases the analyte extraction from the tissue. As a result, it is apparent from **Figure 3.1g** that the aggressive matrix application method used in this instance resulted in heterogeneous crystal formation on the tissue surface. This heterogeneity can produce variation in analyte signal that correlates with the local matrix concentration. This technique, however, led to the observation of lapatinib as $[M+H]^+$ (**Figure 3.1h**) as well as twenty-four metabolites of lapatinib directly from the dog liver tissue. The distributions for these metabolites are similar to the one shown for lapatinib (**Figure 3.1h**) but can be found in **Figure 3.3**. Lapatinib and its metabolites were detected homogeneously throughout the liver at this spatial resolution. As was observed in the IR-MALDESI MSI analysis, lapatinib was not detected in the regions around the blood vessels. The ion image for *m/z* 725.5575 (**Figure 3.1i**), tentatively identified as SM(34:0) or PE-Cer(37:1), relates to the location of these blood vessels and an overlay with the lapatinib distribution is given in **Figure 3.1j**. Comparison of **Figure 3.1c** (IR-MALDESI lapatinib distribution) and **Figure 3.1h** (UV-MALDI lapatinib distribution) highlights that both techniques provide similar results. The UV-MALDI MSI technique was able to detect more of the lesser abundant metabolites, however, because these MALDI and MALDESI experiments were performed on two different mass spectrometers, it is difficult to discern whether this improved sensitivity is directly related to differences in the ionization sources.

DRM	Formula	Exact Mass $[M+H]^+$	Distribution
Lapatinib	$C_{29}H_{26}ClFN_4O_4S$	581.1420	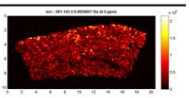
M1	$C_{22}H_{21}ClN_4O_4S$	473.1045	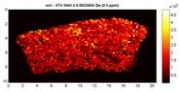
M2	$C_{26}H_{18}ClFN_4O_2$	473.1175	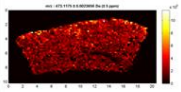
M3	$C_{22}H_{21}ClN_4O_5S$	489.0994	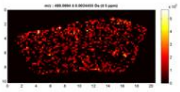
M4	$C_{26}H_{20}ClFN_4O_2$	475.1332	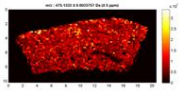
M5	$C_{29}H_{24}ClFN_4O_4S$	579.1264	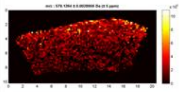
M6/7	$C_{29}H_{24}ClFN_4O_5S$	595.1213	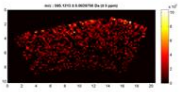
M8	$C_{29}H_{26}ClFN_4O_5S$	597.1369	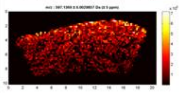
M9/10	$C_{26}H_{18}ClFN_4O_3$	489.1124	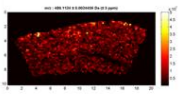
M11	$C_{26}H_{17}ClFN_3O_3$	474.1015	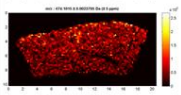
M12	$C_{26}H_{17}ClFN_3O_4$	490.0964	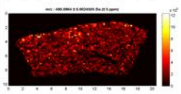

DRM	Formula	Exact Mass $[M+H]^+$	Distribution
	$C_{26}H_{17}ClFN_3O_2$	458.1066	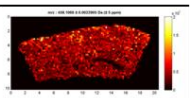
	$C_{26}H_{19}ClFN_3O_2$	460.1223	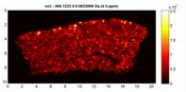
	$C_{22}H_{19}ClN_4O_4S$	471.0888	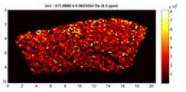
	$C_{22}H_{19}ClN_4O_4S$	476.1172	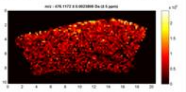
	$C_{25}H_{19}ClN_3O_4$	480.1121	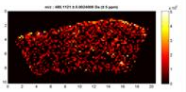
	$C_{26}H_{20}ClFN_4O_3$	491.1281	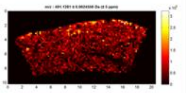
	$C_{27}H_{20}ClFN_4O_3$	503.1281	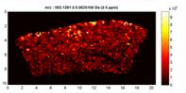
	$C_{26}H_{18}ClFN_4O_5S$	553.0743	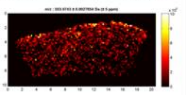
	$C_{30}H_{26}ClFN_4O_5S$	625.1318	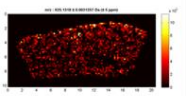
	$C_{32}H_{26}ClFN_4O_8$	649.1496	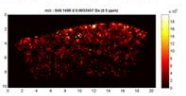
	$C_{32}H_{26}ClFN_4O_9$	665.1445	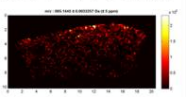
	$C_{32}H_{25}ClFN_3O_{10}$	666.1285	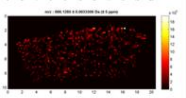
	$C_{33}H_{28}ClFN_4O_9$	679.1602	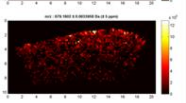
	$C_{36}H_{34}ClFN_4O_{12}S$	801.1639	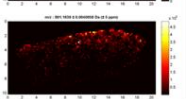

Figure 3.3 Ion maps for all drug related material (lapatinib and metabolites) that were observed from the UV-MALDI MSI analysis.

3.3.3 Influence of Electrospray Solvent Composition

Comparison of the preliminary IR-MALDESI MSI results with those obtained from UV-MALDI revealed that the latter may be more sensitive as more of the lesser abundant metabolites were observed. In order to improve sensitivity, an optimization of the IR-MALDESI source geometry for tissue imaging experiments was performed.[48] In addition to the source geometry optimization, the influence of the electrospray solvent composition on IR-MALDESI signal was also investigated. It was hypothesized that the composition of the electrospray solvent would impact analyte partitioning into the charged solvent droplets and prior results from other groups using similar ionization sources support this hypothesis.[55,56]

To systematically explore how solvent composition influences the observed IR-MALDESI signal, the syringe pump that normally supplies the isocratic flow of electrospray solvent was replaced with an LC pump to provide a solvent gradient. In short, an imaging experiment was performed over the lapatinib dosed liver tissue while an LC gradient from 5% organic to 95% organic was performed. Both methanol and acetonitrile were investigated as the organic solvent. The results of these experiments are provided in **Figure 3.4**. Optical images of the ROI for each imaging experiment are provided in **Figure 3.4a** for the acetonitrile gradient and **Figure 3.4b** for the methanol gradient. The summed extracted ion chromatograms of several lipids are represented in blue, lapatinib and its metabolites are shown in red, and several ambient ions are shown in green. Also provided is an overlay of the gradient plotted on the secondary y-axis. For both solvent systems the abundance

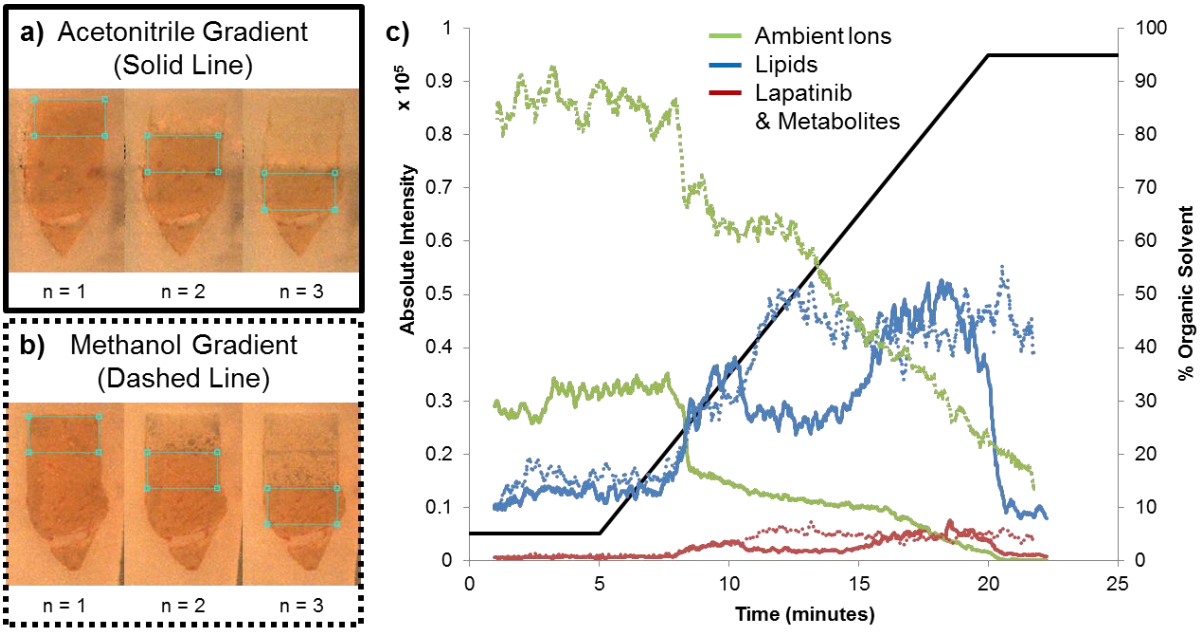

Figure 3.4 Influence of solvent composition on IR-MALDESI MSI signal of tissue related material. **a)** Optical images showing the region of interest for the three imaging experiments performed with an acetonitrile gradient. **b)** Optical images showing the region of interest for the three imaging experiments performed with a methanol gradient. **c)** The summed extracted ion chromatograms for several lipids (blue lines), ambient ions (green lines), and lapatinib and its metabolites (red lines). The solid lines represent data from the acetonitrile gradient and the dashed lines represent data from the methanol gradient.

of the tissue-related ions (lipids and DRM) was low with the high aqueous composition but started to increase by around 20% B. The acetonitrile gradient (solid lines) shows an initial spike around 35% B then the most abundant signal for both groups of tissue-related ions was observed at around 75% B. For the methanol gradient (dashed lines) the tissue-related ions reach their maximum abundance around 50% B then the abundance pretty much plateaus. At the optimal solvent composition for both solvent systems, the maximum abundance for both tissue-related ion groups (lipids and DRM) was essentially the same. However, the major

difference between the two was the abundance of the ambient ions. As can be observed in **Figure 3.4c**, at 50% B in the methanol gradient, where the tissue-related signal is maximized, the ambient ions are more abundant than at 75% B in the acetonitrile gradient. Because these ions are being used as internal calibrants for mass recalibration, it is important that they are relatively abundant. Therefore, 50% aqueous methanol with 0.2% formic acid was chosen as the optimal solvent composition for IR-MALDESI MSI of these lapatinib dosed liver tissue sections. Even though this experiment did not exhibit much selectivity between the two tissue-related groups (lipids vs. DRM) it did lead to an overall improvement in tissue-related signal.

3.3.4 IR-MALDESI Imaging with Optimized Geometry and Solvent Composition

Sections of the lapatinib dosed liver tissue were examined by IR-MALDESI using the optimal solvent composition and recently optimized source geometry.[48] This analysis resulted in the observation of several more metabolites that were not previously detected by IR-MALDESI (**Figure 3.5**) as well as an improvement in signal reproducibility (pixel-to-pixel variability). A summary of the results from the optimized IR-MALDESI MSI analysis is shown in **Figure 3.6**. The optical image of the tissue as well as the distributions for lapatinib and the metabolite M1 are presented in **Figure 3.6a, c,** and **d** respectively. Again, the distribution is homogeneous throughout the tissue as was observed in the previous experiments. A new method for evaluating the distribution of drug-related ions is also presented.

DRM	Formula	Exact Mass $[M+H]^+$	Distribution
Lapatinib	$C_{29}H_{26}ClFN_4O_4S$	581.1420	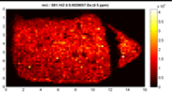
M1	$C_{22}H_{21}ClN_4O_4S$	473.1045	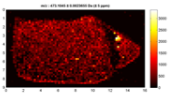
M2	$C_{26}H_{18}ClFN_4O_2$	473.1175	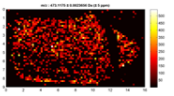
M3	$C_{22}H_{21}ClN_4O_5S$	489.0994	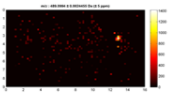
M4	$C_{26}H_{20}ClFN_4O_2$	475.1332	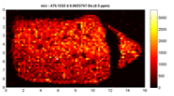
M8	$C_{29}H_{26}ClFN_4O_5S$	597.1369	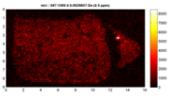
M9/10	$C_{26}H_{18}ClFN_4O_3$	489.1124	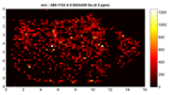
M11	$C_{26}H_{17}ClFN_3O_3$	474.1015	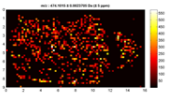
M12	$C_{26}H_{17}ClFN_3O_4$	490.0964	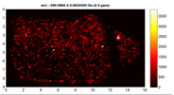

DRM	Formula	Exact Mass $[M+H]^+$	Distribution
	$C_{26}H_{17}ClFN_3O_2$	458.1066	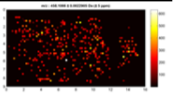
	$C_{22}H_{19}ClN_4O_4S$	476.1172	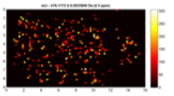
	$C_{27}H_{20}ClFN_4O_3$	503.1281	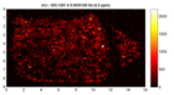
	$C_{30}H_{26}ClFN_4O_5S$	625.1318	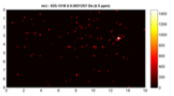
	$C_{35}H_{34}ClFN_4O_{11}S$	773.1690	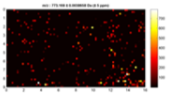
	$C_{36}H_{34}ClFN_4O_{12}S$	801.1639	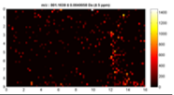

Figure 3.5 Ion maps for all drug related material (lapatinib and metabolites) that were observed from the optimized IR-MALDESI MSI analysis.

By summing the intensities for all drug-related ions on a pixel-by-pixel basis, the image in **Figure 3.6b** can be obtained. Normalizing lapatinib or one of its metabolites to this total DRM image provides the composition of DRM at each pixel. For lapatinib, the % DRM image (**Figure 3.6e**) shows that it makes up roughly 70% of all drug-related intensity homogeneously over the tissue while not being detected in the blood vessels. In contrast, M1 (**Figure 3.6f**) was roughly 3% of the total DRM over most of the tissue but around the blood vessels the M1 makes up a larger

portion of the total DRM. This implies that it is one of the only metabolites observed in this region. This information is not as obvious when looking at the M1 ion distribution (**Figure 3.6d**) alone which supports the utility of determining the % DRM distribution.

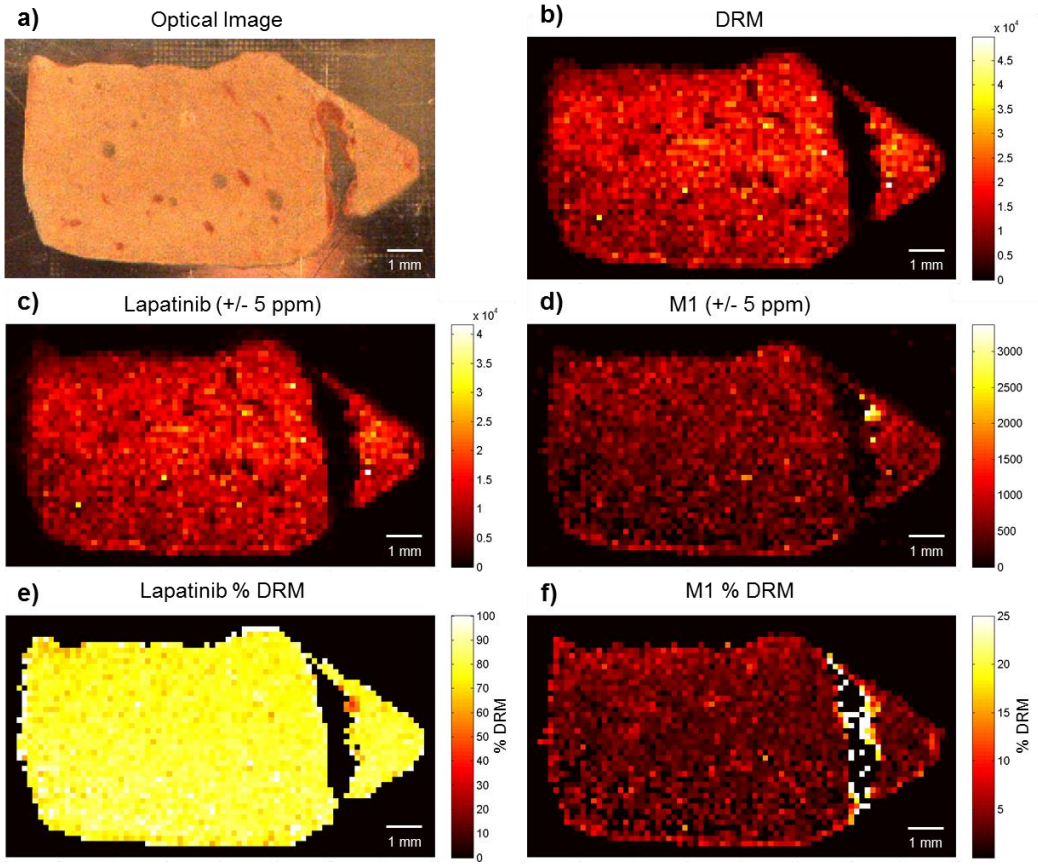

Figure 3.6 IR-MALDESI MSI of lapatinib dosed liver tissue section after optimization of solvent composition and geometrical parameters. **a)** Optical image of the liver tissue section prior to ice matrix deposition. **b)** Ion map depicting the pixel-by-pixel sum of all drug related material. **c)** Ion map of lapatinib $[M+H]^+$. **d)** Ion map of metabolite M1 $[M+H]^+$. **e)** Distribution of the lapatinib composition of the total drug related material. **f)** Distribution of the M1 composition of the total drug related material.

3.4 Conclusion

These experiments serve as proof of principle that IR-MALDESI MSI coupled to FT-ICR can be used to determine the distribution of a dosed drug and its metabolites directly from tissue. The influence of the electrospray solvent composition on IR-MALDESI signal for tissue related ions was also investigated and it was determined that a 50% aqueous methanol solution provided the best results. Furthermore, through analysis of a serial tissue section with the more commonly used UV-MALDI MSI, it was demonstrated that both techniques offer complementary information. Due to the heterogeneity of the matrix crystallization that was observed for the UV-MALDI experiments, attention must be paid to assure an even coating and reduction in analytical variability. In addition, the IR-MALDESI source is currently being coupled to the Q Exactive which has demonstrated improved ion transmission compared to the LTQ-FT and could result in observation of the lesser abundant metabolites.

3.5 References

(1) Lanao, J. M.; Fraile, M. A. Drug Tissue Distribution: Study Methods and Therapeutic Implications. *Curr. Pharm. Des.* **2005**, *11*(29), 3829-3845.

(2) Eichler, H.-G.; Müller, M. Drug Distribution. *Clin. Pharmacokinet.* **1998**, *34*(2), 95-99.

(3) Jespersen, S.; Niessen, W. M. A.; Tjaden, U. R.; van der Greef, J.; Litborn, E.; Lindberg, U.; Roeraade, J.; Hillenkamp, F. Attomole detection of proteins by matrix-assisted laser desorption/ionization mass spectrometry with the use of picolitre vials. *Rapid Commun. Mass Spectrom.* **1994**, *8*(8), 581-584.

(4) Troendle, F. J.; Reddick, C. D.; Yost, R. A. Detection of pharmaceutical compounds in tissue by matrix-assisted laser desorption/ionization and laser desorption/chemical ionization tandem mass spectrometry with a quadrupole ion trap. *J. Am. Soc. Mass Spectrom.* **1999**, *10*(12), 1315-1321.

(5) Todd, P. J.; Schaaff, T. G.; Chaurand, P.; Caprioli, R. M. Organic ion imaging of biological tissue with secondary ion mass spectrometry and matrix-assisted laser desorption/ionization. *J. Mass Spectrom.* **2001**, *36*(4), 355-369.

(6) Reyzer, M. L.; Hsieh, Y.; Ng, K.; Korfmacher, W. A.; Caprioli, R. M. Direct analysis of drug candidates in tissue by matrix-assisted laser desorption/ionization mass spectrometry. *J. Mass Spectrom.* **2003**, *38*(10), 1081-1092.

(7) Hsieh, Y.; Casale, R.; Fukuda, E.; Chen, J.; Knemeyer, I.; Wingate, J.; Morrison, R.; Korfmacher, W. Matrix-assisted laser desorption/ionization imaging mass spectrometry for direct measurement of clozapine in rat brain tissue. *Rapid Commun. Mass Spectrom.* **2006**, *20*(6), 965-972.

(8) Khatib-Shahidi, S.; Andersson, M.; Herman, J. L.; Gillespie, T. A.; Caprioli, R. M. Direct Molecular Analysis of Whole-Body Animal Tissue Sections by Imaging MALDI Mass Spectrometry. *Anal. Chem.* **2006**, *78*(18), 6448-6456.

(9) Drexler, D. M.; Garrett, T. J.; Cantone, J. L.; Diters, R. W.; Mitroka, J. G.; Prieto Conaway, M. C.; Adams, S. P.; Yost, R. A.; Sanders, M. Utility of imaging mass spectrometry (IMS) by matrix-assisted laser desorption ionization (MALDI) on an ion trap mass spectrometer in the analysis of drugs and metabolites in biological tissues. *J. Pharmacol. Toxicol. Methods* **2007**, *55*(3), 279-288.

(10) Hsieh, Y.; Chen, J.; Korfmacher, W. A. Mapping pharmaceuticals in tissues using MALDI imaging mass spectrometry. *J. Pharmacol. Toxicol. Methods* **2007**, *55*(2), 193-200.

(11) Signor, L.; Varesio, E.; Staack, R. F.; Starke, V.; Richter, W. F.; Hopfgartner, G. Analysis of erlotinib and its metabolites in rat tissue sections by MALDI quadrupole time-of-flight mass spectrometry. *J. Mass Spectrom.* **2007**, *42*(7), 900-909.

(12) Stoeckli, M.; Staab, D.; Schweitzer, A. Compound and metabolite distribution measured by MALDI mass spectrometric imaging in whole-body tissue sections. *Int. J. Mass Spectrom.* **2007**, *260*(2–3), 195-202.

(13) Kertesz, V.; Van Berkel, G. J.; Vavrek, M.; Koeplinger, K. A.; Schneider, B. B.; Covey, T. R. Comparison of Drug Distribution Images from Whole-Body Thin Tissue Sections Obtained Using Desorption Electrospray Ionization Tandem Mass Spectrometry and Autoradiography. *Anal. Chem.* **2008**, *80*(13), 5168-5177.

(14) Trim, P. J.; Atkinson, S. J.; Princivalle, A. P.; Marshall, P. S.; West, A.; Clench, M. R. Matrix-assisted laser desorption/ionisation mass spectrometry imaging of lipids in rat brain tissue with integrated unsupervised and supervised multivariant statistical analysis. *Rapid Commun. Mass Spectrom.* **2008**, *22*(10), 1503-1509.

(15) Wiseman, J. M.; Ifa, D. R.; Zhu, Y.; Kissinger, C. B.; Manicke, N. E.; Kissinger, P. T.; Cooks, R. G. Desorption electrospray ionization mass spectrometry: Imaging drugs and metabolites in tissues. *Proceedings of the National Academy of Sciences* **2008**, *105*(47), 18120-18125.

(16) Acquadro, E.; Cabella, C.; Ghiani, S.; Miragoli, L.; Bucci, E. M.; Corpillo, D. Matrix-Assisted Laser Desorption Ionization Imaging Mass Spectrometry Detection of a Magnetic Resonance Imaging Contrast Agent in Mouse Liver. *Anal. Chem.* **2009**, *81*(7), 2779-2784.

(17) Goodwin, R. J. A.; Scullion, P.; MacIntyre, L.; Watson, D. G.; Pitt, A. R. Use of a Solvent-Free Dry Matrix Coating for Quantitative Matrix-Assisted Laser Desorption Ionization Imaging of 4-Bromophenyl-1,4-diazabicyclo(3.2.2)nonane-4-carboxylate in Rat Brain and Quantitative Analysis of the Drug from Laser Microdissected Tissue Regions. *Anal. Chem.* **2010**, *82*(9), 3868-3873.

(18) Nilsson, A.; Fehniger, T. E.; Gustavsson, L.; Andersson, M.; Kenne, K.; Marko-Varga, G.; Andrén, P. E. Fine Mapping the Spatial Distribution and Concentration of Unlabeled Drugs within Tissue Micro-Compartments Using Imaging Mass Spectrometry. *PLoS One* **2010**, *5*(7), e11411.

(19) Koeniger, S. L.; Talaty, N.; Luo, Y.; Ready, D.; Voorbach, M.; Seifert, T.; Cepa, S.; Fagerland, J. A.; Bouska, J.; Buck, W.; Johnson, R. W.; Spanton, S. A quantitation method for mass spectrometry imaging. *Rapid Commun. Mass Spectrom.* **2011**, *25*(4), 503-510.

(20) Manier, M. L.; Reyzer, M.; Goh, A.; Dartois, V.; Via, L.; Barry, C., III; Caprioli, R. Reagent Precoated Targets for Rapid In-Tissue Derivatization of the Anti-Tuberculosis Drug Isoniazid Followed by MALDI Imaging Mass Spectrometry. *J. Am. Soc. Mass Spectrom.* **2011**, *22*(8), 1409-1419.

(21) Prideaux, B.; Dartois, V. r.; Staab, D.; Weiner, D. M.; Goh, A.; Via, L. E.; Barry Iii, C. E.; Stoeckli, M. High-Sensitivity MALDI-MRM-MS Imaging of Moxifloxacin Distribution in Tuberculosis-Infected Rabbit Lungs and Granulomatous Lesions. *Anal. Chem.* **2011**, *83*(6), 2112-2118.

(22) Castellino, S.; Groseclose, M. R.; Sigafoos, J.; Wagner, D.; de Serres, M.; Polli, J. W.; Romach, E.; Myer, J.; Hamilton, B. Central Nervous System Disposition and Metabolism of Fosdevirine (GSK2248761), a Non-Nucleoside Reverse Transcriptase Inhibitor: An LC-MS and Matrix-Assisted Laser Desorption/Ionization Imaging MS Investigation into Central Nervous System Toxicity. *Chem. Res. Toxicol.* **2012**, *26*(2), 241-251.

(23) Hamm, G.; Bonnel, D.; Legouffe, R.; Pamelard, F.; Delbos, J.-M.; Bouzom, F.; Stauber, J. Quantitative mass spectrometry imaging of propranolol and olanzapine using tissue extinction calculation as normalization factor. *Journal of Proteomics* **2012**, *75*(16), 4952-4961.

(24) Nilsson, A.; Forngren, B.; Bjurström, S.; Goodwin, R. J. A.; Basmaci, E.; Gustafsson, I.; Annas, A.; Hellgren, D.; Svanhagen, A.; Andrén, P. E.; Lindberg, J. In Situ Mass Spectrometry Imaging and Ex Vivo Characterization of Renal Crystalline Deposits Induced in Multiple Preclinical Drug Toxicology Studies. *PLoS One* **2012**, *7*(10), 1-10.

(25) Pirman, D. A.; Reich, R. F.; Kiss, A.; Heeren, R. M. A.; Yost, R. A. Quantitative MALDI Tandem Mass Spectrometric Imaging of Cocaine from Brain Tissue with a Deuterated Internal Standard. *Anal. Chem.* **2012**, *85*(2), 1081-1089.

(26) Takai, N.; Tanaka, Y.; Inazawa, K.; Saji, H. Quantitative analysis of pharmaceutical drug distribution in multiple organs by imaging mass spectrometry. *Rapid Commun. Mass Spectrom.* **2012**, *26*(13), 1549-1556.

(27) Vismeh, R.; Waldon, D. J.; Teffera, Y.; Zhao, Z. Localization and Quantification of Drugs in Animal Tissues by Use of Desorption Electrospray Ionization Mass Spectrometry Imaging. *Anal. Chem.* **2012**, *84*(12), 5439-5445.

(28) Atkinson, S. J.; Loadman, P. M.; Sutton, C.; Patterson, L. H.; Clench, M. R. Examination of the distribution of the bioreductive drug AQ4N and its active metabolite AQ4 in solid tumours by imaging matrix-assisted laser desorption/ionisation mass spectrometry. *Rapid Commun. Mass Spectrom.* **2007**, *21*(7), 1271-1276.

(29) Castellino, S.; Groseclose, M. R.; Wagner, D. MALDI imaging mass spectrometry: bridging biology and chemistry in drug development. *Bioanalysis* **2011**, *3*(21), 2427-2441.

(30) Römpp, A.; Guenther, S.; Takats, Z.; Spengler, B. Mass spectrometry imaging with high resolution in mass and space (HR^2 MSI) for reliable investigation of drug compound distributions on the cellular level. *Anal. Bioanal. Chem.* **2011**, *401*(1), 65-73.

(31) Goodwin, R. J. A.; Iverson, S. L.; Andren, P. E. The significance of ambient-temperature on pharmaceutical and endogenous compound abundance and distribution in tissues sections when analyzed by matrix-assisted laser desorption/ionization mass spectrometry imaging. *Rapid Commun. Mass Spectrom.* **2012**, *26*(5), 494-498.

(32) Shariatgorji, M.; Nilsson, A.; Goodwin, R. J. A.; Svenningsson, P.; Schintu, N.; Banka, Z.; Kladni, L.; Hasko, T.; Szabo, A.; Andren, P. E. Deuterated Matrix-Assisted Laser Desorption Ionization Matrix Uncovers Masked Mass Spectrometry Imaging Signals of Small Molecules. *Anal. Chem.* **2012**, *84*(16), 7152-7157.

(33) Cornett, D. S.; Frappier, S. L.; Caprioli, R. M. MALDI-FTICR Imaging Mass Spectrometry of Drugs and Metabolites in Tissue. *Anal. Chem.* **2008**, *80*(14), 5648-5653.

(34) Dekker, L. J. M.; van Kampen, J. J. A.; Reedijk, M. L.; Burgers, P. C.; Gruters, R. A.; Osterhaus, A. D. M. E.; Luider, T. M. A mass spectrometry based

imaging method developed for the intracellular detection of HIV protease inhibitors. *Rapid Commun. Mass Spectrom.* **2009**, *23*(8), 1183-1188.

(35) Végvári, Á.; Fehniger, T. E.; Gustavsson, L.; Nilsson, A.; Andrén, P. E.; Kenne, K.; Nilsson, J.; Laurell, T.; Marko-Varga, G. Essential tactics of tissue preparation and matrix nano-spotting for successful compound imaging mass spectrometry. *Journal of Proteomics* **2010**, *73*(6), 1270-1278.

(36) Marko-Varga, G.; Fehniger, T. E.; Rezeli, M.; Döme, B.; Laurell, T.; Végvári, Á. Drug localization in different lung cancer phenotypes by MALDI mass spectrometry imaging. *Journal of Proteomics* **2011**, *74*(7), 982-992.

(37) Fehniger, T. E.; Végvári, Á.; Rezeli, M.; Prikk, K.; Ross, P.; Dahlbäck, M.; Edula, G.; Sepper, R.; Marko-Varga, G. Direct Demonstration of Tissue Uptake of an Inhaled Drug: Proof-of-Principle Study Using Matrix-Assisted Laser Desorption Ionization Mass Spectrometry Imaging. *Anal. Chem.* **2011**, *83*(21), 8329-8336.

(38) Shahidi-Latham, S. K.; Dutta, S. M.; Prieto Conaway, M. C.; Rudewicz, P. J. Evaluation of an Accurate Mass Approach for the Simultaneous Detection of Drug and Metabolite Distributions via Whole-Body Mass Spectrometric Imaging. *Anal. Chem.* **2012**, *84*(16), 7158-7165.

(39) Herniman, J.; Langley, G.; Bristow, T.; O'Connor, G. The validation of exact mass measurements for small molecules using FT-ICRMS for improved confidence in the selection of elemental formulas. *J. Am. Soc. Mass Spectrom.* **2005**, *16*(7), 1100-1108.

(40) Crossman, L.; McHugh, N. A.; Hsieh, Y.; Korfmacher, W. A.; Chen, J. Investigation of the profiling depth in matrix-assisted laser desorption/ionization imaging mass spectrometry. *Rapid Commun. Mass Spectrom.* **2006**, *20*(2), 284-290.

(41) Marshall, P.; Toteu-Djomte, V.; Bareille, P.; Perry, H.; Brown, G.; Baumert, M.; Biggadike, K. Correlation of Skin Blanching and Percutaneous Absorption for Glucocorticoid Receptor Agonists by Matrix-Assisted Laser Desorption Ionization Mass Spectrometry Imaging and Liquid Extraction Surface Analysis with Nanoelectrospray Ionization Mass Spectrometry. *Anal. Chem.* **2010**, *82*(18), 7787-7794.

(42) Blatherwick, E. Q.; Berkel, G. J. V.; Pickup, K.; Johansson, M. K.; Beaudoin, M.-E.; Cole, R. O.; Day, J. M.; Iverson, S.; Wilson, I. D.; Scrivens, J. H.; Weston, D. J. Utility of spatially-resolved atmospheric pressure surface

sampling and ionization techniques as alternatives to mass spectrometric imaging (MSI) in drug metabolism. *Xenobiotica* **2011**, *41*(8), 720-734.

(43) Eikel, D.; Vavrek, M.; Smith, S.; Bason, C.; Yeh, S.; Korfmacher, W. A.; Henion, J. D. Liquid extraction surface analysis mass spectrometry (LESA-MS) as a novel profiling tool for drug distribution and metabolism analysis: the terfenadine example. *Rapid Commun. Mass Spectrom.* **2011**, *25*(23), 3587-3596.

(44) Parson, W. B.; Koeniger, S. L.; Johnson, R. W.; Erickson, J.; Tian, Y.; Stedman, C.; Schwartz, A.; Tarcsa, E.; Cole, R.; Van Berkel, G. J. Analysis of chloroquine and metabolites directly from whole-body animal tissue sections by liquid extraction surface analysis (LESA) and tandem mass spectrometry. *J. Mass Spectrom.* **2012**, *47*(11), 1420-1428.

(45) Schadt, S.; Kallbach, S.; Almeida, R.; Sandel, J. Investigation of Figopitant and Its Metabolites in Rat Tissue by Combining Whole-Body Autoradiography with Liquid Extraction Surface Analysis Mass Spectrometry. *Drug Metab. Dispos.* **2012**, *40*(3), 419-425.

(46) Robichaud, G.; Barry, J. A.; Garrard, K. P.; Muddiman, D. C. Infrared Matrix-Assisted Laser Desorption Electrospray Ionization (IR-MALDESI) Imaging Source Coupled to a FT-ICR Mass Spectrometer. *J. Am. Soc. Mass Spectrom.* **2013**, *24*(1), 92-100.

(47) Sampson, J.; Hawkridge, A.; Muddiman, D. Generation and detection of multiply-charged peptides and proteins by matrix-assisted laser desorption electrospray ionization (MALDESI) fourier transform ion cyclotron resonance mass spectrometry. *J. Am. Soc. Mass Spectrom.* **2006**, *17*(12), 1712-1716.

(48) Robichaud, G.; Barry, J. A.; Muddiman, D. C. IR-MALDESI Mass Spectrometry Imaging of Biological Tissue Sections using Ice as a Matrix. *J. Am. Soc. Mass Spectrom.* **2014**1-10.

(49) Barry, J. A.; Robichaud, G.; Muddiman, D. C. Mass Recalibration of FT-ICR Mass Spectrometry Imaging Data Using the Average Frequency Shift of Ambient Ions. *J. Am. Soc. Mass Spectrom.* **2013**, *24*(7), 1137-1145.

(50) Kessner, D.; Chambers, M.; Burke, R.; Agus, D.; Mallick, P. ProteoWizard: open source software for rapid proteomics tools development. *Bioinformatics* **2008**, *24*(21), 2534-2536.

(51) Robichaud, G.; Garrard, K. P.; Barry, J. A.; Muddiman, D. C. MSiReader: An Open-Source Interface to View and Analyze High Resolving Power MS Imaging Files on Matlab Platform. *J. Am. Soc. Mass Spectrom.* **2013**, *24*(5), 718-721.

(52) Castellino, S.; O'Mara, M.; Koch, K.; Borts, D. J.; Bowers, G. D.; MacLauchlin, C. Human Metabolism of Lapatinib, a Dual Kinase Inhibitor: Implications for Hepatotoxicity. *Drug Metab. Dispos.* **2012**, *40*(1), 139-150.

(53) Dreisewerd, K.; Berkenkamp, S.; Leisner, A.; Rohlfing, A.; Menzel, C. Fundamentals of matrix-assisted laser desorption/ionization mass spectrometry with pulsed infrared lasers. *Int. J. Mass Spectrom.* **2003**, *226*(1), 189-209.

(54) Smith, C. A.; O'Maille, G.; Want, E. J.; Qin, C.; Trauger, S. A.; Brandon, T. R.; Custodio, D. E.; Abagyan, R.; Siuzdak, G. METLIN: a metabolite mass spectral database. *Ther. Drug Monit.* **2005**, *27*(6), 747-751.

(55) Peng, I. X.; Ogorzalek Loo, R. R.; Shiea, J.; Loo, J. A. Reactive-Electrospray-Assisted Laser Desorption/Ionization for Characterization of Peptides and Proteins. *Anal. Chem.* **2008**, *80*(18), 6995-7003.

(56) Liu, J.; Zhang, C.; Sun, J.; Ren, X.; Luo, H. Laser desorption dual spray post-ionization mass spectrometry for direct analysis of samples via two informative channels. *J. Mass Spectrom.* **2013**, *48*(2), 250-254.

CHAPTER 4

Mass Recalibration of FT-ICR Mass Spectrometry Imaging Data Using the Average Frequency Shift of Ambient Ions

The following work was reprinted with permission from:
Barry, J. A.; Robichaud, G.; Muddiman, D. C. J. Am. Soc. Mass Spectrom. 2013, 24(7), 1137-1145.
Copyright © 2013 The American Society for Mass Spectrometry.
The original publication may be accessed directly via the World Wide Web.

4.1 Introduction

In The ability to obtain high resolving power (RP) mass spectra with high mass measurement accuracy (MMA) is one of the key advantages of Fourier transform mass spectrometry (FTMS).[1,2] When applied to complex sample analysis these benefits of FTMS cannot be understated.[3] High RP allows for the resolution of ions that are closely arranged in *m/z* space. This effective increase in the mass spectral peak capacity is of the utmost importance in the analysis of complex mixtures, specifically the molecular imaging analysis of biological tissue sections where prior chromatographic separations are not typically feasible.[4-6] While high RP may not be innately required to obtain high mass measurement accuracy, the resolution of isobaric species is a prerequisite to accurate mass measurement. In addition, the ability to make highly accurate mass measurements can greatly reduce the number of possible elemental compositions that map to a particular mass thereby increasing the confidence of ion identification.[7-11]

A linear and *m/z*-independent systematic shift in the cyclotron frequency with increasing ion populations was observed in the early ion cyclotron resonance (ICR)

and Fourier transform ICR (FT-ICR) literature and was mainly attributed to the effects of Coulombic space charge.[12-15] Similar space charge effects have also been shown to influence the axial frequency in Orbitrap mass spectrometers.[16-18] Thus, the ability to control the magnitude of the ion population from scan to scan is vital for maintaining accurate mass measurements with external calibration throughout an experiment in both FT-ICR and Orbitrap mass spectrometers. One method for achieving ion population control in hybrid FTMS instruments is to externally trap the ions and utilize automatic gain control (AGC).[19-21] For some instruments, AGC is a short prescan event that is used to essentially determine the rate at which ions are being generated by measuring the ion current obtained from the mass range of interest for a given period of time. For continuous ionization sources, such as electrospray ionization (ESI), the length of time that the ions are accumulated in the subsequent analytical scan is adjusted in order to reach a target number of ions (AGC target) based on the ionization rate determined during the prescan event.[22] For pulsed ionization sources, like matrix-assisted laser desorption ionization (MALDI), the prescan event determines the number of ions generated per laser pulse. The number of pulses required to reach the AGC target is then varied for the analytical scan.[23,24] This hardware control over the magnitude of the ion population from spectrum to spectrum allows for the use of an external calibration that is obtained at the same ion density. However, despite the incorporation of such controls, there are a few applications, including molecular imaging, where varying the accumulation time or number of laser pulses from scan to scan may not be

desired or applicable. One such example is the case of IR laser ablation where the penetration depth and amount of material removed per pulse is significantly large, thereby limiting the number of allowable pulses in one position. [25]

Aside from implementing hardware controls, a number of researchers have also investigated various calibration techniques to combat the effects of space charge and maintain high mass accuracy. Conversion of the observed cyclotron frequency to *m/z* in FT-ICR is typically accomplished through the two-parameter calibration function proposed by either Francl (**Equation 4.1**) or Ledford (**Equation 4.2**).[26,27] These two equations have been shown to provide very similar results[28] and they serve as the framework for most of the proposed FT-ICR re-calibration techniques.

$$\frac{m}{z} = \frac{A}{f+B} \qquad \text{(Equation 4.1)}$$

$$\frac{m}{z} = \frac{A}{f} + \frac{B}{f^2} \qquad \text{(Equation 4.2)}$$

In both of these equations the A term is related to the magnetic field strength and the B term accounts for the magnetron motion as well as the electric field generated primarily from the trapping potentials with some contribution from the ion population itself. Wang et al. were able to improve MMA through the inclusion of two more terms and a C parameter to the Ledford calibration.[29] The third term accounted for up to 20 ppm of the observed mass error whereas the fourth term was found to be relatively negligible with only a sub-ppm contribution. A few others have

observed MMA improvements by including a third term to account for the influence of the individual ion abundance.[30-36] The basis for the addition of this third term is founded on the notion that ions of the same *m/z* will only influence and feel influence from ions of different *m/z*, i.e. an ion cloud of one *m/z* won't space charge itself.[37-39] Despite there being some experimental evidence that suggests this assumption may not be entirely valid,[26,40] recent simulations identified these shits as relating to image charge interactions rather than space charge effects.[41] Given that a majority of the observed shift in cyclotron frequency is linearly dependent on the total ion population, other calibration methods include a term that relates to the total ion abundance allowing for MMA in the low ppm range.[33-36,42,43] While some of the external calibration methods are capable of achieving mass accuracies within 5 ppm, it has been demonstrated that internal calibration can provide significant improvement and in some cases reach the ppb range. [44,45] These internal calibrants can be mixed with the sample or introduced from a secondary ion source[46-54]; however, it is also possible to utilize constituents of the sample[55-61] or ambient PDMS[62] ions as calibrants.[42,57,58,63]

There have also been a few calibration methods introduced for the Orbitrap that correct for systematic shifts in axial frequency. The simplified conversion from axial frequency to *m/z* for the Orbitrap is based on a single parameter equation (**Equation 4.3**).[64]

$$\frac{m}{z} = \frac{A}{f} \qquad \textbf{(Equation 4.3)}$$

Olsen et al. used an ambient PDMS ion as a lock mass to re-calculate a new A parameter for each scan to account for systematic frequency shifts.[63] This lock mass calibration has been incorporated into the software for Orbitrap based instrumentation and was capable of maintaining most of the identified ions within 1 ppm. Because of the origin of these PDMS ions (volatile compounds from deodorants and shampoos), their abundances can vary significantly. To stabilize the signal from the PDMS ions throughout an LC-MS run, Lee and coworkers simply placed a stick of deodorant near the inlet to the mass spectrometer.[65] Another lock mass approach was proposed by Wenger and Coon that employed a proportional *m/z* correction using fluoranthene cations generated from the chemical ionization reaction in the ETD chamber as an internal calibrant.[66] This approach highlights several advantages in that the calibration method is not instrument specific, given that it is a proportional correction in *m/z* space, and the internal calibrants are created within the instrument so the common drawbacks of using internal calibrants (e.g. charge competition and ion suppression between the analyte and calibrant) are avoided. Recently, Gorshkov has demonstrated that space charge effects can be accounted for by introducing a two parameter calibration including a term that is proportional to the square root of the AGC target for the Orbitrap.[64]

Matrix-assisted laser desorption electrospray ionization (MALDESI) was introduced in 2006 as a hybrid ambient ionization source that uses a laser to resonantly excite an endogenous or exogenous matrix to facilitate the desorption of neutral material that is post-ionized by electrospray ionization (ESI).[67] The

description of this process is independent of laser wavelength given that one would choose a matrix which strongly absorbs in the wavelength region of the laser emission. The imaging capabilities of the IR-MALDESI source have recently been summarized including the use of exogenous ice as a matrix and synchronization between the pulsing of the laser and collection of mass spectra to greatly improve spot-to-spot reproducibility.[68] Herein we describe the application of a cyclotron frequency correction to account for space charge induced frequency shifts that are observed during an IR-MALDESI MSI experiment coupled to an FT-ICR mass spectrometer. The frequency correction is determined by calculating the average offset of the observed frequency from the expected frequency for a series of PDMS ions. This correction provided part per billion mass accuracy and was the most precise when compared with a few other calibration techniques.

4.2 Experimental

4.2.1 Materials

Formic acid was purchased from Sigma Aldrich (St. Louis, MO, USA). HPLC grade acetonitrile and water were purchased from Burdick & Jackson (Muskegon, MI, USA). All materials were used as received without further purification.

4.2.2 Methods

The electrospray solution was prepared by mixing one part acetonitrile and one part water (v/v) with 0.1 % formic acid. Liver tissue was obtained from a

laboratory animal dosed with the pharmaceutical Tykerb. Mouse brain tissue was snap frozen in liquid nitrogen and stored at -80°C. Both tissue types were sectioned on a cryostat into 50 µm sections that were thaw-mounted onto a glass microscope slide.

4.2.3 LTQ-FT Ultra Mass Spectrometer

The IR-MALDESI source was coupled to a Thermo Scientific LTQ-FT Ultra mass spectrometer (Thermo Scientific, West Palm Beach, FL, USA) that is fitted with an actively shielded 7 T superconducting magnet. The AGC was not applicable to the imaging experiments due to the pulsed nature of the source and was turned off. The ion injection time (IT) determines the length of time the ions are accumulated in the ion trap and this value was set to 200 ms in order to collect the ions generated from the three laser pulses at 20 Hz fired at each spot (pixel), which would take roughly 150 ms. Full mass spectra (*m/z* 190-1900) were acquired at 100000 RP (FWHM) at each pixel, though for the IR-MALDESI imaging experiments, tissue related ions are typically observed between *m/z* 200-1200.

4.2.4 IR-MALDESI Imaging

A more detailed description of the optimized IR-MALDESI source parameters as well as the imaging source parameters has been provided previously.[68,69] In short a thin layer of ice is deposited on the tissue section using a liquid cooled Peltier stage. A wavelength tunable mid-IR laser (IR-Opolette, Opotek, Carlsbad,

CA) is pulsed into the sample to excite the ice matrix and facilitate the desorption of tissue related material. This desorbed material, consisting primarily of neutral molecules and particulate matter, partitions into an orthogonal plume of charged electrospray droplets and is post-ionized through an ESI-like process. The IR-MALDESI imaging source allows for synchronization of the triggering of both the laser and mass spectrometer.[68]

4.2.5 Data Analysis

The .RAW files were converted to mzXML using the freely available conversion tool (http://proteowizard.sourceforge.net/index.shtml).[70] A MATLAB® (The MathWorks Inc, Natick, MA) script was written to import the mzXML file and obtain the centroid mass and intensity for a list of ions from each individual spectrum. These ions included several protonated or ammonium adducted ambient ions that are used as internal calibrants, the protonated ion for Tykerb, protonated cholesterol after water loss, and a protonated lipid (PC(38:4) or PE(41:4)) at the higher end of the mass range. **Table 4.1** lists these ions, their chemical formulas, and exact masses. The tissue related peaks (Tykerb, cholesterol, and the protonated lipid) are homogenously distributed throughout the liver tissue section as determined from their ion maps from the imaging experiment (data not shown). The centroid algorithm used to calculate the observed *m/z* is based on fitting a parabola to three points of each peak (local maxima and adjacent datapoints) has been described previously.[71,72] The calculated centroid for each peak was identical to

Table 4.1 The formula, observed ion, and exact ion mass for the several PDMS ions that were used as internal calibrants and three homogenously distributed tissue related species.

Type	Ion	Formula	Adduct	Ion Exact Mass
Ambient Ions (Internal Calibrants)	Heptadimethylcyclosiloxane	$C_{14}H_{42}O_7Si_7$	$[M+H]^+$	519.1388_2
	Heptadimethylcyclosiloxane	$C_{14}H_{42}O_7Si_7$	$[M+NH_4]^+$	536.1653_7
	Octadimethylcyclosiloxane	$C_{16}H_{48}O_8Si_8$	$[M+H]^+$	593.1576_1
	Octadimethylcyclosiloxane	$C_{16}H_{48}O_8Si_8$	$[M+NH_4]^+$	610.1841_6
Tissue Related Ions	Cholesterol	$C_{27}H_{46}O$	$[M+H-H_2O]^+$	369.3515_8
	Tykerb	$C_{29}H_{26}ClFN_4O_4S$	$[M+H]^+$	581.1420_1
	PE(41:4) / PC(38:4)	$C_{46}H_{84}NO_8P$	$[M+H]^+$	810.6007_3

those calculated by the instrument software (Thermo Xcalibur). The back conversion from *m/z* space to frequency space was performed using the instrument's external calibration parameters which can be found in the header of the raw file. Even with the AGC off, the instrument will use the calibration parameters that were determined for the AGC target that is set. After extraction of this information, several different calibration methods were performed and their effect on mass accuracy was evaluated by plotting cumulative frequency and a scatter plot with color-coded density that was designed in MATLAB®.

For the generation of the ion maps the mzXML files were loaded into the MSiReader software (available at www.msireader.com), a MATLAB® based software program which was developed in-house. This software is capable of generating ion

maps from high resolution MS data. The images that are displayed in this manuscript have been linearly interpolated to an order of 2.[73]

4.3 Results and Discussion

4.3.1 Frequency Shift Recalibration

With no direct control over the magnitude of the ion population from spectrum to spectrum, space charge effects will result in systematic fluctuations in the observed cyclotron frequency. A number of groups have shown that this frequency shift is linearly dependent on the ion population and that the primary contribution to the shift is independent of *m/z*.[12-15] Despite this observation, a large portion of the proposed recalibration techniques involve adding new parameters or calculating new calibration constants to account for the shift in frequency.[29-36,42,43] If the magnitude of this shift can be quantified, then correcting for *m/z*-independent space charge effects could be as straightforward as adding that shift to all of the observed frequencies then converting into *m/z* space. However, the quantification of the space charge induced frequency shift would require some form of internal standard. With ESI and ESI-based ambient ionization techniques, such as IR-MALDESI, PDMS molecules present in the ambient laboratory readily ionize and are consistently present in each mass spectrum. Despite initially being viewed as a contaminant,[62] the use of these ions as internal calibrants is becoming more prevalent.[63] In our laboratory a distribution of several of these ambient ions are commonly observed in every IR-MALDESI spectrum. **Table 4.1** shows those

ambient ions that are typically most abundant, including the protonated and ammonium adducted heptamer and octamer. A key feature of IR-MALDESI is the option to add internal calibrants to the electrospray solution without directly interfering with the sample.[74] However, this was not necessary given that the four PDMS ions were consistently observed in all 5,000 mass spectra from the tissue imaging experiment.

A schematic of the proposed calibration technique using these ions as internal calibrants is shown in **Figure 4.1**. For each scan, the observed *m/z* values are converted back into frequency space using the instruments external calibration equation. The exact mass of each of the ambient ions listed in **Table 4.1** are also converted into frequency space using this external calibration equation. The difference between the exact and observed frequencies for each of the ambient ions is then determined (Δf). The average of these four values represents the average space charge induced frequency shift (avg Δf) that is then added to all of the observed frequencies. These calibrated frequencies are converted back into *m/z* space using the instruments external calibration equation to obtain a calibrated mass spectrum. This workflow is then repeated for every mass spectrum. Using a MATLAB® script for the average frequency shift recalibration routine, an imaging experiment with 5000 scans can be processed in a little over two minutes.

In order to evaluate the effectiveness of this calibration, the MMA of the PDMS ions as well as several tissue related ions was determined for the externally calibrated spectra and the spectra calibrated using the observed frequency shift. It

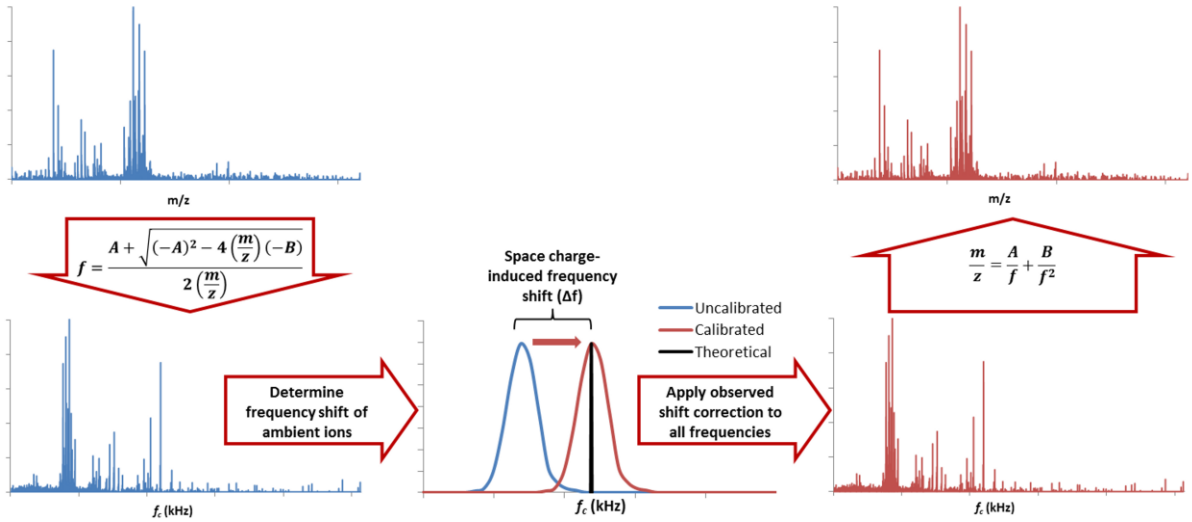

Figure 4.1 Typical workflow of the average frequency shift recalibration technique that involve conversion of each mass spectrum into frequency space, determination of the average frequency shift, correction of the shift, and conversion back to *m/z* space.

is important to note that only the ambient ions in **Table 4.1** were used as internal calibrants and the tissue related ions were used to identify the effectiveness of the calibration. **Figure 4.2** shows scatter plots of the MMA for these ions with respect to the total ion current (TIC) along with cumulative percentage plots for both calibrations. Given the large number of data points in the scatter plots (roughly 38,000 points), a majority of them overlap. To account for this, the data was distributed into 500 equally spaced bins along each axis (histograms are shown adjacent to each axis). The points were then color coded according to the number of points in each bin of the two dimensional histogram to illustrate the density of the data points. Even with the AGC off, the external calibration (**Figure 4.2a**) still maintained a majority of the data within 2 ppm. The average MMA for the externally

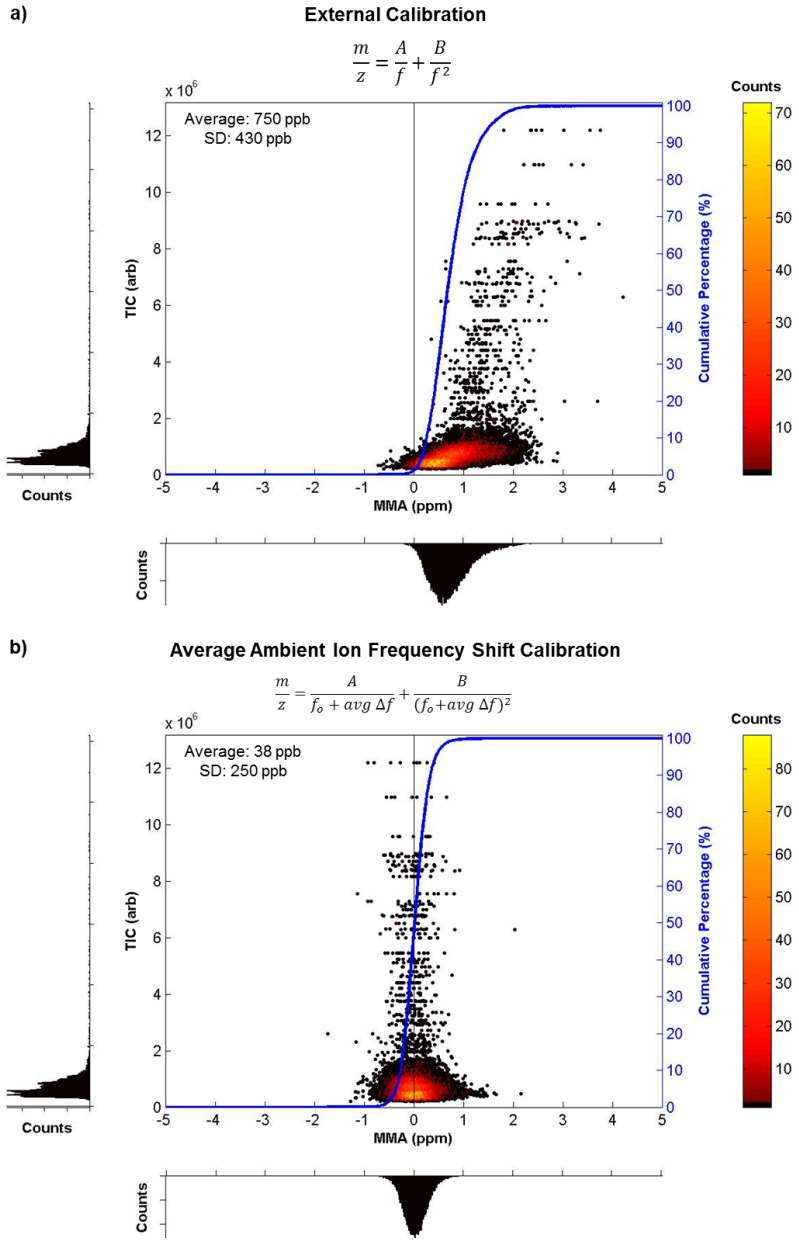

Figure 4.2 Scatter plots of the mass accuracy against total ion current (TIC) of the PDMS ions as well as several tissue related ions over the course of an IR-MALDESI imaging experiment. **a)** The external calibration with the AGC off shows a systematic deterioration in mass accuracy with increasing total ion current indicating a frequency shift due to space charge effects. **b)** Correcting for this frequency shift using the average ambient ion frequency shift calibration, the points are more closely centered around zero and the mass shift associated with the space charge effects is reduced.

calibrated spectra was 750 ppb with a standard deviation of 430 ppb. However, there is a systematic positive shift in MMA with increasing ion current which most likely caused by space charge effects. This shift is corrected for using the proposed calibration as seen in the centering of a majority of the points around zero even at high TIC (**Figure 4.2b**). The average MMA for this method was found to be 38 ppb with a standard deviation of 250 ppb.

4.3.2 Comparison with Other Calibration Methods

As alluded to earlier, there have been a large number of calibration techniques proposed in the literature. In order to evaluate the average ambient ion frequency shift calibration, the same data set was calibrated using several of these other methods. The results of this comparison are shown in **Table 4.2**. Each of the calibration techniques tested were able to achieve an average MMA in the ppb range with varying degrees of precision. The most accurate calibration method was the altered Francl calibration (method 6 in **Table 4.2**), proposed by Muddiman and coworkers, that includes an additional term to account for the individual ion abundance (I).[33] While this method was the most accurate, it was also the least precise with a standard deviation that was almost twice as large as the external calibration. The modified Francl equation, also proposed by Muddiman, that includes terms to account for individual ion abundance as well as total ion abundance (method 5 in **Table 4.2**) has recently been used for recalibrating a FT-ICR imaging dataset.[75] Smith et al. found this method to provide the highest mass

Table 4.2 Comparison of several calibration methods.

Method	Calibration Equation	Avg. MMA (ppm)	SD (ppm)	Ref.
1	$\frac{m}{z} = \frac{A}{f} + \frac{B}{f^2}$	0.750	0.430	26
2	$\frac{m}{z} = \frac{A}{f_o + \Delta f} + \frac{B}{(f_o + \Delta f)^2}$	0.175	0.316	This work
3	$\frac{m}{z} = \frac{A}{f_o + avg\ \Delta f} + \frac{B}{(f_o + avg\ \Delta f)^2}$	0.038	0.250	This work
4	$\frac{m}{z} = \frac{A}{f} + \frac{B}{f^2} + \frac{C \times TIC}{f^2}$	0.085	0.326	42
5	$\frac{m}{z} = \frac{B}{f - (A + C \times I + D \times TIC)}$	0.052	0.471	33*
6	$\frac{m}{z} = \frac{B}{f - (A + C \times I)}$	-0.006	0.844	33*
7	$\frac{m}{z} = \left(\frac{m}{z}\right)_{observed} \times \left[\frac{\left(\frac{m}{z}\right)_{exact}}{\left(\frac{m}{z}\right)_{observed}}\right]_{calibrant}$	0.208	0.360	67*

*The terms in these equations have been modified to correlate with the terminology of the manuscript.

accuracy; however the technique proposed here (method 3 in **Table 4.2**) is shown to provide significant improvement in both mass measurement accuracy and precision when compared to each of the methods that were tested. One possible explanation for the improvement that is realized using the frequency shift recalibration is that it is a direct correction in frequency space, whereas the other techniques utilize intensity measurements to adjust the *m/z* scale. The measurement of intensity is not

necessarily accurate and thus the error in the intensity measurement can propagate into the error of the mass measurement when utilizing total ion current or individual ion abundance for mass calibration. Another interesting observation is demonstrated in the comparison of methods 2 and 3 where the determination of the frequency shift using a series of ambient ions is significantly more accurate and precise than relying on a single ion. It should also be noted that while ambient PDMS ions are used here as internal calibrants, this calibration method should work for any series of internal calibrants. In addition, this method of determining the frequency shift using internal calibrants could also be applied to calibration of the Orbitrap. However, since the Orbitrap is externally calibrated using a single parameter equation, this would likely give results that are similar to the lock mass function that is already integrated into the Orbitrap software.

4.3.3 High Resolving Power Mass Spectrometry Imaging

In mass spectrometry imaging of biological tissue sections, a large number of ions spanning a variety of molecular classes (metabolites, lipids, glycans, proteins, etc.) can be detected simultaneously. Given that chromatographic separation of these species is not typically feasible; the RP of the mass spectrometer is relied upon to resolve these species through separation by *m/z*. An example of the importance of using high RP and accurate mass measurements for mass spectrometry imaging is demonstrated in **Figure 4.3**. The black trace is a portion of a mass spectrum from an IR-MALDESI FT-ICR MSI analysis of a mouse brain tissue

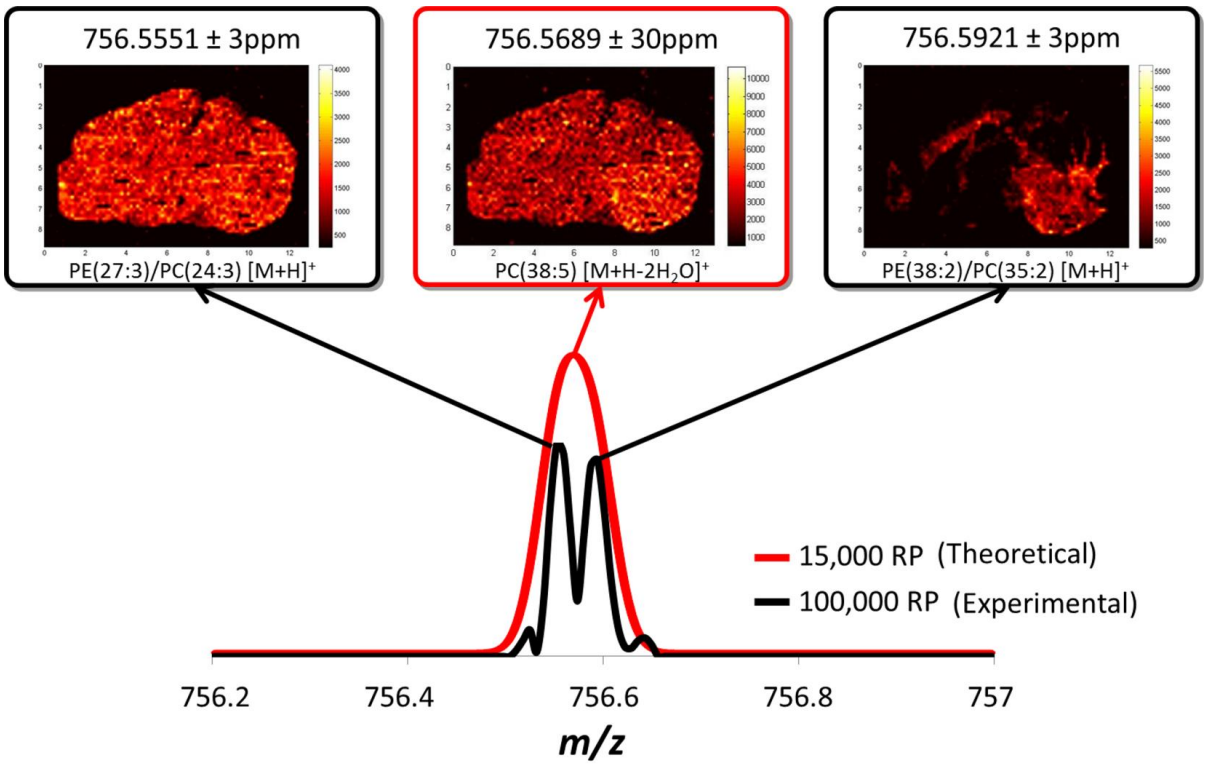

Figure 4.3 Demonstration of the importance of high resolving power and accurate mass measurements in mass spectrometry imaging.

section. The two peaks correspond to two phospholipid species that are resolved at 100,000 RP (FWHM at *m/z* 400). These two lipids have dramatically different spatial distributions in the section that was analyzed (black boxes in **Figure 4.3**). The accurate mass obtained from the centroid of these peaks leads to their preliminary identification as PE(27:3)/PC(24:3) for 756.5551 and PE(38:2)/PC(35:2) for 756.5921. The red trace represents a theoretical spectrum of these two peaks at 15,000 RP (FWHM at *m/z* 400). At the lower RP, these peaks are unresolved and combined under the same peak. The spatial distribution would then appear as a sum of both peaks (red box in **Figure 4.3**) which demonstrates the loss of spatial

information from the latter peak. More importantly, the centroid of this peak would then correlate more closely to a species that is not actually present. In addition, the average frequency shift recalibration was also performed on this mouse brain data set (data not shown). For both peaks shown in **Figure 4.3** the average mass accuracy was improved from roughly 1.3 ppm with the external calibration to about 0.7 ppm with the proposed calibration, thereby improving the confidence of the identification. This also shows that the calibration routine works equally well for species that may not be homogeneously distributed.

4.4 Conclusions

It has been shown that an increase in the total ion population can result in a systematic shift in the observed cyclotron frequency in FT-ICR. Without direct control over the size of this ion population from scan to scan, external calibration can lead to significant errors in mass measurement. The calibration technique that is described here uses a series of ambient PDMS ions as internal calibrants to quantify this space charge induced frequency shift allowing for proper adjustment of the observed cyclotron frequency. This method is capable of achieving part per billion mass accuracy with the highest precision of the calibration techniques tested for an IR-MALDESI imaging dataset. Also, given that this calibration routine is executed in MATLAB®, we are working on integrating this workflow and perhaps other universal mass calibration techniques[66] into our freely available and vendor neutral MSI analysis software, MSiReader.[73]

4.5 References

(1) Comisarow, M. B.; Marshall, A. G. Fourier transform ion cyclotron resonance spectroscopy. *Chem. Phys. Lett.* **1974**, *25*(2), 282-283.

(2) Makarov, A. Electrostatic Axially Harmonic Orbital Trapping: A High-Performance Technique of Mass Analysis. *Anal. Chem.* **2000**, *72*(6), 1156-1162.

(3) Marshall, A. G.; Hendrickson, C. L. High-Resolution Mass Spectrometers. *Annu. Rev. Anal. Chem.* **2008**, *1*(1), 579-599.

(4) Park, S.-G.; Murray, K. K. Infrared laser ablation sample transfer for on-line liquid chromatography electrospray ionization mass spectrometry. *J. Mass Spectrom.* **2012**, *47*(10), 1322-1326.

(5) Kertesz, V.; Van Berkel, G. J. Liquid Microjunction Surface Sampling Coupled with High-Pressure Liquid Chromatography−Electrospray Ionization-Mass Spectrometry for Analysis of Drugs and Metabolites in Whole-Body Thin Tissue Sections. *Anal. Chem.* **2010**, *82*(14), 5917-5921.

(6) Ovchinnikova, O. S.; Kertesz, V.; Van Berkel, G. J. Combining Laser Ablation/Liquid Phase Collection Surface Sampling and High-Performance Liquid Chromatography−Electrospray Ionization-Mass Spectrometry. *Anal. Chem.* **2011**, *83*(6), 1874-1878.

(7) Beynon, J. H. Qualitative Analysis of Organic Compounds by Mass Spectrometry. *Nature* **1954**, *174*(4433), 735-737.

(8) Guan, S.; Marshall, A. G.; Scheppele, S. E. Resolution and Chemical Formula Identification of Aromatic Hydrocarbons and Aromatic Compounds Containing Sulfur, Nitrogen, or Oxygen in Petroleum Distillates and Refinery Streams. *Anal. Chem.* **1996**, *68*(1), 46-71.

(9) Herniman, J.; Langley, G.; Bristow, T.; O'Connor, G. The validation of exact mass measurements for small molecules using FT-ICRMS for improved confidence in the selection of elemental formulas. *J. Am. Soc. Mass Spectrom.* **2005**, *16*(7), 1100-1108.

(10) Kim, S.; Rodgers, R. P.; Marshall, A. G. Truly "exact" mass: Elemental composition can be determined uniquely from molecular mass measurement at ~0.1 mDa accuracy for molecules up to ~500 Da. *Int. J. Mass Spectrom.* **2006**, *251*(2–3), 260-265.

(11) Yongdong, W. Improving elemental composition determination. *Pharm. Tech. Eur.* **2007**, *19*(6), 51-57.

(12) Hipple, J. A.; Sommer, H.; Thomas, H. A. A Precise Method of Determining the Faraday by Magnetic Resonance. *PhRv* **1949**, *76*(12), 1877-1878.

(13) Beauchamp, J. L.; Armstrong, J. T. An Ion Ejection Technique for the Study of Ion-Molecule Reactions with Ion Cyclotron Resonance Spectroscopy. *Rev. Sci. Instrum.* **1969**, *40*(1), 123-128.

(14) Ledford, E. B.; Ghaderi, S.; White, R. L.; Spencer, R. B.; Kulkarni, P. S.; Wilkins, C. L.; Gross, M. L. Exact mass measurement by Fourier transform mass spectrometry. *Anal. Chem.* **1980**, *52*(3), 463-468.

(15) Jeffries, J. B.; Barlow, S. E.; Dunn, G. H. Theory of space-charge shift of ion cyclotron resonance frequencies. *Int. J. Mass Spectrom. Ion Processes* **1983**, *54*(1–2), 169-187.

(16) Hu, Q.; Noll, R. J.; Li, H.; Makarov, A.; Hardman, M.; Graham Cooks, R. The Orbitrap: a new mass spectrometer. *J. Mass Spectrom.* **2005**, *40*(4), 430-443.

(17) Makarov, A.; Denisov, E.; Lange, O.; Horning, S. Dynamic range of mass accuracy in LTQ orbitrap hybrid mass spectrometer. *J. Am. Soc. Mass Spectrom.* **2006**, *17*(7), 977-982.

(18) Kharchenko, A.; Vladimirov, G.; Heeren, R.; Nikolaev, E. Performance of Orbitrap Mass Analyzer at Various Space Charge and Non-Ideal Field Conditions: Simulation Approach. *J. Am. Soc. Mass Spectrom.* **2012**, *23*(5), 977-987.

(19) Belov, M. E.; Zhang, R.; Strittmatter, E. F.; Prior, D. C.; Tang, K.; Smith, R. D. Automated Gain Control and Internal Calibration with External Ion Accumulation Capillary Liquid Chromatography-Electrospray Ionization-Fourier Transform Ion Cyclotron Resonance. *Anal. Chem.* **2003**, *75*(16), 4195-4205.

(20) Belov, M. E.; Rakov, V. S.; Nikolaev, E. N.; Goshe, M. B.; Anderson, G. A.; Smith, R. D. Initial implementation of external accumulation liquid chromatography/electrospray ionization Fourier transform ion cyclotron resonance with automated gain control. *Rapid Commun. Mass Spectrom.* **2003**, *17*(7), 627-636.

(21) Syka, J. E. P.; Marto, J. A.; Bai, D. L.; Horning, S.; Senko, M. W.; Schwartz, J. C.; Ueberheide, B.; Garcia, B.; Busby, S.; Muratore, T.; Shabanowitz, J.; Hunt, D. F. Novel Linear Quadrupole Ion Trap/FT Mass Spectrometer: Performance Characterization and Use in the Comparative Analysis of Histone H3 Post-translational Modifications. *J. Proteome Res.* **2004**, *3*(3), 621-626.

(22) Schwartz, J. C. Z., Xaio-Guang; Brier, Mark E. Method and Apparatus of Increasing Dynamic Range and Sensitivity of a Mass Spectrometer. U.S. Patent 5,572,022, **1996**.

(23) Schwartz, J. C. K., Viatcheslav V. Automatic gain control (AGC) method for an ion trap and a temporally non-uniform ion beam. U.S. Patent 7,960,690 B2, **2011**.

(24) Strupat, K.; Kovtoun, V.; Bui, H.; Viner, R.; Stafford, G.; Horning, S. MALDI Produced Ions Inspected with a Linear Ion Trap-Orbitrap Hybrid Mass Analyzer. *J. Am. Soc. Mass Spectrom.* **2009**, *20*(8), 1451-1463.

(25) Dreisewerd, K.; Berkenkamp, S.; Leisner, A.; Rohlfing, A.; Menzel, C. Fundamentals of matrix-assisted laser desorption/ionization mass spectrometry with pulsed infrared lasers. *Int. J. Mass Spectrom.* **2003**, *226*(1), 189-209.

(26) Francl, T. J.; Sherman, M. G.; Hunter, R. L.; Locke, M. J.; Bowers, W. D.; McIver Jr, R. T. Experimental determination of the effects of space charge on ion cyclotron resonance frequencies. *Int. J. Mass Spectrom. Ion Processes* **1983**, *54*(1–2), 189-199.

(27) Ledford, E. B.; Rempel, D. L.; Gross, M. L. Space charge effects in Fourier transform mass spectrometry. II. Mass calibration. *Anal. Chem.* **1984**, *56*(14), 2744-2748.

(28) Shi, S. D. H.; Drader, J. J.; Freitas, M. A.; Hendrickson, C. L.; Marshall, A. G. Comparison and interconversion of the two most common frequency-to-mass calibration functions for Fourier transform ion cyclotron resonance mass spectrometry. *Int. J. Mass Spectrom.* **2000**, *195–196*(0), 591-598.

(29) Wang, M.; Marshall, A. G. Mass shifts induced by negative frequency peaks in linearly polarized Fourier transform ion cyclotron resonance signals. *Int. J. Mass Spectrom. Ion Processes* **1988**, *86*(0), 31-51.

(30) Brown, C. E. S., Martin J.C. The present status and prospects for Fourier transform-ion cyclotron resonance mass spectrometry. *Spectroscopy World* **1990**, *2*(1), 24-30.

(31) Masselon, C.; Tolmachev, A.; Anderson, G.; Harkewicz, R.; Smith, R. Mass measurement errors caused by “local” frequency perturbations in FTICR mass spectrometry. *J. Am. Soc. Mass Spectrom.* **2002**, *13*(1), 99-106.

(32) Easterling, M. L.; Mize, T. H.; Amster, I. J. Routine Part-per-Million Mass Accuracy for High- Mass Ions: Space-Charge Effects in MALDI FT-ICR. *Anal. Chem.* **1999**, *71*(3), 624-632.

(33) Muddiman, D. C.; Oberg, A. L. Statistical Evaluation of Internal and External Mass Calibration Laws Utilized in Fourier Transform Ion Cyclotron Resonance Mass Spectrometry. *Anal. Chem.* **2005**, *77*(8), 2406-2414.

(34) Williams, D. K.; Muddiman, D. C. Parts-Per-Billion Mass Measurement Accuracy Achieved through the Combination of Multiple Linear Regression and Automatic Gain Control in a Fourier Transform Ion Cyclotron Resonance Mass Spectrometer. *Anal. Chem.* **2007**, *79*(13), 5058-5063.

(35) Williams Jr, D. K.; Chadwick, M. A.; Williams, T. I.; Muddiman, D. C. Calibration laws based on multiple linear regression applied to matrix-assisted laser desorption/ionization Fourier transform ion cyclotron resonance mass spectrometry. *J. Mass Spectrom.* **2008**, *43*(12), 1659-1663.

(36) Williams, D.; Kovach, A.; Muddiman, D.; Hanck, K. Utilizing artificial neural networks in matlab to achieve parts-per-billion mass measurement accuracy with a fourier transform ion cyclotron resonance mass spectrometer. *J. Am. Soc. Mass Spectrom.* **2009**, *20*(7), 1303-1310.

(37) Wineland, D.; Dehmelt, H. Line shifts and widths of axial, cyclotron and G-2 resonances in tailored, stored electron (ion) cloud. *Int. J. Mass Spectrom. Ion Phys.* **1975**, *16*(3), 338-342.

(38) Chen, S.-P.; Comisarow, M. B. Simple physical models for coulomb-induced frequency shifts and coulomb-induced inhomogenous broadening for like and unlike ions in fourier transform ion cyclotron resonance mass spectrometry. *Rapid Commun. Mass Spectrom.* **1991**, *5*(10), 450-455.

(39) Chen, S.-P.; Comisarow, M. B. Modelling coulomb effects in Fourier-transform ion cyclotron resonance mass spectrometry by charged disks and charged cylinders. *Rapid Commun. Mass Spectrom.* **1992**, *6*(1), 1-3.

(40) Wong, R. L.; Amster, I. J. Experimental evidence for space-charge effects between ions of the same mass-to-charge in Fourier-transform ion cyclotron resonance mass spectrometry. *Int. J. Mass Spectrom.* **2007**, *265*(2–3), 99-105.

(41) Leach, F.; Kharchenko, A.; Heeren, R.; Nikolaev, E.; Amster, I. Comparison of particle-in-cell simulations with experimentally observed frequency shifts between ions of the same mass-to-charge in fourier transform ion cyclotron resonance mass spectrometry. *J. Am. Soc. Mass Spectrom.* **2010**, *21*(2), 203-208.

(42) Haas, W.; Faherty, B. K.; Gerber, S. A.; Elias, J. E.; Beausoleil, S. A.; Bakalarski, C. E.; Li, X.; Villén, J.; Gygi, S. P. Optimization and Use of Peptide Mass Measurement Accuracy in Shotgun Proteomics. *Mol. Cell. Proteomics* **2006**, *5*(7), 1326-1337.

(43) Zhang, J.; Ma, J.; Dou, L.; Wu, S.; Qian, X.; Xie, H.; Zhu, Y.; He, F. Mass Measurement Errors of Fourier-Transform Mass Spectrometry (FTMS): Distribution, Recalibration, and Application. *J. Proteome Res.* **2009**, *8*(2), 849-859.

(44) Beu, S.; Senko, M.; Quinn, J.; McLafferty, F. Improved fourier-transform ion-cyclotron-resonance mass spectrometry of large biomolecules. *J. Am. Soc. Mass Spectrom.* **1993**, *4*(2), 190-192.

(45) Wu, Q. Multistage Accurate Mass Spectrometry: A “Basket in a Basket” Approach for Structure Elucidation and Its Application to a Compound from Combinatorial Synthesis. *Anal. Chem.* **1998**, *70*(5), 865-872.

(46) Burton, R. D.; Matuszak, K. P.; Watson, C. H.; Eyler, J. R. Exact mass measurements using a 7 tesla fourier transform ion cyclotron resonance mass spectrometer in a good laboratory practices-regulated environment. *J. Am. Soc. Mass Spectrom.* **1999**, *10*(12), 1291-1297.

(47) O'Connor, P. B.; Costello, C. E. Internal Calibration on Adjacent Samples (InCAS) with Fourier Transform Mass Spectrometry. *Anal. Chem.* **2000**, *72*(24), 5881-5885.

(48) Hannis, J.; Muddiman, D. A dual electrospray ionization source combined with hexapole accumulation to achieve high mass accuracy of biopolymers in Fourier transform ion cyclotron resonance mass spectrometry. *J. Am. Soc. Mass Spectrom.* **2000**, *11*(10), 876-883.

(49) Flora, J. W.; Hannis, J. C.; Muddiman, D. C. High-Mass Accuracy of Product Ions Produced by SORI-CID Using a Dual Electrospray Ionization Source Coupled with FTICR Mass Spectrometry. *Anal. Chem.* **2001**, *73*(6), 1247-1251.

(50) Null, A. P.; Muddiman, D. C. Determination of a correction to improve mass measurement accuracy of isotopically unresolved polymerase chain reaction amplicons by electrospray ionization Fourier transform ion cyclotron resonance mass spectrometry. *Rapid Commun. Mass Spectrom.* **2003**, *17*(15), 1714-1722.

(51) Herniman, J. M.; Bristow, T. W. T.; O'Connor, G.; Jarvis, J.; Langley, G. J. Improved precision and accuracy for high-performance liquid chromatography/Fourier transform ion cyclotron resonance mass spectrometric exact mass measurement of small molecules from the simultaneous and controlled introduction of internal calibrants via a second electrospray nebuliser. *Rapid Commun. Mass Spectrom.* **2004**, *18*(24), 3035-3040.

(52) Young, N. L.; Sisto, M. C.; Young, M. N.; Grant, P. G.; Killilea, D. W.; LaMotte, L.; Wu, K. J. J.; Lebrilla, C. B. Steady-State Asymmetric Nanospray Dual Ion Source for Accurate Mass Determination within a Chromatographic Separation. *Anal. Chem.* **2007**, *79*(15), 5711-5718.

(53) Williams, D.; Hawkridge, A.; Muddiman, D. Sub parts-per-million mass measurement accuracy of intact proteins and product ions achieved using a dual electrospray ionization quadrupole fourier transform ion cyclotron resonance mass spectrometer. *J. Am. Soc. Mass Spectrom.* **2007**, *18*(1), 1-7.

(54) Smith, D.; Aizikov, K.; Duursma, M.; Giskes, F.; Spaanderman, D.-J.; McDonnell, L.; O'Connor, P.; Heeren, R. An External Matrix-Assisted Laser Desorption Ionization Source for Flexible FT-ICR Mass Spectrometry Imaging with Internal Calibration on Adjacent Samples. *J. Am. Soc. Mass Spectrom.* **2011**, *22*(1), 130-137.

(55) Bruce, J.; Anderson, G.; Brands, M.; Pasa-Tolic, L.; Smith, R. Obtaining more accurate Fourier transform ion cyclotron resonance mass measurements without internal standards using multiply charged ions. *J. Am. Soc. Mass Spectrom.* **2000**, *11*(5), 416-421.

(56) Yanofsky, C. M.; Bell, A. W.; Lesimple, S.; Morales, F.; Lam, T. T.; Blakney, G. T.; Marshall, A. G.; Carrillo, B.; Lekpor, K.; Boismenu, D.; Kearney, R. E. Multicomponent Internal Recalibration of an LC−FTICR-MS Analysis

Employing a Partially Characterized Complex Peptide Mixture: Systematic and Random Errors. *Anal. Chem.* **2005**, *77*(22), 7246-7254.

(57) de Godoy, L.; Olsen, J.; de Souza, G.; Li, G.; Mortensen, P.; Mann, M. Status of complete proteome analysis by mass spectrometry: SILAC labeled yeast as a model system. *Genome Biol* **2006**, *7*(6), R50.

(58) Palmblad, M.; Bindschedler, L. V.; Gibson, T. M.; Cramer, R. Automatic internal calibration in liquid chromatography/Fourier transform ion cyclotron resonance mass spectrometry of protein digests. *Rapid Commun. Mass Spectrom.* **2006**, *20*(20), 3076-3080.

(59) Wong, R. L.; Amster, I. J. Sub Part-Per-Million Mass Accuracy by Using Stepwise-External Calibration in Fourier Transform Ion Cyclotron Resonance Mass Spectrometry. *J. Am. Soc. Mass Spectrom.* **2006**, *17*(12), 1681-1691.

(60) Savory, J. J.; Kaiser, N. K.; McKenna, A. M.; Xian, F.; Blakney, G. T.; Rodgers, R. P.; Hendrickson, C. L.; Marshall, A. G. Parts-Per-Billion Fourier Transform Ion Cyclotron Resonance Mass Measurement Accuracy with a "Walking" Calibration Equation. *Anal. Chem.* **2011**, *83*(5), 1732-1736.

(61) Jing, L.; Amster, I. An improved calibration method for the matrix-assisted laser desorption/ionization-Fourier transform ion cyclotron resononance analysis of 15N-metabolically- labeled proteome digests using a mass difference approach. *Eur. J. Mass Spectrom.* **2012**, *18*(3), 269-277.

(62) Schlosser, A.; Volkmer-Engert, R. Volatile polydimethylcyclosiloxanes in the ambient laboratory air identified as source of extreme background signals in nanoelectrospray mass spectrometry. *J. Mass Spectrom.* **2003**, *38*(5), 523-525.

(63) Olsen, J. V.; de Godoy, L. M. F.; Li, G.; Macek, B.; Mortensen, P.; Pesch, R.; Makarov, A.; Lange, O.; Horning, S.; Mann, M. Parts per Million Mass Accuracy on an Orbitrap Mass Spectrometer via Lock Mass Injection into a C-trap. *Mol. Cell. Proteomics* **2005**, *4*(12), 2010-2021.

(64) Gorshkov, M.; Good, D.; Lyutvinskiy, Y.; Yang, H.; Zubarev, R. Calibration function for the orbitrap FTMS accounting for the space charge effect. *J. Am. Soc. Mass Spectrom.* **2010**, *21*(11), 1846-1851.

(65) Lee, K. A.; Farnsworth, C.; Yu, W.; Bonilla, L. E. 24-Hour Lock Mass Protection. *J. Proteome Res.* **2010**, *10*(2), 880-885.

(66) Wenger, C. D.; McAlister, G. C.; Xia, Q.; Coon, J. J. Sub-part-per-million Precursor and Product Mass Accuracy for High-throughput Proteomics on an Electron Transfer Dissociation-enabled Orbitrap Mass Spectrometer. *Mol. Cell. Proteomics* **2010**, *9*(5), 754-763.

(67) Sampson, J.; Hawkridge, A.; Muddiman, D. Generation and detection of multiply-charged peptides and proteins by matrix-assisted laser desorption electrospray ionization (MALDESI) fourier transform ion cyclotron resonance mass spectrometry. *J. Am. Soc. Mass Spectrom.* **2006**, *17*(12), 1712-1716.

(68) Robichaud, G.; Barry, J. A.; Garrard, K. P.; Muddiman, D. C. Infrared Matrix-Assisted Laser Desorption Electrospray Ionization (IR-MALDESI) Imaging Source Coupled to a FT-ICR Mass Spectrometer. *J. Am. Soc. Mass Spectrom.* **2013**, *24*(1), 92-100.

(69) Barry, J. A.; Muddiman, D. C. Global optimization of the infrared matrix-assisted laser desorption electrospray ionization (IR MALDESI) source for mass spectrometry using statistical design of experiments. *Rapid Commun. Mass Spectrom.* **2011**, *25*(23), 3527-3536.

(70) Kessner, D.; Chambers, M.; Burke, R.; Agus, D.; Mallick, P. ProteoWizard: open source software for rapid proteomics tools development. *Bioinformatics* **2008**, *24*(21), 2534-2536.

(71) Giancaspro, C.; Comisarow, M. B. Exact Interpolation of Fourier Transform Spectra. *Appl. Spectrosc.* **1983**, *37*(2), 153-166.

(72) Verdun, F. R.; Ricca, T. L.; Marshall, A. G. Beating the Nyquist Limit by Means of Interleaved Alternated Delay Sampling: Extension of Lower Mass Limit in Direct-Mode Fourier Transform Ion Cyclotron Resonance Mass Spectrometry. *Appl. Spectrosc.* **1988**, *42*(2), 199-203.

(73) Robichaud, G.; Garrard, K.; Barry, J.; Muddiman, D. MSiReader: An Open-Source Interface to View and Analyze High Resolving Power MS Imaging Files on Matlab Platform. *J. Am. Soc. Mass Spectrom.* **2013**DOI: 10.1007/s13361-013-0607-z.

(74) Sampson, J. S.; Hawkridge, A. M.; Muddiman, D. C. Direct characterization of intact polypeptides by matrix-assisted laser desorption electrospray ionization quadrupole Fourier transform ion cyclotron resonance mass spectrometry. *Rapid Commun. Mass Spectrom.* **2007**, *21*(7), 1150-1154.

(75) Smith, D.; Kharchenko, A.; Konijnenburg, M.; Klinkert, I.; Paša-Tolić, L.; Heeren, R. Advanced Mass Calibration and Visualization for FT-ICR Mass Spectrometry Imaging. *J. Am. Soc. Mass Spectrom.* **2012**, *23*(11), 1865-1872.

CHAPTER 5

Mapping Antiretroviral Drugs in Tissue by IR-MALDESI MSI Coupled to the Q Exactive and Comparison with LC-MS/MS SRM Assay

The following work was reprinted from the recently submitted manuscript: Barry, J. A.; Robichaud, G.; Thompson, C.; Sykes, C.; Kashuba, A. D. M.; Muddiman, D. C. *J. Am. Soc. Mass Spectrom.* **2014**, *Submitted:* January 6, 2014.

5.1 Introduction

Mass spectrometry imaging (MSI) is a method by which mass spectra are generated from discrete locations in a two dimensional array across a sample surface.[1] This combination of spatial information with the specificity and sensitivity of mass spectrometric detection make MSI a valuable tool in a variety of scientific fields.[2-9] One such example is the potential that MSI has demonstrated in the analysis of pharmaceuticals in tissue sections.[10-12] Knowledge of the distribution of a drug, and in some cases its metabolites, within certain compartments or sub-compartments of a particular tissue can have numerous implications in the areas of drug pharmacokinetics and pharmacodynamics.[13,14] Whole-body autoradiography (WBA) is the predominant technique for the determination of drug distribution in tissue.[15] While WBA is a valuable quantitative technique, it shares an inherent flaw with all radiolabeled studies in that it only follows the distribution of the radiolabel and provides no information as to which form of the drug is being detected (parent or metabolite). Given that MSI is based on mass spectrometric detection, it is capable of distinguishing between the parent drug and its metabolites. Perhaps one of the most enticing attributes of MSI is its label-free nature that precludes the use of

expensive radiolabels and allows for the simultaneous analysis of xenobiotics and endogenous compounds in a single global experimental approach. In some cases the additional knowledge gained from endogenous distributions can provide valuable insight on the impact of the drug on the local environment, implications for site-specific efficacy and toxicity, and can be used to identify certain histological features.[11,16-18] MSI is befitting to drug discovery and development where the early understanding of preclinical drug distribution (and without requiring a radiolabel) can improve efficiency by narrowing the list of potential candidates.

Matrix-assisted laser desorption/ionization (MALDI) is perhaps the most common ionization technique that is currently used for MSI. Several characteristics of MALDI that make it a suitable match for MSI include its high sensitivity and small spot size which are prerequisites for high spatial resolution imaging.[19] There are, however, several issues regarding this technique including the requirement that the sample must be amenable to high vacuum as well as the extensive sample preparation that is involved prior to analysis.[20,21] Other ionization methods such as desorption electrospray (DESI), liquid extraction surface analysis (LESA), and matrix-assisted laser desorption electrospray ionization (MALDESI) have demonstrated promise for pharmaceutical tissue imaging with little to no prior sample preparation.[22-24]

MALDESI refers to any technique which involves resonant excitation of an endogenous or exogenous matrix to facilitate analyte desorption followed by post-ionization through ESI. The matrix described here refers to any molecule present in

large excess that strongly absorbs the laser energy and leads to analyte ejection.[25] The first MALDESI publication was presented in 2006 by Muddiman as proof of principle using a UV laser (UV-MALDESI) and a ubiquitin solution mixed with an organic acid matrix.[26] This resulted in the detection of multiply charged ubiquitin with a charge state distribution that was indistinguishable from that obtained by direct infusion ESI which affirmed electrospray post-ionization in the MALDESI mechanism. Muddiman, as well as several other research groups, have also explored the utility of other laser wavelengths for MALDESI in each case utilizing a matrix that strongly absorbed within the wavelength region of the laser emission.[27-31] An exciting combination arose with the use of a Mid-IR laser (2.94 μm) with endogenous or exogenous water as the laser energy absorbing matrix (IR-MALDESI) which offers certain intrinsic benefits including the lack of matrix interference in the mass spectra and the natural occurrence of water in most biological samples. While the use of water as a matrix for IR laser desorption was not an entirely new concept,[32] ion yields for IR-MALDI using ice were typically low.[33] Thus, post-ionization of the larger fraction of neutral molecules in the ablation plume using ESI could result in improved ion yields.[34] MSI using laser ablation electrospray ionization (LAESI), an analogue of IR-MALDESI, has been presented using the endogenous water in the tissue as a laser energy absorbing matrix.[35] However, we have found that depositing a uniform ice matrix over the sample surface provides improved reproducibility from pixel to pixel resulting in higher image quality.[24,36,37]

Due to the complex nature of biological tissue samples, MSI techniques rely heavily on the mass spectrometer to resolve species by *m/z*. Several groups have demonstrated the utility of coupling imaging sources with high resolving power mass spectrometers in order to resolve several unique species with the same nominal mass that often times have different spatial distributions.[11,19,36,38-42] The primary benefits to imaging with Fourier transform (FT) mass spectrometers include not only the ability to increase the spectral peak capacity but also the ability to obtain accurate mass measurements that improve the confidence of ion identification. However, due to the relatively slow acquisition rates, FT imaging can be a time consuming process. The hybrid quadrupole orbitrap mass spectrometer (Q Exactive) has several unique features that make it highly amenable to MSI.[43] In addition to using the enhanced FT (eFT) to reduce the required transient times, the Q Exactive also allows for multiplexing capabilities to improve the overall duty cycle. Several groups demonstrated the application of the Q Exactive for MSI.[44-46]

The use of MSI to visually evaluate the distribution of drugs in tissue is of particular interest in the field of human immunodeficiency virus (HIV), an intracellular infection primarily of CD4+ T cells. In this disease, current limitations in assessing mucosal tissue antiretroviral drug distribution have slowed the progress of small molecule research in the prevention of HIV infection.[47] Moreover, an understanding of antiretroviral distribution in HIV tissue reservoirs, where low-level viral replication may still be occurring in the face of clinically effective antiretroviral therapy[48] will form the foundation of successful eradication strategies. Previous uses of MALDI in the

HIV field have focused on the quantification of antiretrovirals in plasma,[49] and more recently MSI has been used to examine the disposition of a novel antiretroviral in brain tissue.[50] A reliable method of visually evaluating antiretroviral exposure in tissues relevant to HIV infection will greatly inform the development of novel therapies for HIV treatment, prevention, and cure.

Herein, we present on the coupling of the IR-MALDESI imaging source to the Q Exactive to determine the distribution of several commonly used antiretroviral drugs in incubated tissues. Imaging is performed as either a broadband acquisition to obtain a global perspective of the three drugs of interest with endogenous species or as a more selective targeted MS^2 acquisition. In addition, tissue sections that are adjacent to those used for imaging were homogenized and analyzed by LC-MS/MS to quantify the total amounts of each drug present in the tissue. These values were then compared with the relative abundances from the imaging experiments to determine the quantitative capabilities of IR-MALDESI MSI.

5.2 Experimental

5.2.1 Materials

HPLC Grade methanol and water were purchased from Burdick and Jackson (Muskegon, MI) and formic acid was purchased from Sigma-Aldrich (St. Louis, MO). Emtricitabine, tenofovir and raltegravir were obtained from the NIH AIDS Reagent Program, directed by the Pathogenesis and Basic Research Branch, Basic Sciences

Table 5.1 Incubation Concentrations for the three HIV drugs.

Drug	Abbreviation	Monoisotopic Mass of $[M+H]^+$	Low Conc. (μg/mL)	High Conc. (μg/mL)
Tenofovir	TFV	288.0856	3.8	100.0
Emtricitabine	FTC	248.0499	18.0	100.0
Raltegravir	RAL	445.1630	28.88	100.0

Program, Division of AIDS (DAIDS), NIAID, NIH. All materials were used as purchased without further purification.

5.2.2 Samples

Cervical tissues were obtained from surgical waste via the University of North Carolina Tissue Procurement Facility through UNC IRB # 09-0921. Written informed consent was obtained from all patients. After harvest, tissues were placed immediately in culture media [Iscove's Modified Dulbecco's Media (Gibco, Grand Island, NY), 10% fetal bovine serum (Gibco), 240 units/mL nystatin (Sigma, St. Louis, MO), 100 units/mL penicillin-streptomycin (Gibco), and MEM vitamin solution (Sigma)] and kept on ice until receipt into the laboratory. Once received into the lab, tissues were trimmed of fat and other connective tissue with sterile scissors and cut into approximately $1cm^2$ pieces. Pieces were placed into individual wells of a 24-well tissue culture plate with 1mL culture media containing low or high concentrations of the nucleoside reverse transcriptase inhibitors emtricitabine (FTC) and tenofovir (TFV) and the integrase strand transfer inhibitor raltegravir (RAL).

Here, low concentrations were defined as 10 times the reported plasma C_{max} value in humans for each drug: 18,000 ng/mL FTC, 3,800 ng/mL TFV, and 28,880 ng/mL RAL. High concentration was defined as 100,000 ng/mL for all three drugs. These concentrations were selected to mimic mucosal tissue concentrations seen clinically in Phase I studies.[51,52] The incubation concentration along with the exact monoisotopic mass for each drug is also presented in **Table 5.1**. All tissues were incubated for 24 hours at 37°C. After 24 hours, tissues were removed from drug and rinsed with fresh culture media before being frozen with dry ice vapor and stored at -80°C. Each tissue was sectioned at -20°C using a Leica CM1950 cryomicrotome (Buffalo Grove, IL) into 10, 25, or 50 µm thick sections. The sections were then thaw-mounted onto glass microscope slides for imaging. Sections of each tissue were mounted adjacent to each other so that each glass slide contained a section of each tissue in the low and high concentrations at the same thickness. Sections that were serial cuts to those used for imaging were also collected for LC-MS quantitation.

5.2.3 IR-MALDESI Imaging

A more detailed description of the IR-MALDESI imaging source can be found elsewhere.[36,37] In short, the tissue sample is placed on a liquid cooled thermoelectric stage that is cooled to -10°C while under nitrogen purge and is then exposed to the ambient environment in order to deposit a thin layer of ice over the surface of the tissue. Once the ice layer has been deposited, the enclosure around

the source is purged with nitrogen to maintain a relative humidity of around 10 % which we have found to be the point where ice deposition and sublimation are close to equilibrium to preserve a consistent ice matrix layer throughout the course of the imaging experiment. A mid-IR laser tuned to 2.94 μm (IR-Opolette 2371, Opotek, Carlsbad, CA) is used to resonantly excite the ice matrix layer and facilitate the desorption of neutral molecules from the tissue section. These neutrals then partition into the charged solvent droplets of an electrospray plume where ions are generated through an ESI-like process. The geometry of the IR-MALDESI source has recently been optimized for tissue imaging.[37] For the imaging experiments, 50% (v/v) aqueous methanol with 0.2% formic acid was used for the electrospray solvent as this composition has been shown to work well for small molecules and lipids.[24] All imaging experiments were performed with a spot-to-spot distance of 100 μm.

5.2.4 Q Exactive

The IR-MALDESI imaging source was fully synchronized with a Thermo Fisher Scientific Q Exactive (Bremen, Germany) such that ion accumulation was triggered to overlap with the pulsing of the laser resulting in a single orbitrap acquisition at each pixel. The automatic gain control (AGC) of the instrument was turned off for all imaging experiments due to its incompatibility with our pulsed ionization source. The AGC is normally used to maintain a consistent number of ions in the orbitrap. It does so by determining the rate of ion generation during a prescan and varying the amount of time that ions are accumulated to reach a target

number of ions (AGC target) for the analytical scan. With the AGC off, ions are accumulated for a set period of time according to the maximum ion injection time (IT). Even with the AGC off, mass accuracy was verified to be maintained within 1 ppm by using two diisooctyl phthalate peaks (391.2843 $[M+H]^+$ and 413.266 $[M+Na]^+$) as lock-masses in the instrument control software.

For broadband acquisition, two laser pulses were performed at 20 Hz (50 ms/pulse) with a 150 ms IT to accumulate ions from both laser pulses in the C-trap followed by a single Orbitrap acquisition. The mass range for the orbitrap acquisition was set to 150-600 *m/z*. The mass resolution was set to 140,000 at *m/z* 200.

For MS^2 acquisition, a targeted MS^2 method file was created using an inclusion list for isolating the protonated ion of RAL (*m/z* 445.16302) with a maximum IT of 150 ms. Two IR pulses were performed at each pixel (20 Hz) where ions from each pulse were isolated with a 4 *m/z* window and a 1.5 *m/z* offset followed by ion accumulation in the C-trap. The accumulated ion packet was then fragmented in the HCD cell at a normalized collision energy of 20. All resulting fragments were analyzed in a single orbitrap acquisition. The normalized collision energy was optimized through the direct infusion of a RAL standard. Unique transitions for RAL were also determined during the direct infusion of the drug standards. The mass resolution was set to 140,000 at *m/z* 200 for the MS^2 acquisition in the orbitrap in order to obtain high mass accuracies for the fragments.

5.2.5 Data Analysis

For individual ion images, the raw data (.raw) from the Thermo Q Exactive was converted to the mzXML format using the MSConvert software from Proteowizard[53] For the stacked ion images, the raw files were converted to mzML files using the MSConvert software from Proteowizard and were then converted to individual imzML files using imzMLConverter.[54] The imzML Converter was then used to stack the individual imzmL files into one master imzML file. The mzXML or imzML files were then loaded into the standalone version of MSiReader which is freely available software developed in our lab for processing MSI data.[55] In order to demonstrate the quality of the raw data, ion images presented in this manuscript were neither interpolated nor normalized (unless otherwise specified). MSiReader was used to extract peak intensities to the regions around the low and high concentration tissues in order to determine the average peak intensity for comparison with the absolute amounts determined by LC-MS/MS. A modified 'hot' colorscale was used to demonstrate changes in intensity. Despite its widespread use in visualizing data, the 'rainbow' or 'jet' colorscale leads to misleading and non-intuitive distinctions between intensity values and was thus not used here.[56-59]

5.2.6 LC-MS/MS Quantitation

Tissue sections (10, 25, and 50 µm) from the low and high concentration tissue samples were extracted and analyzed by LC-MS/MS for TFV, FTC, and RAL concentrations. Sections were homogenized and extracted in 1 mL of 70:30

acetonitrile:1 mM ammonium phosphate (pH 7.4) using a Precellys® 24 tissue homogenizer. Calibration standards were prepared at 0.3, 0.6, 1.5, 6, 15, 30, 75, 150, 255, and 300 ng/mL in 70:30 acetonitrile:1 mM ammonium phosphate (pH 7.4). Quality control (QC) samples were prepared at 0.9, 21, and 240 ng/mL in 70:30 acetonitrile:1 mM ammonium phosphate (pH 7.4). Following centrifugation, 300 µL of each standard/QC/sample was mixed with 50 µL of an internal standard solution ($^{13}C_5$-TFV, $^{13}C^{15}N_2$-FTC, and RAL-d_3 at 50 ng/mL in 50:50 methanol:water). The resulting solutions were evaporated to dryness under nitrogen at 50^{o}C. Samples were reconstituted in 100 µL of 1 mM ammonium phosphate (pH 7.4) and transferred to a 96-well plate for LC-MS/MS analysis.

A Shimadzu HPLC system (SIL-20AC autosampler, LC-20AD pumps, and CTO-20A column oven; Shimadzu Scientific Instruments, Columbia, MD) was used for this analysis. A Waters Atlantis T3 column (2.1 mm × 100 mm, 3 µm, Waters, Milford, MA) was utilized at 35^{o}C. A gradient elution using water with 0.1% formic acid (Mobile Phase A) and acetonitrile with 0.1% formic acid (mobile Phase B) was used to perform chromatographic separation. A Sciex API 5000 Triple Quad mass spectrometer (AB Sciex, Foster City, CA) equipped with a Turbo spray interface was used as the detector. TFV and $^{13}C_5$-TFV were detected in negative ion mode with mass transitions of 286 → 107 and 291 →111, respectively. FTC, $^{13}C^{15}N_2$-FTC, RAL, and RAL-d_3 were detected in positive ion mode with mass transitions of 248 → 130, 251 →133, 445 → 361, 448 →109, respectively.

Calibration standards and QCs for all three analytes were within 15% of nominal concentrations. With the tissue samples being extracted in 1 mL of solvent, the final result (in ng/mL) was equivalent to mass extracted (in ng) from each sample. The tissues (all < 1mg) provided negligible volume to the homogenized sample allowing for the direct correlation between ng/mL and ng extracted. Since the tissue slices were too small to weigh, the final drug concentrations were not adjusted for tissue mass and are presented as ng extracted per slice.

5.3 Results and Discussion

5.3.1 Full Acquisition IR-MALDESI MSI

Cervical tissues were incubated in either a high or low concentration of the three HIV drugs tenofovir (TFV), emtricitabine (FTC), and raltegravir (RAL). Two adjacent 10 µm sections of the high concentration tissue were thaw-mounted onto glass microscope slides. These two tissue sections were then imaged either with or without an ice matrix in order to validate the use of ice as a matrix for IR-MALDESI MSI.[37] The optical images of the tissues for both conditions as well as the corresponding ion maps for the protonated ions of the three incubated drugs are shown in **Figure 5.1**. The ion images for each drug provide clear evidence of the degree of improvement that can be achieved when using ice as a matrix. Also, the average pixel intensity and frequency of pixels in the tissue-related area where signal was detected (number of non-zero pixels/total number of pixels for the tissue-related area) are also provided for each drug under both conditions to provide a

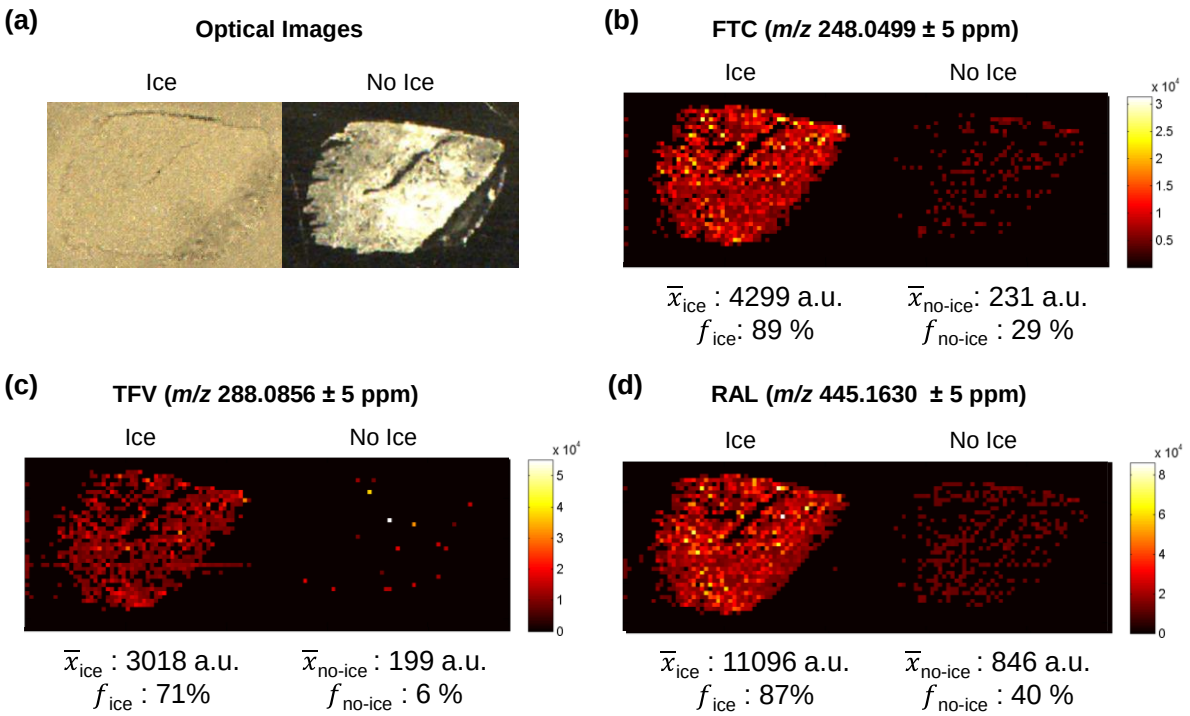

Figure 5.1 Validation of the use of ice as a matrix for IR-MALDESI MSI. Optical images **(a)** of two 10 µm serial sections of the high concentration tissue either with or without (respectively) a deposited layer of ice. Ion maps of **(b)** emtricitabine as $[M+H]^+$, **(c)** tenofovir as $[M+H]^+$, and **(d)** raltegravir as $[M+H]^+$. In addition, the average intensity and frequency of the pixels with signal within the tissue area is provided for each of the ions under both conditions (with or without ice matrix) to demonstrate the degree of improvement that is achieved when using the ice matrix.

more objective comparison. The average pixel intensity is shown to be between about 15 fold higher for the tissue with ice as a matrix compared to the tissue without a matrix. While it is likely linked to the improvement in overall intensity, there is also marked improvement in the frequency of pixels with signal in the imaging experiment with ice which is especially clear for tenofovir which is the least abundant of the three incubated drugs. The results of these experiments help to validate the use of ice as a matrix for IR-MALDESI MSI and support our previous conclusions.[37]

The high and low concentration incubated tissues were then cryo-sectioned into several thicknesses (10, 25, and 50 μm) to investigate the influence of tissue thickness on the imaging experiment. IR-MALDESI MSI was then performed on each set of tissues (high and low concentration at each tissue thickness) using a broadband acquisition method where at each image pixel a single full mass spectrum (*m/z* 150-600) was collected. This broadband acquisition allows for the observation of all three drugs as well as any endogenous species that fall within the *m/z* range. For each tissue thickness a single imaging experiment was conducted which encompassed both the low and high concentration tissue sections. Ion images for the protonated forms of all three drugs as well as the optical images of the tissue sections are shown in **Figure 5.2**. All of the ion maps shown in **Figure 5.2** are on the same intensity scale to demonstrate the relative intensities of all three drugs across the different tissue thicknesses. Coupling the IR-MALDESI imaging source with the Q Exactive has demonstrated a vast improvement in the analysis time necessary to complete a high resolving power imaging experiment. On the Q Exactive, the broadband imaging experiments were acquired at a rate of 1.6 scans/second. For reference, the acquisition rate for the same experiment on our LTQ-FT is roughly 0.5 scans/second, which represents a nearly three-fold improvement in acquisition speed with the Q Exactive. This improvement is likely due to the eFT which allows for shorter transients in addition to the multiplexing capabilities of the Q Exactive where ions can be accumulated for the next acquisition while the FT analysis is being performed.

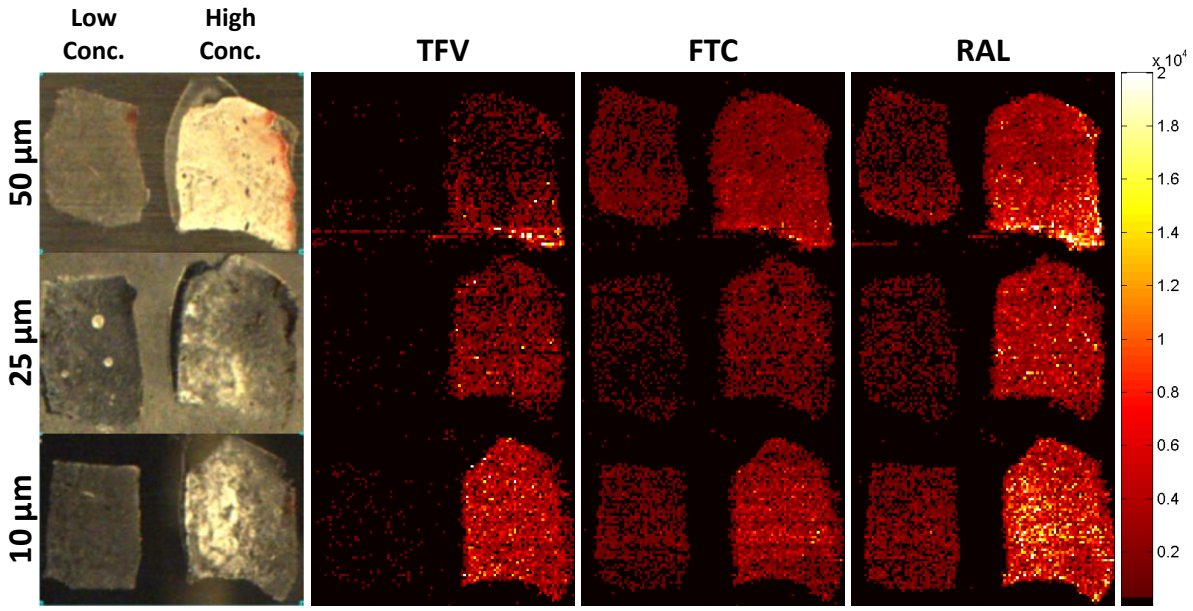

Figure 5.2 IR-MALDESI MSI analysis of cervical tissues incubated in either a low or high concentration of three HIV drugs including emtricitabine (FTC), tenofovir (TFV), and raltegravir (RAL). Three different tissue thicknesses were investigated (10, 25, and 50 µm). The ion maps for all three drugs at each tissue thickness are shown on the same intensity scale to highlight relative differences in abundance.

At each pixel, the laser ablates all the way through the tissue and therefore it may be expected that the intensity for any of the drugs from the 50 µm section should be roughly five times that of the 10 µm section since there is five times more material (this assumption is validated from the LC-MS/MS quantification presented later). This, however, was not observed and the signal from all three thicknesses appears to be relatively similar. The lack of correlation between tissue thickness and the signal abundance could be occurring for several reasons. One possible explanation is that in IR-MALDESI the ablated material interacts with the charged solvent droplets of the electrospray plume where the analyte is extracted into the solvent droplets and is later ionized through an ESI-like process. The efficiency of

Table 5.2 Absolute drug quantities determined by LC-MS/MS.

Incubated Conc.	Tissue Thickness	TFV (ng/Tissue)	FTC (ng/Tissue)	RAL (ng/Tissue)
Low	10	0.877	3.36	2.29
	25	1.91	6.95	4.90
	50	4.04	14.4	10.6
High	10	8.82	9.19	12.5
	25	21.9	23.1	33.2
	50	43.3	44.7	64.6

this neutral capture event may inversely scale with the amount of material that is ablated. In essence, the extraction of analyte may be limited because there are a finite number of droplets present that are available for interaction with the tissue material. Despite this, **Figure 5.2** shows that for a given tissue thickness there is an observable difference in intensity between the low and high concentrations and in fact the ratio of the average intensity of the low and high concentrations is consistent for all three tissue thicknesses.

5.3.2 Comparison of IR-MALDESI MSI with LC-MS/MS Quantitation

Tissue sections serial to those imaged by IR-MALDESI MSI were homogenized and analyzed by LC-MS/MS to quantify the amount of each drug that was present in both the high and low concentration tissues for all three tissue thicknesses. **Table 5.2** shows the results of this analysis and provides the absolute amount of each drug per tissue section (ng/tissue). The ratio of low to high concentration was determined for each set of tissues and these values were then

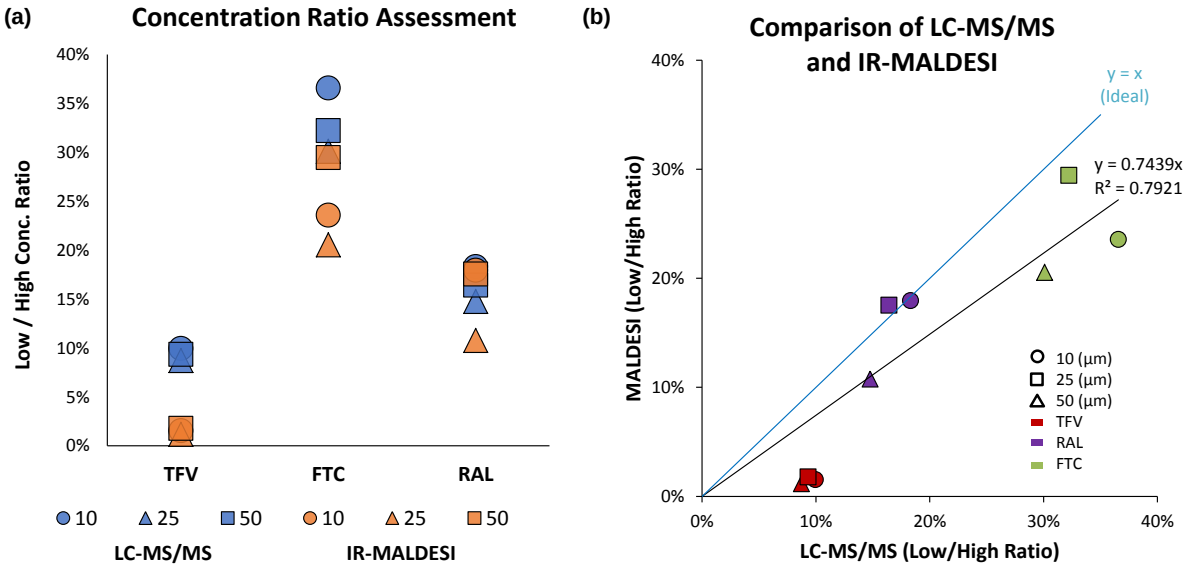

Figure 5.3 Comparison of data from LC-MS/MS and IR-MALDESI. **(a)** Plot of the low to high concentration ratios of all three drugs across the three tissue thicknesses that were investigated. **(b)** Plot of the data from both methods (LC-MS/MS vs. IR-MALDESI). A slope near 1 indicates relatively good agreement between the results from the LC-MS/MS and IR-MALDESI MSI experiments.

compared with the corresponding average intensity ratios from the IR-MALDESI imaging experiments. This comparison is shown in **Figure 5.3**. It should be noted that differential uptake of these drugs precludes the ability to compare their incubated concentrations with ratios observed by LC-MS and IR-MALDESI (data not shown). **Figure 5.3a** shows the relative intensity ratio from the low to the high concentration tissues for each of the three drugs. It is evident that for both techniques and the different tissue thicknesses, the low/high ratio clusters together for a given drug. To compare the two methods, the low/high concentration ratios are plotted as a function of the method, thus a slope of 1 indicates agreement between the two methods (**Figure 5.3b**). The slope of the least-squares fit line through the

data (forcing the intercept to 0) was around 0.74 with a correlation coefficient of close to 0.8. The deviation from an ideal slope of 1 is likely due to an underestimation of the low/high ratio by IR-MALDESI. The cause of this underestimation of the ratio is possibly due to the decreased frequency of detection of these drugs in the low concentration tissue which is a result of being near the detection limit as evidenced by **Figure 5.2**. While there obviously room for improvement, the low/high concentration ratios between LC-MS/MS and IR-MALDESI are in fairly good agreement. A correlation between MSI and LC-MS/MS has been demonstrated previously for other ionization methods including MALDI [18,50,60-70] and DESI,[22,71,72] but this is the first example of agreement between IR-MALDESI MSI with LC-MS/MS. Given that LC-MS/MS is a validated quantitation method; the correlation between the average intensities from IR-MALDESI with the absolute quantities determined by LC-MS/MS provides a foundation for quantification directly from an imaging experiment. Direct quantitation from an MSI experiment would be ideal (especially for heterogeneous tissues) and is the focus of research efforts from several groups.[40,61,63-70,72-77]

A potential limitation of this study is the use of mucosal tissue explants incubated in drug-containing media, rather than utilizing tissue biopsies obtained from patients receiving the drug. It is possible that antiretroviral uptake into explants ex-vivo differs from that observed in-vivo. However, the human tissue explant model has previously been validated for generating pharmacokinetic/ pharmacodynamic (PK/PD) relationships that are clinically useful.[78,79] With the promising data

generated from this current investigation, future drug distribution experiments evaluating tissues obtained from animals and humans dosed with these drugs are being planned.

5.3.3 MS^2 IR-MALDESI MSI

IR-MALDESI MSI was performed as a targeted MS^2 experiment for the drug RAL. Ions generated from two laser pulses were filtered for the protonated form of RAL using the selection quadrupole followed by accumulation in the C-Trap. The ions were then fragmented in the HCD cell and mass analyzed in the orbitrap at 140,000 RP (at *m/z* 200) to obtain accurate mass data on the fragment ions. This process was then repeated over the surface of the tissue such that a fragment ion 'scan' was acquired at each pixel in the image. The acquisition rate for the targeted MS^2 imaging experiment was 1.5 scans/second, implying that very little overhead was incurred with the added step of fragmentation. Ion maps for the several RAL transitions are shown in **Figure 5.4a**. The colocalization of all of the transitions with the parent ion distribution at *m/z* 445 demonstrates the higher selectivity that can be achieved with an MRM-MSI approach. In addition, the ion abundance ratios from this pseudo MRM imaging experiment were compared with those obtained from the direct infusion ESI-MS experiment that was used to determine the optimal collision energy (**Figure 5.4b**). As shown, the ion abundance ratios are nearly identical between the two techniques. This implies also that the internal energy imparted

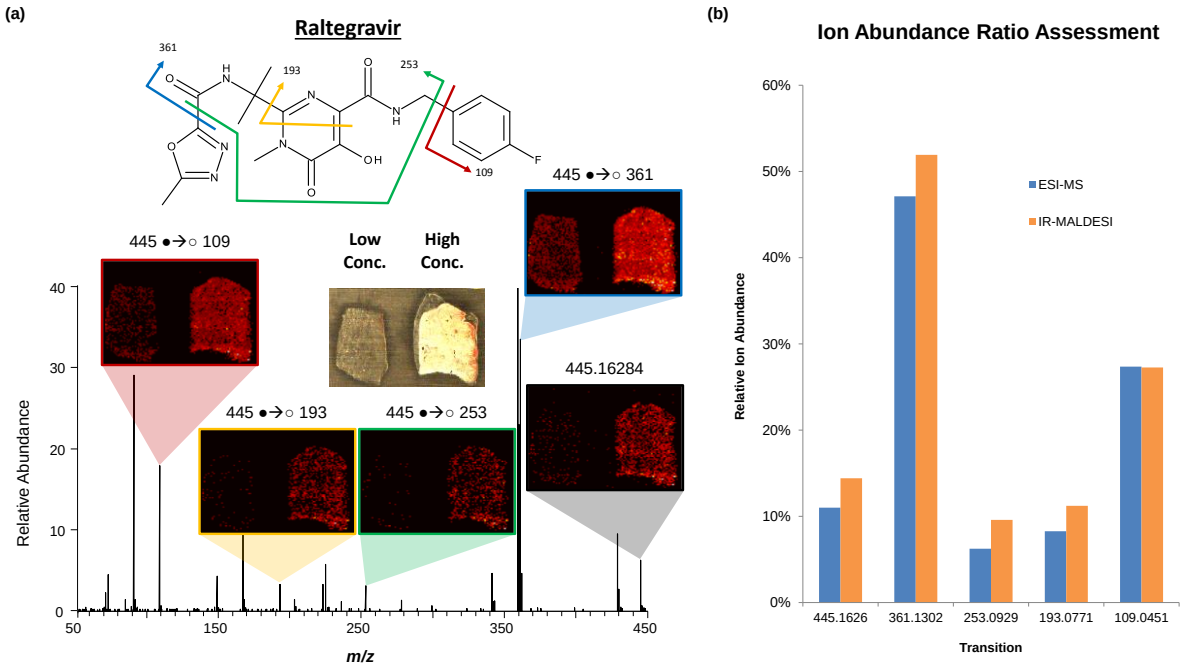

Figure 5.4 Results of MRM Imaging. **(a)** Ion maps for the several unique transitions for raltegravir (RAL) that were observed from the targeted MS^2 IR-MALDESI MSI experiment. The colocalization of all of the transitions demonstrates the increased selectivity that can be realized with targeted MS^2 imaging techniques. **(b)** Comparison of the ion abundance ratios for selected transitions of raltegravir for both IR-MALDESI and LC-MS/MS.

during ionization in IR-MALDESI is comparable to the softness of ionization in ESI as has been previously mentioned.[80]

5.4 Conclusions

We have demonstrated the capabilities of IR-MALDESI MSI coupled with the Q Exactive mass spectrometer. Tissue sections that were incubated with several potent and commonly utilized antiretroviral drugs were analyzed by IR-MALDESI MSI as well as LC-MS/MS. A comparison of these two methods demonstrated that

the average intensities determined from the imaging experiments agreed well with the absolute abundances determined from a validated quantitation method. These experiments serve as a foundation for direct quantitation from tissue using IR-MALDESI MSI. In addition, a targeted MS^2 imaging experiment was also conducted to show the added selectivity that can be attained for this type of analysis.

5.5 References

(1) Caprioli, R. M.; Farmer, T. B.; Gile, J. Molecular Imaging of Biological Samples: Localization of Peptides and Proteins Using MALDI-TOF MS. *Anal. Chem.* **1997**, *69*(23), 4751-4760.

(2) Caldwell, R. L.; Caprioli, R. M. Tissue Profiling by Mass Spectrometry: A Review of Methodology and Applications. *Mol. Cell. Proteomics* **2005**, *4*(4), 394-401.

(3) Burnum, K. E.; Frappier, S. L.; Caprioli, R. M. Matrix-Assisted Laser Desorption/Ionization Imaging Mass Spectrometry for the Investigation of Proteins and Peptides. *Annu. Rev. Anal. Chem.* **2008**, *1*(1), 689-705.

(4) Murphy, R. C.; Hankin, J. A.; Barkley, R. M. Imaging of lipid species by MALDI mass spectrometry. *J. Lipid Res.* **2009**, *50*(Supplement), S317-S322.

(5) Svatoš, A. Mass spectrometric imaging of small molecules. *Trends Biotechnol.* **2010**, *28*(8), 425-434.

(6) Greer, T.; Sturm, R.; Li, L. Mass spectrometry imaging for drugs and metabolites. *J. Proteomics* **2011**, *74*(12), 2617-2631.

(7) Oppenheimer, S. R.; Drexler, D. M. Tissue analysis by imaging MS. *Bioanalysis* **2012**, *4*(1), 95-112.

(8) Schwamborn, K. Imaging mass spectrometry in biomarker discovery and validation. *J. Proteomics* **2012**, *75*(16), 4990-4998.

(9) Liu, J.; Ouyang, Z. Mass spectrometry imaging for biomedical applications. *Anal. Bioanal. Chem.* **2013**, *405*(17), 5645-5653.

(10) Goodwin, R. J.; Pitt, A. R. Mass spectrometry imaging of pharmacological compounds in tissue sections. *Bioanalysis* **2010**, *2*(2), 279-293.

(11) Castellino, S.; Groseclose, M. R.; Wagner, D. MALDI imaging mass spectrometry: bridging biology and chemistry in drug development. *Bioanalysis* **2011**, *3*(21), 2427-2441.

(12) Castellino, S. MALDI imaging MS analysis of drug distribution in tissue: the right time!(?). *Bioanalysis* **2012**, *4*(21), 2549-2551.

(13) Eichler, H.-G.; Müller, M. Drug Distribution. *Clin. Pharmacokinet.* **1998**, *34*(2), 95-99.

(14) Lanao, J. M.; Fraile, M. A. Drug Tissue Distribution: Study Methods and Therapeutic Implications. *Curr. Pharm. Des.* **2005**, *11*(29), 3829-3845.

(15) Solon, E. G.; Balani, S. K.; Lee, F. W. Whole-Body Autoradiography In Drug Discovery. *Curr. Drug Metab.* **2002**, *3*(5), 451-462.

(16) Atkinson, S. J.; Loadman, P. M.; Sutton, C.; Patterson, L. H.; Clench, M. R. Examination of the distribution of the bioreductive drug AQ4N and its active metabolite AQ4 in solid tumours by imaging matrix-assisted laser desorption/ionisation mass spectrometry. *Rapid Commun. Mass Spectrom.* **2007**, *21*(7), 1271-1276.

(17) Römpp, A.; Guenther, S.; Takats, Z.; Spengler, B. Mass spectrometry imaging with high resolution in mass and space (HR^2 MSI) for reliable investigation of drug compound distributions on the cellular level. *Anal. Bioanal. Chem.* **2011**, *401*(1), 65-73.

(18) Nilsson, A.; Forngren, B.; Bjurström, S.; Goodwin, R. J. A.; Basmaci, E.; Gustafsson, I.; Annas, A.; Hellgren, D.; Svanhagen, A.; Andrén, P. E.; Lindberg, J. In Situ Mass Spectrometry Imaging and Ex Vivo Characterization of Renal Crystalline Deposits Induced in Multiple Preclinical Drug Toxicology Studies. *PLoS One* **2012**, *7*(10), 1-10.

(19) Römpp, A.; Spengler, B. Mass spectrometry imaging with high resolution in mass and space. *Histochem. Cell Biol.* **2013**, *139*(6), 759-783.

(20) Kaletaş, B. K.; van der Wiel, I. M.; Stauber, J.; Lennard, J. D.; Güzel, C.; Kros, J. M.; Luider, T. M.; Heeren, R. M. A. Sample preparation issues for tissue imaging by imaging MS. *Proteomics* **2009**, *9*(10), 2622-2633.

(21) Goodwin, R. J. A. Sample preparation for mass spectrometry imaging: Small mistakes can lead to big consequences. *J. Proteomics* **2012**, *75*(16), 4893-4911.

(22) Wiseman, J. M.; Ifa, D. R.; Zhu, Y.; Kissinger, C. B.; Manicke, N. E.; Kissinger, P. T.; Cooks, R. G. Desorption electrospray ionization mass spectrometry: Imaging drugs and metabolites in tissues. *Proc. Natl. Acad. Sci. U.S.A.* **2008**, *105*(47), 18120-18125.

(23) Eikel, D.; Vavrek, M.; Smith, S.; Bason, C.; Yeh, S.; Korfmacher, W. A.; Henion, J. D. Liquid extraction surface analysis mass spectrometry (LESA-MS) as a novel profiling tool for drug distribution and metabolism analysis: the terfenadine example. *Rapid Commun. Mass Spectrom.* **2011**, *25*(23), 3587-3596.

(24) Barry, J. A.; Groseclose, M. R.; Robichaud, G.; Castellino, S.; Muddiman, D. C. Assessing drug and metabolite detection in liver tissue by IR-MALDESI mass spectrometry imaging coupled to FT-ICR MS. *Int. J. Mass Spectrom.* **Submitted 12/31/2013**.

(25) Levis, R. J. Laser Desorption and Ejection of Biomolecules From the Condensed Phase into the Gas Phase. *Annu. Rev. Phys. Chem.* **1994**, *45*(1), 483-518.

(26) Sampson, J.; Hawkridge, A.; Muddiman, D. Generation and detection of multiply-charged peptides and proteins by matrix-assisted laser desorption electrospray ionization (MALDESI) fourier transform ion cyclotron resonance mass spectrometry. *J. Am. Soc. Mass Spectrom.* **2006**, *17*(12), 1712-1716.

(27) Sampson, J. S.; Murray, K. K.; Muddiman, D. C. Intact and Top-Down Characterization of Biomolecules and Direct Analysis Using Infrared Matrix-Assisted Laser Desorption Electrospray Ionization Coupled to FT-ICR Mass Spectrometry. *J. Am. Soc. Mass Spectrom.* **2009**, *20*(4), 667-673.

(28) Rezenom, Y. H.; Dong, J.; Murray, K. K. Infrared laser-assisted desorption electrospray ionization mass spectrometry. *Analyst* **2008**, *133*(2), 226-232.

(29) Nemes, P.; Vertes, A. Laser Ablation Electrospray Ionization for Atmospheric Pressure, in Vivo, and Imaging Mass Spectrometry. *Anal. Chem.* **2007**, *79*(21), 8098-8106.

(30) Sampson, J. S.; Muddiman, D. C. Atmospheric pressure infrared (10.6 μm) laser desorption electrospray ionization (IR-LDESI) coupled to a LTQ Fourier transform ion cyclotron resonance mass spectrometer. *Rapid Commun. Mass Spectrom.* **2009**, *23*(13), 1989-1992.

(31) Jorabchi, K.; Smith, L. M. Single Droplet Separations and Surface Partition Coefficient Measurements Using Laser Ablation Mass Spectrometry. *Anal. Chem.* **2009**, *81*(23), 9682-9688.

(32) Nelson, R.; Rainbow, M.; Lohr, D.; Williams, P. Volatilization of high molecular weight DNA by pulsed laser ablation of frozen aqueous solutions. *Sci* **1989**, *246*(4937), 1585-1587.

(33) Berkenkamp, S.; Karas, M.; Hillenkamp, F. Ice as a matrix for IR-matrix-assisted laser desorption/ionization: mass spectra from a protein single crystal. *Proc. Natl. Acad. Sci. U. S. A.* **1996**, *93*(14), 7003-7.

(34) Vertes, A.; Nemes, P.; Shrestha, B.; Barton, A.; Chen, Z.; Li, Y. Molecular imaging by Mid-IR laser ablation mass spectrometry. *Appl. Phys. A: Mater. Sci. Process.* **2008**, *93*(4), 885-891.

(35) Nemes, P.; Barton, A. A.; Li, Y.; Vertes, A. Ambient Molecular Imaging and Depth Profiling of Live Tissue by Infrared Laser Ablation Electrospray Ionization Mass Spectrometry. *Anal. Chem.* **2008**, *80*(12), 4575-4582.

(36) Robichaud, G.; Barry, J. A.; Garrard, K. P.; Muddiman, D. C. Infrared Matrix-Assisted Laser Desorption Electrospray Ionization (IR-MALDESI) Imaging Source Coupled to a FT-ICR Mass Spectrometer. *J. Am. Soc. Mass Spectrom.* **2013**, *24*(1), 92-100.

(37) Robichaud, G.; Barry, J. A.; Muddiman, D. C. IR-MALDESI Mass Spectrometry Imaging of Biological Tissue Sections using Ice as a Matrix. *J. Am. Soc. Mass Spectrom.* **2014**, *25*(3), 319-328.

(38) Cornett, D. S.; Frappier, S. L.; Caprioli, R. M. MALDI-FTICR Imaging Mass Spectrometry of Drugs and Metabolites in Tissue. *Anal. Chem.* **2008**, *80*(14), 5648-5653.

(39) Manicke, N. E.; Dill, A. L.; Ifa, D. R.; Cooks, R. G. High-resolution tissue imaging on an orbitrap mass spectrometer by desorption electrospray ionization mass spectrometry. *J. Mass Spectrom.* **2010**, *45*(2), 223-226.

(40) Fehniger, T. E.; Végvári, Á.; Rezeli, M.; Prikk, K.; Ross, P.; Dahlbäck, M.; Edula, G.; Sepper, R.; Marko-Varga, G. Direct Demonstration of Tissue Uptake of an Inhaled Drug: Proof-of-Principle Study Using Matrix-Assisted Laser Desorption Ionization Mass Spectrometry Imaging. *Anal. Chem.* **2011**, *83*(21), 8329-8336.

(41) Shahidi-Latham, S. K.; Dutta, S. M.; Prieto Conaway, M. C.; Rudewicz, P. J. Evaluation of an Accurate Mass Approach for the Simultaneous Detection of Drug and Metabolite Distributions via Whole-Body Mass Spectrometric Imaging. *Anal. Chem.* **2012**, *84*(16), 7158-7165.

(42) Korte, A.; Lee, Y. Multiplex Mass Spectrometric Imaging with Polarity Switching for Concurrent Acquisition of Positive and Negative Ion Images. *J. Am. Soc. Mass Spectrom.* **2013**, *24*(6), 949-955.

(43) Michalski, A.; Damoc, E.; Hauschild, J.-P.; Lange, O.; Wieghaus, A.; Makarov, A.; Nagaraj, N.; Cox, J.; Mann, M.; Horning, S. Mass Spectrometry-based Proteomics Using Q Exactive, a High-performance Benchtop Quadrupole Orbitrap Mass Spectrometer. *Mol. Cell. Proteomics* **2011**, *10*(9).

(44) Bhandari, D.; Shen, T.; Römpp, A.; Zorn, H.; Spengler, B. Analysis of cyathane-type diterpenoids from Cyathus striatus and Hericium erinaceus by high-resolution MALDI MS imaging. *Anal. Bioanal. Chem.* **2013**1-10.

(45) Janfelt, C.; Wellner, N.; Hansen, H. S.; Hansen, S. H. Displaced dual-mode imaging with desorption electrospray ionization for simultaneous mass spectrometry imaging in both polarities and with several scan modes. *J. Mass Spectrom.* **2013**, *48*(3), 361-366.

(46) Lanekoff, I.; Burnum-Johnson, K. E.; Thomas, M.; Short, J.; Carson, J. P.; Cha, J.; Dey, S. K.; Yang, P.; Prieto Conaway, M. C.; Laskin, J. High-Speed MS/MS in Situ Imaging by Nanospray Desorption Electrospray Ionization Mass Spectrometry. *Anal. Chem.* **2013**.

(47) Thompson, C. G.; Cohen, M. S.; Kashuba, A. D. M. Antiretroviral Pharmacology in Mucosal Tissues. *JAIDS J. Acquired Immune Defic. Syndromes* **2013**, *63*S240-S247

(48) Smith, M. Z.; Wightman, F.; Lewin, S. R. HIV Reservoirs and Strategies for Eradication. *Current HIV/AIDS Reports* **2012**, *9*(1), 5-15.

(49) Meesters, R. J. W.; van Kampen, J. J. A.; Scheuer, R. D.; van der Ende, M. E.; Gruters, R. A.; Luider, T. M. Determination of the antiretroviral drug tenofovir in plasma from HIV-infected adults by ultrafast isotope dilution MALDI-triple quadrupole tandem mass spectrometry. *J. Mass Spectrom.* **2011**, *46*(3), 282-289.

(50) Castellino, S.; Groseclose, M. R.; Sigafoos, J.; Wagner, D.; de Serres, M.; Polli, J. W.; Romach, E.; Myer, J.; Hamilton, B. Central Nervous System Disposition and Metabolism of Fosdevirine (GSK2248761), a Non-Nucleoside Reverse Transcriptase Inhibitor: An LC-MS and Matrix-Assisted Laser Desorption/Ionization Imaging MS Investigation into Central Nervous System Toxicity. *Chem. Res. Toxicol.* **2012**, *26*(2), 241-251.

(51) Patterson, K. B.; Prince, H. A.; Kraft, E.; Jenkins, A. J.; Shaheen, N. J.; Rooney, J. F.; Cohen, M. S.; Kashuba, A. D. M. Penetration of Tenofovir and Emtricitabine in Mucosal Tissues: Implications for Prevention of HIV-1 Transmission. *Science Translational Medicine* **2011**, *3*(112), 112re4.

(52) Patterson, K. B.; Prince, H. A.; Stevens, T.; Shaheen, N. J.; Dellon, E. S.; Madanick, R. D.; Jennings, S.; Cohen, M. S.; Kashuba, A. D. M. Differential penetration of raltegravir throughout gastrointestinal tissue: implications for eradication and cure. *AIDS* **2013**, *27*(9), 1413-1419 10.1097/QAD.0b013e32835f2b49.

(53) Kessner, D.; Chambers, M.; Burke, R.; Agus, D.; Mallick, P. ProteoWizard: open source software for rapid proteomics tools development. *Bioinformatics* **2008**, *24*(21), 2534-2536.

(54) Race, A. M.; Styles, I. B.; Bunch, J. Inclusive sharing of mass spectrometry imaging data requires a converter for all. *J. Proteomics* **2012**, *75*(16), 5111-5112.

(55) Robichaud, G.; Garrard, K. P.; Barry, J. A.; Muddiman, D. C. MSiReader: An Open-Source Interface to View and Analyze High Resolving Power MS Imaging Files on Matlab Platform. *J. Am. Soc. Mass Spectrom.* **2013**, *24*(5), 718-721.

(56) Rogowitz, B. E.; Treinish, L. A.; Bryson, S. How Not to Lie with Visualization. *ComPh* **1996**, *10*(3), 268-273.

(57) Rogowitz, B.; Treinish, L. A. Data visualization: the end of the rainbow. *Spectrum, IEEE* **1998**, *35*(12), 52-59.

(58) Light, A.; Bartlein, P. J. The end of the rainbow? Color schemes for improved data graphics. *Eos, Transactions American Geophysical Union* **2004**, *85*(40), 385-391.

(59) Borland, D.; Taylor, R. M. Rainbow Color Map (Still) Considered Harmful. *Computer Graphics and Applications, IEEE* **2007**, *27*(2), 14-17.

(60) Reyzer, M. L.; Hsieh, Y.; Ng, K.; Korfmacher, W. A.; Caprioli, R. M. Direct analysis of drug candidates in tissue by matrix-assisted laser desorption/ionization mass spectrometry. *J. Mass Spectrom.* **2003**, *38*(10), 1081-1092.

(61) Hsieh, Y.; Casale, R.; Fukuda, E.; Chen, J.; Knemeyer, I.; Wingate, J.; Morrison, R.; Korfmacher, W. Matrix-assisted laser desorption/ionization imaging mass spectrometry for direct measurement of clozapine in rat brain tissue. *Rapid Commun. Mass Spectrom.* **2006**, *20*(6), 965-972.

(62) Drexler, D. M.; Garrett, T. J.; Cantone, J. L.; Diters, R. W.; Mitroka, J. G.; Prieto Conaway, M. C.; Adams, S. P.; Yost, R. A.; Sanders, M. Utility of imaging mass spectrometry (IMS) by matrix-assisted laser desorption ionization (MALDI) on an ion trap mass spectrometer in the analysis of drugs and metabolites in biological tissues. *J. Pharmacol. Toxicol. Methods* **2007**, *55*(3), 279-288.

(63) Hsieh, Y.; Chen, J.; Korfmacher, W. A. Mapping pharmaceuticals in tissues using MALDI imaging mass spectrometry. *J. Pharmacol. Toxicol. Methods* **2007**, *55*(2), 193-200.

(64) Signor, L.; Varesio, E.; Staack, R. F.; Starke, V.; Richter, W. F.; Hopfgartner, G. Analysis of erlotinib and its metabolites in rat tissue sections by MALDI quadrupole time-of-flight mass spectrometry. *J. Mass Spectrom.* **2007**, *42*(7), 900-909.

(65) Nilsson, A.; Fehniger, T. E.; Gustavsson, L.; Andersson, M.; Kenne, K.; Marko-Varga, G.; Andrén, P. E. Fine Mapping the Spatial Distribution and Concentration of Unlabeled Drugs within Tissue Micro-Compartments Using Imaging Mass Spectrometry. *PLoS One* **2010**, *5*(7), e11411.

(66) Koeniger, S. L.; Talaty, N.; Luo, Y.; Ready, D.; Voorbach, M.; Seifert, T.; Cepa, S.; Fagerland, J. A.; Bouska, J.; Buck, W.; Johnson, R. W.; Spanton, S. A quantitation method for mass spectrometry imaging. *Rapid Commun. Mass Spectrom.* **2011**, *25*(4), 503-510.

(67) Prideaux, B.; Dartois, V. r.; Staab, D.; Weiner, D. M.; Goh, A.; Via, L. E.; Barry Iii, C. E.; Stoeckli, M. High-Sensitivity MALDI-MRM-MS Imaging of Moxifloxacin Distribution in Tuberculosis-Infected Rabbit Lungs and Granulomatous Lesions. *Anal. Chem.* **2011**, *83*(6), 2112-2118.

(68) Hamm, G.; Bonnel, D.; Legouffe, R.; Pamelard, F.; Delbos, J.-M.; Bouzom, F.; Stauber, J. Quantitative mass spectrometry imaging of propranolol and olanzapine using tissue extinction calculation as normalization factor. *J. Proteomics* **2012**, *75*(16), 4952-4961.

(69) Pirman, D. A.; Reich, R. F.; Kiss, A.; Heeren, R. M. A.; Yost, R. A. Quantitative MALDI Tandem Mass Spectrometric Imaging of Cocaine from

Brain Tissue with a Deuterated Internal Standard. *Anal. Chem.* **2012**, *85*(2), 1081-1089.

(70) Takai, N.; Tanaka, Y.; Inazawa, K.; Saji, H. Quantitative analysis of pharmaceutical drug distribution in multiple organs by imaging mass spectrometry. *Rapid Commun. Mass Spectrom.* **2012**, *26*(13), 1549-1556.

(71) Kertesz, V.; Van Berkel, G. J.; Vavrek, M.; Koeplinger, K. A.; Schneider, B. B.; Covey, T. R. Comparison of Drug Distribution Images from Whole-Body Thin Tissue Sections Obtained Using Desorption Electrospray Ionization Tandem Mass Spectrometry and Autoradiography. *Anal. Chem.* **2008**, *80*(13), 5168-5177.

(72) Vismeh, R.; Waldon, D. J.; Teffera, Y.; Zhao, Z. Localization and Quantification of Drugs in Animal Tissues by Use of Desorption Electrospray Ionization Mass Spectrometry Imaging. *Anal. Chem.* **2012**, *84*(12), 5439-5445.

(73) Bunch, J.; Clench, M. R.; Richards, D. S. Determination of pharmaceutical compounds in skin by imaging matrix-assisted laser desorption/ionisation mass spectrometry. *Rapid Commun. Mass Spectrom.* **2004**, *18*(24), 3051-3060.

(74) Goodwin, R. J. A.; Scullion, P.; MacIntyre, L.; Watson, D. G.; Pitt, A. R. Use of a Solvent-Free Dry Matrix Coating for Quantitative Matrix-Assisted Laser Desorption Ionization Imaging of 4-Bromophenyl-1,4-diazabicyclo(3.2.2)nonane-4-carboxylate in Rat Brain and Quantitative Analysis of the Drug from Laser Microdissected Tissue Regions. *Anal. Chem.* **2010**, *82*(9), 3868-3873.

(75) Goodwin, R. J. A.; Mackay, C. L.; Nilsson, A.; Harrison, D. J.; Farde, L.; Andren, P. E.; Iverson, S. L. Qualitative and Quantitative MALDI Imaging of the Positron Emission Tomography Ligands Raclopride (a D2 Dopamine Antagonist) and SCH 23390 (a D1 Dopamine Antagonist) in Rat Brain Tissue Sections Using a Solvent-Free Dry Matrix Application Method. *Anal. Chem.* **2011**, *83*(24), 9694-9701.

(76) Shin, Y.; Dong, T.; Chou, B.; Menghrajani, K. Determination of loperamide in Mdr1a/1b knock-out mouse brain tissue using matrix-assisted laser desorption/ionization mass spectrometry and comparison with quantitative electrospray-triple quadrupole mass spectrometry analysis. *Arch. Pharmacal Res.* **2011**, *34*(11), 1983-1988.

(77) Källback, P.; Shariatgorji, M.; Nilsson, A.; Andrén, P. E. Novel mass spectrometry imaging software assisting labeled normalization and quantitation of drugs and neuropeptides directly in tissue sections. *J. Proteomics* **2012**, *75*(16), 4941-4951.

(78) Harman, S.; Herrera, C.; Armanasco, N.; Nuttall, J.; Shattock, R. J. Preclinical Evaluation of the HIV-1 Fusion Inhibitor L'644 as a Potential Candidate Microbicide. *Antimicrob. Agents Chemother.* **2012**, *56*(5), 2347-2356.

(79) Rohan, L. C.; Moncla, B. J.; Kunjara Na Ayudhya, R. P.; Cost, M.; Huang, Y.; Gai, F.; Billitto, N.; Lynam, J. D.; Pryke, K.; Graebing, P.; Hopkins, N.; Rooney, J. F.; Friend, D.; Dezzutti, C. S. In Vitro and Ex Vivo Testing of Tenofovir Shows It Is Effective As an HIV-1 Microbicide. *PLoS One* **2010**, *5*(2), e9310.

(80) Nemes, P.; Huang, H.; Vertes, A. Internal energy deposition and ion fragmentation in atmospheric-pressure mid-infrared laser ablation electrospray ionization. *Phys. Chem. Chem. Phys.* **2012**, *14*(7), 2501-2507.

CHAPTER 6

Direct Analysis of Textile Fabric Using IR Matrix-Assisted Laser Desorption Electrospray Ionization (MALDESI) Mass Spectrometry

A portion of the following work was reprinted with permission from:
Cochran, K. H.; Barry, J. A.; Muddiman, D. C.; Hinks, D. Anal. Chem. 2012, 85(2), 831-836.
Copyright © 2012 American Chemical Society
The original publication may be accessed directly via the World Wide Web.

6.1 Introduction

Textile fibers are a significant form of trace evidence in forensic investigation. The importance of trace evidence is based primarily on Locard's exchange principle which states that a transfer of evidence occurs when a person comes into contact with any object or another person. This axiom allows for a comparison of fibers to determine the probability of association, *i.e.* fibers from the victim compared to fibers from the suspect, or fibers from the suspect matched against the crime scene, etc. If unrelated fibers positively match, the probability of deliberate contact increases while the probability of coincidental contact decreases.[1] The importance of unrelated fibers being compared with confidence will ensure viability of evidence in court necessitates that the techniques used for analysis be as accurate, time efficient, widely available, and up-to-date as possible. The analytical techniques used for contemporary fiber analysis include both non-destructive and destructive methods. Non-destructive methods yield the fiber polymer, information about the polymer such as refractive indices, luster, and birefringence, and the basic dye color. However,

non-destructive methods will not provide the significantly more conclusive data such as the dye's mass and elemental composition.[2]

Non-destructive techniques include microscopy, spectroscopy, and ultraviolet-visible microspectrophotometry (UV-vis MSP). The forms of microscopy commonly used for forensic purposes are confocal microscopy,[3] Fourier transform infrared (FT-IR) microscopy,[4] polarized light microscopy,[1] comparison microscopy,[2,5] and scanning electron microscopy with energy dispersive spectrometry (SEM-EDS).[1] Microscopy is used primarily to determine and compare fiber polymers of unrelated fibers, examine fraying and cuts, and identify polymer characteristics such as striations, crimp, and cross-sectional shapes.[2] The spectroscopic techniques used in forensics are Raman spectroscopy,[6,7] FT-IR spectroscopy,[4] and X-ray fluorescence spectroscopy.[7] Spectroscopy is used to definitively determine the fiber polymer and polymer composition, and some forms of spectroscopy such as Raman will yield limited qualitative dye information such as basic color spectra and dye concentrations. Spectroscopy will not give the quantitative dye mass or elemental composition.[1,6,7] UV-vis MSP is a combination of both microscopy and spectroscopy. Its forensic use is specifically for comparison purposes because UV-vis MSP can identify spectral characteristics but cannot differentiate dyes and dye mixtures.[1] These techniques have the benefits of being non-destructive while requiring little to no sample preparation. These benefits are crucial to forensic labs, which usually have very small sample sizes, limited analysts, and are on strict time constraints.

Liquid chromatography mass spectrometry (LC-MS) is becoming an increasingly popular method for identifying dye(s) from dyed textile fiber with a high degree of molecular specificity. LC-MS has the benefit of yielding the mass of the dye and in some instances the fiber polymer. A few of the disadvantages, however, include the destructive nature of the analysis as well as the extensive sample preparation procedures which can lead to lengthy analysis times. Prior to LC-MS analysis the dye must first be extracted from the fiber using an extraction solvent specific to the dye class. The extracted dye(s) can then be loaded onto an LC column for separation and subsequent detection by mass spectrometry. The entire extraction/chromatography/mass spectrometry process is lengthy, resulting in analysis times of around an hour, and extraction of the dye from the fiber renders the fiber unusable for any other subsequent characterization.[1,8-12]

Direct analysis of textile fibers can provide information about the dye, similar to that which can be obtained from LC-MS, in a much shorter period of time while requiring little to no sample preparation. Direct analysis techniques such as laser desorption photoionization[13,14] and direct analysis in real time[15] (DART) have been used to identify the dyes present in textiles. Herein, matrix-assisted laser desorption electrospray ionization (MALDESI)[16] coupled to MS is used for the direct analysis of dyes from textile fibers.

In IR-MALDESI, a mid-IR laser tuned to 2.94 μm is pulsed into a water containing sample to desorb neutral molecules which partition into an orthogonal electrospray plume where they are ionized by an ESI-like process.[17,18] The laser

wavelength correlates with the absorption maximum for the symmetric and asymmetric OH stretching modes in water. Using water as a matrix is ideal because it does not interfere with the mass spectrum and produces a low background signal. The low background signal enables better detection of the ions of interest. For the direct analysis of textile fabric that is presented herein, water is added onto the fabric sample to absorb the laser energy and facilitate the desorption of the dye molecules for subsequent post-ionization by ESI. The MALDESI source is coupled to a high mass accuracy-high resolving power hybrid linear ion trap, Fourier transform ion cyclotron resonance (LTQ-FT-ICR) mass spectrometer. The FT-ICR mass spectrometer's high resolving power and high mass accuracy allows the determination of elemental composition of the dyes. It should be noted that new bench-top generations of hybrid FTMS instruments can provide equivalent information. If the molecules are fragmented using tandem mass spectrometry (MS/MS), structural information about the compound can be determined as well. Structural information is very important when identifying dyes in forensics because many of the dyes have similar structures. Some dye structures differ by only a single substituent.[19]

The direct analysis using MALDESI is beneficial in that there is no extraction required, meaning the fiber can be used for multiple analyses because such an insignificant amount of fiber is consumed. MALDESI is time efficient, taking a few seconds to analyze the fiber and dye, while traditional LC-MS methods take around an hour for total analysis. The only sample preparation necessary for MALDESI is

spotting a few droplets of water on the fabric to absorb the laser energy and facilitate the desorption of the dye. Mass Spectrometry Imaging (MSI) of single fibers directly from a tape lift is also presented.

6.2 Experimental

6.2.1 Materials

Dyes were obtained from the stored supplies at the NCSU College of Textiles. Acid black 58, blue 40, and green 16 were purchased from Ciba-Geigy (Dover Township, NJ, USA). Basic Violet 16 was purchased from Clariant (Charlotte, NC, USA). Disperse red 60 and blue 79 were purchased from M. Dohmen (Greenville, NC, USA). Indigo, pigment red 146 and red 112 were purchased Huntsman (Charlotte, NC, USA). Direct red 24 was purchased from Crompton and Knowles (Middlebury, CT, USA). Vat orange 7 was purchased from Dystar (Charlotte, NC, USA). The reactive dyes (red 141, blue 160, and yellow 84) were purchased from the Institute of Dyes and Organic Products (Zgierz, Poland). HPLC grade acetonitrile and water were purchased from Burdick and Jackson (Muskegon, MI, USA). The raw fabrics were also obtained from the NCSU College of Textiles supplies.

6.2.2 Direct Infusion ESI

Dyes from a variety of dye classes (acid, basic, disperse, pigment, vat, and reactive dyes) were chosen for direct analysis from different fabrics (nylon, acetate,

polyester, and cotton). A small database of mass spectra was developed by directly infusing standard solutions made from the raw dye powders. Dye standards were made by dissolving 1 mg of the raw dye powder in 1 mL of 50:50 (v : v) water : acetonitrile then diluting the solution to 1 µM with the electrospray solvent (50 : 50 water : acetonitrile with 0.1% acetic acid). The dye standard solutions were then analyzed by direct infusion ESI in both positive and negative ion modes.

6.2.3 Direct Analysis by IR-MALDESI

The raw un-dyed fabrics were directly analyzed by MALDESI in both positive and negative ion modes to generate representative spectra for each fabric. The raw fabrics were then dyed using the appropriate procedures for the dye class and fabric type (actual procedures can be found in the supplementary material). A 1 cm by 1 cm square was cut from each of the dyed fabrics and these samples were analyzed by MALDESI in both positive and negative ion mode to identify the dye and, in some cases, the fiber polymer. Each fabric was analyzed as a pixel array of 5 pixels per line and 4 lines. Three laser pulses were fired per pixel with a single mass spectrum acquired after the third pulse and the spacing between pixels and lines was set to 0.5 mm. This correlates to a sampled section that was 2.5 mm by 2 mm for each fabric. While such a large section of the fabric was analyzed, it should be noted that signal from the dye and/or fabric can be obtained from a single pixel which corresponds a sample size that is on the order of the laser spot size that has a diameter of roughly 200 µm. Multiple pixels were analyzed across the fabric surface

in order to determine the average response. Microscopic images of the dyed fabric surfaces were obtained both before and after MALDESI analysis to provide qualitative information on the level of destruction to the fabric caused by the laser ablation.

6.2.4 IR-MALDESI Source

The IR-MALDESI source parameters were recently optimized using a design of experiments[18] and control over the laser ablation and mass spectrometer scanning features have been implemented. Briefly, electrospray solvent (50 % aqueous acetonitrile with 0.1% acetic acid) is pumped through a 75 µm fused silica emitter which is tapered to 30 µm at the tip (New Objective, Woburn, MA) at a flow rate of 200 nL/min. A potential of around 2 kV was applied to a stainless steel microtight union (Upchurch Scientific, Oak Harbor, WA, USA) just before the emitter to generate a stable electrospray. The emitter was held 9 mm from and on axis with the inlet to the mass spectrometer. The fabric sample was placed on a glass microscope slide and was wet with roughly 20 µL of water. It should be noted that this wetting process could theoretically extract some of the dye from the fabric. The fabric sample (dyed or un-dyed) was then placed on a vertical translation stage mounted on a motion controlled XY stage (LTA-HS, Newport Corporation, Irvine, CA, USA) such that the top of the fiber sample was 5 mm below the electrospray axis. A tunable wavelength mid infrared laser (IR Opolette, Opotek, Carlsbad, CA, USA) was used to ablate the fiber sample. The wavelength was tuned to 2.94 µm,

corresponding with the symmetric and asymmetric OH stretching frequency, allowing for the water added to the fabric sample to act as an exogenous matrix by absorbing the laser energy and facilitating the desorption of particulates of fiber. The laser beam was steered by three silver coated mirrors (Newport Corporation, Irvine, CA, USA) and was focused onto the sample by a CaF_2 plano-convex lens (Edmund Optics, Barrington, NJ, USA)

6.2.5 LTQ-FT Mass Spectrometer

The IR-MALDESI source was coupled to a LTQ-FT-ICR Ultra (Thermo Fisher Scientific, San Jose, Ca, USA). An extended capillary was used to allow the stage clearance while rastering the sample. An extended ion transfer tube was used which protruded 23mm from the instrument. The internal diameter of the ion transfer tube was 0.596 mm to maintain the conductance and pressure in the first pumping stage as compared to the original instrument ion transfer tube. For positive mode analyses, the capillary temperature and voltage were set at 250℃ and 37 V respectively with a tube lens voltage of 110 V. For negative mode analysis, these values were set to 250℃, -45 V, and -30 V respectively. The resolving power of the FT-ICR was set to 100 000 $_{FWHM}$ at *m/z* 400 unless otherwise specified. The automatic gain control (AGC) on the LTQ is a short prescan which roughly determines the number of ions that are currently entering the instrument and adjusts the ion trap injection time accordingly such that a similar number of ions are sent to the ICR cell which each scan.[20] This adjustment is used to reduce space charge

effects and maintain accurate mass measurements.[21] For the direct infusion ESI experiments the AGC was set to 5 x 10^5. In the MALDESI experiment, ions are generated in distinct packets, milliseconds after each laser pulse, rather than being continuously generated. Considering this, the ions would not be present during the AGC prescan, making it impractical to use. For this reason the AGC was turned off and the ion injection time was set to 150 ms to capture ions from all three laser pulses (3 pulses at 20 Hz takes roughly 100 ms from the first pulse). While turning off the AGC can result in poor mass measurement accuracy, the dye ions detected were within 2 ppm of their theoretical mass which is within the instrument specifications.

6.2.6 Data Analysis

Using high resolving power and high mass accuracy instrumentation, such as the FT-ICR, allows for resolution of elemental contributions to isotopic peaks (such as the contribution of ^{34}S in the A+2 peak of a sulfur containing ion).[22] Sulfur counting was carried out by comparing the relative abundance of the sulfur peak to the monoisotopic peak and multiplying by the ratio of the isotopic distributions for ^{32}S and ^{34}S (^{32}S:^{34}S), **Equation 6.1** (adapted from equation 3 in reference 23). $A+2_{Experimental}$ is the experimental peak intensity of the ^{34}S peak and $A_{Experimental}$ is the experimental peak intensity of the monoisotopic peak. $^{32}S_{Theoretical}$ and $^{34}S_{Theoretical}$ are the natural isotopic distributions of the ^{32}S and ^{34}S isotopes, respectively, as reported by the NIST.[23]

$$\frac{A+2_{Exp.}}{A_{Exp.}} \times \frac{^{32}S_{Theo.}}{^{34}S_{Theo.}} = \#\ of\ Sulfur\ Atoms \qquad \textbf{(Equation 6.1)}$$

Carbon counting is carried out the same way except the carbon isotopes ^{12}C and ^{13}C replace ^{32}S and ^{34}S, respectively, and the A+1 carbon peak is used in place of the A+2 sulfur peak, **Equation 6.2.**

$$\frac{A+2_{Exp.}}{A_{Exp.}} \times \frac{^{32}S_{Theo.}}{^{34}S_{Theo.}} = \#\ of\ Sulfur\ Atoms \qquad \textbf{(Equation 6.2)}$$

6.3 Results and Discussion

The dyes that successfully yielded spectral results were Acid Black 58 (nylon), Acid Blue 40 (nylon), Acid Green 16 (nylon), Basic Violet 16 (acetate), and Disperse Red 60 (polyester). The only polymer peaks that were observed were nylon 6 peaks from the acid dyed fabrics. 487 and 713 as well as 511 and 737 are 226 mass to charge (*m/z*) units apart which corresponds to a monomer of nylon 6, detectable in negative ion mode. There were no distinguishing peaks for acetate, polyester, or cotton.

Acid Black 58 was detected in negative ion mode as $[M]^-$. The observed mass from the MALDESI analysis was within 0.68 ppm of the theoretical monoisotopic mass based on the structure provided by the Colour Index International. The theoretical isotopic distribution was calculated and plotted as red

circles over the experimental isotopic distribution from direct infusion ESI (**Figure 6.1a**) and the direct analysis by MALDESI (**Figure 6.1b** inlay). The presence of chromium in the structure gives rise to the characteristic shifts seen in the isotopic distribution. The peak pairs at *m/z* 487 and 713 as well as 511 and 737 in the full scan MALDESI spectrum correspond to polymers of nylon 6 (green squares in **Figure 6.1b)**. The mass difference between each pair (226 *m/z* units) relates to the loss of a monomer of nylon 6. **Figure 6.1c** shows the before image of the fabric prior to analysis, the portion of the fabric that was analyzed (white square), as well as an image of the sampled area taken after the analysis. This particular fabric had the appearance of damaged fibers across the entire sample, but the "before MALDESI" microscopic image (**Figure 6.1c**) clearly shows frizzy, ravaged fibers even prior to analysis. The "after MALDESI" image (**Figure 6.1c**) shows the sampled region in the upper left corner of the fabric that appears to be more damaged.

The MALDESI analysis of Acid Blue 40 in nylon led to the observation that the experimental mass of the dye ion $[M-H]^-$ (423.0649) did not match the monoisotopic mass (based on the 450.0765) structure provided by the Colour Index International (**Figure 6.3a**). It is unknown whether this is due to degradation or contamination of the dye, however, the dye mass observed in the MALDESI analysis (**Figure 6.2b)** correlated with the mass observed from the direct infusion ESI of the dye standard (**Figure 6.2a)**. This correlation implies that the mass discrepancy with the Colour Index structure is not due to a fragmentation specifically during the MALDESI

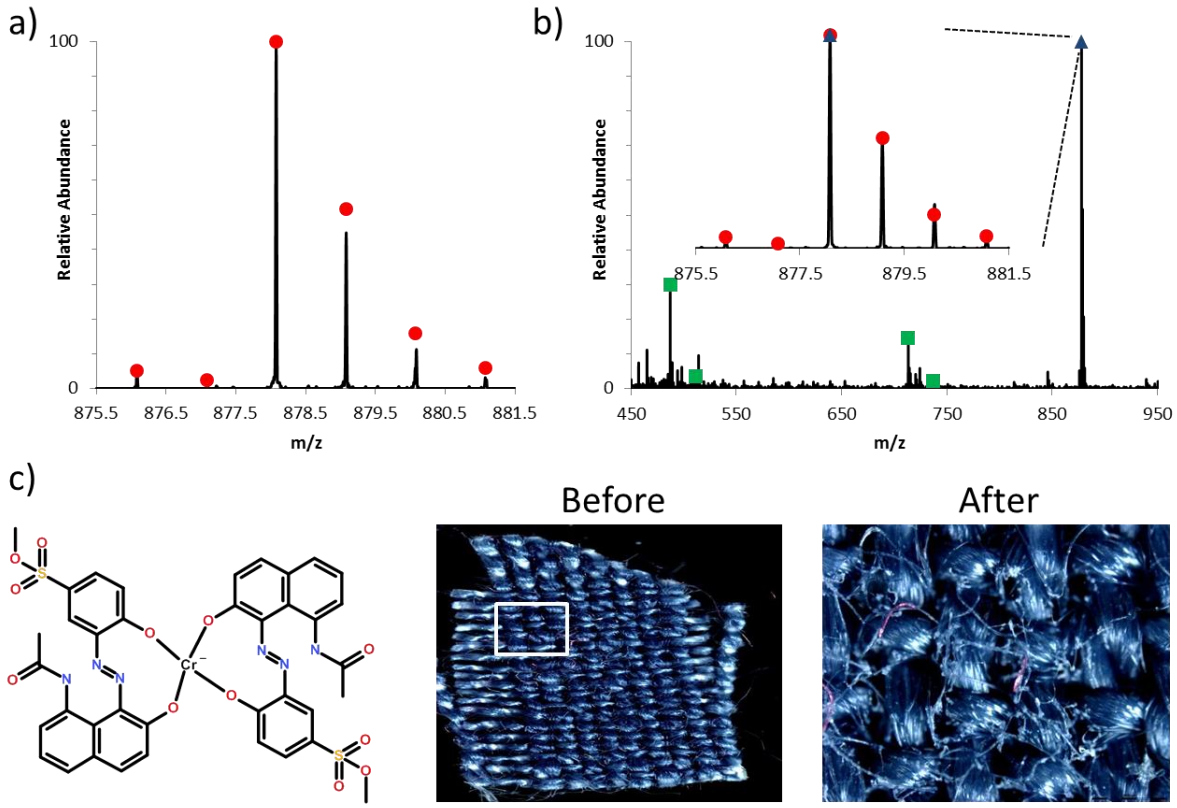

Figure 6.1 Mass spectra and microscopic images of Acid Black 58 in nylon. **a)** Mass spectrum of Acid Black 58 from direct infusion ESI, with the theoretical isotopic distribution (red circles). **b)** Full scan mass spectrum from direct analysis of the dyed fabric by MALDESI with the dye peak (blue triangle) and nylon peaks (green squares) labeled. The inlay shows a zoomed portion of the most abundant dye peak (blue triangle) with the theoretical isotopic distribution (red circles). **c)** Dye structure as given by the Colour Index International and microscopic images of the dyed fabric before and after MALDESI analysis. The white square indicates the analyzed section displayed in the "after" image.

analysis. To further investigate this discrepancy, the dye standard was directly infused (negative ion mode) and analyzed by tandem MS with collision-induced dissociation (CID) to elucidate its structure. The fragmentation of the parent ion at

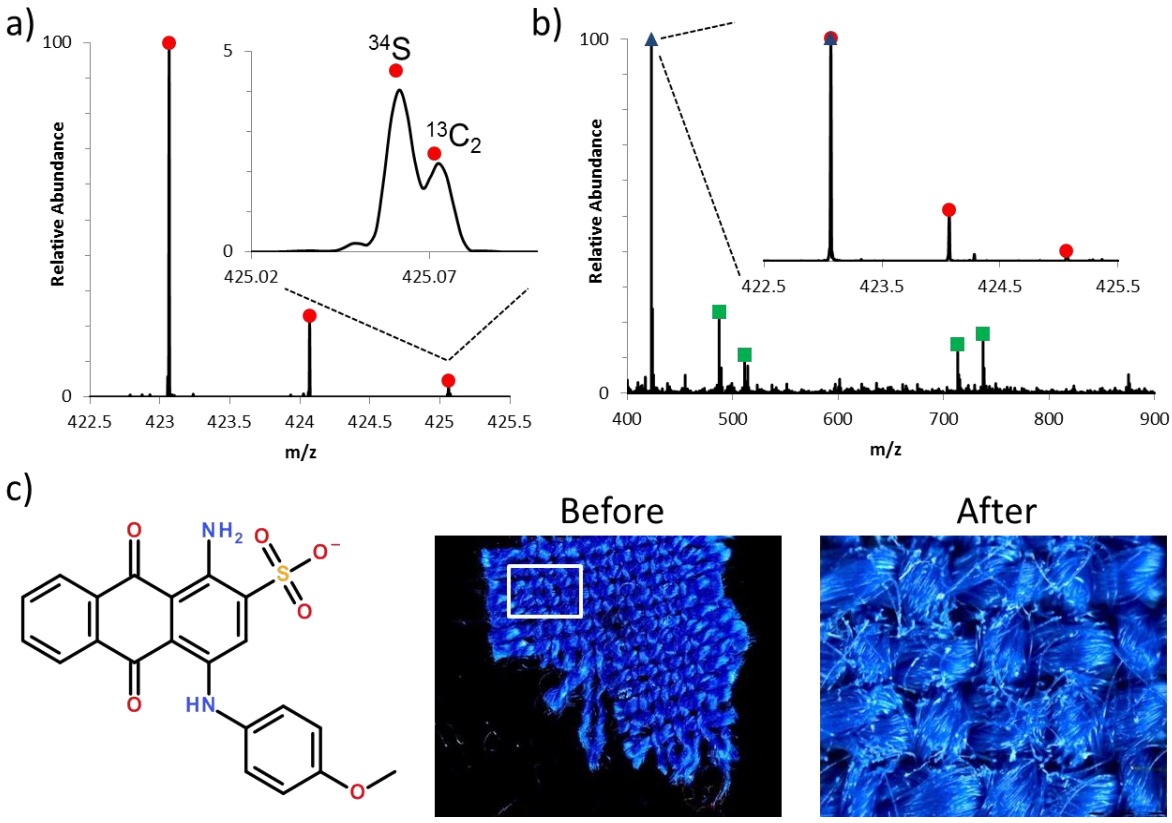

Figure 6.2 Mass spectra and microscopic images of Acid Blue 40 in nylon. **a)** Mass spectrum of Acid Blue 40 from direct infusion ESI, theoretical isotopic distribution (red circles) and the proposed structure based on accurate mass and MS/MS fragmentation. The inlay shows the resolution of the ^{34}S and $^{13}C_2$ contributions to the A+2 peak. **b)** Full scan mass spectrum from direct analysis of the dyed fabric by MALDESI with the dye peak (blue triangle) and nylon peaks (green squares) labeled. The inlay shows a zoomed portion of the dye peak (blue triangle) with the theoretical isotopic distribution (red circles). **c)** The proposed dye structure based on accurate mass, isotopic distribution, and MS/MS fragmentation as well as microscopic images of the dyed fabric before and after MALDESI analysis. The white square indicates the analyzed section displayed in the "after" image.

423 led to a major fragment at 408.0430, a neutral loss of 15.0219 *m/z*, which is most likely a loss of a methyl group. A methyl loss is not a likely fragment to come from the structure from the Colour Index. At a resolving power of 100 000 the

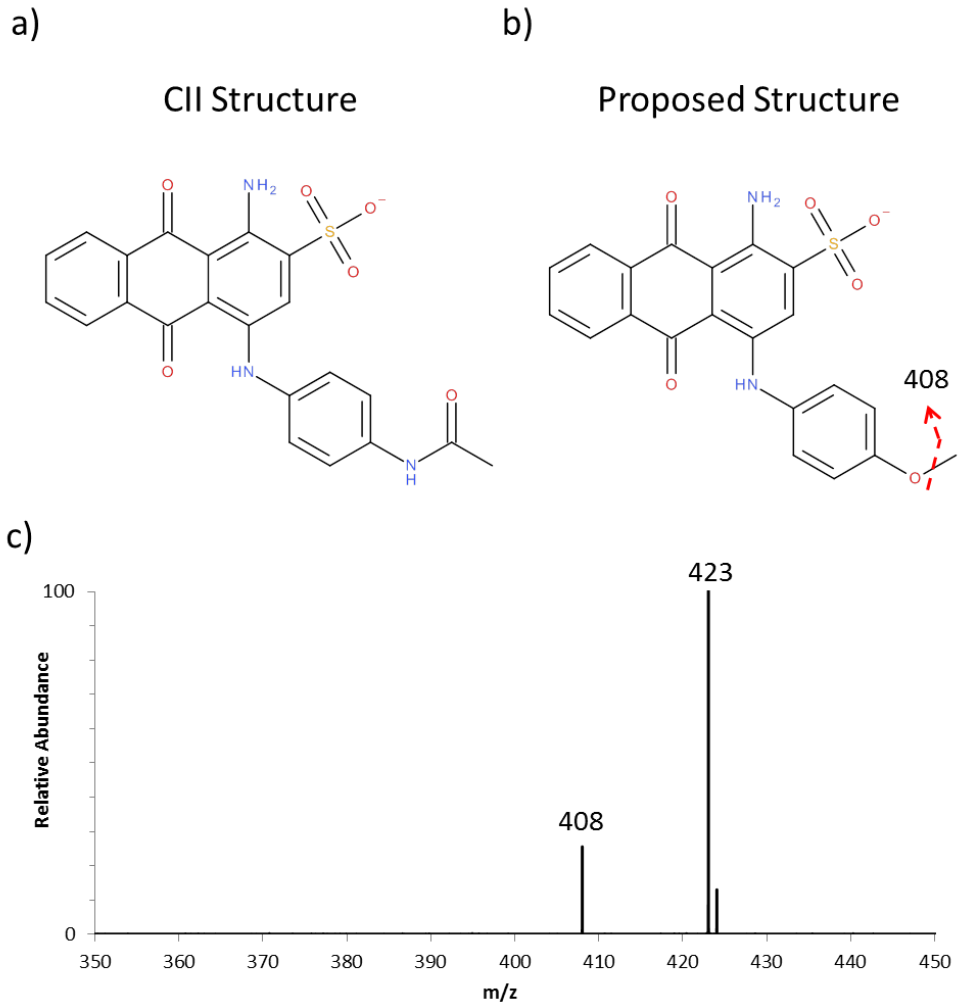

Figure 6.3 Acid Blue 40 structures and tandem mass spectra. **a)** Structure of Acid Blue 40 from the Colour Index International. **b)** Proposed structure of Acid Blue 40 based on accurate mass measurement, carbon counting, sulfur counting, and CID fragmentation pattern from MS/MS experiment. The red dashed lines correspond to the location of fragmentation during the MS/MS experiment. **c)** Tandem mass spectrum of Acid Blue 40 (423) with CID fragmentation.

contribution of ^{34}S in the A+2 peak can be resolved allowing for sulfur counting to be performed. Using equation 1, it was determined that the molecule contains a single sulfur and carbon counting, using equation 2, was performed and yielded around 21

carbons. With the accurate mass of the parent ion and the information obtained from the MS/MS data, sulfur counting, and carbon counting, a new structure was proposed (**Figure 6.3c**). It is likely that the anthraquinonesulfonic acid portion of the structure is conserved since it is, in part, responsible for its classification as an acid dye. The proposed structure differs from the Colour Index structure by replacing the acetamide group on the para position of the benzene ring with a methoxy group. The monoisotopic mass and isotopic distribution of the proposed structure (red circles in **Figure 6.2a** and **Figure 6.2b** inlay) correlate with the observed mass and isotopic distribution from direct infusion ESI and MALDESI analyses within -0.98 and -1.6 ppm respectively. Also, the proposed structure is more likely to produce a neutral loss of a methyl group when fragmented. Peaks which correlated with nylon polymer were observed in the MALDESI analysis (green squares in **Figure 6.2b**). The destruction to the fabric was rather minimal, with a few fibers that were visibly melted (**Figure 6.2c**). Some of the top fibers of the weave were shredded, but most of the fibers in that section of the weave were not affected at all by the laser. The remaining fabric surface is untouched and as undamaged as prior to analysis.

The analysis of Acid Green 16 in nylon also resulted in an experimental mass of the $[M-2H]^-$ ion that did not match the theoretical monoisotopic mass of the main structure provided by the Colour Index (**Figure 6.4a**). It should be noted that this dye contains a quaternary ammonium cation which is why the loss of two protons gives an overall charge of -1. However, the observed mass was greater than what the given structure indicated it should be. The experimental mass was 593.1793 but

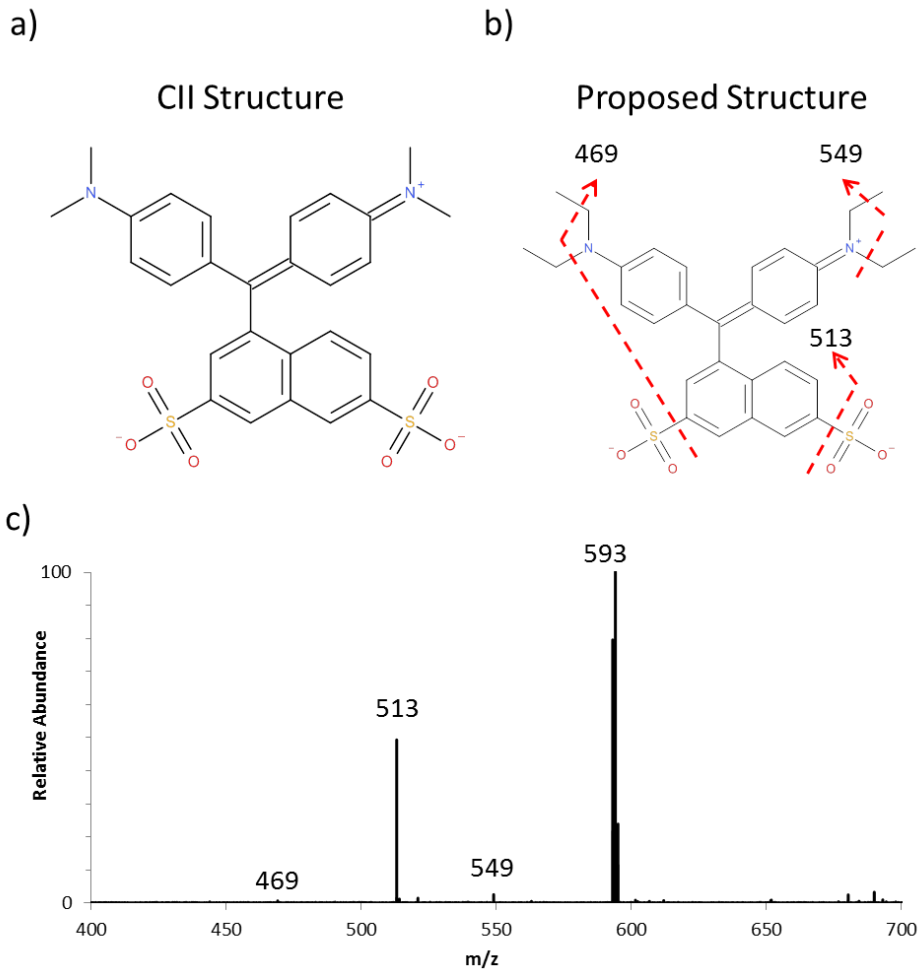

Figure 6.4 Acid Green 16 structures and tandem mass spectra. **a)** Structure of Acid Green 16 from the Colour Index International. **b)** Proposed structure of Acid Green 16 based on accurate mass measurement, carbon counting, sulfur counting, and CID fragmentation pattern from MS/MS experiment. The red dashed lines correspond to the location of fragmentation during the MS/MS experiment. **c)** Tandem mass spectrum of Acid Green 16 (593) with CID fragmentation.

the monoisotopic mass is supposed to be 537.1159, a mass difference of 56.0634. Acid Green 16 was then analyzed using high resolving power mass spectrometry and MS/MS in negative ion mode to elucidate the structure. Performing sulfur and carbon counting on the high resolution experimental data indicated that the structure

contains two sulfurs and about 30 carbons. The fragmentation of the ion at 593 resulted in a major fragment ion at 513.2218 (loss of 79.9568) and two minor fragment ions at 549.1166 (loss of 44.0620) and 469.1510 (loss of 124.0205) (**Figure 6.4c**). The major fragment at 513 corresponds to a loss of a sulfonic acid which is a possible fragment based on the expected structure. However, the minor loss at 549 (C_3H_8) does not match the Colour Index structure. The fragment ion at 469 resulted from a loss of a sulfonic acid and C_3H_8. A new structure was proposed for this dye as well to match the accurate mass, fragmentation patterns, and carbon and sulfur counting (**Figure 6.4b**). The proposed structure differs from the Colour Index structure by replacing both dimethylamines with diethylamines. The monoisotopic mass and isotopic distribution of the proposed structure (red circles) matched the observed masses from the direct infusion ESI and MALDESI analyses, as shown in **Figure 6.5a** and the inlay in **Figure 6.5b**, with mass accuracies of -0.11 and 1.7 ppm respectively. The loss of C_3H_8 from the proposed structure is possible by the sequential loss of C_2H_5 and CH_3 which has been demonstrated to be a common fragment for diethyphenylammonium ions.[24] After further investigation it was discovered that both the proposed structure and the structure given by the Colour Index are possible structures for Acid Green 16. As with the other nylon fabrics analyzed by MALDESI, the fabric was not shredded completely through (**Figure 6.5c**). Only the top few fibers of the threads in the weave were damaged. The remaining fabric surface was undamaged.

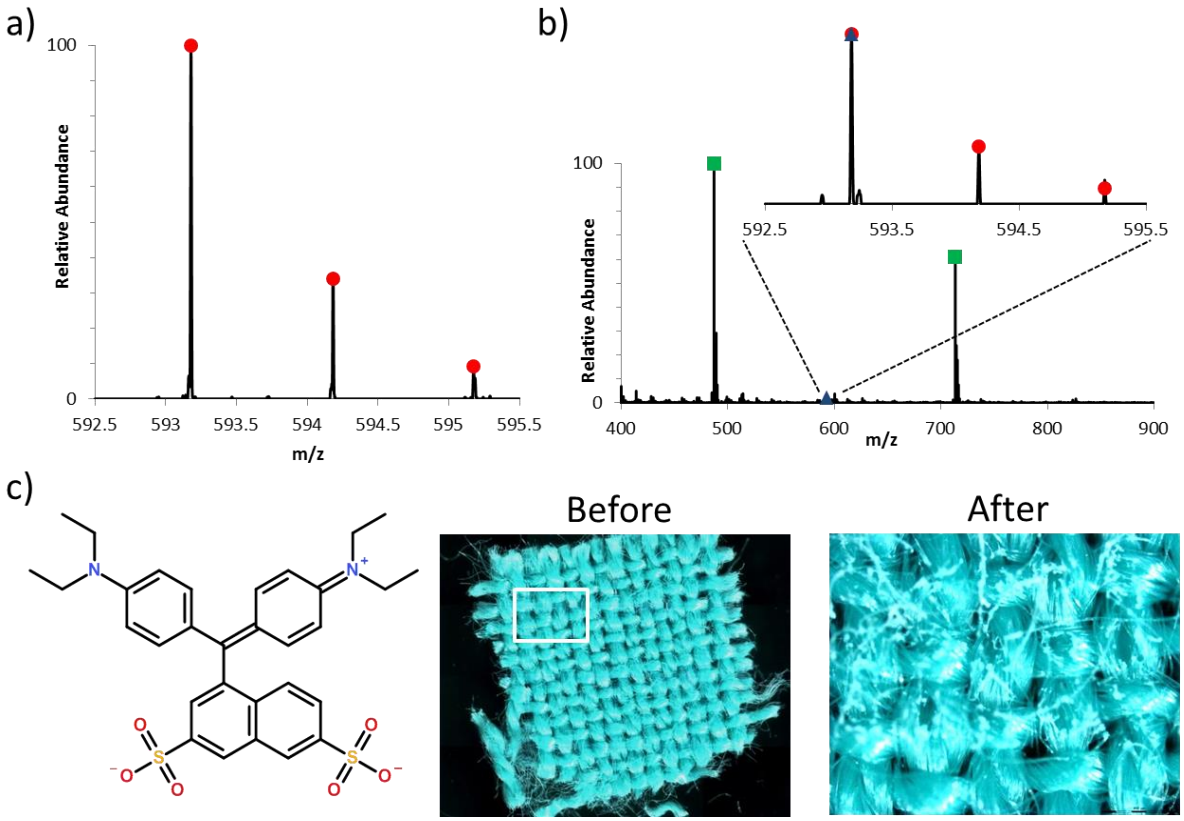

Figure 6.5 Mass spectra and microscopic images of Acid Green 16 in nylon. (a) Mass spectrum of Acid Green 16 from direct infusion ESI, theoretical isotopic distribution (red circles) and the proposed structure based on accurate mass and MS/MS fragmentation. (b) Full scan mass spectrum from direct analysis of the dyed fabric by MALDESI with the dye peak (blue triangle) and nylon peaks (green squares) labeled. The inlay shows a zoomed portion of the dye peak (blue triangle) with the theoretical isotopic distribution (red circles). (c) Microscopic pictures of the dyed fabric before MALDESI and after MALDESI. The white square indicates the analyzed section displayed in the "after" image.

Basic Violet 16 was detected in positive ion mode from the acetate fabric as $[M]^+$. The mass of the dye from the MALDESI experiment (333.2325) corresponded to the theoretical monoisotopic mass (333.2325) with a mass accuracy of -0.075 ppm. The plot of the theoretical distribution (red circles) over the direct infusion ESI (**Figure 6.6a**) and MALDESI (**Figure 6.6b**) spectra also corroborates the accuracy of

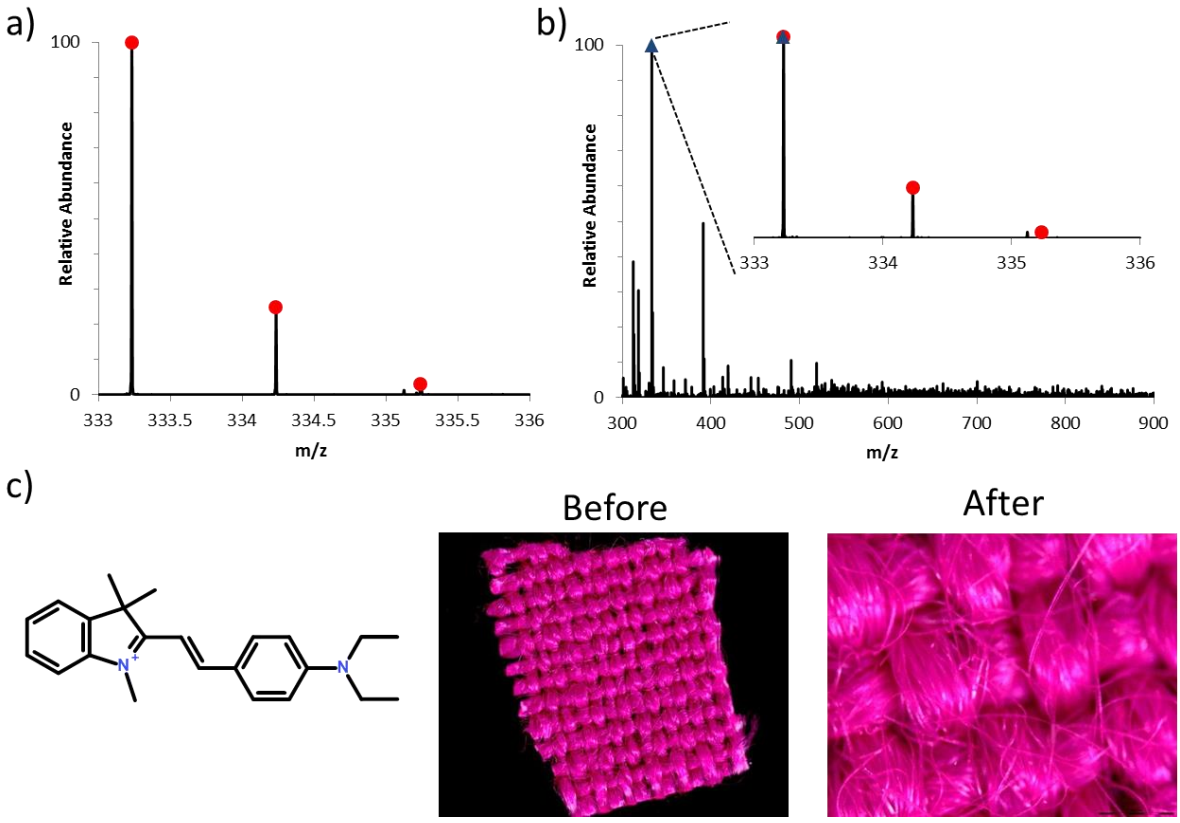

Figure 6.6 Mass spectra and microscopic images of Basic Violet 16 in acetate. **a)** Mass spectrum of Basic Violet 16 from direct infusion ESI, theoretical isotopic distribution (red circles). **b)** Full scan mass spectrum from direct analysis of the dyed fabric by MALDESI. The inlay shows a zoomed portion of the dye peak (blue triangle) with the theoretical isotopic distribution (red circles). **c)** Dye structure as given by the Colour Index International and microscopic images of the dyed fabric before and after MALDESI analysis. The white square indicates the analyzed section displayed in the "after" image.

the match. In order to demonstrate its accuracy, the carbon counting technique was used to predict the number of carbons in the basic violet 16 structure where the theoretical mass matched the observed mass. This technique predicted around 22-23 carbons which correlates with the expected structure which has 23 carbons. There was very little observable damage caused by the laser after the MALDESI

analysis of the acetate fabric (**Figure 6.6c**). On the "after MALDESI" overall fabric image, the damage is visibly undetectable. Even when looking closely at the microscopic image of the blast site, only a few fibers are cut and show the melted beads indicative of the laser's shots.

Disperse Red 60 in polyester was also detected in positive ion mode as $[M+H]^+$ with an observed *m/z* that corresponded to the theoretical mass with a mass accuracy of 0.63 ppm. The overlay of the theoretical distribution (red circles) on the direct infusion ESI (**Figure 6.7a**) and MALDESI (**Figure 6.7b** inlay) spectra corroborate the match. The polyester was even less damaged than the Basic Violet 16 acetate (**Figure 6.7c**). There is no visible destruction to the fabric on either the whole fabric overview or the specific image of the blast site. The "after" image of the polyester looks just as undamaged as the "before" image.

Along with dyed fabrics, fabric prints were also analyzed by MALDESI. The fabric print was pasted on 100% bleached cotton using a paste comprised of a binder, a thickener, and the pigment red 2b (146) dye. During the mass spectrometric analysis of the prints, a highly abundant polyethylene glycol (PEG) signal out-competed the signal from the pigment dye. To isolate the source of the PEG, the pigment dye and the un-pigmented print paste (just the binder and thickener) were separately analyzed and it was determined that a majority of the PEG signal was coming from the thickener. In an attempt to reduce the PEG saturation, the prints were washed with a surfactant and water at 160^o F. The entire washing and drying process took roughly 30 minutes (5 minute wash and 25 minute

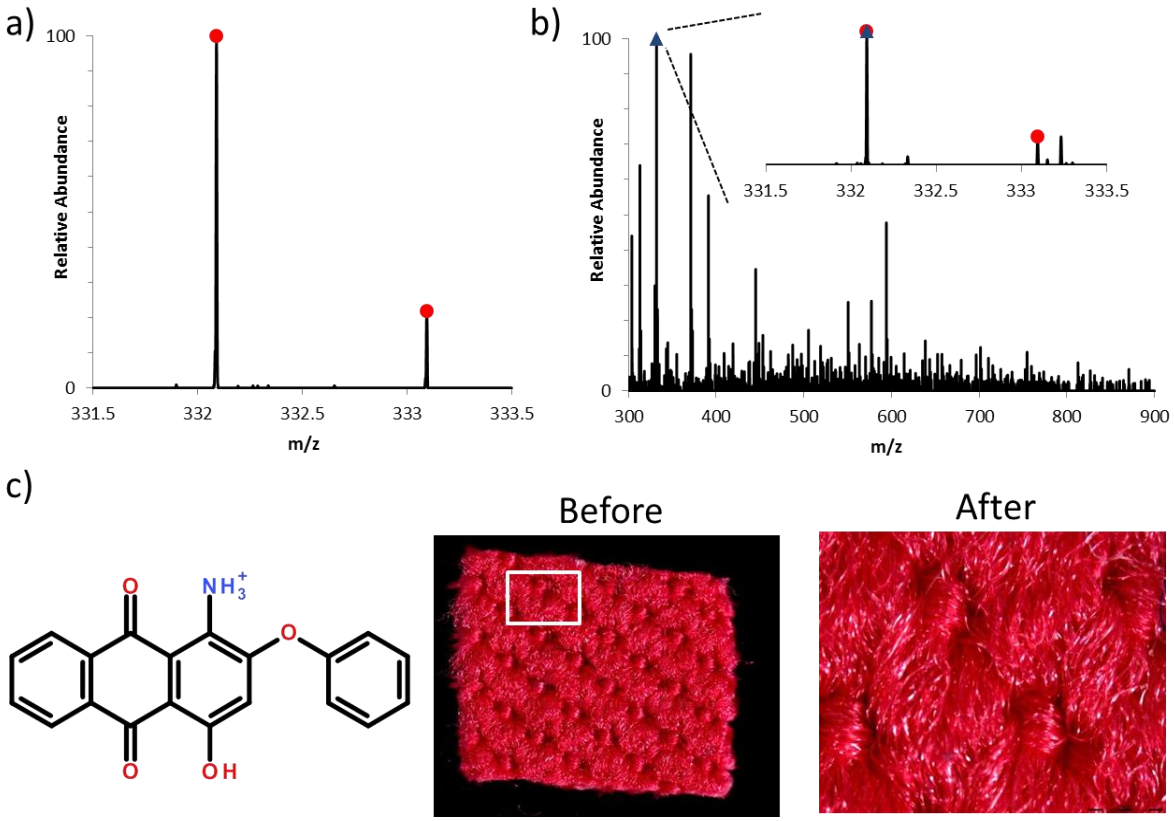

Figure 6.7 Mass spectra and microscopic images of Disperse Red 60 in polyester. **a)** Mass spectrum of Disperse Red 60 from direct infusion ESI, theoretical isotopic distribution (red circles). **b)** Full scan mass spectrum from direct analysis of the dyed fabric by MALDESI. The inlay shows a zoomed portion of the dye peak (blue triangle) with the theoretical isotopic distribution (red circles). **c)** Dye structure as given by the Colour Index International and microscopic images of the dyed fabric before and after MALDESI analysis. The white square indicates the analyzed section displayed in the "after" image.

to dry). When the prints were analyzed again, the polyethylene glycol levels were decreased by a significant amount, allowing pigment red 146 to be detected in positive ion mode as $[M+H]^+$, although in low abundance (**Figure 6.8a**). **Figure 6.8b,** a zoom in portion of the spectra in **Figure 6.8a**, shows the isotopic distribution of the dye with an overlay of the theoretical distribution (red circles).

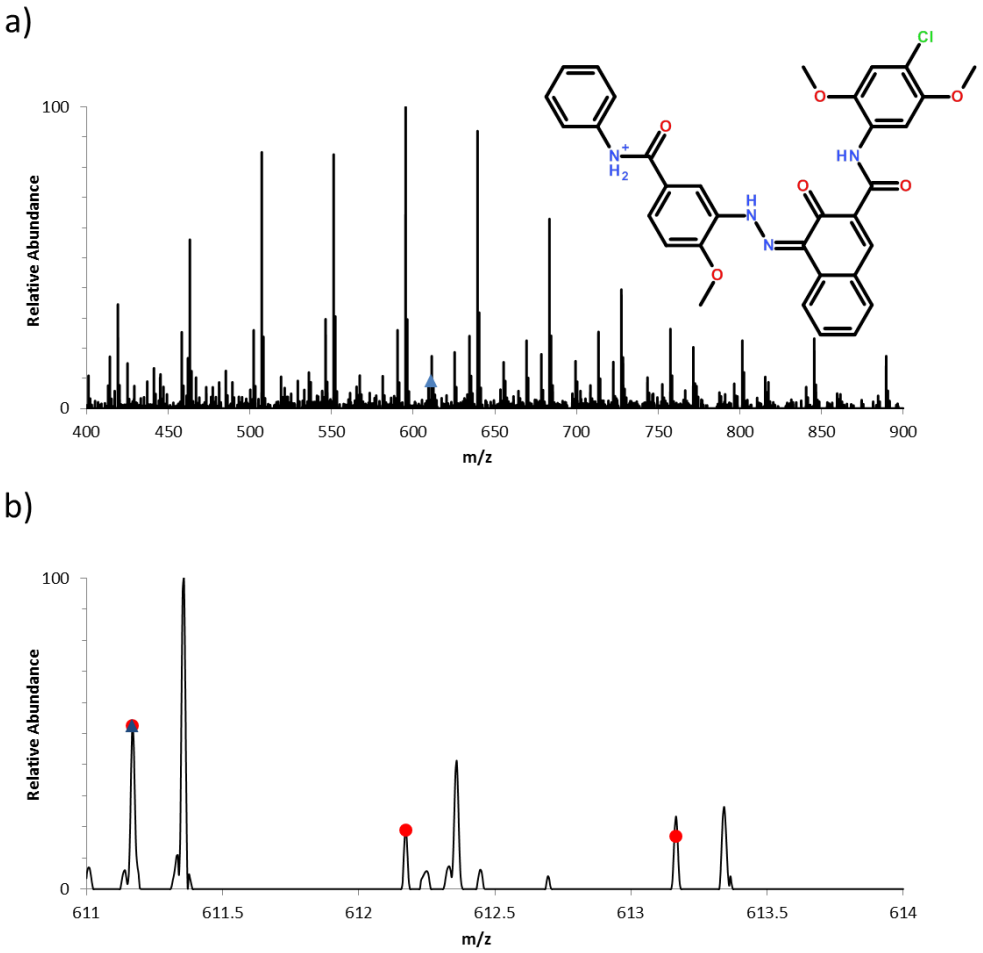

Figure 6.8 Mass spectra of Pigment Red 146 on bleached cotton. **a)** Full scan mass spectrum from direct analysis of the dyed fabric by MALDESI and the dye structure as given by the Colour Index International. **b)** A zoomed portion of the full scan showing the dye peak (blue triangle) with the theoretical isotopic distribution (red circles).

There were a few dyes that were not detected by the direct analysis. However, it was not only when using MALDESI as a source that they were undetectable; the dyes not observed with MALDESI also could not be observed by direct infusion ESI, the contemporary source typically used. Most of the undetectable dyes are ionizable, except Vat Orange 7 and indigo, so it is unclear

why this was the case. The dyes that were not detected include Acid Red 186 (nylon), Disperse Blue 79 (polyester), Indigo/Pigment Blue 66/Vat Blue 1 (cotton), Vat Orange 7 (cotton), Direct Red 24 (cotton and mercerized cotton), Reactive Red 141 (cotton), Reactive Blue 160 (cotton), Reactive Yellow 84 (cotton), and Pigment Red 112 (bleached cotton after washing). Adding a few drops of an aqueous extraction solvent that was appropriate for the dye and fabric in place of just water as the matrix just prior to MALDESI-mass spectrometric analysis was also tried. While this approach was helpful for increasing the signal to noise of the dye ions that were previously detected, those that were undetected using water as a matrix also went unobserved when using the extraction solvent.

6.4 Conclusions

MALDESI-MS has been demonstrated as an effective technique for the direct analysis of dyes from dyed textile fabric with minimal sample pretreatment. Compared to the more contemporary approach of dye extraction followed by either direct infusion ESI or LC-MS, this direct analysis approach provides similar spectral information about the dye (and fiber polymer in some cases) but in a significantly shorter period of time. Another benefit to the direct analysis is that the destruction to the fabric was minimal if present at all. The nylon displayed the most destruction, but even this damage was very small. The polyester showed almost no damage, and the acetate (viewed microscopically) did not show any damage at all. As a future consideration, the analysis of a single fiber or thread and fibers dyed with

multiple dyes will be analyzed using MALDESI as a source since these conditions are more applicable to forensic cases.

6.5 References

(1) Goodpaster, J. V.; Liszewski, E. A. Forensic analysis of dyed textile fibers. *Anal. Bioanal. Chem.* **2009**, *394*(8), 2009-2018.

(2) SWGMAT. Forensic Fiber Examination Guidelines. *Forensic Science Communications* **1999**, *1*(1), 1-59.

(3) Kirkbride, K. P.; Tridico, S. R. The application of laser scanning confocal microscopy to the examination of hairs and textile fibers: an initial investigation. *Forensic Sci. Int.* **2010**, *195*(1-3), 28-35.

(4) Tungol, M. W.; Bartick, E. G.; Montaser, A. Forensic analysis of acrylic copolymer fibers by infrared microscopy. *Appl. Spectrosc.* **1993**, *47*(10), 1655-1658.

(5) Wiggins, K. G. Forensic textile fiber examination across the USA and Europe. *J. Forensic Sci.* **2001**, *46*(6), 1303-1308.

(6) Zieba-Palus, J.; Borusiewicz, R.; Kunicki, M. PRAXIS-combined mu-Raman and mu-XRF spectrometers in the examination of forensic samples. *Forensic Sci. Int.* **2008**, *175*(1), 1-10.

(7) Thomas, J.; Buzzini, P.; Massonnet, G.; Reedy, B.; Roux, C. Raman spectroscopy and the forensic analysis of black/grey and blue cotton fibres. *Forensic Sci. Int.* **2005**, *152*(2), 189-197.

(8) Tuinman, A. A.; Lewis, L. A.; Lewis, S. A. Trace-Fiber Color Discrimination by Electrospray Ionization Mass Spectrometry: A Tool for the Analysis of Dyes Extracted from Submillimeter Nylon Fibers. *Anal. Chem.* **2003**, *75*(11), 2753-2760.

(9) Petrick, L. M.; Wilson, T. A.; Ronald Fawcett, W. High-Performance Liquid Chromatography–Ultraviolet–Visible Spectroscopy–Electrospray Ionization Mass Spectrometry Method for Acrylic and Polyester Forensic Fiber Dye Analysis*. *Journal of Forensic Sciences* **2006**, *51*(4), 771-779.

(10) Stefan, A. R.; Dockery, C. R.; Nieuwland, A. A.; Roberson, S. N.; Baguley, B. M.; Hendrix, J. E.; Morgan, S. L. Forensic analysis of anthraquinone, azo, and metal complex acid dyes from nylon fibers by microextraction and capillary electrophoresis. *Analytical and Bioanalytical Chemistry* **2009**, *394*(8), 2077-2085.

(11) Stefan, A. R.; Dockery, C. R.; Baguley, B. M.; Vann, B. C.; Nieuwland, A. A.; Hendrix, J. E.; Morgan, S. L. Microextraction, capillary electrophoresis, and mass spectrometry for forensic analysis of azo and methine basic dyes from acrylic fibers. *Analytical and Bioanalytical Chemistry* **2009**, *394*(8), 2087-2094.

(12) Dockery, C. R.; Stefan, A. R.; Nieuwland, A. A.; Roberson, S. N.; Baguley, B. M.; Hendrix, J. E. Automated extraction of direct, reactive, and vat dyes from cellulosic fibers for forensic analysis by capillary electrophoresis. *Analytical and Bioanalytical Chemistry* **2009**, *394*(8), 2095-2103.

(13) Dale, M. J.; Jones, A. C.; Langridge-Smith, P. R. R.; Costello, K. F.; Cummins, P. G. Laser desorption laser photoionization time-of-flight mass spectrometry of dyes. *Anal. Chem.* **1993**, *65*(6), 793-801.

(14) Dale, M. J.; Zhan, Q.; Zenobi, R.; Costello, K.; Langridge-Smith, P. R. R. Analysis of dyestuffs on polyester using laser desorption-laser photoionisation mass spectrometry. *Anal. Methods Instrum.* **1995**, *2*(2), 101-105.

(15) Selvius DeRoo, C.; Armitage, R. A. Direct Identification of Dyes in Textiles by Direct Analysis in Real Time-Time of Flight Mass Spectrometry. *Anal. Chem.* **2011**, *83*(18), 6924-6928.

(16) Sampson, J.; Hawkridge, A.; Muddiman, D. Generation and detection of multiply-charged peptides and proteins by matrix-assisted laser desorption electrospray ionization (MALDESI) fourier transform ion cyclotron resonance mass spectrometry. *J. Am. Soc. Mass Spectrom.* **2006**, *17*(12), 1712-1716.

(17) Sampson, J. S.; Murray, K. K.; Muddiman, D. C. Intact and Top-Down Characterization of Biomolecules and Direct Analysis Using Infrared Matrix-Assisted Laser Desorption Electrospray Ionization Coupled to FT-ICR Mass Spectrometry. *J. Am. Soc. Mass Spectrom.* **2009**, *20*(4), 667-673.

(18) Barry, J. A.; Muddiman, D. C. Global optimization of the infrared matrix-assisted laser desorption electrospray ionization (IR MALDESI) source for mass spectrometry using statistical design of experiments. *Rapid Commun. Mass Spectrom.* **2011**, *25*(23), 3527-3536.

(19) Huang, M.; Yinon, J.; Sigman, M. E. Forensic identification of dyes extracted from textile fibers by liquid chromatography mass spectrometry (LC-MS). *J. Forensic Sci.* **2004**, *49*(2), 238-249.

(20) Belov, M. E.; Zhang, R.; Strittmatter, E. F.; Prior, D. C.; Tang, K.; Smith, R. D. Automated Gain Control and Internal Calibration with External Ion Accumulation Capillary Liquid Chromatography-Electrospray Ionization-Fourier Transform Ion Cyclotron Resonance. *Anal. Chem.* **2003**, *75*(16), 4195-4205.

(21) Jeffries, J. B.; Barlow, S. E.; Dunn, G. H. Theory of space-charge shift of ion cyclotron resonance frequencies. *Int. J. Mass Spectrom. Ion Processes* **1983**, *54*(1–2), 169-187.

(22) Blake, S.; Walker, S.; Muddiman, D.; Hinks, D.; Beck, K. Spectral Accuracy and Sulfur Counting Capabilities of the LTQ-FT-ICR and the LTQ-Orbitrap XL for Small Molecule Analysis. *J. Am. Soc. Mass Spectrom.* **2011**, *22*(12), 2269-2275.

(23) NIST Atomic Weights and Isotopic Compositions for All Elements. http://physics.nist.gov/cgi-bin/Compositions/stand_alone.pl?ele=&ascii=html&isotype=all (accessed June-July 2012).

(24) Harrison, A. G. Fragmentation reactions of alkylphenylammonium ions. *J. Mass Spectrom.* **1999**, *34*(12), 1253-1273.